

JSCSEN 77(10)1311–1481(2012)

ISSN 1820-7421 (Online)

Journal of the Serbian Chemical Society

ersion
lectronic

Society
115th
Anniversary
1897 - 2012

VOLUME 77

No 10

BELGRADE 2012

Available on line at



www.shd.org.rs/JSCS/

The full search of JSCS
is available through

DOAJ DIRECTORY OF
OPEN ACCESS
JOURNALS
www.doaj.org



CONTENTS

S. Ž. Drmanić, J. B. Nikolić, A. D. Marinković and B. Ž. Jovanović: A comparative study of the linear solvation energy relationship for the reactivity of pyridine carboxylic acids with diazodiphenylmethane in protic and aprotic solvents (Authors' review) 1311

Organic Chemistry

U. C. Mashelkar, M. S. Jha and B. U. Mashelkar: Synthesis of 2-azetidinones substituted coumarin derivatives 1339

S. Jain, B. S. Keshwal and D. Rajguru: A clean and efficient L-proline-catalyzed synthesis of polysubstituted benzenes in the ionic liquid 1-butyl-3-methylimidazolium hexafluorophosphate 1345

Biochemistry and Biotechnology

B. B. Sokmen, H. C. Onar, A. Yusufoglu and R. Yanardag: Anti-elastase, anti-urease and antioxidant activities of (3–13)-monohydroxyeicosanoic acid isomers 1353

P. M. Mitrović, D. Z. Orčić, Z. O. Sakač, A. M. Marjanović-Jeromela, N. L. Grahovac, D. M. Milošević and D. P. Marisavljević: Characterization of sirodesmins isolated from the phytopathogenic fungus *Leptosphaeria maculans*..... 1363

S. M. Savatović, G. S. Četković, J. M. Čanadanović-Brunet and S. M. Djilas: Kinetic behaviour of the DPPH radical-scavenging activity of tomato waste extracts 1381

Inorganic Chemistry

M. Đorđević, D. Jeremić, K. Anđelković, M. Gruden-Pavlović, V. Divjaković, M. Šumar Ristović and I. Brčeski: Cobalt(II) and cadmium(II) compounds with adamantane-1-sulfonic acid..... 1391

Theoretical Chemistry

I. Gutman, J. Đurđević, Z. Matović and M. Marković: Verifying the modes of cyclic conjugation in tetrabenzo[bc,ef,op,rs]circumanthracene..... 1401

Electrochemistry

V. Radulović, M. M. Aleksić and V. Kapetanović: An electrochemical study of the adsorptive behaviour of varenicline and its interaction with DNA 1409

Analytical Chemistry

P. Džodić, Lj. Živanović, A. Protić, I. Ivanović, R. Veličković-Radovanović, M. Spasić, S. Lukić and S. Živanović: Development and validation of a solid phase extraction-HPLC method for the determination of carbamazepine and its metabolites, carbamazepine epoxide and carbamazepine *trans*-diol, in plasma 1423

M. Čakar and G. Popović: Determination of lisinopril in pharmaceuticals by a kinetic spectrophotometric method (Note) 1437

El H. M. A. Rabtti, M. M. Natić, D. M. Milojković-Opsenica, J. Đ. Trifković, T. Tosti, I. M. Vučković, V. Vajs and Ž. Lj. Tešić: Quantitative structure–toxicity relationship study of some natural and synthetic coumarins using retention parameters..... 1443

Polymers

M. Balaban, V. Antić, M. Pergal, I. Francolini, A. Martinelli and J. Djonlagić: The effect of polar solvents on the synthesis of poly(urethane–urea–siloxane)s 1457

Published by the Serbian Chemical Society
Karnegijeva 4/III, 11000 Belgrade, Serbia
Printed by the Faculty of Technology and Metallurgy
Karnegijeva 4, P.O. Box 35-03, 11120 Belgrade, Serbia





J. Serb. Chem. Soc. 77 (10) 1311–1338 (2012)
JSCS–4354

AUTHORS' REVIEW

**A comparative study of the linear solvation energy relationship
for the reactivity of pyridine carboxylic acids with
diazodiphenylmethane in protic and aprotic solvents**

SAŠA Ž. DRMANIĆ^{1*#}, JASMINA B. NIKOLIĆ^{1#}, ALEKSANDAR D. MARINKOVIĆ^{1#}
and BRATISLAV Ž. JOVANOVIĆ^{2#}

¹Department of Organic Chemistry, Faculty of Technology and Metallurgy, University of Belgrade, Karnegijeva 4, Belgrade, Serbia and ²Institute of Chemistry, Technology and Metallurgy, University of Belgrade, Njegoševa 12, Belgrade, Serbia

(Received 13 July, revised 19 July 2012)

Abstract: The effects of protic and aprotic solvents on the reactivity of picolinic, nicotinic and isonicotinic acid, as well as of some substituted nicotinic acids, with diazodiphenylmethane (DDM) were investigated. In order to explain the kinetic results through solvent effects, the second-order rate constants for the reaction of the examined acids with DDM were correlated using the Kamlet–Taft Solvatochromic Equation. The correlations of the kinetic data were realized by means of multiple linear regression analysis and the solvent effects on the reaction rates were analyzed in terms of the contributions of the initial and the transition state. The signs of the coefficients of the Equation support the already known reaction mechanism. Solvation models for all the investigated acids are suggested and related to their specific structure.

Keywords: pyridine carboxylic acids; linear solvation energy relationship; diazodiphenylmethane; protic and aprotic solvents.

CONTENTS

1. INTRODUCTION
2. SOLVENT EFFECTS ON THE KINETICS OF THE REACTION OF PYRIDINE CARBOXYLIC ACIDS WITH DIAZODIPHENYLMETHANE
3. THE KAMLET–TAFT METHOD FOR THE EXAMINATION OF SOLVENT EFFECTS ON THE REACTIVITY OF PYRIDINE CARBOXYLIC ACIDS WITH DIAZODIPHENYLMETHANE
 - 3.1. Pyridine carboxylic acids
 - 3.2. Substituted nicotinic acids

* Corresponding author. E-mail: drmana@tmf.bg.ac.rs

Serbian Chemical Society member.

doi: 10.2298/JSC120713078D

3.2.1. 2-Substituted nicotinic acids

3.2.2. 6-Substituted nicotinic acids

4. CONCLUDING REMARKS

1. INTRODUCTION

The effect of different solvents on the rates of chemical changes was one of the earliest kinetic problems to be studied¹⁻³ and the development of the correlation analysis in the area of solvent effects has recently proved to be one of the most efficient ways to perform this task. The application of the techniques of multiple regressions has proved quite successful and has considerably increased the understanding of the role of solvents. The reaction rate constant (usually expressed as $\log k$) or the standard Gibbs energy of the transition state in the examined reaction (ΔG^\ddagger) may be correlated with a physical parameter describing some characteristic of the solvent, for example, dielectric constant, solubility parameter, viscosity, *etc.*, or with an empirical solvent parameter, such as Y , Z , Et , *etc.*⁴⁻⁶ This manner of analysis was extended to multiple linear correlations with a number of solvent parameters, notably by Mather and Shorter⁷ for the reaction of diazodiphenylmethane (DDM) and benzoic acid, and more generally by Koppel and Palm⁸ and by Kamlet and Taft and their co-workers.⁹⁻¹¹ The modification of this approach was to separate the solvent effect on $\log k$ or ΔG^\ddagger into contributions of the reactants (initial state) and the transition state, followed, where possible, by a comparison of effects of a solvent on the transition state with the effects of the solvent on solutes that might function as suitable models for the transition state. This method has proved itself efficient enough for application to a number of standard organic reactions and also to organometallic reactions and inorganic reactions.

Two groups of workers set out the general equations for the correlations of solvent effects through multiple regression analysis. Koppel and Palm⁸ used the four-parameter equation (1):

$$\log k = \log k_0 + gf(\epsilon) + pf(n) + eE + bB \quad (1)$$

in which $f(\epsilon)$ is a dielectric constant function, usually $Q = (\epsilon - 1)/(2\epsilon + 1)$, $f(n)$ is a refractive index function $(n^2 - 1)/(n^2 + 2)$ and E and B are measures of the electrophilic solvation ability and the nucleophilic solvation ability of the solvent, respectively. Koppel and Palm⁸ and later Mather and Shorter⁷ applied Eq. (1) quite successfully to a variety of reaction types.

The Kamlet and Taft group of workers¹¹ used the alternative equation (2):

$$\log k = A_0 + s\pi^* + a\alpha + b\beta \quad (2)$$

in which π^* is a measure of solvent dipolarity/polarizability, β represents the scale of the solvent hydrogen bond acceptor basicity, and α represents the scale of solvent hydrogen bond donor acidity, and A_0 is the regression value of the

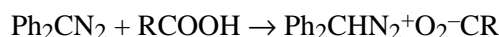
solute property in the reference solvent, cyclohexane. The regression coefficients s , a and b measure the relative susceptibilities of the solvent-dependent solute property ($\log k$ or as ΔG^\ddagger) to the corresponding solvent parameters.

Both Eq. (1) and (2) are general enough to be applied to almost any type of reaction.

This review demonstrates how the linear solvation energy relationship (LSER) method can be used to explain and present the multiple interacting effects of the solvent on the reactivity of pyridine carboxylic acids in their reaction with DDM. The solvent effects on the reaction rates were analyzed in terms of the initial and the transition state contributions, and are expressed quantitatively and discussed.

2. SOLVENT EFFECTS ON THE KINETICS OF THE REACTION OF PYRIDINE CARBOXYLIC ACIDS WITH DIAZODIPHENYLMETHANE

The reactivity of all carboxylic acids, including also pyridine carboxylic acids, with diazodiphenylmethane (DDM) is closely related to the molecular structure of the acid and the solvent present. The main advantage that makes this esterification appropriate for examining the influence of solvent and structure on the carboxylic acid reactivity is that a catalyst is not required for this reaction. It may vary in rate, but occurs without any additional support and in protic and aprotic solvents, it follows the second-order kinetics.¹²⁻¹⁴ The mechanism of this reaction has been thoroughly examined¹⁵⁻¹⁷ and it was established that the rate-determining step involves a proton transfer from the carboxylic acid to DDM to form a diphenylmethanediazonium-carboxylate ion pair, which rapidly reacts to give esters in the subsequent product-determining step in aprotic solvents, or ethers in the case of hydroxylic solvents:



Taking into consideration the reaction mechanism, it could be noticed that, because of the charge separation in the transition state, a solvent of high polarity can stabilize this state, making the reaction faster; the electrophilic ability of a solvent can have a similar effect, affecting the carboxylic anion that also exists in the transition state. On the contrary, nucleophilic solvating ability could be prominent in the initial state, stabilizing the carboxylic proton and hence, retarding the reaction.

Multiple linear regression analysis (MLRA) is very useful in separating and quantifying such interactions on the examined reactivity. The first comprehensive application of multiple linear regression analysis to kinetic phenomena was that of Koppel and Palm,⁸ who listed regression constants for the simple Koppel-Palm Equation for various processes. Aslan *et al.*¹⁴ showed that correlation analysis of the second-order rate constants for the reaction of benzoic acid with DDM in hydroxylic solvents did not give satisfactory results with the Koppel-Palm Model. They concluded that the possibility of Koppel-Palm analysis of data re-

lated to protic solvents depends on the fitting of data in a regression with the main lines being determined by a much larger number of aprotic solvents.

The influence of hydroxylic solvents on the rate constants of the reaction between carboxylic acids and DDM is rather complex. In these amphiprotic solvents, complications can arise from self-association, type AB hydrogen bonding, and multiple type A and type B interactions. In type A hydrogen bonding, the solute acts as an HBA base and the solvent as an HBD acid. In type B hydrogen bonding, the roles are reversed. Type AB represents hydrogen bonding in which the solute acts as both an HBD acid and an HBA base, associating thereby with at least two molecules of amphiprotic solvent in a probably cyclic complex. Under these circumstances where both solvent and solute are hydrogen bond donors, it was proven to be quite difficult to untangle solvent dipolarity/polarizability, type B hydrogen bonding and variable self-association effects from usual multiple type A hydrogen bonding interactions.

Aprotic solvents influence the reaction mainly by their polarity/polarizability, which has an accelerating effect and the HBA activity, which causes a decrease in the reaction rate. The general effect of an aprotic solvent depends on the prevailing solvent property. Some of the aprotic solvents can even show HBD activity (*e.g.*, chloroform) which additionally increases the reaction rate.

In already published studies,^{18–23} the reactivity of various substituted and unsubstituted pyridine carboxylic acids with DDM in various solvents were investigated.

The interesting observation for all the investigated acids was the possible modes of influence of the solvent on their reactivity, considering the two sites in the initial and in the transition states of the pyridine carboxylic acids molecules, which are presented in Fig. 1.

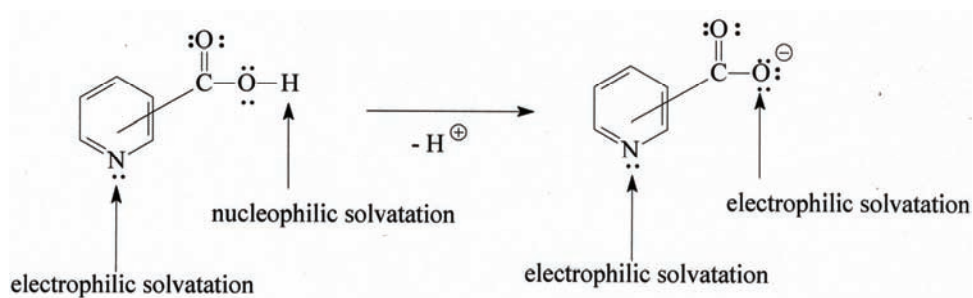


Fig. 1. The structure of a pyridine carboxylic acid and its anion.

Both electrophilic and nucleophilic solvation are present in the initial state, however only electrophilic solvation is present in the anion that exists in the transition state of the examined reaction. The effect of the electrophilic solvation of the pyridine nitrogen exists in both states, especially if a protic solvent is used.

Electrophilic solvation also plays a dominant role in the transition state, due to the structure of the molecule with two electrophilic centers. As electrophilic solvation is present in both the initial and the transition state, its influence may be complicated. Nucleophilic solvation is present only in the initial state and the classical solvation is present in both states, however it is more prominent in the transition state due to the charge increase.

The rate data for the examined acids were correlated with the Kamlet–Taft Equation. The results showed that linear free energy relationships (LFER) are applicable to the kinetic data for the investigated acid systems.

The correlation equations obtained by stepwise regression for all the examined acids showed that the best approach, which helps in the understanding of the effects of hydroxylic solvents on the reaction, lies in the separate correlations of the kinetic data with the hydrogen bond donating (HBD) and hydrogen bond accepting (HBA) ability of a solvent. For aprotic solvents, it is often the case that the effects can be considered together.

3. THE KAMLET–TAFT METHOD FOR THE EXAMINATION OF SOLVENT EFFECTS ON THE REACTIVITY OF CARBOXYLIC ACIDS WITH DIAZODIPHENYLMETHANE

Kamlet *et al.*⁹ established that the effect of a solvent on the reaction rate should be given in terms of the following properties: *i*) the behavior of the solvent as a dielectric, facilitating the separation of opposite charges in the transition state, *ii*) the ability of the solvent to donate a proton in a solvent-to-solute hydrogen bond and thus stabilize the carboxylate anion in the transition state and *iii*) the ability of the solvent to donate an electron pair and therefore stabilize the initial carboxylic acid, by way of a hydrogen bond between the carboxylic proton and the solvent electron pair. The parameter π^* is an appropriate measure of the first property, while the second and the third properties are governed by the effects of the solvent acidity and basicity, quantitatively expressed by the parameters α and β , respectively. The solvent parameters (π^* , α and β) for hydrogen bond donor and non-hydrogen bond donor solvents (Eq. (2)), taken from the literature,¹¹ are given in Table I. The linear dependence (LSER) on the solvent parameters were used to correlate and predict a wide variety of solvent effects, as well as to provide an analysis in the terms of knowledge and the theoretical concepts of molecular structural effects.⁹

TABLE I. Solvent parameters¹¹

Solvent	π^*	β	α
Methanol	0.60	0.62	0.93
Ethanol	0.54	0.77	0.83
Cyclopentanol	0.45	0.84	0.66
Butan-2-ol	0.40	0.80	0.69
2-Methylbutan-2-ol	0.40	0.93	0.28

TABLE I. Continued

Solvent	π^*	β	α
Pentan-1-ol	0.40	0.86	0.84
Benzyl alcohol	0.98	0.52	0.60
Dimethyl sulfoxide	1.00	0.75	0.00
<i>N,N</i> -Dimethylacetamide	0.88	0.76	0.00
<i>N</i> -Methylpyrrolidone	0.92	0.77	0.00
<i>N,N</i> -Dimethylformamide	0.88	0.69	0.00
<i>N</i> -Methylformamide	0.90	0.80	0.62
Acetophenone	0.90	0.49	0.04
Acetone	0.71	0.43	0.08
Ethyl benzoate	0.74	0.41	0.00
Isobutyl methyl ketone	0.65	0.48	0.02
2-Pyrrolidinone	0.85	0.77	0.36
Sulfolan	0.98	0.39	0.00
Butan-2-one	0.67	0.48	0.06
Chloroform	0.58	0.00	0.44
Acetonitrile	0.19	0.31	0.85
Diethyl carbonate	0.45	0.40	0.00
Methyl acetate	0.60	0.42	0.00
Ethyl acetate	0.55	0.45	0.00
Butyl ethanoate	0.46	0.45	0.00
Tetrahydrofuran	0.58	0.55	0.00
Dioxane	0.55	0.37	0.00

The present review demonstrates how the linear solvation energy relationship method can be used to quantify, correlate and rationalize the multiple interacting effects of the selected solvent set on the reactivity parameters of pyridine carboxylic acids in their reaction with DDM.

3.1. Pyridine carboxylic acids

Protic solvents

The values of second-order rate constants for the reaction of the picolinic (**1**), nicotinic (**2**) and isonicotinic acid (**3**), Fig. 2, in a protic solvent set are given in Table II.

TABLE II. Rate constants ($\text{dm}^3 \text{mol}^{-1} \text{min}^{-1}$) for the reaction of nicotinic, isonicotinic and picolinic acid with DDM at 30 °C in various alcohols^{18,19}

Solvent	Picolinic acid	Nicotinic acid	Isonicotinic acid
Methanol	10.96	10.69	19.95
Ethanol	7.24	5.37	12.02
Butan-2-ol	4.36	3.46	5.75
Cyclopentanol	3.74	3.67	5.82
2-Methylbutan-2-ol	1.26	0.87	1.86
Pentan-1-ol	4.26	3.71	7.24
Benzyl alcohol	28.18	26.53	42.94

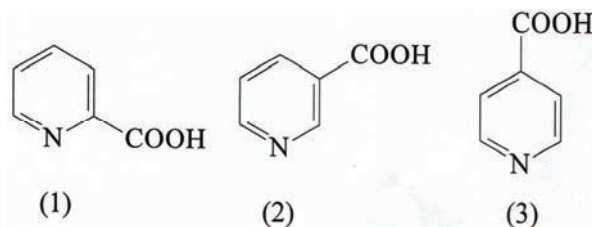


Fig. 2. The structures of the examined compounds.

The observation that isonicotinic acid exhibits the highest reaction rates and picolinic and nicotinic acid have rather similar lower values can be explained by the negative inductive and resonance effects (electron-withdrawing effects) of the present nitrogen, which stabilize the carboxylic anion of the isonicotinic acid and enhances the acidity. In the case of nicotinic acid, which has the lowest reaction rate constants, the nitrogen exerts an inductive effect, which could stabilize the anion, however the same effect is stronger in the molecule of picolinic acid. For picolinic acid, there is a possibility of the formation of an intramolecular hydrogen bond between the carboxylic proton and the neighboring nitrogen; such a hydrogen bond could hinder the removal of the proton, but as picolinic acid react faster than nicotinic acid, it obviously does not prevail over the electron-withdrawing effects of the nitrogen. The fact that the described hydrogen bond exists can be seen from the comparison of picolinic and isonicotinic reaction rate constants. These two compounds have the same resonance and inductive effects, but there is hydrogen bond that decreases the reaction rate only in the case of picolinic acid, Fig. 3.

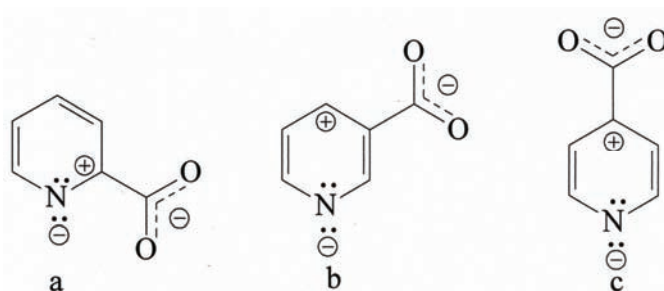


Fig. 3. The carboxylic anions of a) picolinic, b) nicotinic and c) isonicotinic acid.

The Kamlet–Taft parameters of the applied solvent set are given in Table I. The set of seven solvents was chosen to match the solubility of all the examined compounds, so that all the results could be clearly and reliably compared.

In order to separate the effects that influence the initial and the transition state in the examined reaction in protic solvents, the total solvatochromic equation was divided into two parts:

$$\log k = \log k_0 + s\pi^* + a\alpha \quad (3a)$$

$$\log k = \log k_0 + a\alpha + b\beta \quad (3b)$$

Equation (3a) describes the solvent effects influencing the transition state and (3b) the initial state, electrophilic solvation (HBD) exists in the initial state for nicotinic acids because of the presence of the nitrogen in the ring.

By this approach, the following results were obtained:

Nicotinic acid:

$$\log k = -1.02 + (1.83 \pm 0.18)\pi^* + (1.04 \pm 0.17)\alpha \quad (4a)$$

$$R = 0.987, s = 0.09, n = 7$$

$$\log k = 2.61 + (0.23 \pm 0.21)\alpha - (2.70 \pm 0.31)\beta \quad (4b)$$

$$R = 0.979, s = 0.103, n = 7$$

For all three compounds examined in this chapter, there appeared to be the similar problem, the low significance of the HBD coefficient parameter in the initial state. As the value for the HBA solvent effect was much higher and completely reliable, it could be concluded that the HBA effects dominate in the initial state and mask the electrophilic solvation directed to the nitrogen. In order to obtain clear results, α was excluded from the correlation for the initial state and the equation was given in the following form, for nicotinic acid:

$$\log k = 3.01 - (3.05 \pm 0.43)\beta \quad (4c)$$

$$R = 0.953, s = 0.15, n = 7$$

This is not to say that electrophilic solvation does not exist in the initial state for nicotinic acids, it is just not prominent enough to be compared with the HBA solvation in the given solvent set.

Therefore, the following results were taken into consideration:

Picolinic acid:

$$\log k = -0.79 + (1.71 \pm 0.14)\pi^* + (0.91 \pm 0.13)\alpha \quad (5a)$$

$$R = 0.990, s = 0.07, n = 7$$

$$\log k = 2.90 - (2.81 \pm 0.37)\beta \quad (5b)$$

$$R = 0.958, s = 0.13, n = 7$$

Isonicotinic acid:

$$\log k = -0.70 + (1.74 \pm 0.05)\pi^* + (1.04 \pm 0.05)\alpha \quad (6a)$$

$$R = 0.999, s = 0.03, n = 7$$

$$\log k = 3.15 - (2.89 \pm 0.42)\beta \quad (6b)$$

$$R = 0.950, s = 0.15, n = 7$$

The results of the above correlations confirm the reaction mechanism and describe the influence of the solvent by classic electrophilic and nucleophilic solvation. It is evident that the solvent polarity/polarizability and HBD effect increased the reaction rate by stabilizing the transition state, which was proved by the positive signs of the coefficients s and a .

The correlation with the HBA parameter (β) proved also to be successful and from these correlations, it can be seen that this property decreased the reaction rate, which is in agreement with the assumption that this solvent property stabilizes the initial state.

With the intention of analyzing the effect of the presence of nitrogen in the ring, the described results were compared to those for benzoic acid:¹⁸

$$\log k = -1.99 + (2.25 \pm 0.26)\pi^* + (1.15 \pm 0.25)\alpha \quad (7a)$$

$$R = 0.980, s = 0.130, n = 7$$

$$\log k = 2.81 - (3.66 \pm 0.55)\beta \quad (7b)$$

$$R = 0.948, s = 0.190, n = 7$$

The higher value of the coefficient of polarity/polarizability parameter signifies a difference in the solvation between the benzoic and the pyridine carboxylic acids. This can be explained by the higher demand for the solvent polarity/polarizability effect as the anion of the benzoic acid is more polarizable. The presence of nitrogen in the ring decreases the difference in the electronic density in the anion of the pyridine carboxylic acids, in comparison with that of the anion of benzoic acid.

The quantitative analysis of solvent effects showed that in all cases, classical solvation prevails over the proton-donor solvent activity, but that the proton-acceptor (HBA) activity was also significant.

The HBA activity was somewhat higher for benzoic acid as in this case, there is no electronegative nitrogen in the ring that could facilitate the removal of the proton.

The HBD activity was also slightly higher for benzoic acid, as it is directed only to the reactive center, the carboxylic group in the transition state. In the case of pyridine carboxylic acids, it is divided between the carboxylic group and the nitrogen, which is not directly involved in the reaction mechanism.

Regarding the solvent parameter coefficients for the pyridine carboxylic acids, it could be noticed that the picolinic acid had the lowest value of the HBA (β) coefficient. It could be explained by the formation of a hydrogen bond between the carboxylic proton and the neighboring nitrogen, which stabilizes the proton in the initial state; hence, nucleophilic stabilization by solvent is not so necessary (Fig. 4).

Considering that there is only the inductive effect of nitrogen in the case of nicotinic acid, the nucleophilic solvent effect will act the strongest on this compound. As the anion of nicotinic acid is the least stable of the three examined compound because of the absence of the electron-withdrawing effect of nitrogen, it has the highest demand for classical solvation, Fig. 3b.

For isonicotinic acid, the coefficients of which lie in the middle, it could be concluded that there is no intramolecular hydrogen bond. A negative inductive effect of the nitrogen exists that is weaker than for the other two examined com-

pounds, but also an electron-withdrawing effect of the nitrogen, which can make the carboxylic anion more stable, Fig. 3c.

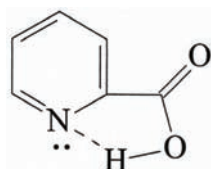


Fig. 4. Hydrogen bond in the molecule of picolinic acid.

The high positive value of the coefficient s indicates that the effect of classical solvation is the main solvent effect influencing the transition state of the reaction of the examined pyridine carboxylic acids with DDM. According to the smaller value of the coefficient a , electrophilic solvation of the transition state is less pronounced than classic solvation, but also increases the reaction rate.

Various solvents containing no hydroxyl group

The same approach as for protic solvents was applied to the kinetic data of nicotinic acid in various solvents containing no hydroxyl group (Table III).

TABLE III. Rate constants ($\text{dm}^3 \text{mol}^{-1} \text{min}^{-1}$) for the reaction of nicotinic, isonicotinic and picolinic acids with DDM at 30 °C in various solvents¹⁹

Solvent	Picolinic acid	Nicotinic acid	Isonicotinic acid
Dimethyl sulfoxide	0.21	0.35	0.10
<i>N,N</i> -Dimethylacetamide	0.12	0.21	0.04
<i>N</i> -Methylpyrrolidone	0.12	0.22	0.037
<i>N,N</i> -Dimethylformamide	0.25	0.44	0.098
Acetophenone	5.17	1.69	1.36
2-Pyrrolidinone	0.15	0.11	0.14
Sulfolan	14.79	Insoluble	3.97
<i>N</i> -Methylformamide	0.94	1.12	1.35
Butan-2-one	2.51	1.49	0.19
Acetone	1.56	3.52	0.19
Chloroform	40.36	Insoluble	13.24
Ethyl benzoate	3.37	Insoluble	6.25
Acetonitrile	12.80	Insoluble	1.76
Diethyl carbonate	Insoluble	Insoluble	0.049
Methyl acetate	1.39	Insoluble	0.88
Butyl ethanoate	0.72	Insoluble	0.16
Isobutyl methyl ketone	1.39	0.98	0.21
Ethyl acetate	1.22	0.88	0.16
Tetrahydrofuran	1.83	0.30	Insoluble
Dioxane	0.24	0.58	Insoluble

In order to obtain a reliable correlation, tetrahydrofuran, butyl ethanoate and ethyl acetate were excluded from the calculations for nicotinic acid, Eq. (8):

$$\log k = 0.13 + (3.22 \pm 0.64)\pi^* + (1.53 \pm 0.41)\alpha - (5.14 \pm 0.48)\beta \quad (8)$$

$$R = 0.955, s = 0.26, n = 16$$

The above result indicates that the influence of the solvent on the rate is mainly the result of the strong basic character of applied solvent molecules, which is reflected in the high values of the coefficient b . Nucleophilic solvation, the basicity of the applied solvent, is the main solvent effect that affects a decrease in the reaction rate of the investigated acid with DDM. The percentage contributions of the individual solvent effects for nicotinic acid are 33 % classical solvation, 15 % electrophilic solvation and 52 % nucleophilic solvation. In this case, the HBD solvent effect and classical solvation increase the reaction rate. One correlation was found in the literature²⁴ that includes all three solvent parameters in the correlation for benzoic acid in solvents not allegedly possessing HBD character:

$$\log k = 0.20 + 1.21 \pi^* + 2.71\alpha - 3.70\beta \quad (9)$$

$$R = 0.980, s = 0.17, n = 44$$

The percentage contributions of the individual solvent effects calculated from the Eq. (9) are: $\pi^* = 16$ %, $\alpha = 35$ %, $\beta = 49$ %. A comparative study of these results (Eq. (9)) with those for nicotinic acid (Eq. (8)) leads to the conclusion that classical solvation is more important for nicotinic acid, while electrophilic stabilization, *i.e.*, the HBD solvent effect, is more important for benzoic acid. For both acids, the basicity of a solvent, or the nucleophilic stabilization of the initial state of the molecules, which decreases the reaction rate, is the main factor affecting their reactivity. This effect is more pronounced in the correlation for nicotinic acid because of its higher acidity.

The surprisingly high values of the coefficient a for applied solvents in the two previous equations, especially the one for benzoic acid, indicate the important role of the HBD effect of applied solvents, which increases the reaction rate by stabilizing the acid anion.

The correlation of the $\log k$ values for isonicotinic acid with the parameters π^* , α and β for applied solvents gave the following results:

$$\log k = 0.075 + (1.67 \pm 0.43)\pi^* + (1.26 \pm 0.23)\alpha - (2.87 \pm 0.47)\beta \quad (10)$$

$$R = 0.953, s = 0.12, n = 9$$

Classical and electrophilic solvation increase the reaction rate of this acid, while nucleophilic solvation of the initial state decreases it. The percentage contributions of the individual solvent parameters are: 29 % for classical solvation, 21 % for electrophilic solvation and 50 % for nucleophilic solvation.

Although a better solvation of the carboxylic group proton of isonicotinic acid in the initial state was expected because it is more acidic than nicotinic acid, there is only a small difference between the values of the contribution of coef-

efficient b for isonicotinic and nicotinic acids, due to negative inductive and electron-withdrawing effects.

The kinetic data for nicotinic and isonicotinic acids in applied solvents (Table III) show interesting results as the rate constants strongly depend on the effects of solvents which is reflected in the value of coefficient b . The higher value of electrophilic solvation in the transition state for isonicotinic acid can be explained by the joint effect of solvation of either the forming carboxylate anion or the partial negative charge on the nitrogen of the pyridyl group. The better classical solvation of nicotinic acid is caused, probably, by a less pronounced direct resonance interaction than in isonicotinic acid, leading to a more polarizable structure, resulting in better solvation by the dipolar solvent effect.

The correlation of the $\log k$ values for picolinic acid with the parameters π^* , α and β for applied solvents gave the following results:

$$\log k = -0.46 + (2.80 \pm 0.43)\pi^* + (2.27 \pm 0.37)\alpha - (4.44 \pm 0.41)\beta \quad (11)$$

$$R = 0.956, s = 0.24, n = 17$$

The high negative value of coefficient b shows that solvation by the HBA solvent effect, namely nucleophilic solvation of the initial state, is a more important effect than the other two. The positive signs of the coefficients s and a indicate significant classical and electrophilic solvation, but they are of less significance than nucleophilic solvation. The calculations of the percentage contributions of the partial solvent effect gave the following results: $\pi^* = 29\%$; $\alpha = 24\%$ and $\beta = 47\%$.

The overall comparison of the results of solvent effects on the reactivity of the pyridine carboxylic acids is presented in Table IV.

TABLE IV. Percentage contribution of the Kamlet–Taft solvatochromic parameters to the reactivity of the investigated acids in various solvents

Acids	$P_{\pi^*} / \%$	$P_{\alpha} / \%$	$P_{\beta} / \%$
Nicotinic	33	15	52
Picolinic	29	21	50
Isonicotinic	29	24	47
Benzoic	16	35	49

The data from Table III indicate that the HBD solvent effect (acidity) significantly affected the stabilization of the transition state, and that this solvent effect is more important for picolinic than for isonicotinic and nicotinic acids. The higher value of the HBA parameter, which expresses the effect of electrophilic solvation, for picolinic acid can, most probably, be explained in the following way: the carboxylate anion forming in the transition state is very close to the pyridine nitrogen, causing, to some extent, a repulsion between the identical negative charges, resulting in the planar carboxylate anion being in a perpendicular

position with respect to the pyridine ring, which is therefore subjected to a better electrophilic solvation. As can be seen, the highest value of the HBD effect for benzoic acid is most probably influenced by the exclusive stabilization of the carboxylate ion, with no stabilization of the negative charge on the pyridine nitrogen, as is the case for the isomeric pyridine carboxylic acids.

Classical solvation (π^*) is more pronounced for nicotinic acid because its molecule has a more distinct dipolar structure than the molecules of the other two investigated pyridine mono-carboxylic acids.

The percentage contribution of the HBA solvent effect shows a small decrease for picolinic acid. This can be explained, probably, by the ability of picolinic acid to create an intramolecular hydrogen bond in the initial state, which decreases the influence of solvents.

3.2. Substituted nicotinic acids

In order to analyze the effect of substituents on the reactivity of pyridine carboxylic acids with DDM, two types of substituted nicotinic acids were examined in the same solvent set.

3.2.1. 2-Substituted nicotinic acids

Protic solvents

The second order rate constants for the reaction of 2-substituted nicotinic acids with DDM in various alcohols at 30 °C are given in Table V. The results show that the rate constants increased with the polarity of the solvents. This is in accordance with the already described reaction mechanism.

TABLE V. Rate constants ($\text{dm}^3 \text{mol}^{-1} \text{min}^{-1}$) for the reaction of 2-substituted nicotinic acids with DDM at 30 °C in various alcohols²⁰

Solvent	H	Cl	OH	CH ₃
Methanol	10.70	38.10	44.80	9.77
Ethanol	5.40	22.20	28.30	4.80
Butan-2-ol	3.45	9.40	12.10	2.70
Cyclopentanol	3.67	9.27	10.70	2.70
2-Methylbutan-2-ol	1.26	3.42	4.72	0.76
Pentan-1-ol	3.72	11.10	15.90	3.00
Benzyl alcohol	26.50	100.90	137.10	23.10

All investigated 2-substituted nicotinic acids are more reactive than the correspondingly substituted benzoic acids in the same solvent set.²⁴ This is understandable considering the highly electron attracting pyridine nucleus. In both reaction series, the hydroxyl-substituted acids were more reactive than the other substituted acids.²⁴ This is generally accepted to be due to the existence of a hydrogen bond between the hydrogen from the hydroxyl group and the oxygen from the carboxylic anion. This interaction is potentially possible in both salicylic acid

and 2-hydroxynicotinic acid, and is probably responsible for enhanced acidity by facilitating the release of the carboxylic proton.

It can be also noticed that the reaction rate constants increase in the presence of electron-acceptor substituents, which stabilize the negative charge in the transition state, such as chlorine in this case. The only investigated compound with an electron-donor substituent (methyl group) has the lowest reaction rates, and the rate constants for the unsubstituted compound lie in the middle, as could have been expected.

The rate constants were examined using the solvatochromic equation (Eq. (2)), and the parameters given in Table I.

The correlation analysis of investigated acids with solvent parameters π^* , α and β in protic solvents showed that there were no satisfactory results for the three-parameter equation (Eq. (2)). Further examination by dividing the solvent effects into those supporting the transition state (π^* and α) and the one supporting the initial state before the reaction starts (β), as in the previous chapter, proved to be successful.

Nicotinic acid:

$$\log k = -1.02 + (1.83 \pm 0.18)\pi^* + (1.04 \pm 0.17)\alpha \quad (4a)$$

$$R = 0.987, s = 0.09, n = 7$$

$$\log k = 3.01 - (3.05 \pm 0.43)\beta \quad (4c)$$

$$R = 0.953, s = 0.15, n = 7$$

2-Chloronicotinic acid:

$$\log k = -0.54 + (2.01 \pm 0.06)\pi^* + (0.97 \pm 0.06)\alpha \quad (12a)$$

$$R = 0.995, s = 0.032, n = 7$$

$$\log k = 3.67 - (3.23 \pm 0.37)\beta \quad (12b)$$

$$R = 0.976, s = 0.130, n = 7$$

2-Hydroxynicotinic acid:

$$\log k = -0.39 + (2.02 \pm 0.09)\pi^* + (0.91 \pm 0.09)\alpha \quad (13a)$$

$$R = 0.985, s = 0.097, n = 7$$

$$\log k = 3.75 - (3.15 \pm 0.38)\beta \quad (13b)$$

$$R = 0.965, s = 0.890, n = 7$$

2-Methylnicotinic acid:

$$\log k = -1.14 + (1.89 \pm 0.12)\pi^* + (1.05 \pm 0.12)\alpha \quad (14a)$$

$$R = 0.994, s = 0.063, n = 7$$

$$\log k = 3.02 - (3.16 \pm 0.38)\beta \quad (14b)$$

$$R = 0.965, s = 0.136, n = 7$$

Judging by the similar coefficient values for the compounds with different substituents, it could be stated that the nature of substituent does not considerably change the solvent effect. From a comparison with the unsubstituted acid (Eq.

(4)), it can be seen that the influence of the solvent polarity was higher on all the substituted nicotinic acids than on the unsubstituted one. This observation could be explained by the higher polarity of the substituted acids molecules than of the unsubstituted one. The only compound with an alkyl substituent (2-methylnicotinic acid) should differ the least in polarity from nicotinic acid; this is supported by the polarity/polarizability solvent parameter coefficient (s) being the most similar to those of nicotinic acid.

The kinetic results show that in all cases the polarity/polarizability parameter (π^*) was the dominating factor supporting the transition state and increases the reaction rate, which is in agreement with the known mechanism.

The sign of the α coefficient is also positive in all equations, which means that electrophilic stabilization of the transition state existed. This stabilization is explained by a hydrogen bond interaction between the carboxylate anion and the proton of the protic solvent molecule. The effect of both inductive and resonance stabilization of the negative charge on the carboxylate anion by a substituent decreases the necessity of electrophilic solvation, in this way decreasing the influence of the solvent on the reactivity of these acids.

The sign of the coefficients of the β term in all equations is negative, which could be expected considering that this parameter defines the nucleophilic stabilization of the initial state, which slows down the examined reaction.

A comparison with the corresponding 2-substituted benzoic acids²¹ revealed that the signs are also in agreement with the reaction mechanism, as can be seen from Eqs. ((15)–(17)):

2-Chlorobenzoic acid:

$$\log k = -1.19 + (2.20 \pm 0.23)\pi^* + (1.04 \pm 0.22)\alpha \quad (15a)$$

$$R = 0.984, s = 0.120, n = 7$$

$$\log k = 3.44 - (3.59 \pm 0.39)\beta \quad (15b)$$

$$R = 0.972, s = 0.140, n = 7$$

2-Hydroxybenzoic acid:

$$\log k = -0.45 + (2.01 \pm 0.20)\pi^* + (0.49 \pm 0.20)\alpha \quad (16a)$$

$$R = 0.972, s = 0.120, n = 7$$

$$\log k = 3.04 - (3.04 \pm 0.33)\beta \quad (16b)$$

$$R = 0.965, s = 0.890, n = 7$$

2-Methylbenzoic acid:

$$\log k = -2.22 + (2.85 \pm 0.23)\pi^* + (1.32 \pm 0.22)\alpha \quad (17a)$$

$$R = 0.987, s = 0.114, n = 7$$

$$\log k = 2.85 - (3.82 \pm 0.55)\beta \quad (17b)$$

$$R = 0.965, s = 0.136, n = 7$$

The most prominent difference between the 2-substituted nicotinic and the 2-substituted benzoic acids is again the coefficient of the solvent polarity/pola-

rizability parameter, with higher values for the latter. This confirms the tentative explanation from the previous chapter. The higher polarizability of the anion of benzoic acids causes a greater demand for stabilization by the solvent polarity.

Considering the coefficient of the HBD parameter, the values are similar for both sets of acids, except for the OH-substituted acid for which it is considerably lower for benzoic than for nicotinic acid (0.49 and 0.91, respectively). As a strong hydrogen bond in the transition state exists in both compounds (Fig. 5), the demand for electrophilic stabilization should be about the same. However, in the molecule of 2-hydroxynicotinic acid, the nitrogen also requires electrophilic stabilization and hence the higher value for the HBD effect (Fig. 5).

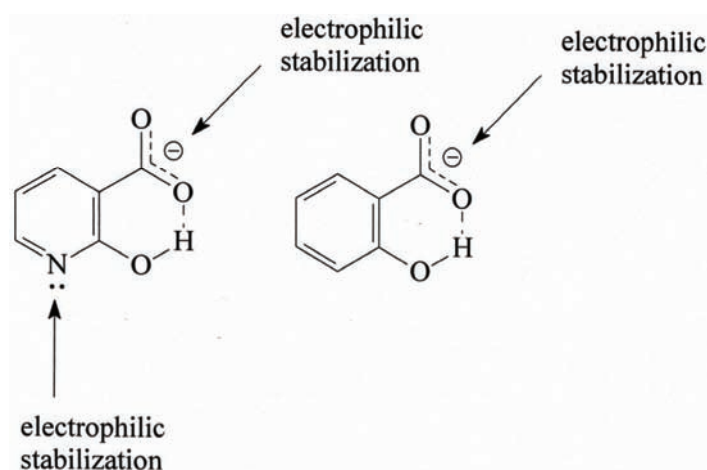


Fig. 5. The electrophilic stabilization of the anion of 2-hydroxynicotinic and 2-hydroxybenzoic acid.

The sign of the HBA parameter coefficient is negative in all equations, as expected considering the known reaction mechanism – the solvation of the proton in the initial state is responsible for the decrease in the reaction rate. The somewhat lower values of the β coefficients for the nicotinic acids could be understood as the lower demand for nucleophilic stabilization by the solvent in the presence of the pyridine nitrogen, which, by its electron-acceptor effect increases the acidity. Therefore, the carboxylic proton is more easily detached from the acid molecule and less stabilized by the HBA solvent effect.

Various solvents containing no hydroxyl group

In order to explain the solvent effect on the reactivity of the 2-substituted nicotinic acids with DDM, the reaction rate constants of the examined compounds were determined in a set of nine various solvents (Table I). The reaction rate constants are given in Table VI.

TABLE VI. Rate constants ($\text{dm}^3 \text{mol}^{-1} \text{min}^{-1}$) for the reaction of 2-substituted nicotinic acids with DDM at 30 °C in various solvents²¹

Solvent	H	2-Cl	2-OH	2-CH ₃	2-Br	2-SH
Dimethyl sulfoxide	0.21	1.011	0.93	0.24	1.01	0.90
<i>N,N</i> -Dimethylacetamide	0.11	0.55	0.63	0.14	0.57	0.74
<i>N</i> -Methylpyrrolidone	0.12	0.74	1.38	0.16	0.73	0.76
<i>N,N</i> -Dimethylformamide	0.24	0.97	1.48	0.33	0.96	1.57
<i>N</i> -Methylformamide	0.94	1.26	0.44	1.74	1.29	2.38
Acetophenone	5.18	22.03	Insoluble	5.64	23.60	17.02
Acetone	1.55	2.824	Insoluble	3.34	3.21	5.24
Ethyl benzoate	3.37	12.25	Insoluble	7.24	12.08	7.85
Isobutyl methyl ketone	1.39	4.04	Insoluble	2.05	4.477	5.64

The correlation results are presented in the following equations. Here, the correlation results for the nicotinic acid are also given for comparison.

Nicotinic acid:

$$\log k = 0.82 + (2.45 \pm 0.85)\pi^* + (1.72 \pm 0.32)\alpha - (5.18 \pm 0.63)\beta \quad (18)$$

$$R = 0.977, s = 0.17, n = 9$$

2-Chloronicotinic acid:

$$\log k = 0.70 + (3.12 \pm 1.23)\pi^* + (0.78 \pm 0.46)\alpha - (4.90 \pm 0.91)\beta \quad (19)$$

$$R = 0.938, s = 0.25, n = 9$$

2-Methylnicotinic acid:

$$\log k = 1.50 + (1.91 \pm 0.60)\pi^* + (1.99 \pm 0.22)\alpha - (5.30 \pm 0.44)\beta \quad (20)$$

$$R = 0.990, s = 0.12, n = 9$$

2-Bromonicotinic acid:

$$\log k = 0.81 + (3.03 \pm 1.21)\pi^* + (0.80 \pm 0.45)\alpha - (4.93 \pm 0.89)\beta \quad (21)$$

$$R = 0.942, s = 0.24, n = 9$$

2-Mercaptonicotinic acid:

$$\log k = 1.31 + (1.78 \pm 0.92)\pi^* + (1.03 \pm 0.35)\alpha - (3.99 \pm 0.68)\beta \quad (22)$$

$$R = 0.955, s = 0.18, n = 9$$

The correlation equations obtained by multiple linear regressions for all the examined acids confirmed the supposed reaction mechanism, as the solvent polarity and its proton-donor (HBD) activity increased the reaction rate constant and the proton-acceptor (HBA) ability decreased it. It could be noticed that the HBA effect was the most prominent one in this solvent set.

From the values of the regression coefficients (s , a and b), the percentage contribution of each parameter to the reactivity of the investigated compounds was calculated and the results are listed in Table VII.

It could be noticed that in the case of the electron withdrawing substituents, the values for the HBD parameter (α) were lower than for the unsubstituted acid

and the acid with the electron-donor substituent (CH_3). The negative inductive effect of the electron-acceptor substituents additionally stabilizes the carboxylic anion, and so the HBD solvent effect is less involved.

TABLE VII. Percentage contribution of the Kamlet–Taft solvatochromic parameters to the reactivity of the investigated acids in various solvents

Acid	$P_{\pi^*} / \%$	$P_{\alpha} / \%$	$P_{\beta} / \%$
H	26	18	56
2-Cl	35	9	56
2- CH_3	22	20	58
2-Br	35	9	56
2-SH	26	15	59

The results from Table VII, lead to the following conclusions:

a) The rate of the reaction was mostly influenced by the rate-decreasing HBA parameter, as its percentage prevailed over the other two rate-increasing parameters.

b) The non-specific interaction has a greater influence (higher percentage value) than HBD on the reaction rate in all cases, meaning that the classical or non-specific solute–solvent interactions dominate in the transition state and increase the reaction rate.

When the correlation results obtained here were compared with the previously published results for the corresponding 6-substituted nicotinic acids,¹⁰ the solvent effect disposition was similar considering the dominant HBA effect. However, the percentage values for the non-specific and the HBD interactions were different; the proton-donor ability had a higher influence on the 6-substituted acids. This could be explained by the strong negative inductive effect of most of the substituents present that is considerably stronger in the C-2 position, as it is next to the reactive center, than in the C-6 position of the ring, with three atoms separating them from the reactive center. Comparing the reaction rate constants for both types of nicotinic acid, it could be noticed that the 2-substituted acids generally reacted faster, due to the additional stabilization of the anion in the transition state by the negative inductive substituent effect. The fact that of the only examined acids with an electron-donor substituent, the methyl group, the 2-substituted acid also reacted faster than the 6-substituted one can be explained by the steric effect of the substituent, which twists the carboxylic group out of the plane of the ring and makes it more approachable for the DDM molecule. The higher value of the HBD coefficient (α) shows that electron-donor support from the solvent is more necessary in this case, as there is no negative inductive substituent effect to stabilize the transition state. The inductive effect of the substituents in C-2 position, which is based on their electronegativity, is additionally proved by the value of the HBD coefficient for 2-mercaptanicotinic acid; sulfur

is less electronegative than chlorine and bromine, and this compound has an α coefficient higher than the other two acids, but also somewhat lower than the unsubstituted and the methyl-substituted acids.

The peculiarity of 2-hydroxynicotinic acid with its unsuccessful correlation, mentioned before, also draws attention. The 6-hydroxynicotinic acid, unlike the 2-hydroxynicotinic acid, gave a successful correlation in the same solvents, with the expected arithmetic signs of the coefficients:

6-Hydroxynicotinic acid:²²

$$\log k = -1.92 + (2.37 \pm 0.36)\pi^* + (1.99 \pm 0.09)\alpha - (2.20 \pm 0.51)\beta \quad (23)$$
$$R = 0.982, s = 0.26, n = 5$$

Due to the ability of forming strong hydrogen bonds between the oxygen and nitrogen on both carboxylic acids and the hydroxyl group, both compounds are insoluble in many solvents; however, the set of five solvents given here, in which they both dissolve, was found.

The exception of the unsuccessful correlation for 2-hydroxynicotinic acid could be explained by its specific structure. As can be seen in Fig. 5, this compound forms a strong intramolecular hydrogen bond, helped by the electron-donor resonance effect of the hydroxylic group, which significantly decreases its reactivity in the form of the anion. When the carboxylic proton leaves the molecule, the strong hydrogen bond is formed between the carboxylic group and the hydroxylic proton, preventing the anion from further reaction in the chosen solvent set.

Contrary to this, in case of 6-hydroxynicotinic acid, there is also a possibility of the formation of intermolecular hydrogen bonds that, as can be concluded from the successful application of the Kamlet–Taft Equation, does not interfere significantly with its reactivity in the examined reaction.

It could be concluded that, because of its complex possibilities for the formation of intramolecular hydrogen bonds, 2-hydroxynicotinic acid is not an appropriate compound for an investigation of the reaction mechanism of carboxylic acids with DDM and the effect solvent on it, as it cannot be analyzed by the Kamlet–Taft Equation.

None of the other examined 2-substituted nicotinic acid possesses an ability to form such an intramolecular hydrogen bond, except for 2-mercaptynicotinic acid. However, it is obvious that in this case, the hydrogen bond is not strong enough to influence the reactivity of the compound as it has a similar behavior to that of the other examined acids in their reaction with DDM.

3.2.2. 6-Substituted nicotinic acids

Protic solvents

The analysis of the kinetics of the reaction of the 6-substituted nicotinic acids with DDM gave the following results.

In accordance to previous results, as it could be seen in Eqs. (24)–(26), the signs of the solvatochromic parameters are again in agreement with the reaction mechanism.

Nicotinic acid:

$$\log k = -1.02 + (1.83 \pm 0.18)\pi^* + (1.04 \pm 0.17)\alpha \quad (4a)$$

$$R = 0.987, s = 0.09, n = 7$$

$$\log k = 3.01 - (3.05 \pm 0.43)\beta \quad (4c)$$

$$R = 0.953, s = 0.15, n = 7$$

6-Chloronicotinic acid:

$$\log k = -0.58 + (1.77 \pm 0.09)\pi^* + (0.71 \pm 0.09)\alpha \quad (24a)$$

$$R = 0.995, s = 0.047, n = 7$$

$$\log k = 2.97 - (2.76 \pm 0.33)\beta \quad (24b)$$

$$R = 0.966, s = 0.116, n = 7$$

6-Hydroxynicotinic acid:

$$\log k = -1.28 + (1.95 \pm 0.12)\pi^* + (1.00 \pm 0.11)\alpha \quad (25a)$$

$$R = 0.994, s = 0.060, n = 7$$

$$\log k = 2.86 - (3.15 \pm 0.43)\beta \quad (25b)$$

$$R = 0.956, s = 0.151, n = 7$$

6-Methylnicotinic acid:

$$\log k = -1.09 + (1.92 \pm 0.13)\pi^* + (0.94 \pm 0.12)\alpha \quad (26a)$$

$$R = 0.993, s = 0.065, n = 7$$

$$\log k = 2.93 - (3.07 \pm 0.43)\beta \quad (26b)$$

$$R = 0.954, s = 0.151, n = 7$$

Once again, the solvent polarity/polarizability is the dominating effect in the transition state. The effect supporting the initial state, the HBA solvent activity, was in the range similar to those of the previous investigations in this study. The positive sign of the HBD solvent parameter once again describes the support this effect gives to the transition state and the increase in the reaction rate. The somewhat lower value of this parameter coefficient for the chloro-substituted acid may be explained by its acidity, higher than those of the other examined compounds because of the presence of the electronegative chlorine, which additionally stabilizes the anion. Such a structure has a lower demand for electrophilic stabilization.

Contrary to 2-hydroxynicotinic acid, 6-hydroxynicotinic acid displays the lowest reaction rate constants. This observation could be explained by the decrease in its acidity because of the electron-donor resonance effect of the hydroxyl group. The increase of the electronic density in the ring destabilizes the carboxylic anion (Fig. 6).

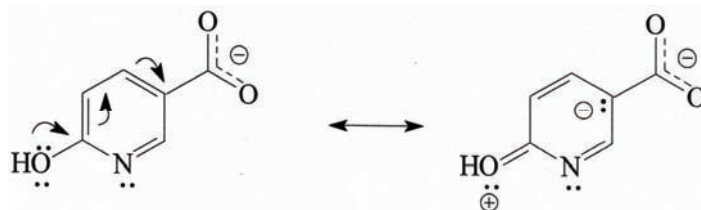


Fig. 6. The carboxylic anion of 6-hydroxynicotinic acid.

The highest value of the π^* coefficient for the 6-hydroxy-substituted acid could be explained by its additional need for stabilization of the anion by the solvent, because the charge separation in the transition state is the highest for this acid. The same compound also has the highest coefficients for the HBD and HBA solvent parameters. The strongest solvent influence on 6-hydroxynicotinic acid is due to lowest stability of the anion of this acid, considering the series examined in this chapter. The negative inductive effect of the oxygen atom seems to be negligibly weak in comparison to the positive resonance one (electron-donor effect).

6-Methylnicotinic acid has lower reaction rate constants than nicotinic and 6-chloronicotinic acids, which is probably due to the positive inductive effect of the methyl group. However, it seems that its anion is more stable than the one of the 6-hydroxynicotinic acid, as 6-hydroxynicotinic has even lower reaction rate constants. The solvent effect on this compound is slightly higher than on the unsubstituted and chloro-substituted nicotinic acids, but lower than on 6-hydroxynicotinic acid, meaning that its demand for stabilization by solvent effects is intermediate between them.

For comparison, the same equations were determined for the same substituted benzoic acids in the same solvent set²³, as in the previous section:

6-Chlorobenzoic acid

$$\log k = -1.48 + (1.96 \pm 0.22)\pi^* + (0.99 \pm 0.22)\alpha \quad (27a)$$

$$R = 0.980, s = 0.116, n = 7$$

$$\log k = 2.71 - (3.21 \pm 0.43)\beta \quad (27b)$$

$$R = 0.957, s = 0.153, n = 7$$

6-Hydroxybenzoic acid

$$\log k = -2.59 + (2.42 \pm 0.22)\pi^* + (1.37 \pm 0.21)\alpha \quad (28a)$$

$$R = 0.988, s = 0.113, n = 7$$

$$\log k = 2.73 - (4.02 \pm 0.58)\beta \quad (28b)$$

$$R = 0.950, s = 0.207, n = 7$$

6-Methylnicotinic acid

$$\log k = -2.09 + (2.19 \pm 0.23)\pi^* + (1.17 \pm 0.23)\alpha \quad (29a)$$

$$R = 0.984, s = 0.119, n = 7$$

$$\log k = 2.64 - (3.59 \pm 0.54)\beta \quad (29b)$$

$$R = 0.948, s = 0.191, n = 7$$

Again the major difference between the two acids systems analyzed in this chapter is the value of the coefficient of the π^* parameter. Once more it was proved that the benzoic acids, although substituted at a different position from the set considered in the previous chapter, have more polarizable anions, which demand additional stabilization by the polarity/polarizability solvent effect. Furthermore, the somewhat higher values for the HBD solvent parameter, in other words more pronounced electrophilic stabilization of the benzoic acids, can again be explained by the fact that it is directed only to the reactive center, the carboxylic group in the transition state.

Various solvents containing no hydroxyl group

The reaction rate constants for the chosen series of 6-substituted nicotinic acids are given in Table VIII.

TABLE VIII. Rate constants ($\text{dm}^3 \text{mol}^{-1} \text{min}^{-1}$) for the reaction of 6-substituted nicotinic acids with DDM at 30 °C in various solvents²²

Solvent	H	6-Cl	6-OH	2-CH ₃	6-Br	6-SH
Acetophenone	5.17	7.55	Insoluble	2.24	8.32	6.16
Acetone	1.55	2.34	Insoluble	1.38	2.51	2.09
Chloroform	40.73	208.92	Insoluble	31.62	281.8	158.5
Ethyl benzoate	3.37	4.36	Insoluble	2.82	4.49	3.04
Isobutyl methyl ketone	1.39	3.55	Insoluble	0.88	4.11	2.24
<i>N</i> -Methylformamide	0.94	1.51	0.49	0.76	1.41	1.20
Dimethyl sulfoxide	0.85	0.42	0.76	0.12	0.45	0.42
<i>N,N</i> -Dimethylacetamide	0.11	0.25	0.71	0.76	0.27	0.35
<i>N,N</i> -Dimethylformamide	0.24	0.58	0.05	0.16	1.58	0.69
<i>N</i> -Methylpyrrolidone	0.12	0.33	0.04	0.08	0.49	0.35

The results from Table VIII show that the influence of a solvent on the reactivity is complex, due to the many types of solvent to solute interactions (dipolarity, HBD and HBA effects), acting not only on the electrophilic and nucleophilic acid sites (Fig. 1), but also on the substituents, where they could cause modifications of the electronic properties. Solvents of high dipolarity/polarizability and/or high proton-acceptor capability caused a significant decrease in the reaction rate. The highest value of the reaction rates in chloroform could be explained by the highest proton-donor ability of this solvent, as well as by its lowest proton-acceptor capability, considering its values of the α and β parameters from Table I.

As stated in the literature,²⁵ carboxylic acids dissolved in chloroform exist in the form of dimers. A dimer could appear in two forms, cyclic and open, the latter being a very reactive form because it can easily lose a proton and convert into a resonance-stabilized anion. As the carboxylic anion is the reacting species in this system, it is continuously converted into the product and this is a probable

reason why the open chain dimer, which stabilizes the anion, is the dominant form.²⁵ Being a solvent of low polarity, chloroform influences a weaker stabilization of the ion-pair intermediate, making it easily convertible into the final product. Solvation of an ion-pair intermediate with a solvent of lower polarizability could have a higher contribution than with one of higher polarizability to a less negative activation entropy and thus to a more spontaneous reaction.

The results of the correlations of the reaction rate with the solvatochromic parameters π^* , α and β using the solvatochromic Eq. (2) are presented in the following equations.

Nicotinic acid:

$$\log k = 0.80 + (2.05 \pm 1.08)\pi^* + (1.61 \pm 0.39)\alpha - (4.63 \pm 0.67)\beta \quad (30)$$

$$R = 0.974, s = 0.22, n = 10$$

6-Chloronicotinic acid:

$$\log k = 1.48 + (1.70 \pm 0.71)\pi^* + (1.58 \pm 0.27)\alpha - (4.77 \pm 0.47)\beta \quad (31)$$

$$R = 0.990, s = 0.16, n = 10$$

6-Hydroxynicotinic acid:

$$\log k = -1.92 + (2.37 \pm 0.36)\pi^* + (1.99 \pm 0.09)\alpha - (2.20 \pm 0.51)\beta \quad (23)$$

$$R = 0.982, s = 0.26, n = 5$$

6-Methylnicotinic acid:

$$\log k = 1.02 + (1.35 \pm 0.97)\pi^* + (1.73 \pm 0.35)\alpha - (4.34 \pm 0.61)\beta \quad (32)$$

$$R = 0.980, s = 0.20, n = 10$$

6-Bromonicotinic acid:

$$\log k = 1.64 + (1.68 \pm 0.77)\pi^* + (1.50 \pm 0.28)\alpha - (4.91 \pm 0.48)\beta \quad (33)$$

$$R = 0.989, s = 0.16, n = 10$$

6-Mercaptonicotinic acid:

$$\log k = 1.18 + (1.89 \pm 0.77)\pi^* + (1.40 \pm 0.28)\alpha - (4.56 \pm 0.48)\beta \quad (34)$$

$$R = 0.986, s = 0.16, n = 10$$

From the values of regression coefficients (s , a and b), the contribution of each parameter to the reactivity of the investigated compounds on the percentage basis was calculated and the results are listed in Table IX.

TABLE IX. Percentage contribution of the Kamlet-Taft solvatochromic parameters to the reactivity of the investigated acids in various solvents

Acid	$P_{\pi^*} / \%$	$P_{\alpha} / \%$	$P_{\beta} / \%$
H	27	23	60
6-Cl	21	20	59
6-OH	36	30	34
6-CH ₃	18	23	59
6-Br	21	19	60
6-SH	24	18	58

The results from Table IX lead to the following conclusions:

1) The rate of the reaction is strongly influenced by specific solute–solvent interactions, as indicated by the percentage contributions of the α and β parameters ($P_\alpha + P_\beta$).

2) The positive sign of the coefficient of the α term suggests that the specific interaction between the transition state and the solvent (Fig. 1), through HBD properties is stronger than that between the reactant and solvent, *i.e.*, the HBD solvent effect or electrophilic solvation increases the reaction rate.

3) The negative sign of the coefficient of the β term suggest that the specific interaction between the reactant and solvent, through HBA properties, is stronger than that between the transition state and the solvent, *i.e.*, the HBA effect or nucleophilic solvation decreases the reaction rate.

4) The solvent dipolarity/polarizability, as indicated by P_{π^*} also plays an appreciable role in governing the reactivity. The positive sign of the coefficient of this term proves that classical or non-specific solute–solvent interactions dominate in the transition state and increase the reaction rate.

From a comparison with the already mentioned Eq. (9) for benzoic acid, it could be observed that the higher contribution of the HBA solvent effect for substituted nicotinic acids is affected by their higher acidity and the strong proton accepting character of some of the aprotic solvents. Classical solvation has a higher influence on the reactivity of 6-hydroxynicotinic acid, while the electrophilic stabilization, *i.e.* the HBD solvent effect, is more pronounced for benzoic acid. The significant contribution of the HBD solvent effect, reflected in value of the coefficient a for the chosen solvent set, in all previous equations, and especially for benzoic acid, indicate an important role of the HBD solvent effect. The proton donor ability of a solvent to stabilize nucleophilic sites on an acid anion in forming increases the reaction rate, while stabilization of the initial state decreases it. These results could be supported by the observation that dipolar non-HBD solvents, in spite of their high relative permittivities and dipole moments, could favor acid ionization and charge separation, and the created carboxylate anion–diazodiphenylmethane cation ion pair could be stabilized by applied solvents. Furthermore, the significantly higher value of P_α for benzoic acid leads to the conclusion that the strong electron-accepting character of the pyridine nitrogen has an undesirable contribution to HBD solvent stabilization in the transition state. The small and definitely increased contribution of the HBD solvent effect for 6-hydroxynicotinic acid could probably be a manifestation of the specific solvation of the acidic hydrogen of the hydroxyl group, causing stabilization and a definite modification of the electron-donating properties of this group.

4. CONCLUDING REMARKS

From the presented results, the conclusion can be drawn that the Kamlet–Taft Total Solvatochromic Equation can be applied to analyze the solvent effect on the reaction of pyridine carboxylic acids with DDM in both protic and aprotic solvents. A set of seven protic solvents in which all the examined compounds are soluble was chosen in order to obtain clear and comparable results. The arithmetic signs of the equation parameters are in agreement with the known reaction mechanism. The different demands for solvation and stabilization of the examined compounds, which are a consequence of their structure, reflected themselves in the coefficient values. Hence, it could be stated that the applied equation, apart from a quantitative description of the solvent effect on reactivity, also displays the structure effect on reactivity of the examined compounds to some extent, in the given solvent set.

It could be concluded that in the applied solvent set, the classical solvation effect dominates the reaction; it is the main effect that causes an increase in the reaction rate. The proton-donor (HBD) solvent effect has two electrophilic centers available for attack, the nitrogen in the initial state, and the nitrogen and carboxylic anion in the transition state; however, its principal influence is on the carboxylic anion in the transition state. The electrophilic solvent effect on nitrogen in the initial state seems to be masked by the stronger nucleophilic solvent effect. This proton-acceptor solvent effect (HBA) is present in the initial state before the reaction commences and it is directed to the carboxylic proton, decreasing the reaction rate.

The presence of the nitrogen in the ring of the pyridine carboxylic acids could also be noticed by the lower polarizability of its anion. The smaller difference in the electron density of the anion of pyridine carboxylic acids, than in the anion of the corresponding benzoic acids, was proved by the lower values of the coefficients of the solvent polarity/polarizability parameter for the pyridine carboxylic acids. The pyridine ring has a greater electron density than the benzene ring, therefore the anion of the carboxylic acid containing the latter ring has a more polarizable structure and higher demands for stabilization by the polarity/polarizability solvent effect.

The observation that isonicotinic acid has higher reaction rate values than, picolinic and nicotinic acid, which have rather similar values, could be explained by the electron-withdrawing effects of the nitrogen in isonicotinic acid that stabilize the carboxylic anion and increase its acidity. In the case of nicotinic acid, which reacts the slowest, there is only the inductive effect of nitrogen, which gives weaker support than for isonicotinic acid. In the molecule of picolinic acid, an intramolecular hydrogen bond can be formed between the carboxylic proton and the neighboring nitrogen and make the removal of the proton more difficult, but, as picolinic acid reacts faster than nicotinic acid, it obviously does not pre-

vail over the electron-withdrawing effects of the nitrogen. However, the presence of the mentioned hydrogen bond cannot be neglected, judging from a comparison of reaction rate constants for picolinic and isonicotinic acids. These two compounds have the same electron-withdrawing effects, but a hydrogen bond exists only in the case of picolinic acid, which decreases the reaction rate.

The 2-substituted nicotinic acids have higher reaction rate constants than the unsubstituted acid, except for 2-methylnicotinic acid. The strong negative inductive effect increases the acidity in the case of 2-chloronicotinic acid. In the case of the 2-hydroxy-substituted acid, a hydrogen bond between the carboxylic anion and the hydroxylic proton can stabilize the anion and enhance the acidity, therefore the reactivity of this compound with DDM. For the 2-methyl substituted acids, it was observed that the electron-donor effect of the methyl group reduces the acidity, as the reaction rate constants were lower than those of nicotinic acid were.

When comparing 2- and 6-substituted acids, it could be noticed that the negative inductive effect of chlorine was less prominent when coming from C-6. Therefore, 6-chloronicotinic acid has lower reaction rate constants than 2-chloronicotinic acid, however it was still the fastest in the 6-substituted acids series.

Contrary to 2-hydroxynicotinic acid, 6-hydroxynicotinic acid displays the lowest reaction rate constants. This observation could be explained by the decrease of its acidity because of the electron-donor resonance effect of the hydroxyl group. The increase of the electron density in the ring destabilizes the carboxylic anion. There is no possibility for an intramolecular hydrogen bond, as in the case of 2-hydroxynicotinic acid. 2-Hydroxynicotinic acid has high values of the reaction rate constants because of the existence of the hydrogen bond between the hydrogen from the hydroxyl group and the carboxylic anion. This interaction is probably responsible for enhanced acidity of the 2-hydroxynicotinic acid, because it facilitates the release of the carboxylic proton.

The difference between 2- and 6-substituted acids was the smallest in the case of the methyl-substituted acids, which could be expected, as it is the substituent with the weakest electronic effect of all the examined substituents. The positive inductive effect of the methyl group reduces the acidity and the reactivity of these acids with DDM. It could be expected that this effect would be more prominent for 2-methylnicotinic acid, however, 6-methylnicotinic had the lower reaction rate constants. This could be explained by the steric effect that could exist in the case of 2-methylnicotinic acid, which could slightly enhance its reactivity in comparison with 6-methylnicotinic acid. The steric interaction between the methyl group and the carboxylic group can twist out the carboxylic group and make it more accessible for DDM, thereby increasing the reactivity. There is no possibility that such an effect could oppose the positive inductive effect of the methyl group in the case of 6-methylnicotinic acid.

In various solvents containing no hydroxyl group, the Kamlet–Taft Equation could be employed in its full three-parameter form, however it was not possible to find a mutual solvent set for all the examined series of pyridine carboxylic acids. The three-parameter equation makes the solvent properties influence easily comparable, and it can be concluded that the proton acceptor solvent activity, which decreases the reaction rate, is the dominant factor for all the compounds. The interesting difference in reactivity between 2-hydroxynicotinic acid and 6-hydroxynicotinic acid in aprotic solvents could be explained by the presence of an intramolecular hydrogen bond in the molecule of the former. The mentioned hydrogen bond could reverse the effect on the reactivity of the hydroxyl substituent of 2-hydroxynicotinic acid depending on the solvent. In protic solvents, it makes the anion stable and the compound more reactive toward DDM and in aprotic solvents, where there is no stabilization by the proton-donor solvent effect, it blocks the anion and prevents it from reacting further.

Acknowledgements. The authors acknowledge the financial support of the Ministry of Education, Science and Technological Development of the Republic of Serbia (Project 172013).

ИЗВОД

КОМПАРАТИВНА СТУДИЈА ЛИНЕАРНЕ КОРЕЛАЦИЈЕ СЛОБОДНИХ ЕНЕРГИЈА ЗА РЕАКТИВНОСТ ПИРИДИН-КАРБОКСИЛНИХ КИСЕЛИНА СА ДИАЗОДИФЕНИЛ-МЕТАНОМ У ПРОТИЧНИМ И АПРОТИЧНИМ РАСТВОРАЧИМА

САША Ж. ДРМАНИЋ¹, ЈАСМИНА Б. НИКОЛИЋ¹, АЛЕКСАНДАР Д. МАРИНКОВИЋ²
и БРАТИСЛАВ Ж. ЈОВАНОВИЋ²

¹*Катедра за органску хемију, Технолошко–металуршки факултет, Универзитет у Београду, Карнегијева 4, Београд* и ²*Институт за хемију, технологију и металургију, Универзитет у Београду, Њешићева 12, Београд*

У овом раду анализиран је утицај протичних и апротичних растварача на реактивност пиколинске, никотинске и изоникотинске киселине, као и неколико супституисаних никотинских киселина са диазодифенилметаном (DDM). Да би се добијени кинетички подаци могли објаснити помоћу ефеката растварача, константе другог реда за реакцију испитиваних киселина и DDM-а су корелисане Камлет–Тафтовом тоталном солватохромном једначином. Корелација кинетичких података урађена је вишеструком линеарном регресионом анализом и ефекат растварача је посматран са стране основног стања, односно реактаната, и прелазног стања у реакцији. Аритметички знаци испред коефицијената у једначини су у складу са познатим механизмом испитиване реакције. Солватациони модели за све испитиване киселине су предложени и повезани са специфичностима њихових структура.

(Примљено 13. јула, ревидирано 19. јула 2012)

REFERENCES

1. E. D. Hughes, C. K. Ingold, *J. Chem. Soc.* (1935) 244
2. J. G. Kirkwood, *J. Phys. Chem.* **2** (1934) 351

3. E. Grunwald, S. Winstein, *J. Am. Chem. Soc.* **70** (1948) 846
4. M. H. Abraham, *Prog. Phys. Org. Chem.* **11** (1974) 1
5. E. F. Caldin, *Pure Appl. Chem.* **51** (1979) 2067
6. C. Reichardt, *Pure Appl. Chem.* **54** (1982) 1867
7. D. Mather, J. Shorter, *J. Chem. Soc., Perkin Trans. 2* (1983) 1179
8. I. A. Koppel, V. A. Palm, in *Advanced Linear Free Energy Relationships*, N. B. Chapman, J. Shorter, Eds., Plenum Press, London, 1972, Ch. 5
9. M. J. Kamlet, J. L. M. Abboud, R. W. Taft, *Prog. Phys. Org. Chem.* **13** (1981) 485
10. M. H. Abraham, R. W. Taft, M. J. Kamlet, *J. Org. Chem.* **46** (1981) 3053
11. M. J. Kamlet, J. L. M. Abboud, M. H. Abraham, R. W. Taft, *J. Org. Chem.* **48** (1983) 2877
12. M. H. Abraham, *Pure Appl. Chem.* **57** (1985) 1055
13. M. H. Aslan, A. G. Burden, N. B. Chapman, J. Shorter, *J. Chem. Soc., Perkin Trans. 2* (1981) 500
14. M. H. Aslan, G. Collier, J. Shorter, *J. Chem. Soc., Perkin Trans. 2* (1981) 1572
15. K. Bowden, N. B. Chapman, J. Shorter, *J. Chem. Soc.* (1963) 5329
16. J. Shorter, *Correlation Analysis of Organic Reactivity*, Wiley, Chichester, UK, 1982, p. 130
17. M. H. Abraham, L. P. Grellier, J. L. M. Abboud, M. R. Doherty, R. W. Taft, *Can. J. Chem.* **66** (1988) 2673
18. B. Jovanović, S. Drmanić, M. Mišić-Vuković, *J. Chem. Res. (S)* (1998) 554
19. A. Marinković, S. Drmanić, B. Jovanović, M. Mišić-Vuković, *J. Serb. Chem. Soc.* **70** (2005) 557
20. S. Drmanić, B. Jovanović, A. Marinković, M. Mišić-Vuković, *J. Serb. Chem. Soc.* **68** (2003) 515
21. S. Drmanić, J. Nikolić, B. Jovanović, *J. Serb. Chem. Soc.* **77** (2012) 569
22. S. Drmanić, A. Marinković, B. Jovanović, *J. Serb. Chem. Soc.* **74** (2009) 1359
23. S. Drmanić, B. Jovanović, M. Mišić-Vuković, *J. Serb. Chem. Soc.* **65** (2000) 481.
24. C. Reichardt, *Solvents and Solvent Effects in Organic Chemistry*, VCH, Weinheim, Germany, 1990, p. 398
25. N. B. Chapman, M. R. J. Dack, D. J. Newman, J. Shorter, R. Wilkinson, *J. Chem. Soc., Perkin Trans. 2* (1974) 962.



J. Serb. Chem. Soc. 77 (10) 1339–1344 (2012)
JSCS–4355

Synthesis of 2-azetidinones substituted coumarin derivatives

UDAY C. MASHELKAR*, MUKESH S. JHA** and BEENA U. MASHELKAR

*Organic Research Laboratory, S. S. and L. S. Patkar College, Goregaon (West),
Mumbai 400 062, India*

(Received 24 October 2011, revised 5 April 2012)

Abstract: α -Naphthol was converted into 4-methyl-2*H*-benzo[*h*]chromen-2-one by reacting with ethyl acetoacetate in the presence of bismuth trichloride. The product was oxidized to 2-oxo-2*H*-benzo[*h*]chromene-4-carbaldehyde and then condensed with aromatic primary amines to give Schiff bases **3a–d**. These Schiff bases were then reacted with acid chlorides in the presence of a base in toluene to give 1,3,4-substituted 2-azetidinones.

Keywords: α -naphthol; selenium dioxide; aromatic amine; acid chloride; ethyl acetoacetate; tri-*n*-butylamine; 2-azetidinone.

INTRODUCTION

The β -lactam class of compounds has served an important and highly successful role in the pharmaceutical industry. Miracle drugs, such as penicillins and cephalosporins have significantly improved human health and life expectancy.

Developments in the field of β -lactams^{1–4} during the last decades indicate that the only essential feature for antibacterial activity in these compounds is the presence of the β -lactam (2-azetidinone) ring. It was reported that the presence of an aliphatic substituent on the nitrogen and a carbonyl group on the imine carbon does not give any β -lactam *via* the di-anion–imine cycloaddition reaction.⁵ However, van der Veen reported the formation of *cis*- β -lactams *via* [2+2] cycloaddition reaction involving an *in situ* prepared ketene and an imine derived from phenyl glyoxal and 2-phenylethylamine.⁶ Azetidinone derivatives are also recognized as transcatheter arterial chemoembolization (TACE) inhibitors⁷ and agents with new biological activities, such as anticancer,⁸ anticoccidial,⁹ cardiovascular,¹⁰ antiviral,¹¹ mutagenic,¹² anticonvulsant and anti-inflammatory agents.^{13,14}

A number of publications and patents have appeared in recent years discussing the synthesis of different types of coumarin derivatives and their antibacte-

Corresponding authors. E-mail: (*)ucmashelkar@rediffmail.com;
(**)Jhamukesh1@rediffmail.com
doi: 10.2298/JSC111024045M

rial,¹⁵ antifungal¹⁶ and other biological¹⁷ properties. The coumarin skeleton is also present in novobiocin¹⁸ and other recently discovered antibiotics, such as coumermycin¹⁹ and chartreusin.²⁰ Coumarins substituted with different heterocycles at the position 4 have been shown to possess promising antibacterial activity.²¹ Bearing this in mind, it was decided to synthesize 2-azetidinones that have a coumarin moiety substituent at position 4.

RESULTS AND DISCUSSION

The 4-methyl coumarin derivative was obtained in excellent yield (92 %)²² by reacting α -naphthol with ethyl acetoacetate in the presence of bismuth trichloride (5 mol %). The IR spectrum of compound **1** showed a band at 1711 cm^{-1} for C=O stretching along with other bands. The $^1\text{H-NMR}$ spectrum of compound **1** in CDCl_3 showed a doublet at δ 2.56 ppm for methyl protons and a quartet at δ 6.41 ppm for $\text{C}_3\text{-H}$. It was then oxidized to the corresponding formyl derivative **2** with selenium dioxide. The IR spectrum of compound **2** in KBr showed peaks at 1727 and 1706 cm^{-1} for the two carbonyl groups and the $^1\text{H-NMR}$ spectrum of **2** showed the presence of signal at δ 10.23 ppm for the aldehydic proton. The formyl compound **2** was condensed with various aromatic amines to yield the Schiff bases **3a-d**.²³ The IR spectra of the compounds **3a-d** showed an absorption for only one carbonyl group and band for C=N at 1634 cm^{-1} . The $^1\text{H-NMR}$ spectra showed the absence of an aldehydic proton and presence of the -CH=N- proton at δ 8.8 ppm. These Schiff bases were then reacted with acid chlorides in the presence of base to give the 1,3,4-substituted 2-azetidinones **4a-l**. The IR spectra of compounds **4a-l** showed absorptions for two carbonyls. In the $^1\text{H-NMR}$ spectra there were two doublets for $\text{C}_3\text{-H}$ and $\text{C}_4\text{-H}$. The envisaged reaction sequence is depicted in Scheme 1.

Structures of the compounds **4a-l** were established by their IR and $^1\text{H-NMR}$ spectra. Their *cis/trans* stereochemistry depends mainly on the substituent present on the ketene part, as usually the imine is presumed to exist in the more stable *E*-configuration. The results can be better explained through a zwitter ion intermediate formed by the attack of the nitrogen lone pair of the imine on the ketene, occurring through the less hindered side of the latter.^{24,25} The origin of the diastereoselectivity and influence of reaction conditions on the diastereoselectivity in the Staudinger synthesis have been carefully investigated recently.²⁶ The results indicated that:

1) The diastereoselectivity is controlled by the competition between the direct ring-closure and the isomerization of the imine moiety in the zwitter ionic intermediates generated from imines and ketenes;

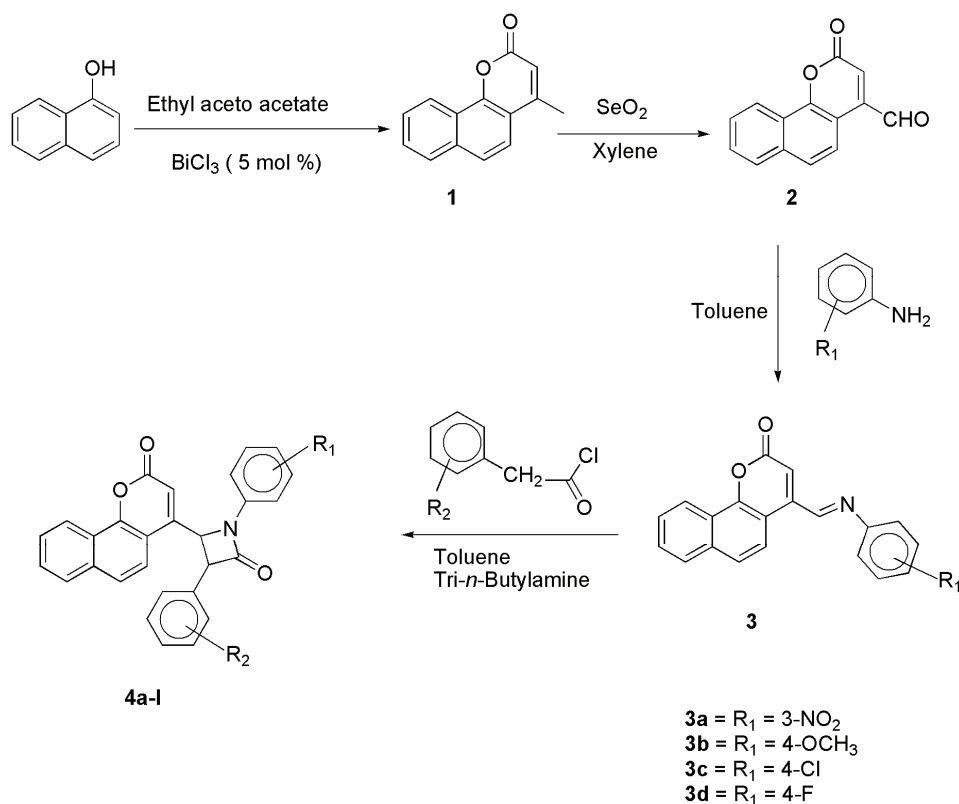
2) electron donating ketene substituents and electron withdrawing imine substituents accelerate the direct ring closure, leading to a preference for a *cis*- β -lactam formation, while electron withdrawing ketene substituents and electron do-

nating imine substituents slow the direct ring closure, leading to a preference for *trans*- β -lactam formation;

3) the electronic effect of the substituents on the isomerization is a minor factor in influencing the diastereoselectivity;

4) different ketene-generation pathways, solvent, additives usually existing in the reaction system, and photo- and microwave-irradiations do not affect the diastereoselectivity;

5) the reaction temperature really influences the diastereoselectivity for some reactions and can be used to tune the same. The stereoselectivity was determined by $^1\text{H-NMR}$. The *cis* isomer shows a higher value of coupling constant than the *trans* isomer (Table I).²⁷



Scheme 1. Synthesis route of 4-methylcoumarin derivative.

EXPERIMENTAL

All the compounds were identified by examination of their spectral data and physical properties. The reported yields refer to the isolated yields of the desired products. Melting points were determined on a Buchi-545 melting point apparatus and are uncorrected. The progress of the reaction was monitored by TLC. The IR spectra were recorded by Perkin

Elmer Spectrum-1 (FTIR) using the KBr disc technique, The $^1\text{H-NMR}$ and $^{13}\text{C-NMR}$ spectra were recorded in CDCl_3 using a Bruker Avance 400 MHz spectrometer (chemical shifts, δ , are in ppm) with TMS as the internal standard. The mass spectra were recorded on a Thermo Finigan Ion Trap GCMS Polaris Q instrument. The dry reactions were performed under nitrogen with magnetic/mechanical stirring.

TABLE I. Stereochemistry of compounds **4a–l**

Compound	R ₁	R ₂	Isolated isomer
4a	4-F	H	<i>Trans</i>
4b	4-Cl	H	<i>Trans</i>
4c	4-OCH ₃	H	<i>Cis</i>
4d	3-NO ₂	H	<i>Trans</i>
4e	4-F	4-Cl	<i>Trans</i>
4f	4-Cl	4-Cl	<i>Trans</i>
4g	4-OCH ₃	4-Cl	<i>Cis</i>
4h	3-NO ₂	4-Cl	<i>Trans</i>
4i	4-F	4-OCH ₃	<i>Cis</i>
4j	4-Cl	4-OCH ₃	<i>Cis</i>
4k	4-OCH ₃	4-OCH ₃	<i>Cis</i>
4l	3-NO ₂	4-OCH ₃	<i>Trans</i>

4-Methyl-2H-benzo[h]chromen-2-one (**1**)

A mixture of α -naphthol (5 mmol) and ethyl acetoacetate (5 mmol) and BiCl_3 (5 mol %) was heated at 110 °C for 2 h. The completion of the reaction was monitored by TLC. The reaction mixture was cooled to room temperature and poured into 10 g of crushed ice. The crystalline product was collected by filtration under vacuum suction and washed with cold water. The pure product was obtained by recrystallization from hot ethanol.

2-Oxo-2H-benzo[h]chromene-4-carbaldehyde (**2**)

Compound **1** (0.10 mmol) was dissolved in xylene (50 ml) at 60–70 °C, and then SeO_2 (0.13 mmol) was added to the solution, which was refluxed for 6–7 h. The hot reaction mixture was filtered to remove the insoluble selenium. The filtrate gave fine crystalline product on cooling to 10 °C.

General procedure for the synthesis of 4-[(phenylimino)methyl]benzo[h]chromen-2-ones (**3a–d**)

An intimate mixture of the 4-formyl derivative compound (**2**) (10 mmol) and corresponding aromatic primary amine (11 mmol) was refluxed in toluene for 6–7 h with azeotropic removal of the water formed during the reaction. The reaction was monitored by TLC. After completion of the reaction, the reaction mass was cooled to 10 °C and the product was washed with cold toluene to obtain the solid products.

General procedure for synthesis of 4-(2-oxo-2H-benzo[h]chromen-4-yl)-1,3-diphenylazetidines (**4a–l**)

An intimate mixture of the 4-imino coumarin derivatives (10 mmol) (**3a–d**), the required acid chloride (20 mmol) and tri-*n*-butylamine (30 mmol) in toluene was refluxed for 3–4 h. The reaction was monitored by TLC until the absence of 4-imino coumarins. Reaction mass was then cooled to room temperature and 40–50 ml 1:1 $\text{HCl:H}_2\text{O}$ added. The organic layer that separated was washed with water followed by NaHCO_3 solution and finally with water.

After drying over anhydrous Na₂SO₄, the solvent was removed under reduced pressure. Compound was isolated using flash chromatography and thereafter crystallized using ethanol.

CONCLUSION

In conclusion, novel 4-(2-oxo-2H-benzo[h]chromen-4-yl)-1,3-diphenylazetidin-2-ones were synthesized under mild conditions starting from α -naphthol.

SUPPLEMENTARY MATERIAL

Analytic and spectral data of the synthesized compounds are available electronically from <http://www.shd.org.rs/JSCS/>, or from the corresponding author on request.

Acknowledgements. The authors are thankful to the management of Ipcal Laboratories, Dr. Suneel Dike, Dr. S. R. Soudagar, Dr Gaurav Sahal and Mr. Brajesh Sharma, for providing the necessary support for this study.

ИЗВОД

СИНТЕЗА 2-АЗЕТИДИНОН-СУПСТИТУИСАНИХ ДЕРИВАТА КУМАРИНА

UDAY C. MASHELKAR, MUKESH S. JHA и VEENA U. MASHELKAR

Organic Research Laboratory, S. S. and L. S. Patkar College, Goregaon (West), Mumbai 400 062, India

У реакцији α -нафтола и етил-ацетоацетата, у присуству бизмут-трихлорида, добијен је 4-метилбензо[h]хромен-2-он. Оксидацијом производа добијен је 2-оксо-2H-бензо[h]-хромен-4-карбалдехид који кондензацијом са ароматичним примарним аминима даје Шифове базе **3a–d**. Шифове базе у реакцији са хлоридима киселина, у присуству базе, у толуену као производ дају супституисане 2-азетидиноне.

(Примљено 24. октобра 2011, ревидирано 5. априла 2012)

REFERENCES

1. S. D. Sharma, U. Mehra, *J. Sci. Ind. Res.* **47** (1988) 451
2. L. R. Verma, C. S. Narayanan, *Indian J. Chem., Sect. B* **30** (1991) 676
3. E. Grochowski, K. Papek, *Tetrahedron*, **47** (1991) 6759
4. M. S. Manhas, D. R. Wagle, J. Ciang, A. K. Bose, *Heterocycles* **27** (1988) 1755
5. G. T. Georg, J. Kant, H. S. Gill, *J. Am. Chem. Soc.* **109** (1987) 1129
6. J. M. van der Veen, S. S. Bari, I. Krishnan, M. S. Manhas, A. K. Bose, *J. Org. Chem.* **54** (1989) 5758
7. B. G. Rao, U. K. Bandarage, T. Wang, J. H. Come, E. Perola, Y. W. S.-K. Tian, J. O. Saunders, *Bioorg. Med. Chem. Lett.* **17** (2007) 2250
8. B. K. Banik, I. Banik, F. F. Becker, *Bioorg. Med. Chem.* **13** (2005) 3611
9. G.-B. Liang, X. Qian, D. Feng, M. Fisher, T. Crumley, S. J. Darkin-Rattray, P. M. Dulski, A. Gurnett, P. S. Leavitt, P. A. Liberator, A. S. Misura, S. Samaras, T. Tamas, D. M. Schmatz, M. Wyvratta, T. Biftu, *Bioorg. Med. Chem. Lett.* **18** (2008) 2019
10. S. Takai, D. Jin, M. Muramatsu, Y. Okamoto, M. Miyazaki, *Eur. J. Pharmacol.* **501** (2004) 1
11. W. W. Ogilvie, C. Yoakim, F. Do, B. Hache, L. Lagace, J. Naud, J. A. Omeara, R. Deziel, *Bioorg. Med. Chem.* **7** (1999) 1521
12. H. Valette, F. Dolle, M. Bottlaender, F. Hinnen, D. Marzin, *Nucl. Med. Biol.* **29** (2002) 849

13. P. Kohli, S. D. Srivastava, S. K. Srivastava, *J. Indian. Chem. Soc.* **85** (2008) 326
14. S. K. Srivastava, S. Srivastava, S. D. Srivastava, *Indian J. Chem., Sect B* **38** (1999) 183
15. T. Ukita, D. Mizuno, T. Tamura, T. Yamkawa, S. Nojima, *J. Pharm. Soc. Jpn.* **71** (1951) 2334
16. D. P. Chakraborty, A. Dasgupta, P. K. Bose, *Ann. Biochem. Exp. Med.* **17** (1957) 59, *CA* **52** (1958) 1352
17. Troponwerke Dinklag, Co Belgium Patent (1976), 843
18. C. G. Smith, A. Dietz, W. T. Soholoski, G. M. Savage, *Antibiot. Chemother.* **6** (1956) 135
19. H. Kawaguchi, H. Tsukiura, M. Okanishi, T. Miyaki, T. Ohmori, K. Fujisawa, H. Koshiyama, *J. Antibiot. Tokyo* **18** (1965) 1, *CA* **63** (1965) 430
20. E. Simonitsch, W. Eisenhuth, O. A. Stamm, H. Schmid, *Helv. Chim. Acta* **43** (1960) 58
21. U. C. Mashelkar, A. A. Audi, *J. Indian Chem. Soc.* **82** (2005) 254
22. S. K. De, R. A. Gibbs, *Synthesis* **8** (2005) 12331
23. U. C. Mashelkar, A. A. Audi, *Indian J. Chem., B* **45** (2006) 1463
24. W. T. Braddy, Y. Q. Gu, *J. Org. Chem.* **54** (1989) 2838
25. L. S. Hegedus, J. Montgomery, Y. Narukawa, D. C. Snustad, *J. Am. Chem. Soc.* **113** (1991) 5784
26. J. Xu, *ARKIVOC* (2009) 21
27. M. Browne, D. A. Burnett, M. A. Caplen, L.-Y. Chen, J. W. Clader, M. Domalski, S. Dugar, P. Pushpavanam, R. Sher, W. Vaccaro, M. Viziano, H. Zhao, *Tetrahedron Lett.* **36** (1995) 2555.



SUPPLEMENTARY MATERIAL TO

Synthesis of 2-azetidinones substituted coumarin derivatives

UDAY C. MASHELKAR*, MUKESH S. JHA and BEENA U. MASHELKAR

*Organic Research Laboratory, S. S. and L. S. Patkar College, Goregaon (West),
Mumbai 400 062, India*

J. Serb. Chem. Soc. 77 (10) (2012) 1339–1344

PHYSICAL, ANALYTIC AND SPECTRAL DATA FOR THE SYNTHESIZED
COMPOUNDS

Compound 1. White crystals; yield: 92 %; m.p. 170–172 °C; Anal. Calcd. for $C_{14}H_{10}O_2$; C, 79.98; H, 4.79 %. Found: C, 79.96; H, 4.83 %; IR (KBr, cm^{-1}): 3065 (arom-CH), 1711 (C=O); 1H -NMR (400 MHz, $CDCl_3$, δ / ppm): 2.5 (1H, *d*, $J = 1.2$ Hz, CH_3), 6.4 (1H, *q*, $J = 1.2$ Hz, C_3 -H), 7.6–8.6 (6H, *m*, Ar-H); ^{13}C -NMR (100.622 MHz, $CDCl_3$, δ / ppm): 22.1, 112.6, 120.9, 121.5, 123.0, 124.8, 126.2, 126.9, 127.1, 128.6, 133.8, 153.1, 153.6, 161.3; mass (m/z): 210 [M^+].

Compound 2. White crystals; yield: 78 %; m.p. 198–200 °C; Anal. Calcd. for $C_{14}H_8O_3$; C, 75.00; H, 3.60 %; Found: C, 75.05; H, 3.61 %; IR (KBr, cm^{-1}): 3057 (arom-CH), 1727 (C=O), 1706 (C=O); 1H -NMR (400 MHz, $CDCl_3$, δ / ppm): 7.0 (1H, *s*, C_3 -H), 7.6–8.6 (6H, *m*, Ar-H), 10.23 (1H, *s*, CHO); ^{13}C -NMR (100.622 MHz, $CDCl_3$, δ / ppm): 121.7, 122.3, 123.1, 124.4, 125.9, 126.2, 126.9, 127.1, 128.6, 133.8, 153.6, 161.3, 162.3, 185.8; mass (m/z): 224 [M^+].

4-[(3-Nitrophenyl)imino]methyl}-2H-benzo[h]chromen-2-one (3a). Yellow crystals; yield 84 %; m.p. 265 °C; Anal. Calcd. for $C_{20}H_{12}N_2O_4$; C, 69.76; H, 3.51; N, 8.14 %. Found: C, 69.80; H, 3.56; N, 8.19 %; IR (KBr, cm^{-1}): 3078 (arom-CH), 1708 (C=O), 1634 (C=N); 1H -NMR (400 MHz, $CDCl_3$, δ / ppm): 7.0 (1H, *s*, C_3 -H), 7.6–8.6 (10H, *m*, Ar-H), 8.8 (1H, *s*, CH=N); ^{13}C -NMR (100.622 MHz, $CDCl_3$, δ / ppm): 112.2, 117.8, 118.3, 120.9, 121.5, 123.0, 124.3, 126.2, 126.9, 127.1, 128.8, 129.3, 131.5, 133.6, 146.5, 149.1, 149.3, 153.6, 161.3, 163.3; mass (m/z): 344 [M^+].

4-[(4-Methoxyphenyl)imino]methyl}-2H-benzo[h]chromen-2-one (3b). Yellow crystals; yield: 80 %; m.p. 182 °C; Anal. Calcd. for $C_{21}H_{15}NO_3$; C, 76.58; H, 4.59; N, 4.25 %. Found: C, 76.62; H, 4.62; N, 4.29 %; IR (KBr, cm^{-1}): 3080 (arom-CH), 1706 (C=O), 1628 (C=N); 1H -NMR (400 MHz, $CDCl_3$, δ / ppm): 3.9 (3H, *s*, OCH_3), 6.9 (1H, *s*, C_3 -H), 7.0–8.7 (10H, *m*, Ar-H), 8.79 (1H, *s*, CH=N);

* Corresponding author. E-mail: uc mashelkar@rediffmail.com; Jhamukesh1@rediffmail.com

^{13}C -NMR (100.622 MHz, CDCl_3 , δ / ppm): 54.9, 112.2, 115.9, 120.9, 121.5, 123.0, 123.3, 124.3, 126.2, 126.9, 127.7, 128.8, 133.6, 140.6, 146.5, 153.6, 160.0, 161.3, 163.3; mass (m/z): 329 [M^+].

4-[[4-Chlorophenyl]imino]methyl]-2H-benzo[h]chromen-2-one (**3c**). Brown crystals; yield: 82 %; m.p. 243 °C; Anal. Calcd. for $\text{C}_{20}\text{H}_{12}\text{ClNO}_2$: C, 71.97; H, 3.62; N, 4.20 %. Found: C, 71.96; H, 3.64; N, 4.25 %; IR (KBr, cm^{-1}): 3079 (arom-CH), 1707 (C=O) 1633 (C=N); ^1H -NMR (400 MHz, CDCl_3 , δ / ppm): 6.9 (1H, s, $\text{C}_3\text{-H}$), 7.25–8.60 (10H, m, Ar-H), 8.75 (1H, s, CH=N); ^{13}C -NMR (100.622 MHz, CDCl_3 , δ / ppm): 112.2, 120.9, 121.5, 123.0, 124.1, 124.3, 126.2, 126.9, 127.7, 128.8, 129.6, 133.6, 145.2, 146.5, 147.8, 153.6, 161.3, 163.3; mass (m/z): 333 [M^+].

4-[[4-Fluorophenyl]imino]methyl]-2H-benzo[h]chromen-2-one (**3d**). Yellow crystals; yield: 81 %; m.p. 230 °C; Anal. Calcd. for $\text{C}_{20}\text{H}_{12}\text{FNO}_2$: C, 75.70; H, 3.81; N, 4.41 %. Found: C, 75.73; H, 3.86; N, 4.43 %; IR (KBr, cm^{-1}): 3082 (arom-CH), 1704 (C=O), 1622 (C=N); ^1H -NMR (400 MHz, CDCl_3 , δ / ppm): 6.70 (1H, s, $\text{C}_3\text{-H}$), 6.90–8.76 (10H, m, Ar-H), 8.92 (1H, s, CH=N); ^{13}C -NMR (100.622 MHz, CDCl_3 , δ / ppm): 112.2, 115.2, 120.9, 121.5, 123.0, 124.1, 124.3, 126.2, 126.9, 127.7, 128.8, 133.6, 145.1, 146.5, 153.6, 160.9, 162.0, 163.3; mass (m/z): 317 [M^+].

1-(4-Fluorophenyl)-4-(2-oxo-2H-benzo[h]chromen-4-yl)-3-phenylazetid-2-one (**4a**). White crystals; yield: 58 %; m.p. 241–243 °C; Anal. Calcd. for $\text{C}_{28}\text{H}_{18}\text{FNO}_3$: C, 77.23; H, 4.17; N, 3.22 %. Found: C, 77.26; H, 4.15; N, 3.14 %; IR (KBr, cm^{-1}): 3055, 1758, 1726, 1606, 1559, 1509; ^1H -NMR (400 MHz, CDCl_3 , δ / ppm): 4.3 (1H, d, $J = 2.8$ Hz, $\text{C}_3\text{-H}$), 5.3 (1H, d, $J = 2.8$ Hz, $\text{C}_4\text{-H}$), 6.4 (1H, s, CH=C), 7.1–7.7 (15H, m, Ar-H); ^{13}C -NMR (100.622 MHz, CDCl_3 , δ / ppm): 59.9, 64.4, 110.9, 112.0, 116.3, 116.5, 118.5, 118.6, 119.1, 122.6, 123.1, 124.7, 127.7, 127.9, 129.3, 129.5, 132.8, 133.3, 134.8, 151.3, 151.5, 158.3, 160.8, 163.9; mass (m/z): 435 [M^+].

1-(4-Chlorophenyl)-4-(2-oxo-2H-benzo[h]chromen-4-yl)-3-phenylazetid-2-one (**4b**). White crystals; yield: 52 %; m.p. 236–238 °C; Anal. Calcd. for $\text{C}_{28}\text{H}_{18}\text{ClNO}_3$: C, 74.42; H, 4.01; N, 3.10 %. Found: C, 74.3; H, 4.11; N, 3.19 %; IR (KBr, cm^{-1}): 3066, 1760, 1722, 1594, 1561, 1494; ^1H -NMR (400 MHz, CDCl_3 , δ / ppm): 4.3 (1H, d, $J = 2.8$ Hz, $\text{C}_3\text{-H}$), 5.8 (1H, d, $J = 2.8$ Hz, $\text{C}_4\text{-H}$), 6.3 (1H, s, CH=C), 7.1–8.6 (15H, m, Ar-H); ^{13}C -NMR (100.622 MHz, CDCl_3 , δ / ppm): 59.9, 64.4, 112.5, 122.1, 122.7, 123.6, 124.0, 125.8, 127.0, 127.6, 127.8, 128.5, 128.7, 130.1, 130.3, 130.7, 130.9, 135.1, 137.3, 140.6, 155.3, 158.3, 160.8, 163.9; mass (m/z): 451 [M^+].

1-(4-Methoxyphenyl)-4-(2-oxo-2H-benzo[h]chromen-4-yl)-3-phenylazetid-2-one (**4c**). White crystals; yield: 49 %; m.p. 247–249 °C; Anal. Calcd. for $\text{C}_{29}\text{H}_{21}\text{NO}_4$: C, 77.84; H, 4.73; N, 3.13 %. Found: C, 77.70; H, 4.58; N, 3.04 %; IR (KBr, cm^{-1}): 3066, 1749, 1720, 1607, 1560, 1512; ^1H -NMR (400 MHz,

CDCl₃, δ / ppm): 3.7 (3H, s, OCH₃), 5.2 (1H, d, J = 6.0 Hz, C₃-H), 5.8 (1H, d, J = 6.0 Hz, C₄-H), 6.3 (1H, s, CH=C), 6.9–7.7 (15H, m, Ar-H); ¹³C-NMR (100.622 MHz, CDCl₃, δ / ppm): 43.3, 59.9, 64.4, 112.5, 115.8, 122.2, 122.7, 123.0, 123.6, 125.9, 127.1, 127.6, 127.8, 128.6, 128.7, 130.3, 130.7, 135.0, 135.1, 137.4, 153.4, 154.8, 157.0, 160.8, 163.9; mass (m/z): 447 [M⁺].

1-(3-Nitrophenyl)-4-(2-oxo-2H-benzo[h]chromen-4-yl)-3-phenylazetid-2-one (4d). White crystals; yield: 51 %; m.p. 201–203 °C; Anal. Calcd. for C₂₈H₁₈N₂O₅: C, 72.72; H, 3.92; N, 6.06 %. Found: C, 72.56; H, 3.79; N, 5.89 %; IR (KBr, cm⁻¹): 3050, 1773, 1726, 1612, 1560, 1452; ¹H-NMR (400 MHz, CDCl₃, δ / ppm): 4.4 (1H, d, J = 2.8 Hz, C₃-H), 5.4 (1H, d, J = 2.8 Hz, C₄-H), 6.4 (1H, s, CH=C), 7.0–8.6 (15H, m, Ar-H); ¹³C-NMR (100.622 MHz, CDCl₃, δ / ppm): 59.9, 64.5, 116.5, 112.5, 117.8, 122.1, 122.7, 123.8, 124.0, 125.9, 127.1, 127.7, 127.9, 128.5, 128.8, 130.5, 130.7, 130.9, 135.2, 137.4, 149.6, 150.6, 152.3, 154.8, 160.8, 163.9; mass (m/z): 462 [M⁺].

3-(4-Chlorophenyl)-1-(4-fluorophenyl)-4-(2-oxo-2H-benzo[h]chromen-4-yl)-azetid-2-one (4e). White crystals; yield: 44 %; m.p. 212–214 °C; Anal. Calcd. for C₂₈H₁₇ClFNO₃: C, 71.57; H, 3.65; N, 2.98 %. Found: C, 71.35; H, 3.72; N, 2.85 %; IR (KBr, cm⁻¹): 3071, 1768, 1730, 1607, 1559, 1514; ¹H-NMR (400 MHz, CDCl₃, δ / ppm): 4.3 (1H, d, J = 2.8 Hz, C₃-H), 5.3 (1H, d, J = 2.8 Hz, C₄-H), 6.4 (1H, s, CH=C), 7.1–8.6 (14H, m, Ar-H); ¹³C-NMR (100.622 MHz, CDCl₃, δ / ppm): 59.9, 64.4, 112.6, 116.9, 122.1, 122.7, 123.6, 124.2, 125.9, 127.0, 127.7, 127.9, 128.5, 130.6, 132.3, 134.2, 135.1, 135.5, 138.3, 151.3, 154.3, 158.3, 160.8, 163.9; mass (m/z): 469 [M⁺].

1,3-Bis(4-chlorophenyl)-4-(2-oxo-2H-benzo[h]chromen-4-yl)azetid-2-one (4f). White crystals; yield: 48 %; m.p. 293–295 °C; Anal. Calcd. for C₂₈H₁₇Cl₂NO₃: C, 69.15; H, 3.52; N, 2.88 %. Found: C, 69.26; H, 3.61; N, 2.95; IR (KBr, cm⁻¹): 3085, 1754, 1719, 1598, 1559, 1492; ¹H-NMR (400 MHz, CDCl₃, δ / ppm): 4.3 (1H, d, J = 2.8 Hz, C₃-H), 5.3 (1H, d, J = 2.8 Hz, C₄-H), 6.4 (1H, s, CH=C), 7.1–7.8 (14H, m, Ar-H); ¹³C-NMR (100.622 MHz, CDCl₃, δ / ppm): 59.9, 64.4, 112.5, 122.2, 122.7, 123.6, 124.0, 125.9, 127.0, 127.7, 127.9, 128.7, 130.2, 130.4, 130.9, 132.2, 134.2, 135.2, 135.5, 140.8, 154.3, 158.4, 160.8, 163.9; mass (m/z): 486 [M⁺].

3-(4-Chlorophenyl)-1-(4-methoxyphenyl)-4-(2-oxo-2H-benzo[h]chromen-4-yl)azetid-2-one (4g). White crystals; yield: 53 %; m.p. 248–250 °C; Anal. Calcd. for C₂₉H₂₀ClNO₄: C, 72.27; H, 4.18; N, 2.91 %. Found: C, 72.39; H, 4.25; N, 3.04 %; IR (KBr, cm⁻¹): 3075, 1759, 1713, 1611, 1561, 1498; ¹H-NMR (400 MHz, CDCl₃, δ / ppm): 3.8 (3H, s, OCH₃), 5.1 (1H, d, J = 6.0 Hz, C₃-H), 5.8 (1H, d, J = 6.0 Hz, C₄-H), 6.3 (1H, s, CH=C), 6.9–8.4 (14H, m, Ar-H); ¹³C-NMR (100.622 MHz, CDCl₃, δ / ppm): 43.3, 59.9, 64.4, 112.5, 115.5, 122.3, 122.9, 123.8, 125.9, 127.0, 127.8, 127.9, 128.5, 130.6, 134.2, 134.3, 135.0, 135.1, 135.5, 141.0, 154.3, 155.8, 157.3, 160.8, 163.9; mass (m/z): 481 [M⁺].

3-(4-Chlorophenyl)-1-(3-nitrophenyl)-4-(2-oxo-2H-benzo[h]chromen-4-yl)azetid-2-one (4h). White crystals; yield: 42 %; m.p. 205–207 °C; Anal. Calcd. for C₂₈H₁₇ClN₂O₅: C, 67.68; H, 3.45; N, 5.64 %. Found: C, 67.72; H, 3.34; N, 5.74 %; IR (KBr, cm⁻¹): 3072, 1770, 1732, 1608, 1535, 1505; ¹H-NMR (400 MHz, CDCl₃, δ / ppm): 4.4 (1H, *d*, *J* = 2.8 Hz, C₃-H), 5.4 (1H, *d*, *J* = 2.8 Hz, C₄-H), 6.4 (1H, *s*, CH=C), 7.1–8.1 (14H, *m*, Ar-H); ¹³C-NMR (100.622 MHz, CDCl₃, δ / ppm): 59.9, 64.4, 112.5, 116.5, 116.8, 121.3, 122.7, 123.7, 125.8, 127.2, 127.7, 127.9, 128.6, 128.8, 130.6, 131.0, 132.5, 133.3, 135.1, 135.7, 143.6, 149.6, 154.4, 154.9, 160.8, 163.9; mass (*m/z*): 496 [M⁺].

1-(4-Fluorophenyl)-3-(4-methoxyphenyl)-4-(2-oxo-2H-benzo[h]chromen-4-yl)azetid-2-one (4i). White crystals; yield: 56 %; m.p. 249–250 °C; Anal. Calcd. for C₂₉H₂₀FNO₄: C, 74.83; H, 4.33; N, 3.01 %. Found: C, 74.72; H, 4.25; N, 2.88 %; IR (KBr, cm⁻¹): 3073, 1762, 1730, 1610, 1560, 1506; ¹H-NMR (400 MHz, CDCl₃, δ / ppm): 3.6 (3H, *s*, OCH₃), 5.2 (1H, *d*, *J* = 6.0 Hz, C₃-H), 5.8 (1H, *d*, *J* = 6.0 Hz, C₄-H), 6.3 (1H, *s*, CH=C), 6.5–8.4 (14H, *m*, Ar-H); ¹³C-NMR (100.622 MHz, CDCl₃, δ / ppm): 55.2, 57.4, 60.0, 112.8, 113.1, 113.7, 116.4, 116.8, 119.5, 121.4, 122.0, 122.4, 123.5, 124.3, 127.9, 129.4, 131.1, 134.0, 134.7, 150.2, 151.1, 157.9, 159.0, 159.4, 165.7; mass (*m/z*): 465 [M⁺].

1-(4-Chlorophenyl)-3-(4-methoxyphenyl)-4-(2-oxo-2H-benzo[h]chromen-4-yl)azetid-2-one (4j). White crystals; yield: 53 %; m.p. 208–210 °C; Anal. Calcd. for C₂₉H₂₀ClNO₄: C, 72.27; H, 4.18; N, 2.91 %. Found: C, 72.32; H, 4.30; N, 2.82 %; IR (KBr, cm⁻¹): 3075, 1745, 1711, 1612, 1560, 1508; ¹H-NMR (400 MHz, CDCl₃, δ / ppm): 3.6 (3H, *s*, OCH₃), 5.2 (1H, *d*, *J* = 6.0 Hz, C₃-H), 5.8 (1H, *d*, *J* = 6.0 Hz, C₄-H), 6.3 (1H, *s*, CH=C), 6.5–7.8 (14H, *m*, Ar-H); ¹³C-NMR (100.622 MHz, CDCl₃, δ / ppm): 55.2, 57.4, 60.0, 110.5, 113.8, 122.2, 122.7, 123.6, 124.0, 126.0, 127.0, 127.6, 127.8, 128.5, 129.8, 130.1, 131.0, 131.7, 135.2, 141.0, 154.4, 155.9, 160.7, 161.8, 165.7; mass (*m/z*): 481 [M⁺].

1,3-Bis(4-methoxyphenyl)-4-(2-oxo-2H-benzo[h]chromen-4-yl)azetid-2-one (4k). White crystals; yield: 57 %; m.p. 254–256 °C; Anal. Calcd. for C₃₀H₂₃NO₅: C, 75.46; H, 4.85; N, 2.93 %. Found: C, 75.32; H, 4.92; N, 2.84 %; IR (KBr, cm⁻¹): 3050, 1746, 1714, 1611, 1560, 1508; ¹H-NMR (400 MHz, CDCl₃, δ / ppm): 3.6 (3H, *s*, OCH₃), 3.8 (3H, *s*, OCH₃), 5.1 (1H, *d*, *J* = 6.0 Hz, C₃-H), 5.8 (1H, *d*, *J* = 6.0 Hz, C₄-H), 6.3 (1H, *s*, CH=C), 6.5–8.4 (14H, *m*, Ar-H); ¹³C-NMR (100.622 MHz, CDCl₃, δ / ppm): 55.1, 55.2, 57.4, 60.0, 112.5, 113.5, 115.8, 122.3, 122.7, 123.5, 123.6, 125.8, 127.0, 127.6, 128.0, 128.6, 130.0, 131.7, 133.2, 135.0, 135.2, 154.4, 155.8, 160.6, 161.8, 165.7; mass (*m/z*): 477 [M⁺].

3-(4-Methoxyphenyl)-1-(3-nitrophenyl)-4-(2-oxo-2H-benzo[h]chromen-4-yl)azetid-2-one (4l). White crystals; yield: 42 %; m.p. 257–258 °C; Anal. Calcd. for C₂₉H₂₀N₂O₆: C, 70.73; H, 4.09; N, 5.69 %. Found: C, 70.79; H, 4.18; N, 5.54 %; IR (KBr, cm⁻¹): 3053, 1763, 1723, 1612, 1561, 1515; ¹H-NMR (400 MHz, CDCl₃, δ / ppm): 3.8 (3H, *s*, OCH₃), 4.3 (1H, *d*, *J* = 2.8 Hz, C₃-H), 5.4

(1H, *d*, *J* = 2.8 Hz, C₄-H), 6.3 (1H, *s*, CH=C), 6.9–8.1 (14H, *m*, Ar-H); ¹³C-NMR (100.622 MHz, CDCl₃, δ / ppm): 55.2, 57.4, 60.0, 110.6, 113.6, 114.3, 115.6, 122.2, 122.8, 123.7, 126.0, 127.0, 127.8, 128.0, 128.6, 128.8, 130.0, 131.0, 131.8, 135.2, 143.8, 149.8, 154.4, 155.9, 160.6, 161.8, 165.7; mass (*m/z*): 492 [M⁺].



J. Serb. Chem. Soc. 77 (10) 1345–1352 (2012)
JSCS–4356

A clean and efficient L-proline-catalyzed synthesis of polysubstituted benzenes in the ionic liquid 1-butyl-3-methylimidazolium hexafluorophosphate

SHUBHA JAIN, BALWANT S. KESHWAL* and DEEPIKA RAJGURU

School of Studies in Chemistry, Vikram University, Ujjain, Madhya Pradesh-456010, India

(Received 11 December 2011, revised 20 June 2012)

Abstract: A clean and efficient synthesis of polysubstituted benzenes has been developed *via* sequential vinylogous Michael addition and nucleophilic cyclization reactions of arylolefin malonodinitriles with arylidenemalonodinitriles in the ionic liquid 1-butyl-3-methylimidazolium hexafluorophosphate ([bmim][PF₆]) employing L-proline as a catalyst.

Keywords: polysubstituted benzenes; organocatalysis; ionic liquids; green chemistry.

INTRODUCTION

Polysubstituted benzenes are very useful compounds in organic synthetic chemistry, natural product chemistry, medicinal chemistry and material science.¹ Consequently, enormous numbers of procedures have been developed for their synthesis. Electrophilic² or nucleophilic substitutions,³ coupling reactions catalyzed by transition metals⁴, and metalation functionalization reactions⁵ are considered as traditional approaches. Later, benzannulation reactions including the [3+2+1] Dötz Reaction,⁶ [4+2] cycloaddition,⁷ [3+3] cyclocondensation,⁸ [5+1] benzannulation of alkenoyl ketene-acetals and nitroalkane,⁹ and [4+2] annulation strategy from the Baylis–Hillman Reaction¹⁰ have been developed in recent years.

Milart *et al.* described piperidine-catalyzed cyclocondensations of arylolefin and arylidenemalonodinitriles in acetonitrile.¹¹ Recently, Xue *et al.*¹² and Su *et al.*¹³ reported base-catalyzed cyclocondensations of vinyl malononitriles and nitro-olefins. Xin *et al.*¹⁴ prepared polysubstituted benzenes *via* sequential Michael addition, Knoevenagel condensation and nucleophilic cyclization reactions of chalcones with active methylene compounds in guanidinium ionic liquids. Very recently, Helmy *et al.*¹⁵ achieved the synthesis of polyfunctionally-substituted benzenes by the reaction of the malononitrile dimer with enamines

*Corresponding author. E-mail: bskeshwal2@gmail.com
doi: 10.2298/JSC111211067J

and arylidenemalononitrile in acetic acid in the presence of ammonium acetate. These approaches have received growing interest due to their short sequence and regioselectivity, however; it is still of prime interest and great importance to explore efficient and clean synthetic approaches.

In recent years, ionic liquids, due to their unique properties such as good solvating ability, high thermal stability, negligible vapour pressure, variable polarity, non-flammability and recyclability, have been widely used as “green” solvents for many organic reactions, including transition metal and bio-catalyzed reactions,¹⁶ but they have not been frequently used as the media for organocatalyst catalyzed reactions. Organic reactions catalyzed by small molecule organocatalysts have become very attractive in recent years.^{17–20} Quinine, ephedrine, 2-(*S*)-[(phenylamino)methyl]-4-(*S*)-hydroxypyrrolidine and 2-(*S*)-(diphenylhydroxymethyl)piperidine and its 1-*t*-butoxycarbonyl (1-Boc) derivatives have all been previously used as the catalysts for Michael additions, but they gave only moderate enantiomeric excess (ee) values.^{21–25} Loh *et al.*²⁶ described the excellent results observed for L-proline-catalyzed aldol reactions in imidazolium-based ionic liquids. Rasalkar very recently described the L-proline-catalyzed Michael addition of ketones to nitrostyrene.²⁷ In this study, several ionic liquids were tested and 1-(methoxyethyl)-3-methylimidazolium methanesulphonate ([MOEMIM]OMs) was found to be the best. In order to achieve good yields, it was necessary to prolong the reaction time up to 60 h and the catalyst loading had to be increased to 40 mol % to achieve 75 % ee. Hagiwara²⁸ described organocatalyst-catalysed additions of aliphatic aldehydes to methyl vinyl ketone in the ionic liquid 1-butyl-3-methylimidazolium hexafluorophosphate ([bmim][PF₆]). 2-(*S*)-(Morpholinomethyl)pyrrolidine was found to be the best organocatalyst, but the yields of the product were only average with 11–51 % ee. Kotrusz²⁹ found that L-proline in ionic liquids is a very good catalyst for Michael addition of aliphatic aldehydes and ketones to β -nitrostyrenes. They also described L-proline-catalyzed Michael additions of thiophenols to α,β -unsaturated compounds in [bmim][PF₆].³⁰ Moreover, L-proline, a natural amino acid, is non-toxic, inexpensive and is available in very pure form.

The main aim of the current work was to explore the use of L-proline as a catalyst in ionic liquid media for Michael additions of arylethylidenemalonodinitriles to arylidenemalonodinitriles that could provide a clean synthetic route to polysubstituted benzenes.

RESULTS AND DISCUSSION

When the reactions of arylethylidenemalonodinitriles **1** and arylidenemalonodinitrile **2** were performed in the presence of 10 mol % L-proline in [bmim][PF₆] at 60 °C, the polysubstituted benzene derivatives **3** were obtained in high yields.

In an initial study, the reaction of 2-(1-phenylethylidene)malononitrile (**1a**) and 2-(4-nitrobenzylidene)malononitrile (**2a**) was used as a model reaction to optimize the reaction conditions. The reaction was first performed in [bmim][PF₆] in the absence of L-proline. No reaction occurred at room temperature or at 60 °C. Similar reactions were then attempted in the presence of 5, 10 and 20 mol % of L-proline. The results from Table I (entries 4, 7 and 9) showed that 10 mol % L-proline at 60 °C in [bmim][PF₆] was sufficient to push the reaction forward. Higher loadings of the catalyst did not improve the reaction conditions greatly. To find the optimum reaction temperature, the reaction was first performed with 10 mol % L-proline at room temperature, which yielded only traces of the product, and then at 40, 60 and 80 °C, which resulted in the isolation of **3a** in 64, 76 and 72 % yields (Table I, entries 5–8), respectively. Thus, 10 mol % L-proline and a reaction temperature at 60 °C were the optimal conditions. Furthermore, to determine the most suitable media for the reaction, the model reaction was performed in various ionic liquids as well as in the conventional organic solvent ethanol (Table I, entries 10–14). The best results in terms of reaction time and yield were obtained in [bmim][PF₆].

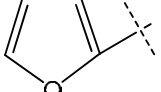
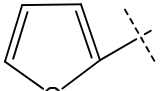
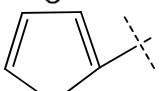
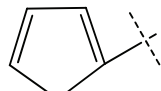
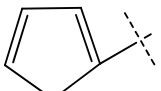
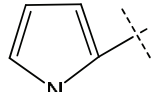
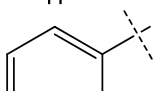
TABLE I. L-Proline-catalyzed synthesis of **3a** under different reaction conditions; r.t. – room temperature; [bmim][PF₆] – 1-butyl-3-methylimidazolium hexafluorophosphate; [bmim]Br – 1-butyl-3-methylimidazolium bromide; [hmim][PF₆] – 1-Hexyl-3-methylimidazolium hexafluorophosphate; [omim][BF₄] – 1-Octyl-3-methylimidazolium hexafluoroborate

Entry	Solvent	Amount of catalyst, mol %	T / °C	Time, h	Yield, %
1	[bmim][PF ₆]	0	r.t.	10	0
2	[bmim][PF ₆]	0	60	10	0
3	[bmim][PF ₆]	5	r.t.	10	Trace
4	[bmim][PF ₆]	5	60	10	43
5	[bmim][PF ₆]	10	r.t.	10	Trace
6	[bmim][PF ₆]	10	40	10	64
7	[bmim][PF ₆]	10	60	4	76
8	[bmim][PF ₆]	10	80	4	72
9	[bmim][PF ₆]	20	60	4	78
10	[bmim][PF ₆]	10	60	4	75
11	[bmim]Br	10	60	6	58
12	[hmim][PF ₆]	10	60	6	61
13	[omim][BF ₄]	10	60	4	72
14	EtOH	10	80	8	54

Having established the optimal conditions for the reaction, various kinds of arylethylidenemalonodinitriles **1** and arylidenemalonodinitriles **2** were reacted to give the corresponding polyfunctionalized benzene derivatives **3**, and representative examples are shown in Table II. All of compounds **1** and **2** gave the expected products in good to high yields under same reaction conditions, regardless of whether they bore electron-withdrawing groups or electron-donating groups.

Thus, it was found that the same product could be synthesized from different arylolethylidene- and arylidenemalonodinitriles with no substantial difference in yields under the given reaction conditions (Table II, entries 1 and 2).

TABLE II. L-Proline-catalyzed synthesis of polysubstituted benzenes **3** in [bmim][PF₆]

Entry	Ar	Ar'	Product	Time, h	Yield, %	M.p. (Lit.), °C
1	C ₆ H ₅	4-NO ₂ C ₆ H ₄	3a	3.5	76	242 (244–246) ¹¹
2	4-NO ₂ C ₆ H ₄	C ₆ H ₅	3a	3.5	65	244 (244–246) ¹¹
3	4-NO ₂ C ₆ H ₄	4-NO ₂ C ₆ H ₄	3b	4	54	350 (352–353) ¹¹
4	C ₆ H ₅	2-CH ₃ OC ₆ H ₄	3c	3	85	166 (168–169) ¹⁴
5	C ₆ H ₅		3d	3.5	82	> 350
6	4-O ₂ NC ₆ H ₄		3e	3	85	277–278
7	4-O ₂ NC ₆ H ₄		3f	3	79	272–273
8			3g	3	84	318
9			3h	4	72	329
10			3i	4	79	315

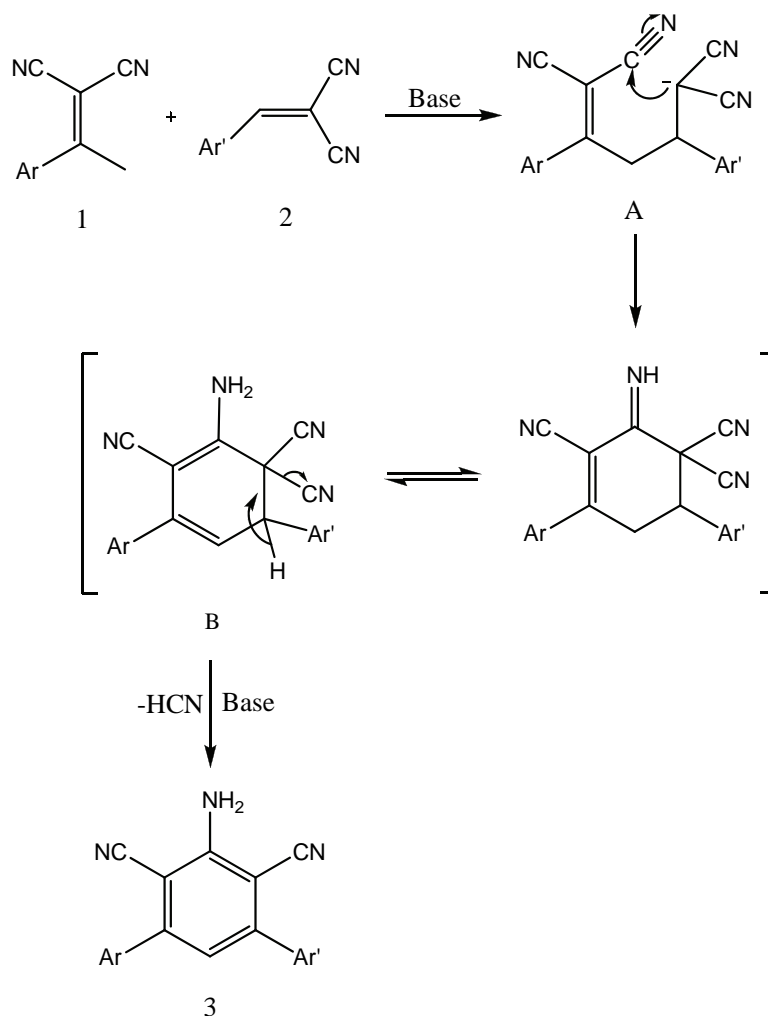
Furthermore, some heteroarylidenemalononitriles were reacted with aryl- or heteroarylethylidenemalononitriles under the same reaction conditions. Surprisingly, these reactions afforded the corresponding benzene derivatives containing heteroaromatic substituents in good yields (Table II, entries 5–10).

The success of the above reactions prompted an investigation of the recyclability of catalyst and ionic liquid. This study was realized using the reaction of **1a** and **2a** in [bmim][PF₆] as a model system. After completion of the reaction, the product was extracted with diethyl ether. The recovered ionic liquid containing L-proline was then used for the next reaction run. Again, the product **3a** was obtained in better yield. Following four consecutive reaction cycles there was a slight decrease in the yield (Table III).

TABLE III. Recycling of the catalyst and ionic liquid in the synthesis of **3a**

Run	1	2	3	4
Yield, %	86	84	82	78

Although the detailed mechanism of the above reaction has not yet been clarified, the formation of polysubstituted benzene derivatives **3** could be tentatively explained by the pathway presented in Scheme 1.

Scheme 1. Tentative pathway for the formation of the polysubstituted benzene derivatives **3**.

In the first step, adduct **A** is obtained according to the vinylogous Michael addition of **1** to arylidenemalononitrile. The addition is followed by the Thorpe

cyclization of the Michael product **A** to the cyclohexadiene system **B**.¹¹ The deprotonation of **B** with *N*-methylimidazole, already contained in imidazolium-based ionic liquids,³¹ followed by the elimination of CN which may occur in the last step afforded the final product **3**. The HCN formed in the reaction is neutralized with the reaction medium that is basic in nature.³² The neutralization of HCN with the reaction media causes a continuous decrease in the yields while recycling the catalyst contained in the ionic liquid.

The synthesis of **3a** was taken as a representative example to show the advantage of the method employed in this study over previously reported procedures. As shown in Table IV, the reaction catalyzed by L-proline in the ionic liquid [bmim][PF₆] gave a comparable yield and took a shorter time than the other method.

TABLE IV. Comparison of the present method with other reported protocols for the synthesis of **3a**

Entry	Catalyst	Conditions	Time, h	Yield, %
1	L-Proline	[bmim][PF ₆], 60 °C	3.5	76 ^a
2	Piperidine	CH ₃ CN, reflux	3	77 ¹¹
3	–	Guanidinium ionic liquid, 60 °C	5	32 ¹⁴

^aThis work

CONCLUSIONS

In summary, a new efficient and clean method for the synthesis of polyfunctionalized benzenes has been established *via* sequential Michael addition and cyclocondensation of arylethylidenemalononitriles with arylidenemalononitriles using L-proline as a catalyst in an ionic liquid, [bmim][PF₆]. According to this methodology, a series of complex aryl compounds such as *m*-terphenyls and benzenes linked to heteroaromatics could be obtained in satisfactory yields. The simplicity, high yields, mild reaction conditions, easy work-up and reusable solvent and catalyst make it a preferred procedure for the preparation of polysubstituted benzenes.

EXPERIMENTAL

General

Chemicals were purchased from Merck and Sigma-Aldrich as “synthesis grade” and were used without further purification. Melting points were determined in open glass capillaries and are uncorrected. The IR spectra were recorded on a Perkin-Elmer-1430 spectrophotometer using KBr pellets. The ¹H- and ¹³C-NMR spectra were obtained at 400 MHz and 100 MHz, respectively, on a Bruker Avance WM-400 spectrometer using DMSO-*d*₆ as the solvent and TMS as an internal standard. The MS spectra were recorded on a Micromass ZMD ESI (70 eV) system. Elemental analysis was performed using a Carlo Erba-1108 analyzer.

Synthesis of the starting arylidenemalonodinitriles

The required arylidene- and arylolethylidenemalonodinitriles were obtained *via* the Knoevenagel reaction of the corresponding aldehyde or ketone with malononitrile, as reported in the literature.³³

General procedure for the synthesis of polysubstituted benzenes 3

To a glass vial charged with L-proline (10 mol %) were added [bmim][PF₆] (5 ml), aryl-ethylidenemalononitrile **1** (1 mmol) and arylidenemalononitrile **2** (1 mmol). The reaction mixture was stirred at 60 °C for 3–4 h. After completion of the reaction (as monitored by TLC), the product was extracted with diethyl ether (4×15 mL) to give the ionic liquid containing L-proline. The recovered ionic liquid containing L-proline was then used for the next reaction run. The combined ether extracts were concentrated and chromatographed on a SiO₂ column using 8:2 hexane/ethyl acetate in all cases. The products were isolated as pure materials. The structures of the already known products were confirmed by their melting point and ¹H-NMR spectra and new compounds were fully characterized.

SUPPLEMENTARY MATERIAL

Analytic and spectral data of the synthesized compounds are available electronically from <http://www.shd.org.rs/JSCS/>, or from the corresponding author on request.

Acknowledgment. We thank the Director, SAIF, Punjab University, Chandigarh, for the NMR and MS spectral data.

ИЗВОД

ЕФИКАСНА СИНТЕЗА ПОЛИСУПСТИТУИСАНИХ ДЕРИВАТА БЕНЗЕНА,
КАТАЛИЗОВАНА L-ПРОЛИНОМ, У ЈОНСКОЈ ТЕЧНОСТИ [bmim][PF₆]

SHUBHA JAIN, BALWANT S. KESHWAL и DEEPIKA RAJGURU

¹*School of Studies in Chemistry, Vikram University, Ujjain, Madhya Pradesh-456010, India*

Развијена је ефикасна синтеза полисупституисаних деривата бензена поступком винилне Мајклове адиције и реакције нуклеофилне циклизације арил-етилиденмалонодинитрила и арилиденмалонодинитрила, катализоване L-пролином, у јонској течности [bmim][PF₆].

(Примљено 11. децембра 2011, ревидирано 20. јуна 2012)

REFERENCES

1. a) D. Astruc, *Modern Arene Chemistry*, Wiley-VCH, Weinheim, Germany, 2002; b) J. Q. Wang, M. Gao, K. D. Miller, G. W. Sledge, Q. H. Zheng, *Bioorg. Med. Chem. Lett.* **16** (2006) 4102
2. a) G. Olah, *Friedel-Crafts and Related Reactions*, Vols. I–IV, Wiley Interscience, New York, 1963; b) D. E. Pearson, C. A. Buehler, *Synthesis* (1972) 533
3. a) M. B. Smith, J. March, *Advanced Organic Chemistry*, 5th ed., Wiley Interscience, New York, 2001, Ch. 13, p. 850; b) E. Buncl, J. M. Dust, F. Terrier, *Chem. Rev.* **95** (1995) 2261
4. J. Hassan, M. Sevignon, C. Gozzi, E. Schulz, M. Lemaire, *Chem. Rev.* **102** (2002) 1359
5. V. Snieckus, *Chem. Rev.* **90** (1990) 879

6. a) K. H. Dotz, P. Tomuschat, *Chem. Soc. Rev.* **28** (1999) 187; b) H. Wang, J. Huang, W. D. Wulff, A. L. Rheingold, *J. Am. Chem. Soc.* **125** (2003) 8980; c) A. V. Vorogushin, W. D. Wulff, H. Hansen, *J. Am. Chem. Soc.* **124** (2002) 6512
7. a) L. V. R. Bonaga, H. C. Zhang, A. F. Moretto, H. Ye, D. A. Gauthier, J. Li, G. C. Leo, B. E. Maryanoff, *J. Am. Chem. Soc.* **127** (2005) 3473; b) S. Saito, Y. Yamamoto, *Chem. Rev.* **100** (2000) 2901
8. a) P. Langer, G. Bose, *Angew. Chem. Int. Ed.* **42** (2003) 4033; b) A. R. Katritzky, J. Li, L. Xie, *Tetrahedron* **55** (1999) 8263
9. a) X. Bi, D. Dong, Q. Liu, W. Pan, L. Zhau, B. Li, *J. Am. Chem. Soc.* **127** (2005) 4578; b) O. Barun, S. Nandi, K. Panda, H. Ila, H. Junjappa, *J. Org. Chem.* **67** (2002) 5398
10. M. J. Lee, K. Y. Lee, S. Gowrisankar, J. N. Kim, *Tetrahedron Lett.* **47** (2006) 1355
11. P. Milart, J. Wilamowski, J. J. Sepiol, *Tetrahedron* **54** (1998) 15643
12. D. Xue, J. Li, Z. T. Zhang, J. G. Deng, *J. Org. Chem.* **72** (2007) 5443
13. W. Su, K. Ding, Z. Chen, *Tetrahedron Lett.* **50** (2009) 636
14. X. Xin, Y. Wang, W. Xu, Y. Lin, H. Duan, D. Dong, *Green Chem.* **12** (2010) 893
15. N. M. Helmy, F. E. M. El-Baih, M. A. Al-Alshaikh, M. S. Moustafa, *Molecules* **16** (2011) 298
16. a) H. Olivier-Bourbigou, L. Magma, *J. Mol. Catal. A: Chem.* **419** (2002) 182; b) J. Dupont, R. F. de-Souza, P. A. Z. Suarez, *Chem. Rev.* **102** (2002) 3667; c) P. Wasserscheid, T. Welton, *Ionic Liquids in Synthesis*, Wiley-VCH, Weinheim, (2003); d) R. Sheldon, *Chem. Commun.* (2001) 2399; e) C. E. Song, *Chem. Commun.* (2004) 1033; f) J. S. Loh, L. C. Feng, H. Y. Yang, J. Y. Yang, *Tetrahedron Lett.* **43** (2002) 8741
17. B. List, R. A. Lerner, C. F. Barbas III, *J. Am. Chem. Soc.* **122** (2000) 2395
18. B. List, *Tetrahedron* **58** (2002) 5573
19. H. Gröger, J. Wilken, *Angew. Chem. Int. Ed.* **40** (2001) 529
20. P. I. Dalko, L. Moisan, *Angew. Chem. Int. Ed.* **40** (2001) 3727
21. H. Hiemstra, H. Wynberg, *J. Am. Chem. Soc.* **103** (1981) 417
22. C. Agami, N. Platzer, C. Puchot, H. Sevestre, *Tetrahedron* **43** (1987) 1091
23. T. Mukaiyama, A. Ikegawa, K. Suzuki, *Chem. Lett.* (1981) 165
24. K. Suzuki, A. Ikegawa, T. Mukaiyama, *Bull. Chem. Soc. Jpn.* **55** (1982) 3277
25. S. Kobayashi, C. Ogawa, M. Kawamura, M. Sugiura, *Synlett* (2001) 983
26. J. S. Loh, L. C. Feng, H. Y. Yang, J. Y. Yang, *Tetrahedron Lett.* **43** (2002) 8741
27. M. S. Rasalkar, M. K. Potdar, S. S. Mohile, M. M. Salunkhe, *J. Mol. Catal., A* **235** (2005) 267
28. H. Hagiwara, T. Okabe, T. Hoshi, T. Suzuki, *J. Mol. Catal., A* **214** (2004) 167
29. P. Kotrusz, S. Toma, H. G. Schmalz, A. Adler, *Eur. J. Org. Chem.* (2004) 1577
30. P. Kotrusz, S. Toma, *ARKIVOC* (2006) 100
31. M. Meciarova, M. Cigan, S. Toma, A. Gaplovsky, *Eur. J. Org. Chem.* **26** (2008) 4408
32. HCN is among the most toxic and rapidly acting of all poisonous substances. Exposure to high doses may be followed by almost instantaneous collapse, rapid cessation of respiration and death. Readers are suggested to take all necessary precautions when working with this procedure.
33. a) D. Xue, Y. C. Chen, X. Cui, Q. W. Wang, J. Zhu, J. G. Deng, *J. Org. Chem.* **70** (2005) 3584; b) S. Suresh, S. Jagir, *Green Chem. Lett. Rev.* **2** (2009) 189; c) C. Mukhopadhyay, A. Datta, *Synth. Comm.* **38** (2008) 2103.



SUPPLEMENTARY MATERIAL TO

A clean and efficient, L-proline-catalyzed synthesis of polysubstituted benzenes in the ionic liquid [bmim][PF₆]

SHUBHA JAIN, BALWANT S. KESHWAL* and DEEPIKA RAJGURU

School of Studies in Chemistry, Vikram University, Ujjain, Madhya Pradesh-456010, India

J. Serb. Chem. Soc. 77 (10) (2012) 1345–1352

ANALYTICAL AND SPECTRAL DATA FOR SELECTED PRODUCTS

5'-Amino-4-nitro-[1,1':3',1''-terphenyl]-4',6'-dicarbonitrile (3a). Yellow needles; yield: 76 %; m.p. 242–244 °C (244–246 °C¹); ¹H-NMR (400 MHz, DMSO-*d*₆, δ / ppm): 6.34 (2H, *s*, amino group), 7.35–7.44 (3H, *m*, phenyl ring), 7.53–7.58 (2H, *m*, phenyl ring), 7.65–7.71 (2H, *m*, phenyl ring), 7.90 (1H, *s*, phenyl ring), 8.20 (2H, *d*, *J* = 7.3 Hz, phenyl ring).

5'-Amino-4,4''-dinitro-[1,1':3',1''-terphenyl]-4',6'-dicarbonitrile (3b). Yellow rods; yield: 54 %; m.p. 350–351 °C (352–353 °C¹); ¹H-NMR (400 MHz, DMSO-*d*₆, δ / ppm): 6.54 (2H, *s*, amino group), 6.98 (1H, *s*, phenyl ring), 7.65–7.67 (4H, *m*, phenyl ring), 7.69–7.70 (4H, *m*, phenyl ring).

5'-Amino-2-methoxy-[1,1':3',1''-terphenyl]-4',6'-dicarbonitrile (3c). White solid; yield: 65 %; m.p. 165–167 °C (168–169 °C²); ¹H-NMR (400 MHz, DMSO-*d*₆, δ / ppm): 3.72 (3H, *s*, methoxy group), 5.92 (2H, *s*, amino group), 6.79–6.81 (2H, *m*, phenyl ring), 7.09–7.12 (2H, *m*, phenyl ring), 7.37–7.43 (4H, *m*, phenyl ring), 7.75–7.77 (2H, *m*, phenyl ring).

3-Amino-5-(furan-2-yl)biphenyl-2,4-dicarbonitrile (3d). Yellow solid; yield: 82 %; m.p. > 350 °C; Anal. Calcd. for C₁₈H₁₁N₃O: C, 75.78; H, 3.89; N, 14.73 %. Found: C, 75.82; H, 3.94; N, 14.66 %; IR (KBr, cm⁻¹): 3474 (ArN–H), 3359 (ArN–H), 2926 (ArC–H), 2215 (ArC≡N), 1653 (ArN–H), 1540 (ArC=C), 1291 (ArC–N), 1049 (ArC–O), 826; ¹H-NMR (400 MHz, DMSO-*d*₆, δ / ppm): 6.30 (2H, *s*, amino group), 6.67–6.69 (2H, *m*, furan ring), 7.41–7.42 (2H, *d*, *J* = 3.6 Hz, phenyl ring), 7.54 (1H, *s*, furan ring), 7.83 (2H, *d*, *J* = 1.6 Hz, phenyl ring), 8.16 (2H, *d*, *J* = 1.5 Hz, phenyl ring); ¹³C-NMR (100 MHz, DMSO-*d*₆, δ / ppm): 88.70, 91.60, 112.52, 112.72, 113.37, 116.04, 116.07, 128.05, 128.49, 128.87, 136.26, 138.38, 141.44, 144.94, 148.41, 154.68; MS (*m/z*): 285 (M⁺).

3-Amino-5-(furan-2-yl)-4'-nitro-biphenyl-2,4-dicarbonitrile (3e). Yellow solid; yield: 74 %; m.p. 277–278 °C; Anal. Calcd. for C₁₈H₁₀N₄O₃: C, 65.45; H, 3.05; N, 16.96 %. Found: C, 65.76; H, 3.27; N, 16.72 %; IR (KBr, cm⁻¹): 3468

*Corresponding author. E-mail: bskeshwal2@gmail.com

(ArN–H), 3358 (ArN–H), 2927 (ArC–H), 2221 (ArC≡N), 1544 (ArC=C), 1284 (ArC–N); ¹H-NMR (400 MHz, DMSO-*d*₆, δ / ppm): 6.60 (2H, *s*, amino group), 6.66–6.68 (1H, *m*, phenyl ring), 7.19 (1H, *s*, phenyl ring), 7.44 (1H, *d*, *J* = 3.5 Hz, phenyl ring), 7.77 (1H, *d*, *J* = 1.7 Hz, phenyl ring), 7.82–7.84 (2H, *m*, phenyl ring), 8.36–8.38 (2H, *m*, phenyl ring); ¹³C-NMR (100 MHz, DMSO-*d*₆, δ / ppm): 89.96, 93.01, 99.49, 112.50, 112.90, 114.01, 115.32, 115.78, 123.52, 129.52, 136.48, 143.68, 144.80, 147.21, 147.77, 148.41, 154.17; MS (*m/z*): 331 (M⁺).

3-Amino-4'-nitro-5-(2-thienyl)biphenyl-2,4-dicarbonitrile (3f). Yellow solid; yield: 68 %; m.p. 272–273 °C; Anal. Calcd. for C₁₈H₁₀N₄O₂S: C, 62.42; H, 2.91; N, 16.18, S, 9.26 %. Found: C, 62.68; H, 2.96; N, 16.34, S, 9.22 %; IR (KBr, cm⁻¹): 3472 (ArN–H), 3382 (ArN–H), 2936 (ArC–H), 2224 (ArC≡N), 1535 (ArC=C), 1326 (ArC–N), 760; ¹H-NMR (400 MHz, DMSO-*d*₆, δ / ppm): 6.74 (2H, *s*, amino group), 6.91 (1H, *s*, phenyl ring), 7.22 (1H, *t*, *J* = 4.6 Hz, phenyl ring), 7.70–7.73 (2H, *m*, phenyl ring), 7.84 (2H, *d*, *J* = 8.6 Hz, phenyl ring), 8.36 (2H, *d*, *J* = 8.6 Hz, phenyl ring); ¹³C-NMR (100 MHz, DMSO-*d*₆, δ / ppm): 96.73, 96.77, 115.00, 115.29, 117.52, 123.54, 128.06, 128.82, 129.68, 133.24, 138.04, 141.75, 143.45, 147.34, 152.28, 154.31; MS (*m/z*): 347 (M⁺).

2-Amino-4,6-bis(furan-2-yl)-1,3-benzenedicarbonitrile (3g). Yellow solid; yield: 84 %; m.p. 318 °C; Anal. Calcd. for C₁₆H₉N₃O₂: C, 69.81; H, 3.30; N, 15.27 %. Found: C, 69.85; H, 3.33; N, 15.25 %. IR (KBr, cm⁻¹): 3475 (ArN–H), 3376 (ArN–H), 2926 (ArC–H), 2212 (ArC≡N), 1654 (ArN–H), 1540 (ArC=C), 1301 (ArC–N), 1032 (ArC–O), 862, 754; ¹H-NMR (400 MHz, DMSO-*d*₆, δ / ppm): 6.58 (2H, *s*, amino group), 6.90–6.95 (2H, *m*, furan ring), 7.21–7.25 (2H, *m*, furan ring), 7.53 (1H, *s*, phenyl ring), 7.87 (2H, *d*, *J* = 1.7 Hz, furan ring); ¹³C-NMR (100 MHz, DMSO-*d*₆, δ / ppm): 93.34, 115.24, 117.83, 121.53, 126.16, 128.71, 134.98, 146.39, 154.60; MS (*m/z*): 275 (M⁺).

2-Amino-4-(furan-2-yl)-6-(1H-pyrrol-2-yl)-1,3-benzenedicarbonitrile (3h). Green solid; yield: 72 %; m.p. 329 °C; Anal. Calcd. for C₁₆H₁₀N₄O: C, 70.06; H, 3.67; N, 20.43 %. Found: C, 70.18; H, 3.72; N, 20.41 %; IR (KBr, cm⁻¹): 3458 (ArN–H), 3260 (ArN–H), 3131, 3088 (ArC–H), 2293 (ArC≡N), 1649 (ArN–H), 1555 (ArC=C), 1342 (ArC–N), 1053 (ArC–O), 790; ¹H-NMR (400 MHz, DMSO-*d*₆, δ / ppm): 6.58 (2H, *s*, amino group), 6.67–6.69 (1H, *m*, pyrrole ring), 7.21–7.23 (1H, *t*, *J* = 4.4 Hz, pyrrole ring), 7.25 (1H, *s*, phenyl ring), 7.42–7.43 (1H, *d*, *J* = 3.5 Hz, pyrrole ring), 7.69–7.70 (2H, *m*, furan ring), 7.83 (*d*, 1H, *J* = 1.6 Hz, furan ring), 8.10 (1H, *s*, pyrrole ring); ¹³C-NMR (100 MHz, DMSO-*d*₆, δ / ppm): 92.98, 108.98, 109.49, 111.41, 114.92, 117.83, 121.53, 126.16, 128.71, 133.35, 134.98, 137.20, 146.39, 155.07, 163.00; MS (*m/z*): 274 (M⁺).

2-Amino-4-(furan-2-yl)-6-(pyridin-3-yl)-1,3-benzenedicarbonitrile (3i). Yellow solid; yield: 79 %; m.p. 315 °C; Anal. Calcd. for C₁₇H₁₀N₄O: C, 71.32; H, 3.52; N, 19.57 %. Found: C, 71.44; H, 3.67; N, 19.56 %; IR (KBr, cm⁻¹): 3472 (ArN–H), 3365 (ArN–H), 2925 (ArC–H), 2212 (ArC≡N), 1637 (ArN–H), 1540

(ArC=C), 1296 (ArC-N), 1039 (ArC-O), 824; $^1\text{H-NMR}$ (400 MHz, DMSO- d_6 , δ / ppm): 6.21 (2H, *s*, amino group), 6.78–6.82 (2H, *m*, furan ring), 7.11 (1H, *s*, pyridine ring), 7.42 (1H, *d*, $J = 3.6$ Hz, furan ring), 7.53 (1H, *s*, phenyl ring), 7.87 (1H, *d*, $J = 1.7$ Hz, pyridine ring), 8.21 (1H, *d*, $J = 1.8$ Hz, pyridine ring), 8.52 (1H, *s*, pyridine ring); $^{13}\text{C-NMR}$ (100 MHz, DMSO- d_6 , δ / ppm): 92.58, 93.34, 109.49, 112.10, 117.83, 121.53, 126.16, 128.71, 133.35, 134.98, 145.82, 146.39, 150.48, 154.00, 155.07; MS (m/z): 286 (M^+).

REFERENCES

1. P. Milart, J. Wilamowski, J. J. Sepiol, *Tetrahedron* **54** (1998) 15643
2. X. Xin, Y. Wang, W. Xu, Y. Lin, H. Duan, D. Dong, *Green Chem.* **12** (2010) 893.



J. Serb. Chem. Soc. 77 (10) 1353–1361 (2012)
JSCS–4357

Anti-elastase, anti-urease and antioxidant activities of (3–13)-monohydroxyeicosanoic acid isomers

BAHAR BILGIN SOKMEN¹, HULYA CELIK ONAR^{2*}, AYSE YUSUFOGLU²
and REFIYE YANARDAG³

¹Department of Chemistry, Faculty of Arts and Sciences, Giresun University, 28049, Giresun, Turkey, ²Faculty of Engineering, Department of Chemistry, Organic Division, Istanbul University, Avcilar-Istanbul, 34320, Turkey and ³Faculty of Engineering, Department of Chemistry, Biochemistry Division, Istanbul University, Avcilar-Istanbul, 34320, Turkey

(Received 5 January, revised 5 April 2012)

Abstract: A series of (3–13)-monohydroxyeicosanoic acid isomers were evaluated for their anti-elastase, anti-urease and antioxidant activities for the first time in this study. All the test compounds exhibited anti-elastase, anti-urease and antioxidant activities. According to the obtained results, the hydroxyeicosanoic acid isomers in which the hydroxyl group is located in the middle or close to the middle of the chain showed higher anti-elastase, anti-urease and antioxidant activities than that of the other isomers. Therefore, (3–13)-monohydroxyeicosanoic acid isomers can be used in agriculture, pharmacy and cosmetic industries due to their excellent anti-elastase, anti-urease and antioxidant activities.

Keywords: anti-elastase; anti-urease; antioxidant; hydroxyeicosanoic acid; enzyme; inhibition.

INTRODUCTION

Elastases are a group of serine proteases that possess the ability to cleave the important connective tissue protein elastin, which is widely distributed in vertebrate tissues, and is particularly abundant in the lung, arteries, skin, and ligaments. These proteases include the neutrophil elastase (NE), also known as leukocyte elastase, the pancreatic elastase (PE), the macrophage elastase (MMP-12) and the fibroblast elastase.^{1–3} There has been increasing interest in elastases in recent years because of their possible involvement in diseases of the connective tissues.⁴ Elastase activity increases significantly with age and results in reduced skin elastic properties, aging and sagging.⁵ Inhibition of the elastase activity could be employed as a useful target to protect against skin aging.⁶

* Corresponding author. E-mail: hcelikonar@gmail.com
doi: 10.2298/JSC120105042S



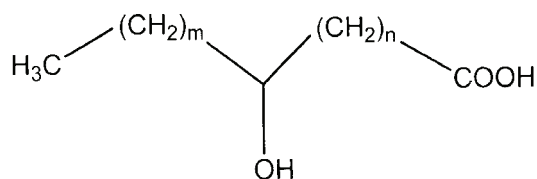
The metalloenzyme urease (urea amidohydrolase; EC 3.5.1.5) catalyzes the hydrolysis of urea into ammonia and carbon dioxide. It is present in a variety of plants, algae, fungi, bacteria and in soil enzymes.⁷ Urease is involved in the pathogenesis of hepatic encephalopathy, hepatic coma urolithiasis, pyelonephritis, ammonia and urinary catheter encrustation.⁸ It is also a major cause of pathologies induced by *Helicobacter pylori* (HP) as this allows bacteria to survive at the low pH of the stomach and hence plays an important role in producing peptic and gastric ulcers.⁹ In agriculture, high urease activity releases abnormally large amounts of ammonia into the atmosphere after urea application and causes significant environmental problems and economical loss. The study of urease inhibition is of medical, agricultural and environmental significance. In the near past, a number of compounds have been proposed as urease inhibitors to reduce environmental problems and enhance the uptake of urea nitrogen by plants.^{10,11}

Recently, interest in finding antioxidants for foods, cosmetics and medicines has increased considerably. Nowadays, antioxidants have become one of the major areas of scientific research. Antioxidants have been extensively studied for their capacity to protect organisms and cells from damage induced by oxidative stress. Scientists in many different disciplines have become more interested in new compounds, either synthesized or obtained from natural sources, that could provide active components to prevent or reduce the impact of oxidative stress on cells.¹² Chemical compounds and endogenous metabolic processes in the human body or in food systems might produce highly reactive free radicals, especially oxygen-derived radicals, which are capable of oxidizing biomolecules, resulting in cell death and tissue damage. Presently, synthetic antioxidant such as butylated hydroxyanisole (BHA), butylated hydroxytoluene (BHT), propyl gallate (PG) and tertiary-butylhydroquinone (TBHQ) are the most commonly used antioxidants. However, their uses have been limited as they may be responsible for liver damage and carcinogenesis.^{13,14} For these reasons, this problem has been overcome by new synthetic or natural compounds.

Hydroxy fatty acids are ubiquitous in nature and have been found as constituents of triacylglycerols, waxes, cerebrosides, and other lipids in plants, animals, insects and microorganisms.^{15–18} The hydroxy fatty acids mentioned in the literature are valuable starting compounds used in the preparation of numerous textile auxiliaries, detergents, dispersion and emulsion reagents¹⁹ and play an important role in cancer chemotherapy.²⁰ Hydroxy fatty acids exhibit an antitumor^{21,22} effect at neutral and acidic pH values in human lung cancer (A 549) cells.²³ In the literature, there is no data on the anti-elastase, anti-urease and antioxidant activities of monohydroxyeicosanoic acid isomers. In this study, the anti-elastase, anti-urease and antioxidant activities of (3–13)-monohydroxyeicosanoic acid isomers were determined for the first time.

EXPERIMENTAL

(3–13)-Hydroxyeicosanoic acids (Scheme 1) were synthesized with high purity by Celik *et al.*^{24,25}. The elastase activity was examined using *N*-succinyl-Ala-Ala-Ala-*p*-nitroanilide (STANA) as a substrate and by the measuring the release of *p*-nitroaniline at 410 nm.²⁶ Urease inhibitory activity was determined according to van Slyke and Archibald.²⁷ The cupric reducing antioxidant capacity of the monohydroxyeicosanoic acids was determined according to the method described by Apak *et al.*²⁸



Scheme 1. Structure of the studied monohydroxyeicosanoic acid isomers; n : 1, 2, 4, 5, 6, 7, 8, 9, 10, 11; $m = 17 - n$.

RESULTS AND DISCUSSION

Fatty acids with one hydroxyl group, called α -hydroxy and β -hydroxy fatty acids, are healing agents in cosmetic and clinical use against skin diseases.²⁹ Hydroxy acids, mainly α -hydroxy acids and polyhydroxy acids, remain timeless in their ability to modulate skin structure and performance, providing both clinical and cosmetic benefits to skin. α -Hydroxy acids (AHAs) are a class of compounds derived from food sources that have become increasingly popular as skin rejuvenating agents. At higher concentrations (50–70 %), AHAs are used for superficial skin peeling, while at low concentrations (8–30 %), they have been reported to act as moisturizing agents and can cause a decrease in corneocytic attachment.^{30,31} β -Hydroxy fatty acids are formed during mitochondrial β -oxidation of fatty acids in mammalian tissues. Increased concentrations of free 3-OH fatty acids in body fluids are indicative of disorders in fatty acid oxidation, which is important for tissues with a high-energy demand.³²

According to a literature survey, no positional fatty acid isomers have been examined to date for their elastase inhibition. This work demonstrates the importance of the positional effect on elastase inhibition. The elastase inhibition activities of the monohydroxy C_{20} acids are given in Table I. The elastase inhibitory activities of monohydroxy C_{20} acids were found to increase in a dose dependent manner, the results are expressed as half maximal inhibitory concentrations (IC_{50}) values, calculated from the regression equations prepared from the concentrations of samples. Amongst them, the best inhibition was found for the 10-hydroxyeicosanoic acid, followed by the 11- and 9-hydroxyeicosanoic acid isomers as seen in Table I. A higher elastase inhibitor activity is associated with a lower IC_{50} value. A high elastase inhibition (55.08 ± 0.95 %) was seen at $1 \mu\text{g mL}^{-1}$ for the 10-hydroxy C_{20} acid and the IC_{50} value was $0.59 \pm 0.004 \mu\text{g mL}^{-1}$. A low elastase inhibition (24.28 ± 0.63 %) was seen at $1 \mu\text{g mL}^{-1}$ for the 12-hydroxy C_{20} acid and IC_{50} value of the 12-hydroxy C_{20} acid was $7.69 \pm 1.77 \mu\text{g mL}^{-1}$.

The (3–13)-hydroxyeicosanoic acid isomers showed good elastase inhibition. The 3-, 4-, 6-, 7-, 8-, 9-, 11- and 13-monohydroxy C₂₀ acids showed nearly the same inhibition (Table I).

TABLE I. The inhibition of elastase activity (mean±SD) by the monohydroxyeicosanoic acid isomers at a concentration of 1 µg mL⁻¹

Hydroxyl position	Inhibition, %	IC ₅₀ / µg mL ⁻¹
3	48.94±1.80	1.24±0.42
4	48.47±0.73	1.43±0.33
6	48.72±0.51	1.19±0.10
7	44.84±0.39	2.10±0.04
8	45.35±1.87	1.42±0.29
9	49.41±1.00	1.08±0.18
10	55.08±0.95	0.59±0.004
11	51.04±0.37	0.88±0.02
12	24.28±0.63	7.69±1.77
13	26.84±2.79	4.9±2.19

Elastase has a serine residue with a free hydroxyl group in its active center. This hydroxyl group may form an ester bond with the carboxyl group of the hydroxyeicosanoic acid isomers. In a previous study, lactones and their derivatives were used as elastase inhibitors.^{33,34} This inhibition was explained by a new transesterification between the hydroxyl group of the serine and carboxyl group of the lactone ring. In the present study, some hydroxyeicosanoic acid isomers were examined for their elastase inhibition activity (Table I). The hydroxyl and carboxyl groups of these isomers may be effective in the inhibition of elastase. The carboxyl group may be more active than the hydroxyl group according to the literature data on the elastase inhibition activity of some saturated and unsaturated fatty acids.^{35,36} The inhibition effect of the hydroxyeicosanoic acid isomers may be explained by the formation of an ester bond between the carboxyl group of the hydroxy acid isomers with the hydroxyl group of serine located in the active center. However, the experimental results obtained in this study showed that the position of the hydroxyl group of the hydroxy acid isomers plays a role on the inhibition effect indicating to a second effect resulting from an interaction between the hydroxyl group of the hydroxy acid isomers and the hydroxyl group of the serine. The best elastase inhibition was found for the 10-hydroxy isomer. This isomer has a symmetrical structure and is like an arrow. The hydroxyl group of the 10-hydroxy isomer is not sterically hindered and is free. The other hydroxy acid isomers showed very similar inhibition, but their degree of inhibition was lower than that of the 10-hydroxy acid isomer. These isomers are less free and more sterically hindered than the 10-hydroxy acid isomer. The 12- and 13-monohydroxy hydroxyeicosanoic acid isomers having the hydroxyl group closer to the end exerted the lowest inhibition. The molecule structure at

these positions may sterically prevent the formation of the hydrogen bridge between the hydroxyl groups of the serine and hydroxy acid isomers, affected probably by van der Waals forces. The hydroxyl group of the 12- and 13-hydroxy isomers is located very far from the carboxyl group. The hydroxyl group of the 3–8 isomers is very close to the carboxyl group. Another effect depending on the position of the hydroxyl may occur between the hydroxyl and carboxyl group. This position effect may be also active on elastase inhibition effect of the hydroxyeicosanoic acid isomers (Table I).

Certain synthetic compounds have shown potential urease inhibition, such as hydroxyurea, flurofamide and hydroxyamic acid. However, the *in vivo* use of some of these is prohibited because of their toxicity or instability, for example, acetohydroxyamic acid was demonstrated to be teratogenic in rats.³⁷ The discovery of potent and safe urease inhibitors is a very important area of pharmaceutical research because of the involvement of urease in different pathological conditions.

The urease inhibition activity of the monohydroxy C₂₀ acids is given in Table II. The urease activity was detected at a lower concentration of the hydroxy acid isomers than the elastase activity. Many synthetic and natural apple polyphenols have shown inhibitory activity against urease activity.^{38,39} Xiao *et al.* explained the urease inhibition activity of polyphenols by the ability of the hydroxyl group to form a complex with the nickel metal located at the active center of urease.³⁸ In this study, the urease inhibition activity of the monohydroxy C₂₀ acid isomers was found to increase dose dependently. The results are expressed as IC₅₀ values calculated from the regression equations prepared from the inhibition and the concentrations of the samples. A high urease inhibition (70.22±1.36 %) was seen at 0.1 µg mL⁻¹ for the 8-hydroxy C₂₀ acid. The IC₅₀ value was 0.000012±±0.0000092 µg mL⁻¹. A low urease inhibition (52.89±2.41 %) was seen at 0.1 µg mL⁻¹ for the 6-hydroxy C₂₀ acid. The IC₅₀ value of the 6-hydroxy C₂₀ acid was 0.0766±0.01 µg mL⁻¹. A number of novel synthetic and natural inhibitors of urease were investigated.^{40,41} Lodhi *et al.* studied triacontanyl palmitate as an effective inhibitor of urease.⁴² The 8-, 10- and 7-hydroxy C₂₀ acid isomers, with the hydroxyl group located in the middle and close to the middle of the chain showed the best inhibition activities. These middle positions make these isomers successful in chelating and, as a result, in the urease inhibition. Moving away from these positions, the urease inhibitory activity decreased due to the molecule symmetry and steric hindrance of the alkyl groups. The activity against urease is the complex building ability of the hydroxyl group with nickel metal.³⁷ The urease inhibition activity of the hydroxy acid isomers in this study can also be attributed to the complex building ability of the hydroxy acid isomers with nickel active center of the urease. The presence of –OH and –COOH group of mono-

hydroxyeicosanoic acid isomers in this study may play together a great role in the inhibition of urease activity.

TABLE II. The inhibition of urease activity (mean \pm SD) by the monohydroxyeicosanoic acid isomers at a concentration of 1 $\mu\text{g mL}^{-1}$

Hydroxyl position	Inhibition, %	$IC_{50} / \mu\text{g mL}^{-1}$
3	59.18 \pm 0.64	0.0509 \pm 0.007
4	66.32 \pm 0.50	0.0174 \pm 0.0002
6	52.89 \pm 2.41	0.0766 \pm 0.01
7	67.41 \pm 2.00	0.0065 \pm 0.0038
8	70.22 \pm 1.36	0.000012 \pm 0.0000092
9	64.85 \pm 1.27	0.0297 \pm 0.00028
10	62.92 \pm 0.28	0.0049 \pm 0.0007
11	67.87 \pm 2.62	0.0234 \pm 0.0043
12	67.20 \pm 1.36	0.0301 \pm 0.000212
13	60.21 \pm 1.46	0.0297 \pm 0.0031

Antioxidants can be reductants, and deactivation of oxidants by reductants can be described as redox reactions in which one reactions species is reduced at the expense of the oxidation of the other. As is known, transition metal ions, such as ferrous and cupric ions, accelerate lipid oxidation by breaking down hydrogen and lipid peroxides to reactive free radicals *via* the Fenton reaction.⁴³ Therefore, chelating agents, known as secondary antioxidants, are important to retard radical degradation. There are several methods for the determination of antioxidant activities. In this study, the cupric reduction antioxidant capacity test (CUPRAC method) was used.²⁸ The CUPRAC method is also used to determine the reducing power of antioxidant compounds.²⁸ This method is based on the reduction of Cu^{2+} to Cu^+ by antioxidants in the presence of neocuprein.⁴⁴ In this method, a higher absorbance indicates a higher cupric ion reduction ability. The CUPRAC method is simultaneously cost effective, rapid, stable, selective and suitable for a variety of antioxidants regardless of the chemical type or hydrophilicity.⁴⁵ The reducing capacity of a compound may serve as a significant indicator of its potential antioxidant activity.⁴⁴

The cupric ion (Cu^{2+}) reducing abilities of the monohydroxyeicosanoic acid isomers are given in Table III. The compounds 12-, 9-, 6- and 13-monohydroxyeicosanoic acid showed the lowest cupric ions (Cu^{2+}) reducing capability (Table III). Compounds, 3-, 4-, 7-, 10- and 11-monohydroxyeicosanoic acids exhibited a moderate reducing power. The highest reducing capacity was found for 8-monohydroxyeicosanoic acid. All the monohydroxyeicosanoic acid isomers are less effective on cupric ions (Cu^{2+}) reducing ability than BHT. This method is based on the chelating ability of the hydroxyl group of some 3–13-monohydroxyeicosanoic acid isomers with Cu^{2+} . The position of the hydroxyl group is important for the chelating activity. The best reducing activity was found for the 8-hydroxy

isomer, in which the hydroxyl is located close to the middle of the chain. This position has no steric hindrance; therefore, the hydroxyl group is free and suitable for chelating with Cu^{2+} . This reducing effect decreased with 3–7- and 9–13-monohydroxyeicosanoic acid isomers because of the molecular symmetry and steric hindrance of the alkyl groups.

TABLE III. The cupric ions reducing antioxidant capacity of the monohydroxyeicosanoic acid isomers (mean \pm SD) at a concentration of 100 $\mu\text{g mL}^{-1}$

Hydroxyl position	CUPRAC reducing power (absorbance)
3	0.35 \pm 0.008
4	0.36 \pm 0.004
6	0.23 \pm 0.004
7	0.37 \pm 0.004
8	0.57 \pm 0.006
9	0.27 \pm 0.001
10	0.37 \pm 0.002
11	0.44 \pm 0.004
12	0.32 \pm 0.002
13	0.24 \pm 0.003
BHT	1.65 \pm 0.045

CONCLUSIONS

A series of (3–13)-monohydroxyeicosanoic acid isomers were synthesized and their anti-elastase, anti-urease and antioxidant activities evaluated. The results showed that all the monohydroxyeicosanoic acid isomers exhibited anti-elastase, anti-urease and antioxidant activities. According to the obtained results, the monohydroxyeicosanoic acid isomers with the hydroxyl group located in the middle or close to the middle of the chain showed higher antioxidant, anti-urease and anti-elastase activities than the other isomers. These monohydroxyeicosanoic acid isomers could be used in the agriculture, pharmacy and cosmetic industries due to their excellent anti-elastase, anti-urease and antioxidant activities.

ИЗВОД

АНТИЕЛАСТАЗНА, АНТИУРЕАЗНА И АНТИОКСИДАТИВНА АКТИВНОСТ НЕКИХ (3–13)-МОНОХИДРОКСИЛНИХ ИЗОМЕРА ЕИКОЗАНСКЕ КИСЕЛИНЕ

BAHAR BILGIN SOKMEN¹, HULYA CELIK ONAR², AYSE YUSUFOGLU² и REFIYE YANARDAG³

¹Department of Chemistry, Faculty of Arts and Sciences, Giresun University, 28049, Giresun, Turkey,

²Faculty of Engineering, Department of Chemistry, Organic Division, Istanbul University,

Avcilar-Istanbul, 34320, Turkey u ³Faculty of Engineering, Department of Chemistry, Biochemistry Division, Istanbul University, Avcilar-Istanbul, 34320, Turkey

Испитана је антиеластазна, антиуреазна и антиоксидативна активност групе (3–13)-монохидроксилних изомера еикозанске киселине. Сва анализирана једињења су испољила све ове активности. Резултати су показали да највећу активност имају изомери код којих је хидроксилна група у средини или близу средине ланца. Према томе, (3–13)-

-монохидроксилни изомери еикозанске киселине, због својих својстава, могу наћи примену у пољопривреди, фармацији и козметичкој индустрији.

(Примљено 5. јануара, ревидирано 5. априла 2012)

REFERENCES

1. W. Bode, E. Meyer, J. C. Powers, *Biochemistry* **28** (1989) 1951
2. N. Tsuji, S. Moriwaki, Y. Suzuki, Y. Takema, G. Imokawa, *Photochem. Photobiol.* **74** (2001) 283
3. S. Nenan, E. Boichot, V. Lagente, C. P. Bertrand, *Mem. Inst. Oswaldo Cruz* **100** (2005) 167
4. B. Siedle, A. Hrenn, I. Merfort, *Planta Med.* **73** (2007) 401
5. L. Robert, *Cosmet. Toiletries* **116** (2001) 61
6. O. Wiedow, J. M. Schroder, H. Gregory, J. A. Young, E. Christophers, *J. Biol. Chem.* **265** (1990) 14791
7. B. Krajewska, *Wiad. Chem.* **56** (2002) 223
8. H.L.T. Mobley, M. D. Island, R. P. Hausinger, *Microbiol. Rev.* **59** (1995) 451
9. H. L. T. Mobley, R. P. Hausinger, *Microbiol. Rev.* **53** (1989) 85
10. G.W. McCarty, J. M. Bremner, J. S. Lee, *Plant Soil* **127** (1990) 269
11. K. M. Khan, A. Wadood, M. Ali, Zia-Ullah, Z. Ul-Haq, M. A. Lodhi, *J. Mol. Graphics Modell.* **28** (2010) 792
12. H. H. Hussain, G. Babic, T. Durst, J. Wright, M. Flueraru, A. Chichirau, *J. Org. Chem.* **68** (2003) 7023
13. H. P. Grice, *Food Chem. Toxicol.* **26** (1988) 717
14. H. C. Wichi, *Food Chem. Toxicol.* **24** (1986) 1127
15. E. Jantzen, A. Sonesson, T. Tangen, J. Eng, *J. Clin. Microbiol.* **31** (1993) 1413
16. I. I. Deridovich, O. V. Reunova, *Comp. Biochem. Physiol., A* **104** (1993) 23
17. N. Murakami, H. Shirahashi, J. Nagatsu, J. Sakakibara, *Lipids* **27** (1992) 776
18. V. M. Dembitsky, T. Rezanka, E. E. Shubina, *Phytochemistry* **34** (1993) 1057
19. R. T. Holman, W. D. Lundberg, T. Malkin, *Prog. Chem. Fats Other Lipids* **3** (1955) 243
20. G. F. Townsend, W. H. Brown, *Can. J. Biochem. Physiol.* **39** (1961) 1765
21. S. Tolnai, J. F. Morgan, *Can. J. Biochem. Physiol.* **40** (1962) 1367
22. Y. Hayashi, Y. Nishikawa, H. Mori, H. Tamura, Y. I. Matsushita, T. Matsui, *J. Ferment. Bioeng.* **86** (1998) 149
23. V. Llado, S. Teres, M. Higuera, R. Alvarez, M. A. Noguera-Salva, J. E. Halver, *Proc. Natl. Acad. Sci. U.S.A.* **106** (2009) 13754
24. H. Celik, *J. Serb. Chem. Soc.* **67** (2002) 473
25. H. Celik, S. Ozeris, *Chim. Acta Turc.* **24** (1996) 23
26. A. E. James, D. W. Timothy, L. Gordon, *Biochemistry* **35** (1996) 9090
27. D. D. van Slyke, R. M. Archibald, *J. Biol. Chem.* **154** (1944) 623
28. R. Apak, K. Güçlü, M. Ozyürek, S. E. Karademir, E. Erçağ, *Int. J. Food Sci. Nutr.* **57** (2006) 292
29. B. A. Green, R. J. Yu, E. J. van Scot, *Clin. Dermatol.* **27** (2009) 495
30. J. C. DiNardo, G. L. Grove, L. S. Moy, *Dermatol. Surg.* **22** (1996) 421
31. F. F. Becker, F. P. Langford, M. G. Rubin, P. Speelman, *Dermatol. Surg.* **22** (1996) 463
32. R. Jenske, W. Vetter, *Food Chem.* **114** (2009) 1122

33. B. Siedle, L. Gustavsson, S. Johansson, R. Murillo, V. Castro, L. Bohlin, I. Merfort, *Biochem. Pharmacol.* **65** (2003) 897
34. D. Dou, G. He, Y. Li, Z. Lai, L. Wei, K. R. Alliston, G. H. Lushington, D. M. Eichhorn, W. C. Groutas, *Bioorg. Med. Chem.* **18** (2010) 1093
35. B. Rennert, M. F. Melzig, *Planta Med.* **68** (2002) 767
36. G. Moroy, E. Bourquet, M. Decarme, J. Sapi, A. J. P. Alix, W. Hornebeck, S. Lorimier, *Biochem. Pharmacol.* **81** (2011) 626
37. Z. P. Xiao, D. H. Shi, H. Q. Li, L. N. Zhang, C. Xu, H. L. Zhu, *Bioorg. Med. Chem.* **15** (2007) 3703
38. Z. P. Xiao, T. W. Ma, X. C. Peng, A. H. Zhang, H. L. Zhu, *Eur. J. Med. Chem.* **45** (2010) 5064
39. E. Pastene, M. Troncoso, G. Figueroa, J. Alarcon, H. Speisky, *J. Agric. Food Chem.* **57** (2009) 416
40. Z. Amtul, A. Rahman, R. A. Siddiqui, M. I. Choudhary, *Curr. Med. Chem.* **9** (2002) 1323
41. Z. Amtul, M. Rasheed, M. I. Choudhary, S. Rosanna, K. M. Khan, A. Rahman, *Biochem. Biophys. Res. Commun.* **319** (2004) 1053
42. M. A. Lodhi, M. A. Abbasi, M. I. Choudhart, V. U. Ahmad, *Nat. Prod. Res.* **21** (2007) 721
43. B. Halliwell, J. M. C. Gutteridge, *Biochem. J.* **219** (1984) 1
44. Y. Çetinkaya, H. Göçer, A. Menzek, İ. Gülçin, *Arch. Pharm. Chem. Life Sci.* (2011) 1
45. E. Köksal, I. Gülçin, S. Beyza, O. Sarıkaya, E. Bursal, *J. Enzyme Inhib. Med. Chem.* **24** (2009) 395.



J. Serb. Chem. Soc. 77 (10) 1363–1379 (2012)
JSCS–4358

Characterization of sirodesmins isolated from the phytopathogenic fungus *Leptosphaeria maculans*

PETAR M. MITROVIĆ^{1*}, DEJAN Z. ORČIĆ², ZVONIMIR O. SAKAČ¹,
ANA M. MARJANOVIĆ-JEROMELA¹, NADA L. GRAHOVAC¹,
DRAGO M. MILOŠEVIĆ³ and DRAGANA P. MARISAVLJEVIĆ⁴

¹*Institute of Field and Vegetable Crops, Maksima Gorkog 30, 21000 Novi Sad, Serbia,*

²*University of Novi Sad, Faculty of Sciences, Dositeja Obradovića 3, 21000 Novi Sad, Serbia,*

³*University of Kragujevac, Faculty of Agronomy, Cara Dušana 34, 32000 Čačak, Serbia and*

⁴*Institute for Plant Protection and Environment, Teodora Drajzera 9, 11000 Belgrade, Serbia*

(Received 31 December 2011, revised 10 April 2012)

Abstract: The pathogenicity of phytopathogenic fungi is associated with phytotoxins, especially with their chemical nature and quantity. Sirodesmins are phytotoxins from the epipolythiodioxopiperazines group, produced by the fungus *Leptosphaeria maculans*, which are a cause of blackleg and stem canker in oilseed rape (*Brassica napus* L.). The aim of this work was to obtain a detailed chemical profile of sirodesmins in five fungal isolates (four from Vojvodina, Serbia, and one from the Centre for Agricultural Research, Rothamsted, UK). Sirodesmins showing different phytotoxicity on treated cotyledons of cv. Quinta were separated and detected by thin layer chromatography in all analysed isolates (L.m, C-3, St-5 and S-11) except K-113, which neither contained sirodesmin congeners nor did it exhibit activity. By use of high performance liquid chromatography coupled with tandem mass spectrometer, it was possible to identify total of 10 sirodesmins, together with their precursor – phomamide. It was found that the dominant epipolythiodioxopiperazines of the investigated *L. maculans* isolates were sirodesmin PL, sirodesmin C, and their de-acetylated derivatives.

Keywords: epipolythiodioxopiperazine; thin layer chromatography; liquid chromatography; mass spectrometry; phytotoxicity.

INTRODUCTION

A number of plant pathogens produce secondary metabolites (toxins) in order to obtain nutrients from plant cells. In some fungi, the toxins have potential toxicity or carcinogenic properties that could endanger the health of humans, animals and plants.¹ In some cases, toxins cause death of plant cells to release nut-

* Corresponding author. E-mail: petar.mitrovic@ifvcns.ns.ac.rs
doi: 10.2298/JSC111231048M

rients or disrupt plant metabolism in favour of the pathogenic fungi.² Sphingolipids originating from fumonisin B₁, produced by *Fusarium* species (*Fusarium verticillioides*), cause cell death by depletion of extracellular ATP.³ Particular races of the pathogenic fungus *Cochliobolus carbonum* produce HC-toxin that does not directly destroy the cell, but inhibits the enzyme histone deacetylase by disrupting the regulatory gene in the plant cell.⁴ Many selective toxins play a role in the virulence of pathogenic fungi.^{2,5} The role of non-selective toxin in virulence is complex and the production of toxins is not always correlated with virulence.⁶ Sirodesmin PL, the product of the pathogenic fungus *Leptosphaeria maculans*, belongs to the class of epipolythiodioxopiperazines (ETPs), and is characterized by the presence of disulphide bridges.^{7,8} The diketopiperazine ring originates from cyclic dipeptides and sulphur bridges are responsible for all the known toxic effects of these molecules.⁹ Gardner⁸ stated that disulphide bridges are a key structural element for the creation of a variety of reactive forms of oxygen and for connection with the cysteine residues of proteins. It is assumed that the toxicity of ETPs could be explained by these reactions. Sirodesmin PL is a non-selective toxin that causes chlorosis and necrosis, inhibits root growth and leads to the extinction of plant cells.^{10,11} In addition, these compounds have antibacterial and antiviral properties.¹²

The aim of this study was to perform crude separation of fungal toxins using TLC, to evaluate phytotoxic effects of the separated components on oilseed rape (*Brassica napus* L.), and to identify individual toxins using liquid chromatography with a tandem mass-spectrometric detector (LC-MS-MS).

EXPERIMENTAL

Isolation of fungi and obtaining monospore culture

Infected plants of oilseed rape were collected during 2009/10 in the region of Vojvodina, Serbia. Diseased plant organs (root, basal and upper stem, leaf, flower, pod and seed) with clearly defined symptoms of the disease were used for the isolation of the fungi. Diseased tissue fragments were soaked in a 3 % solution of sodium hypochlorite for 5–10 min and then washed with sterile water and naturally dried under controlled conditions. After drying, the fragments of diseased tissue were applied to the culture medium of potato dextrose agar (PDA) (Difco, Detroit, USA) that had previously been poured into petri plates. To prevent bacterial growth in the medium, 50 mg of streptomycin sulphate (Galenika, Belgrade, Serbia) was added per litre. The inoculated petri plates were incubated at 25±1 °C. After 5 to 10 days, the formation of pycnidia and pycnidiospores was observed under a stereo microscope. Pure cultures were obtained by the following procedure: pycnidiospores, which were released from pycnidia serving as a single droplet originating from the culture media, were transferred with the tip of a spear needle into plastic tubes to which 2 mL of sterile water had previously been added. The prepared suspension of conidia was applied onto the aqueous agar medium, which had previously been poured into petri plates. After 48 h, germination of the conidia was observed under a stereo microscope. The germinated conidia, together with fragments of the substrate, were transferred onto PDA medium in petri plates and placed in an incubator at 25 °C in order to develop monospore fungal isolates. In this way, 123 isolates of fungi were ob-

tained. All isolates were analysed at the morphological and molecular level. Based on morphological (colony appearance, shape, size and colour of the pycnidia and piconspores^{13,14}) and molecular characteristics (Polymerase Chain Reaction – Restriction Fragment Length Polymorphism, PCR–RFLP¹⁵), it was determined that 115 isolates belonged to *L. maculans* and 8 to *L. biglobosa* (data not shown). Using the method of random selection, four isolates (three of *L. maculans*, St-5, C-3 and S-11, and one of *L. biglobosa*, K-113) were taken for further research.

Extraction and isolation of phytotoxins

Four isolates of *L. maculans* were used for the extraction and isolation of the phytotoxins. Three isolates (C-3, St-5 and S-11) originated from Vojvodina and the fourth, designated L.m. (*L. maculans*) and serving as the reference isolate, was received from the Centre for Agricultural Research, Rothamsted, UK. In addition, an *L. biglobosa* culture (designated K113) was prepared as a known negative. All five isolates were sown in Czapek liquid medium,¹⁶ which had previously been poured into tubes. The tubes were placed in a climate chamber at 20 °C with 12 h photo period. After 30 days, the cultures were filtered to separate the fungus mycelium from the liquid medium.

Culture extracts were prepared and purified according to previously published procedures,^{17,18} but using a two-stage thin layer chromatography (TLC) fractionation. The culture filtrate was first extracted with ethyl acetate (6 mL of ethyl acetate per 5 mL of filtrate). The organic extract was dried with anhydrous sodium sulphate. After removal of sodium sulphate by filtration through a qualitative filter paper, the samples were evaporated under a stream of nitrogen. The residue was redissolved in 100 µL of chloroform at room temperature. The chloroform solution was applied on a TLC plate (silica gel G, 20 cm×20 cm×0.25 mm, Macherey–Nagel) using a glass capillary and the plate was developed using ethyl acetate:chloroform (1:1) as the solvent. After drying, the plate was examined under UV light (254 nm) (Fig. 1). Based on literature data,^{17,19} these spots were tentatively identified as phytotoxins. Based on the preliminary results, a larger-scale experiment (with a greater amount of media) was set up with the purpose of preparative isolation of the phytotoxins (for chemical and phytotoxic activity analysis). The final chloroform solution of the dry extract was applied on a preparative plate (silica gel G, thickness 2 mm, Macherey–Nagel), and the plate was developed by the aforementioned procedure. Three spots were detected under UV light, designated 1 ($R_f = 0.15$), 2 ($R_f = 0.44$) and 3 ($R_f = 0.60$). The spots were removed from plates and individually extracted in absolute ethanol (20 mL) at room temperature with shaking for 2 h. The spot 2 extract was evaporated under a N₂ stream and further separated using an additional TLC plate by the aforementioned procedure, yielding fractions 2a ($R_f = 0.49$), 2b ($R_f = 0.40$), 2c ($R_f = 0.32$) and 2d ($R_f = 0.22$). Spots were removed and extracted as described above. All the obtained extracts were purified on a Sephadex column (SPE Bakerbond Sephadex G-25) previously conditioned with 10 mL of ethanol. The ethanol filtrate was evaporated under a N₂-stream, and the dry residue was used in the identification of phytotoxins using the LC–MS–MS method.

LC–MS–MS characterization of phytotoxins

Chemical composition of obtained fractions was determined by reversed-phase high-performance liquid chromatography (Agilent Technologies Series 1200 Rapid Resolution liquid chromatograph) coupled with tandem mass spectrometric detection (Agilent Technologies Series 6410A Triple-Quad mass spectrometer with an electrospray ion source). 1 µl of undiluted sample was injected into the system. The components were separated using a Zor-

bax Eclipse XDB-C18 rapid resolution column 50 mm×4.6 mm, 1.8 µm (Agilent Technologies), held at 40 °C. The samples were eluted using the gradient mode: 0 min 30 % B, 7–10 min 100 % B (phase A being 0.1 % aqueous formic acid and phase B – 0.1 % formic acid in acetonitrile) with a post time of 2.5 min. The mobile phase flow was 1 mL min⁻¹. The effluent was forwarded into the electrospray ion source (ESI) without flow splitting. The ESI parameters were as follows: nebulizer pressure 40 psi, drying gas temperature 350 °C, drying gas flow 9 L min⁻¹, capillary voltage 4000 V and fragmentor voltage 100 V. All samples were analyzed in the MS2Scan mode (MS¹ experiment), using positive polarity, in the *m/z* range 150–900. Afterwards, the representative sample (St-5/2b) was analyzed in the Product Ion Scan mode (MS² experiment), using [M+H]⁺ of suspected sirodesmins peaks as precursor ions, and a collision voltage of 0–30 V (in 10 V increments). All the acquired data were processed using MassHunter Workstation – Qualitative Analysis software, ver. B.03.01 (Agilent Technologies).

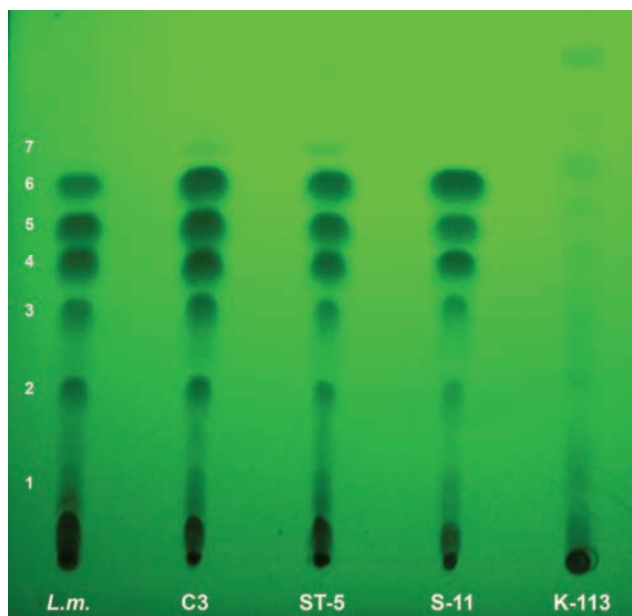


Fig. 1. Thin layer chromatogram of the ethyl acetate fraction from the culture filtrates of four *L. maculans* isolates (*L.m.* St-5, C-3 and S-11) and one *L. biglobosa* isolate (K-113). The ethyl acetate fractions were separated on silica gel with chloroform:ethyl acetate (1:1) as solvent.

The compounds were examined under UV light (254 nm). Fractions 1–7 (*R_f* values: 0.11, 0.17, 0.27, 0.34, 0.42, 0.51 and 0.60). These findings are in accordance with previously published results.^{10–14}

Phytotoxicity test

Fractions 1, 2a, 2b, 2c, 2d and 3 from the preparative plate were extracted in ethanol and diluted with water to final ethanol concentration of 0.5 % by volume. Different toxin fractions were applied as small 5 µL droplets over a puncture wound on cotyledons of the oilseed rape cv. Quinta. Plants were kept at 22±2 °C and 70/80 % relative humidity in a 12 h photoperiod. Symptoms were rated after 2 days using the scale of Badawy and Hoppe:¹⁹ – (no symptoms),

+ (slight lesions), ++ (moderate lesions), +++ (severe lesions). The crude extract of isolate K-113 was used as a negative control.

RESULTS AND DISCUSSION

Identification of phytotoxins

In the LC–MS chromatograms of the investigated samples, a number of peaks were detected (Figs. 2–5) with molecular weights, isotopic profiles and fragmentation patterns in agreement with those of sirodesmins and other secondary biomolecules (Fig. 6), already detected in *Leptosphaeria* species. For convenience, all peaks were given a designation in form P xxx y, where xxx is mono-isotopic molecular weight (M_{mi}) and y is an additional letter added if several isobaric peaks were detected.

The peak with the retention time $t_r = 1.57$ min, designated P444, belongs to a compound with a mono-isotopic molecular weight of 444 Da, corresponding to either sirodesmin J (deacetylsirodesmin A) or its 1-epimer (deacetylsirodesmin PL). In MS¹ spectrum (Table I), weak signals of adduct ions were detected at m/z 445 [M+H]⁺, 467 [M+Na]⁺ and 483 [M+K]⁺, as well as a fragment ion at m/z 381 [M+H–S₂]⁺ as the base peak. The isotopic peak profile, A (100 %), A+1 (22.9 %) and A+2 (12.3 %), is in good agreement with the theoretical profile for C₁₈H₂₄N₂O₇S₂ (100 %, 22.9 %, 12.8 %). The dominant peak in the MS² spectrum is the fragment at m/z 381 [M+H–S₂]⁺. The observed neutral loss of sulphur from a polysulphide bridge is consistent with the behaviour of epipolythiodioxopiperazines (ETPs).²⁰ Both possible isomers have already been detected in *L. maculans* cultures.^{19,21–24} The R_f value of spot 4 in the thin layer chromatogram (Fig. 1) is identical to that of deacetylsirodesmin PL (synthesized from sirodesmin PL) reported by Badawy and Hoppe.¹⁹ However, it should be noted that, without obtaining the R_f value of deacetylsirodesmin A, identification with absolute certainty is not possible, especially since (unlike in the Badawy–Hoppe experiment) the extracts of *L. maculans* described herein contained significant amounts of sirodesmin A in addition to sirodesmin PL.

Peak P454, eluting at 1.42 min, corresponds to sirodesmin H (monosulphide analogue of sirodesmin PL), already identified in *L. maculans* cultures.^{22–24} In addition to the adduct ions at m/z 455 [M+H]⁺, 477 [M+Na]⁺ and 493 [M+K]⁺, the MS¹ spectrum also contains fragment ions at m/z 437 [M+H–H₂O]⁺ and 393 [M+H–H₂O–CO]⁺. The isotopic peaks profile: A (100 %), A+1 (22.6 %), A+2 (8.4 %) is consistent with the theoretical values for C₂₀H₂₆N₂O₈S (100, 24.4 and 8.9 %). In the MS² spectrum, a number of fragments were detected, corresponding to loss of alcoholic OH (as H₂O), acetyl (as ketene, C₂H₂O) and an unidentified group at $m/z=78$: 437 [M+H–H₂O]⁺, 413 [M+H–C₂H₂O]⁺, 393 [M+H–CO₂]⁺, 377 [M+H–78]⁺, 351 [M+H–CO₂–C₂H₂O]⁺, 315 [M+H–CO₂–78]⁺, etc.

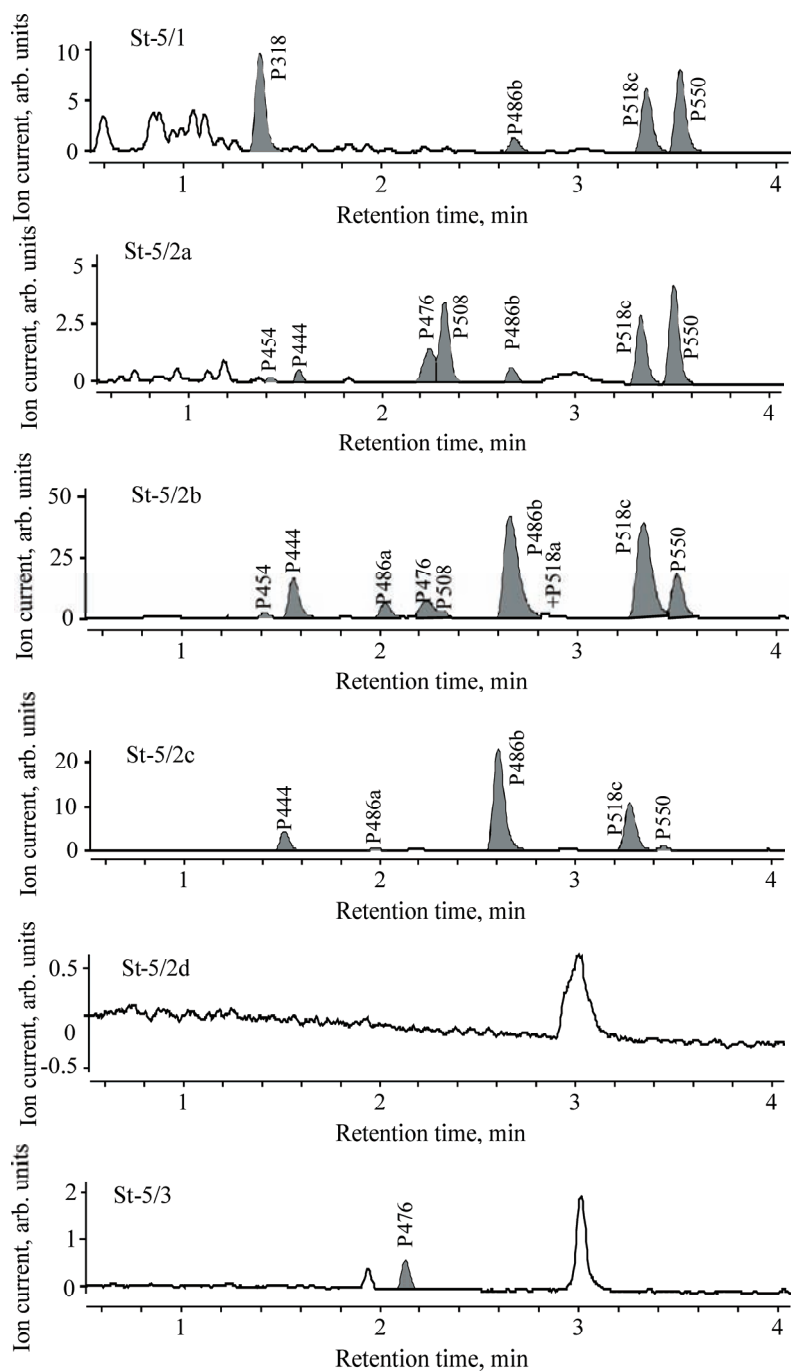


Fig. 2. LC-MS base peak chromatograms of the fractions of the St-5 isolate. The chromatographic conditions are given in the text.

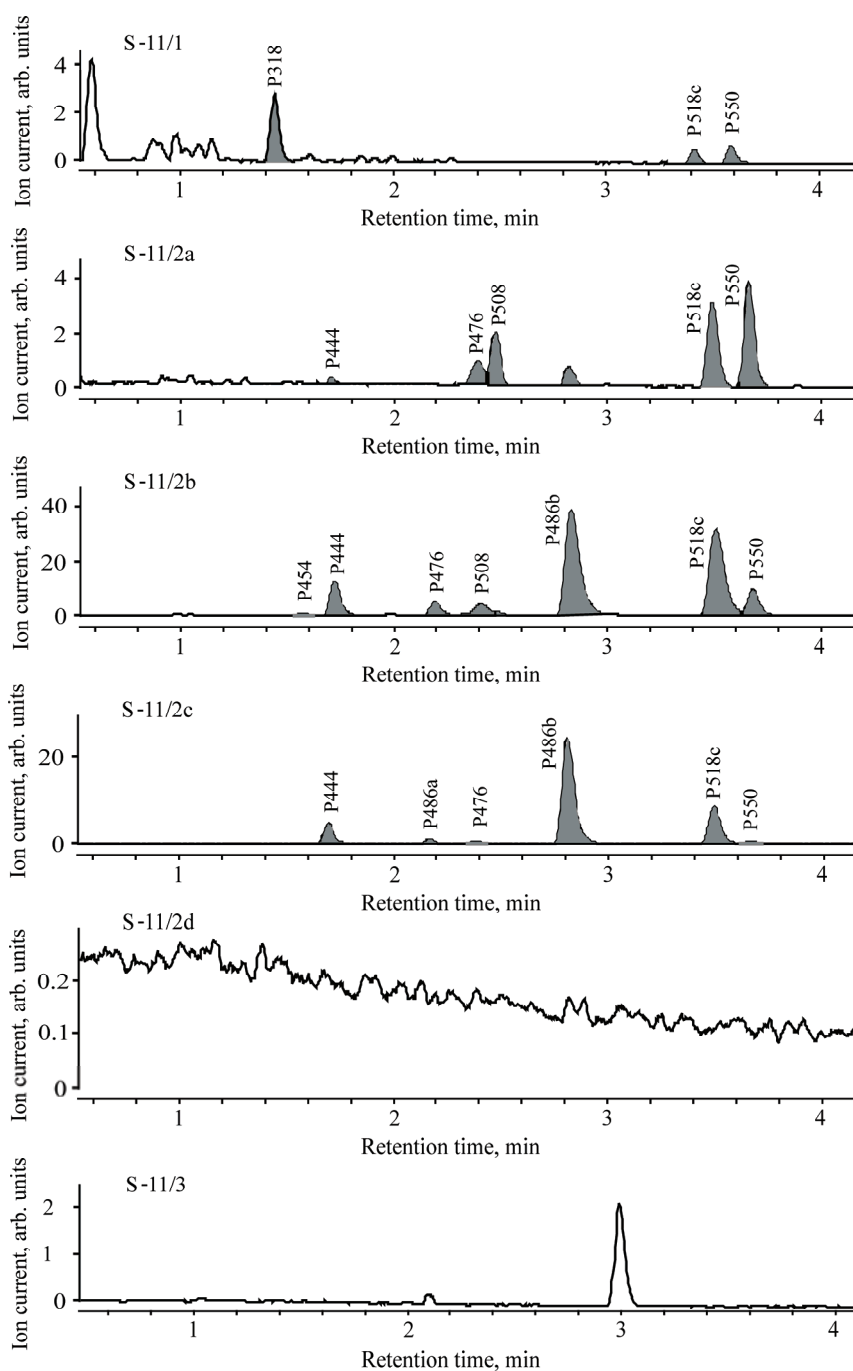


Fig. 3. LC-MS base peak chromatograms of the fractions of the St-11 isolate. The chromatographic conditions are given in the text.

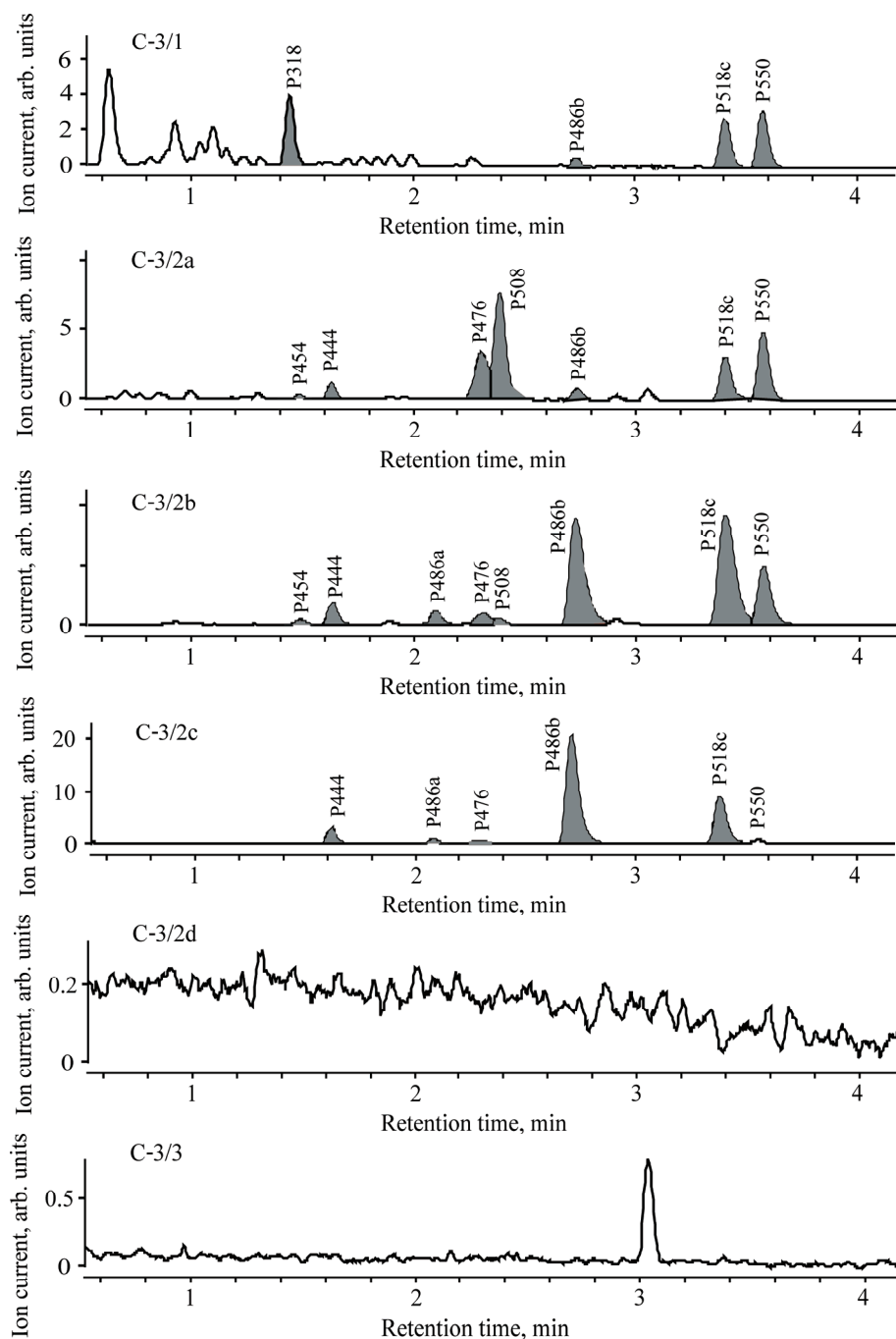


Fig. 4. LC-MS base peak chromatograms of the fractions of the C3 isolate. The chromatographic conditions are given in the text.

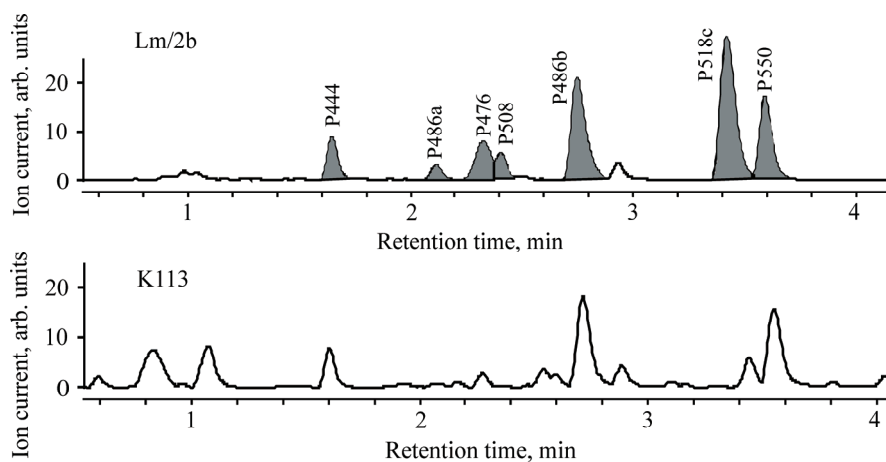
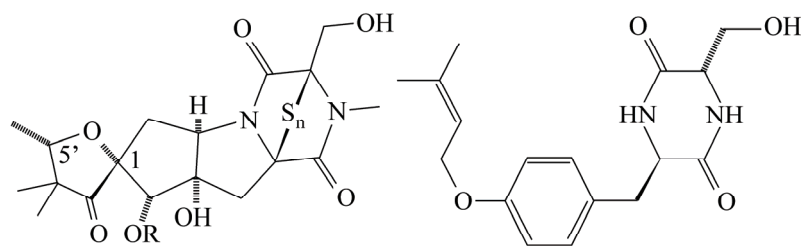


Fig. 5. Comparison of the LC-MS base peak chromatograms of L.m./2b and K-113. While several peaks with similar t_R were detected in both samples, they do not represent same compounds (as they differ completely in their mass spectra).



- n=1, R=Ac sirodesmin H
- n=2, R=H sirodesmin J, 1-*epi*-sirodesmin J
- n=2, R=Ac sirodesmin A, sirodesmin PL
- n=3, R=H de-*O*-acetylsirodesmin C/F
- n=3, R=Ac sirodesmin C/F
- n=4, R=H de-*O*-acetylsirodesmin B/E/K
- n=4, R=Ac sirodesmin B/E/K

phomamide

Fig. 6. Structures of the detected epipolythiodioxopiperazines.

The MS¹ spectrum of peak P476, eluting at 2.22 min, contains (in addition to the low-abundance of adducts with H⁺, Na⁺ and K⁺) an intense peak of a fragment at m/z 381 [M+H-S₃]⁺. The molecular weight and the loss of an S₃-unit point out to deacetylsirodesmin C or F. Badawy and Hoppe already reported deacetylated sirodesmin C as a component of *L. maculans* extract, with an *R_f* value close to that of the spot designated 3 in Fig. 1.¹⁹ However, due to lack of information on its epimer behaviour, compound P476 can only be tentatively identified as deacetylsirodesmin C (which stems from the more abundant epimer, sirodesmin PL). The experimental isotopic peak profile is in good agreement with the theoretical profile for C₁₈H₂₄N₂O₇S₃: 100, 25.0 and 17.2 % vs. 100, 23.7 and

17.4 % for A, A+1 and A+2, respectively. The MS² spectrum features fragment m/z 381 [M+H-S₃]⁺ as a base peak, accompanied by m/z 353 [M+H-S₃-CO]⁺ and 325 [M+H-S₃-2CO]⁺. The same fragment ions were detected in the MS² of peak P444, differing only in the number of sulphur atoms in the bridge, which supports the assumed structure.

TABLE I. Positive ionization MS¹, MS² and pseudo-MS³ spectra of the detected compounds (V_c – collision voltage)

Peak	Id	Order	V_c / V	Adduct and product ions, m/z (abundance)
P318	Phomamide	MS ¹	–	659 (6), 357 (8), 341 (16), 319 (43), 251 (100)
P444	Deacetylsirodesmin J or 1- <i>epi</i> -deacetylsirodesmin J	MS ¹	–	483 (7), 467 (5), 445 (9), 381 (100)
		MS ²	0	445 (30), 381 (100)
			10	381 (100), 363 (10)
			20	381 (100), 363 (22), 158 (6)
			30	381 (100), 353 (47), 325 (41), 229 (53), 205 (95), 193 (42), 140 (47)
P454	Sirodesmin H	MS ¹	–	493 (22), 477 (14), 455 (100), 437 (33), 393 (21)
		MS ²	0	455 (100), 437 (40), 413 (10), 393 (29), 377 (10)
			10	437 (9), 413 (41), 393 (100), 377 (25), 351 (17), 315 (32), 279 (18)
			20	413 (14), 393 (100), 351 (71), 315 (55), 279 (40), 245 (8), 217 (31)
			30	393 (13), 351 (100), 323 (9), 245 (12), 217 (78)
P476	Deacetylsirodesmin C or F	MS ¹	–	515 (8), 477 (13), 381 (100)
		MS ²	0	477 (43), 381 (100)
			10	381 (100)
			20	381 (100)
			30	381 (100), 253 (33), 325 (18), 205 (16), 140 (15)
P486a	Sirodesmin A	MS ¹	–	525 (14), 509 (13), 487 (100), 423 (50)
		MS ²	0	487 (100), 423 (79)
			10	423 (100)
			20	423 (100), 229 (15), 140 (10)
			30	423 (100), 395 (19), 367 (34), 246 (26), 229 (83), 219 (13)
P486b	Sirodesmin PL	MS ¹	–	525 (6), 487 (14), 423 (100)
		MS ²	0	487 (28), 423 (100), 409 (5)
			10	423 (100)
			20	423 (100), 327 (15), 346 (21), 229 (63)
			30	423 (19), 246 (47), 229 (100), 217 (19), 140 (19)
P508	Deacetylsirodesmin B, D, E or K	MS ¹	–	547 (6), 381 (100)

TABLE I. Continued

Peak	Id	Order	V_c / V	Adduct and product ions, m/z (abundance)	
P518a	Sirodesmin F	MS ¹	–	557 (19), 541 (24), 519 (100)	
		MS ²	0	423 (100)	
			10	423 (100)	
			20	423 (100), 229 (8)	
			30	423 (100), 395 (29), 367 (14), 246 (21), 229 (69), 219 (19), 140 (22)	
P518a	Sirodesmin F	MS ^{3a}	0	423 (100)	
			10	423 (100), 327 (19), 229 (33)	
			20	423 (17), 229 (100), 219 (7)	
			30	229 (100), 219 (9), 201 (7), 173 (7)	
			P518b	Unknown	MS ¹
MS ²	0	501 (16), 441 (20), 423 (100), 345 (8)			
	10	423 (100), 345 (41)			
	20	423 (78), 345 (100), 246 (46)			
	30	423 (33), 345 (100), 246 (32), 229 (14), 217 (44), 205 (44)			
MS ³	0	423 (100)			
	10	423 (100)			
	20	423 (100), 395 (25), 367 (41), 305 (15), 229 (22), 223 (12), 219 (25)			
	30	367 (45), 305 (53), 229 (65), 219 (100), 201 (40), 191 (43), 188 (57)			
	P518c	Sirodesmin C			MS ¹
			MS ²	0	423 (100)
10				423 (100)	
20				423 (100), 229 (5)	
30				423 (100), 395 (15), 367 (28), 246 (28), 229 (36), 140 (10)	
MS ³			0	423 (100)	
			10	423 (100), 327 (14), 229 (30)	
	20	423 (25), 229 (100)			
P550	Sirodesmin B	MS ¹	–	589 (4), 423 (100)	

^aPseudo-MS³ spectrum of ion 423 obtained by in-source fragmentation

Two peaks of compounds with a monoisotopic molecular weight of 486 were detected: P486a (eluting at 2.03 min) and P486b (at 2.66 min). The two corresponding compounds, sirodesmin A and sirodesmin PL (also designated G), are epimers and, thus, it was not possible to distinguish them solely using their mass spectra. From their relative amounts and knowing that sirodesmin PL is the dominant phytotoxin of *L. maculans*,^{6,8,20,22–25} it could be assumed that peak P486a corresponds to sirodesmin A, while P486b represents the PL isomer. The *R_f* value of spot 6 (0.51) in the thin layer chromatogram is very similar to that of the sirodesmin PL reference standard (0.50) reported by Badawy and Hoppe.¹⁹

The MS¹ spectrum of both peaks are similar, containing H⁺, Na⁺ and K⁺-adduct ions, as well as an intense fragment peak at m/z 423 [M+H-S₂]⁺, which is in agreement with previous results.⁶ The isotopic peak profile for A, A+1 and A+2 ions is 100, 25.0 and 14.0 % for P486a and 100, 23.6 and 14.2 % for P486b, which supports the assumed formula C₂₀H₂₆N₂O₈S₂ (theoretical profile: 100, 25.2 and 13.5 %). The most abundant fragments in the MS² spectra of both peaks were: 423 [M+H-S₃]⁺, 395 [M+H-S₃-CO]⁺, 367 [M+H-S₃-2CO]⁺, 246 and 229.

Peak at 2.32 min, designated P508, exhibited minute ions at m/z 531 [M+Na]⁺ and 547 [M+K]⁺ and 381 [M+H-S₄]⁺, as the base peak, in the MS¹ spectrum. Based on its molecular weight, as well as the observed loss of an S₄-unit, it could be assumed that the compound is a tetrasulphide homologue of deacetylsirodesmin A or PL, *i.e.*, deacetylsirodesmin B, D, E or K. For a more precise identification, its isolation and acquisition of its NMR spectrum would be necessary. None of possible isomers is indexed in the Dictionary of Natural Products (up to 2007),²⁶ but sirodesmin K has already been found in *L. maculans*.²⁴ It should be noted that Badawy and Hoppe succeeded in synthesising deacetylsirodesmin B (by sulphurization of previously deacetylated sirodesmin PL). While no spot at a corresponding *R_f* value (0.13) was observable in their unmodified *L. maculans* extract,¹⁹ well-defined spots at *R_f* = 0.17 are present in extracts described herein. It remains unclear whether it corresponds to sirodesmin B or one of the other isomers.

Three peaks corresponding to compounds with $M_{mi} = 518$ were detected: the weak P518a ($t_r = 2.71$ min) and P518b (2.92 min) and the abundant P518c (3.34 min). The MS¹ spectra of all three compounds feature H⁺, Na⁺ and K⁺ adducts, as well as intense fragment m/z 423 [M+H-S₃]⁺. Two isomeric trisulphide sirodesmins with $M_{mi} = 518$ are known, *i.e.*, sirodesmin C and F.²⁶ The theoretical isotopic profile for the A, A+1 and A+2 ions of these compounds, with empirical formula C₂₀H₂₆N₂O₈S₃, is 100, 26.0 and 18.1 %, which is in good agreement with the experimental data: 100, 26.5 and 17.2 % for P518a, 100, 26.3 and 16.3 % for P518b and 100, 26.6 and 18.8 % for P518c. Since sirodesmins C and F are 1-epimers, similarity of their MS² spectra is to be expected. Indeed, the MS² fragmentation patterns of P518a and P518c show remarkable similarity, with m/z 423 [M+H-S₃]⁺ as the base peak, accompanied by m/z 395 [M+H-S₃-CO]⁺, 367 [M+H-S₃-2CO]⁺, 246, 229 and 140. It is likely that P518c represents sirodesmin C, which is known to be one of the main sirodesmins in *L. maculans*.¹⁹ In that case, P518a is probably sirodesmin F, which was reported in *Sirodesmium diversum*, but not in *L. maculans* (probably due to co-elution with some of major ETPs – sirodesmin PL in the present experiments).²⁶ The *R_f* value of spot 5 in the TLC chromatogram is identical to that of sirodesmin C, as determined by Badawy and Hoppe.¹⁹ The MS² spectrum of the third peak, P518b, differs significantly from those of the other two – while base peak is m/z 423, several fragment ions that are absent in the other two peaks are observable, including an intense peak at m/z

345 [M+H-S₃-78]⁺, as well as 501 [M+H-H₂O]⁺ and 441 [M+H-78]⁺. It is possible that P518b represents an isomer of sirodesmin C and F with the acetyl attached at a different position (at C2a-OH or hydroxymethyl).

The peak at 3.51 min, designated P550, contains a weak signal at *m/z* 589 [M+K]⁺ and an intense one at *m/z* 423 [M+H-S₄]⁺ in MS¹ spectrum. The molecular weight and the loss of a tetrasulphide unit indicate to a tetrasulphide homologue of sirodesmin A (or one of its isomers), *i.e.*, sirodesmin B, D, E or K. Both sirodesmins B and K have already been reported in *L. maculans* cultures, while sirodesmin E was found in *S. diversum*.^{19,22-24,26}

Peak P318, eluting at 1.39 min, was detected only in fractions designated as 1. The MS¹ spectrum features a fragment at *m/z* 251 as the base peak, as well as adduct ions *m/z* 319 [M+H]⁺, 341 [M+Na]⁺, 357 [M+K]⁺ and 659 [2M+Na]⁺. This peak corresponds to dioxopiperazine phomamide, a biosynthetic precursor of sirodesmins, which was already detected in *L. maculans* cultures²²⁻²⁴. The fragment *m/z* 251 corresponds to the loss of *O*-bound prenyl as C₅H₅. The isotopic peaks profile: A (100 %), A+1 (18.0 %), A+2 (2.8 %) is in agreement with the assumed formula C₁₇H₂₂N₂O₄ (theoretical: 100, 20.1 and 2.7 %).

Phomalide, phomaligols, polanzrazins, leptomaculins and maculansins, previously identified in *L. maculans*, were not detected in the investigated samples. However, it is well known that the nature of the synthesized metabolites is strongly dependent on both growing medium and on *L. maculans* group and subgroup.²⁰⁻²⁵

Chemical profile of L. maculans extracts

Since reference standards for sirodesmins were not available, the absolute concentrations of the detected compounds in the samples could not be determined. However, it was possible to compare the differences in content of each compound throughout the fractions. It was observed that the bulk of the identified sirodesmins were contained within the fraction (preparative TLC spot) designated 2b. For the majority of compounds, only a small percentage was present in fractions 2a and 2c, with the exception of compounds with the strongest signals (sirodesmin PL, sirodesmin C and P444), that diffused into 2c spot to a greater extent. Another exception is P318 (phomamide), which occurs exclusively in fraction 1. Fractions 2d and 3 were practically devoid of sirodesmins.

Due to differences in the response factors, which are to be expected when using ESI-MS, the peak areas (given in Table II) can only be treated as a rough approximation of relative abundances within a sample. However, in our opinion, it is safe to assume the protonation constants of the sirodesmin congeners are sufficiently comparable to be able to state that the dominant ETP components of the investigated *L. maculans* cultures were sirodesmins PL and C, and their deacetylated derivatives, which is in agreement with previous results.¹⁹ These results are also supported by the TLC plates (Fig. 1).

There was no significant difference between investigated *L. maculans* extracts. No sirodesmins were found in the reference extract K113 prepared from an *L. biglobosa* culture (Fig. 5.). This indicates that sirodesmins could be employed as markers for the differentiation of two species – *L. maculans* and *L. biglobosa*.

TABLE II. Relative abundances of sirodesmin congeners, given as peak areas calculated from extracted ion chromatograms. For each compound, all abundant adduct and fragment ions were taken into account

Extract fraction	Peak areas, arb. units										
	P318	P444	P454	P476	P486a	P486b	P508	P518a	P518b	P518c	P550
St-5/1	324	0	46	8	0	45	12	7	1	160	181
St-5/2a	0	16	16	53	0	24	82	5	1	73	89
St-5/2b	0	485	79	290	338	2086	56	119	34	1423	461
St-5/2c	0	121	10	30	38	855	2	9	2	286	22
St-5/2d	0	0	0	0	0	0	0	0	0	0	0
St-5/3	0	0	0	0	0	3	0	0	0	2	0
C-3/1	106	0	17	5	0	15	6	1	0	56	56
C-3/2a	0	35	22	124	4	30	182	10	0	80	104
C-3/2b	0	232	87	164	261	1706	39	138	35	1307	524
C-3/2c	0	80	12	18	41	802	2	10	2	238	18
C-3/2d	0	0	0	0	0	0	0	0	0	0	0
C-3/3	0	0	0	0	0	3	0	0	0	4	1
S-11/1	103	0	6	0	0	5	3	0	0	16	18
S-11/2a	0	12	15	33	2	26	41	1	6	75	79
S-11/2b	0	370	35	159	263	1739	23	76	18	1014	232
S-11/2c	0	137	6	22	50	966	2	9	2	232	12
S-11/2d	0	0	0	0	0	1	0	0	0	2	1
S-11/3	0	0	0	0	0	0	0	0	0	1	0
L.m./2a	0	443	4	136	131	383	0	32	1	90	5
L.m./2b	0	252	31	353	185	924	129	227	19	971	476
L.m./2c	0	24	1	109	13	53	156	30	1	165	200
L.m./2d	0	44	0	121	2	19	121	7	1	45	38
L.m./3	0	141	0	103	10	218	23	8	1	150	29
K113	0	0	0	0	0	0	0	0	2	3	1

Phytotoxicity of the sirodesmin fractions

Fractions 2b and 2c produced the most severe lesions (+++) on cotyledons for all four isolates (C-3, St-5, S-11 and L.m). Fraction 2a showed moderate phytotoxicity (++) except for isolate C-3, which was rated as slightly phytotoxic (+). Slight phytotoxicity was also observed for fraction 1 (all isolates). Fractions 2d and 3 of all isolates of *L. maculans* and K-113 (*L. biglobosa*) did not produce any lesions on cotyledons. The whitish spots on these cotyledons were the consequence of epidermis damage by the needle. The phytotoxicity activity of the fraction (Fig. 7) is in agreement with the results of LC–MS analysis, when the

presence of phytotoxic sirodesmins in fractions 1, 2a, 2b and 2c was clearly confirmed, which is also in accordance with the results of Badawy and Hope.^{10,19}

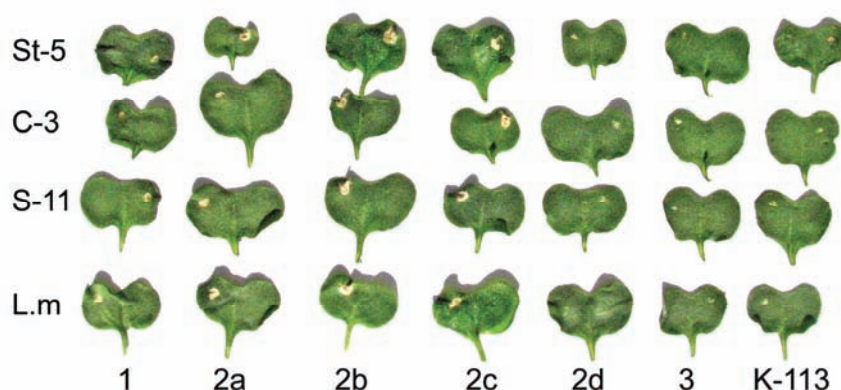


Fig. 7. Phytotoxic effects of the fractionated *Leptosphaeria* isolates on *Brassica napus* cv. Quinta cotyledons.

While it is known that a polysulphide bridge in the diketopiperazine ring is responsible for the observed toxic effects (while the nature of side groups does not affect toxicity), and the reduction thereof leads to complete loss of activity, the exact mechanism of toxicity is still a matter of debate.^{7,8} It was demonstrated that ETPs non-selectively form mixed disulphide bonds with various cysteine-containing proteins, such as NF- κ B (thus accounting for immunosuppressive effects of ETPs) and alcohol dehydrogenase. In addition, they can catalyze the formation of intramolecular disulphide bonds between physically close Cys residues within some proteins, including creatine kinase. However, the exact consequences of ETPs binding to proteins are still unknown. Other theories explain the toxicity of ETPs through redox cycling. A polysulphide bridge is easily reduced in cells; the spontaneous auto-oxidation back to disulphide could generate various reactive oxygen species (ROS), including H_2O_2 and $\text{O}_2^{\bullet-}$, that are known to cause adverse effects on cell constituents. However, the concentrations of ETPs that exhibit toxic effects would cause negligible oxidative stress; moreover, some effects (including apoptosis) were proved not to be ROS-related.⁸

Regardless of the mechanism (or a combination thereof) that is responsible for the phytotoxic effects of ETPs, activity could be expected for all detected polysulphide-bridge containing sirodesmins, although it is likely that only the dominant components contribute significantly, as indicated by Badawy and Hoppe.¹⁹

CONCLUSIONS

The results obtained by thin-layer chromatography and high-performance liquid chromatography with mass spectrometric detection demonstrated the pre-

sence of sirodesmins in all the examined fungal culture isolates from Serbia (C-3, St-5, S-11) except for K-113. It was found that the dominant epipolythiodioxo-piperazines in the investigated *L. maculans* isolates were sirodesmin PL, sirodesmin C, and their deacetylated derivatives. The isolated sirodesmins exhibited phytotoxicity on oilseed rape (*Brassica napus* L.) and may act as virulence factors, contributing to development of *Leptosphaeria maculans*-caused disease. However, no sirodesmins were detected in *L. biglobosa*, suggesting these compounds as markers for the differentiation of the two species. These results are the first indication of the presence of two *Leptosphaeria* species in Serbia – *L. maculans* and *L. biglobosa*.

Acknowledgment. This study is a part of the TR 31025 project financially supported by the Ministry of Education, Science and Technological Development of the Republic of Serbia.

ИЗВОД

КАРАКТЕРИЗАЦИЈА СИРОДЕЗМИНА ИЗОЛОВАНИХ ИЗ ФИТОПАТОГЕНЕ ГЉИВЕ
Leptosphaeria maculans

ПЕТАР М. МИТРОВИЋ¹, ДЕЈАН З. ОРЧИЋ², ЗВОНИМИР О. САКАЧ¹, АНА М. МАРЈАНОВИЋ-ЈЕРОМЕЛА¹,
НАДА Л. ГРАХОВАЦ¹, ДРАГО М. МИЛОШЕВИЋ³ и ДРАГАНА П. МАРИСАВЉЕВИЋ⁴

¹Институт за растарство и површарство, Максима Горког 30, 21000, Нови Сад, ²Природно-математички факултет, Универзитет у Новом Саду, Доситеја Обрадовића 3, 21000, Нови Сад,

³Агрономски факултет, Универзитет у Крагујевцу, Цара Душана 34, 32000 Чачак и

⁴Институт за заштитиу биља и животињу средину, Теодора Драјзера 9, 11000, Београд

Патогеност фитопатогених гљива повезана је са фитотоксинима, а нарочито са њиховом хемијском природом и количином. Сиродезмини су фитотоксини из групе епиполитиодиоксопиперазина, које производи гљива *Leptosphaeria maculans*, узрочник суве трулежи корена и рака стабла уљане репице. Циљ овог рада била је детаљна хемијска карактеризација сиродезмина у пет изолата гљива (четири из Војводине и један из Велике Британије, Центар за пољопривредна истраживања, Rothamsted). Код свих испитиваних изолата (*L. maculans*, C-3, St-3, S-11), осим K-113 (који није садржао сиродезмине нити показивао активност) танкослојном хроматографијом су раздвојени и детектовани сиродезмини који су показали различиту фитотоксичност на третираним котиледонима сорте Quinta. Применом течне хроматографије високе ефикасности, купловане са тандемским масеним спектрометром, било је могуће идентификовати укупно 10 сиродезмина, као и њихов прекурсор – фомамид. Утврђено је да су доминантни епиполитиодиоксопиперазини испитиваних изолата *L. maculans* сиродезмин PL, сиродезмин C и њихови деацетиловани деривати.

(Примљено 31. децембра 2011, ревидирано 10. априла 2012)

REFERENCES

1. M. Bohnert, B. Wackler, D. Hoffmeister, *Appl. Microbiol. Biotechnol.* **87** (2010) 1
2. B. J. Howlett, *Curr. Opin. Plant Biol.* **9** (2006) 371
3. S. Chivasa, K. B. Ndimba, J. W. Simon, K. Lindsey, R. A. Slabas, *Plant Cell* **17** (2005) 3019
4. D. Baidyaroy, G. Brosch, S. Graessle, P. Trojer, D. J. Waton, *Eukaryot. Cell* **1** (2002) 538

5. J. T. Wolpert, D. L. Dunkle, M. L. Ciuffetti, *Annu. Rev. Phytopathol.* **40** (2002) 251
6. E. C. Elliott, M. D. Gardiner, G. Thomas, J. A. Cozijnsen, A. Van de Wouw, B. J. Howlet, *Mol. Plant. Path.* **8** (2007) 791
7. D. M. Gardiner, J. A. Cozijnsen, M. L. Wilson, M. S. C. Pedras, B. J. Howlet, *Mol. Microbiol.* **53** (2004) 1307
8. D. M. Gardiner, P. Waring, B. J. Howlet, *Microbiology* **151** (2005) 1021
9. A. Mullbacher, P. Waring, U. Tiwari-Palni, D. R. Eichner, *Mol. Immunol.* **23** (1986) 231
10. H. M. A. Badawy, H. H. Hoppe, *J. Phytopathol.* **127** (1989) 137
11. M. E. Fox, B. J. Howlet, *Mycol. Res.* **112** (2008) 162
12. T. Rouxel, Y. Chupeau, R. Fritz, A. Kollmann, F. J. Bousquet, *Plant Sci.* **57** (1988) 45
13. E. Punithalingam, P. Holliday, *Phoma lingam, C.M.I. Description of pathogenic fungi and bacteria*, No. 331, Commonwealth Mycological Institute, Kew, UK, 1972
14. B. D. L. Fitt, H. Brun, M. J. Barbetti, S. R. Rimmer, *Eur. J. Plant Pathol.* **114** (2006) 3
15. M. H. Balesdent, M. Jedryczka, L. Jain, E. Mendes-Pereira, J. Bertrand, T. Rouxel, *Phytopathology* **88** (1998) 1210
16. C. D. McGee, A. G. Petrie, *Phytopathology* **68** (1978) 625
17. E. Koch, A. M. H. Badawy, H. H. Hoppe, *J. Phytopathol.* **124** (1989) 52
18. M. S. C. Pedras, J. C. Bisesenthal, *Phytochemistry* **58** (2001) 905
19. H. M. A. Badawy, H. H. Hoppe, *J. Phytopathol.* **127** (1989) 146
20. B. J. Howlett, A. Idnurm, M. S. C. Pedras, *Fungal Genet. Biol.* **33** (2001) 1
21. M. S. C. Pedras, P. B. Chumala, Y. Yu, *Can. J. Microbiol.* **53** (2007) 364
22. M. S. C. Pedras, Y. Yu, *Bioorg. Med. Chem.* **16** (2008) 8063
23. M. S. C. Pedras, Y. Yu, *Phytochemistry* **69** (2008) 2966
24. M. S. C. Pedras, G. Séguin-Swartz, *Can. J. Plant Pathol.* **14** (1992) 67
25. Z. J. Wu, G. Y. Li, D. M. Fang, H. Y. Qi, W. J. Ren, G. L. Zhang, *Anal. Chem.* **80** (2008) 217
26. J. Buckingham, Ed., *Dictionary of Natural Products*, Version 15.1 on CD-ROM, Chapman & Hall/CRC, Boca Raton, USA, 2007.



J. Serb. Chem. Soc. 77 (10) 1381–1389 (2012)
JSCS–4359

Kinetic behaviour of the DPPH radical-scavenging activity of tomato waste extracts

SLADJANA M. SAVATOVIĆ, GORDANA S. ČETKOVIĆ*^{##},
JASNA M. ČANADANOVIĆ-BRUNET[#] and SONJA M. DJILAS[#]

*Faculty of Technology, University of Novi Sad, Bulevar cara Lazara 1,
21000 Novi Sad, Serbia*

(Received 10 April, revised 16 June 2012)

Abstract: The kinetic behaviour of tomato waste extracts (obtained from six genotypes) and standard antioxidant compounds (ascorbic and caffeic acid) were investigated using the 2,2-diphenyl-1-picrylhydrazyl radical test. Based on the time required for the reaction to reach steady state, the investigated extracts showed very slow (steady state ≥ 180 min) antiradical behaviour, ascorbic acid acted as a rapid antioxidant (steady state < 5 min) while caffeic acid is a rapid–intermediate antioxidant ($5 \text{ min} < \text{steady state} < 20 \text{ min}$). The efficient concentrations at different kinetic times $EC_{50,t}$ were determined for all extracts, as well as for ascorbic and caffeic acid. The $EC_{50,t}$ was used as a parameter to screen and compare antiradical activities of food extracts with slow kinetic action. Irrespective of the time considered, a comparison of the $EC_{50,t}$ values for extracts of tomato waste obtained from different tomato genotypes showed that their DPPH radicals-scavenging activity decreased in the order $O_2 > \text{Knjaz} > \text{Bačka} > \text{Saint Pierre} > \text{Rutgers} > \text{Novosadski niski}$. The tomato waste extracts showed very slow kinetic action, which is probably the result of the different kinetic behaviour of the phenolic compounds present in tomato waste, as well as other antioxidants (vitamins, carotenoids, *etc.*).

Keywords: tomato waste; DPPH radicals; free radical scavenger; kinetic behaviour.

INTRODUCTION

By-products of fruits and vegetables processing represent a major disposal problem for the industry concerned, but they are also promising sources of antioxidant compounds, which may be used for various purposes in the food, pharmaceutical and cosmetic industries.¹ The most abundant vegetable-processing waste is tomato pomace, produced in tomato juice and paste factories. It consists

* Corresponding author. E-mail: cetkovic@tf.uns.ac.rs

[#] Serbian Chemical Society member.

doi: 10.2298/JSC120410065S

of tomato peel, seeds and a part of the pulp, and contains valuable nutritional compounds (on a dry weight basis): mainly fibres (59.03 % d.w.), total sugars (25.73 % d.w.), proteins (19.27 % d.w.), pectins (7.55 % d.w.), total fats (5.85 % d.w.), minerals (3.92 % d.w.) and antioxidants.²⁻⁴

Several methods have been proposed to measure the antioxidant activity of pure compounds and plant extracts, such as FRAP (Ferric Reducing Antioxidant Power), ORAC (Oxygen Radical Absorbance Capacity), ESR (Electron Spin Resonance), ABTS (2,2-azinobis(3-ethyl-benzothiazoline-6-sulphonate) and DPPH (2,2-diphenyl-1-picrylhydrazyl).⁵ Usually, the antioxidant activity is examined at a fixed endpoint, which may not consider the kinetic characteristics of the antioxidant. However, an investigation of the kinetic behaviour could provide more complete information about the antioxidant properties and could be more important than the total antioxidant capacities determined at a fixed endpoint.⁶

The DPPH test is one of the oldest and the most frequently used methods for the determination of the antioxidant activity of food extracts.⁷⁻⁹ Some authors used different initial DPPH radical concentrations and reaction times in order to define the kinetic model for understanding the antioxidant behaviour. In the case of food extracts with very slow kinetic behaviour, the treatment of DPPH test data could be simplified to easily screen food extracts.¹⁰

The main objective of this study was to evaluate the kinetic behaviour of radical scavenging activity of tomato waste (from juice processing, obtained from different tomato genotypes – Bačka, Knjaz, Novosadski niski, O₂, Rutgers and Saint Pierre).

MATERIALS AND METHODS

Chemicals and materials

2,2-Diphenyl-1-picrylhydrazyl (DPPH), caffeic acid and L-ascorbic acid were obtained from Sigma (St. Louis, USA). All other chemicals and reagents were of the highest analytical grade.

Tomato genotypes (Bačka, Knjaz, Novosadski niski, O₂, Rutgers and Saint Pierre) grown in the fields of the Institute of Field and Vegetable Crops, Novi Sad, Serbia were taken for the experiments. The materials include new (Bačka, Knjaz, Novosadski niski and O₂) and traditional (Rutgers and Saint Pierre) genotypes.

Waste preparation and extraction procedure

Tomatoes (1 kg) of each genotype were washed and cut into four pieces and tomato juice was prepared using a juice processor Neo, SK-400. Fresh tomato waste was dried (25 °C, 1.03 mbar, 15 h, and 30 °C, 0.001 mbar, 4.5 h) in a vacuum-dryer (Alpha 2-4 LSC Martin Christ, Osterode, Germany). The weights of the dry tomato wastes were measured in triplicate.

Samples of dried tomato waste (5 g) were treated with *n*-hexane to remove non-polar compounds, then extracted with ethanol at room temperature, using a high performance homogenizer, Heidolph DIAX 900 (Heidolph Instruments, Kelheim, Germany). The extraction was performed three times with different amounts of 80 % ethanol: 80 ml in 30 min, 40 ml in 30 min and 40 ml in 15 min at room temperature. The obtained three extracts were combined and

evaporated to dryness under reduced pressure at 40 °C on a water bath. The weights of the extracts, *i.e.*, ethanol extractive values, were taken as the average of triplicate analyses.

DPPH Radical scavenging activity

The DPPH radicals scavenging activity of the tomato waste extracts was determined spectrophotometrically using the DPPH method of Espin *et al.*,¹¹ modified for this assay. Briefly, 0.5 ml of a solution containing from 0.05 to 2 mg of extract in distilled water or 0.5 ml of distilled water (control) were mixed with 1.5 ml of a 90 µM DPPH radical solution and 3 ml of methanol. The mixture was shaken vigorously and incubated at room temperature for 120 min. The absorbance at 515 nm was measured at different intervals (after 10, 20, 30, 60, 120, 150 and 180 min) using a UV-1800 spectrophotometer (Shimadzu, Kyoto, Japan) against a blank that had been prepared in a similar manner as the control, by replacing the DPPH radicals solution with methanol. The level of remaining DPPH• in the reaction medium was calculated using the following equation:

$$\text{Remaining DPPH}^\bullet (\%) = 100 \times A_{\text{Sample}} / A_{\text{Control}}$$

where A_{Control} is the absorbance of the control reaction and A_{Sample} is the absorbance in the presence of the extract measured at different time intervals.

The efficient concentration at different times $EC_{50,t}$ (mg extract mg^{-1} DPPH•) was the amount of the extracts in relation to the amount of initial DPPH•, which was calculated using the following equation:

$$EC_{50,t} = IC_{50,t} / [\text{DPPH}^\bullet]_{t=0}$$

where $IC_{50,t}$ is the inhibitory concentration at different times, defined as the concentration of extract (mg mL^{-1}) required to scavenge 50 % of DPPH• and $[\text{DPPH}^\bullet]_{t=0}$ is the initial concentration of DPPH• (mg mL^{-1}).

Ascorbic and caffeic acid were used as reference radical scavengers.

Statistical analysis

All measurements were performed in triplicate and the results are presented as mean \pm SD. The IC_{50} values were calculated using Microsoft Office Excel 2003.

RESULTS AND DISCUSSION

Waste from six tomato genotypes were obtained as by-products in juice processing. In a previous study,¹² it was shown that tomato waste contained significant amounts of hydrophilic antioxidants, polyphenolics and ascorbic acid, which were identified as being responsible for antiradical activities. Based on the significant antioxidant activity of the selected tomato waste at a fixed end-point, as well as the well known health benefits of polyphenolics and ascorbic acid, this by-product has potential as value-added ingredients for functional foods. The results of the antioxidant activity based on measurements at a fixed end-point together with those based on kinetic data provide comprehensive information on the total antioxidant property of sample.¹³ In this work, kinetic parameters were evaluated to clarify the antioxidant activity of tomato waste extracts.

The scavenging stable DPPH radicals is a widely used method to evaluate antioxidant activities due to its simple, rapid, sensitive and reproducible procedure.^{14,15} A freshly prepared DPPH solution exhibits a deep purple colour with

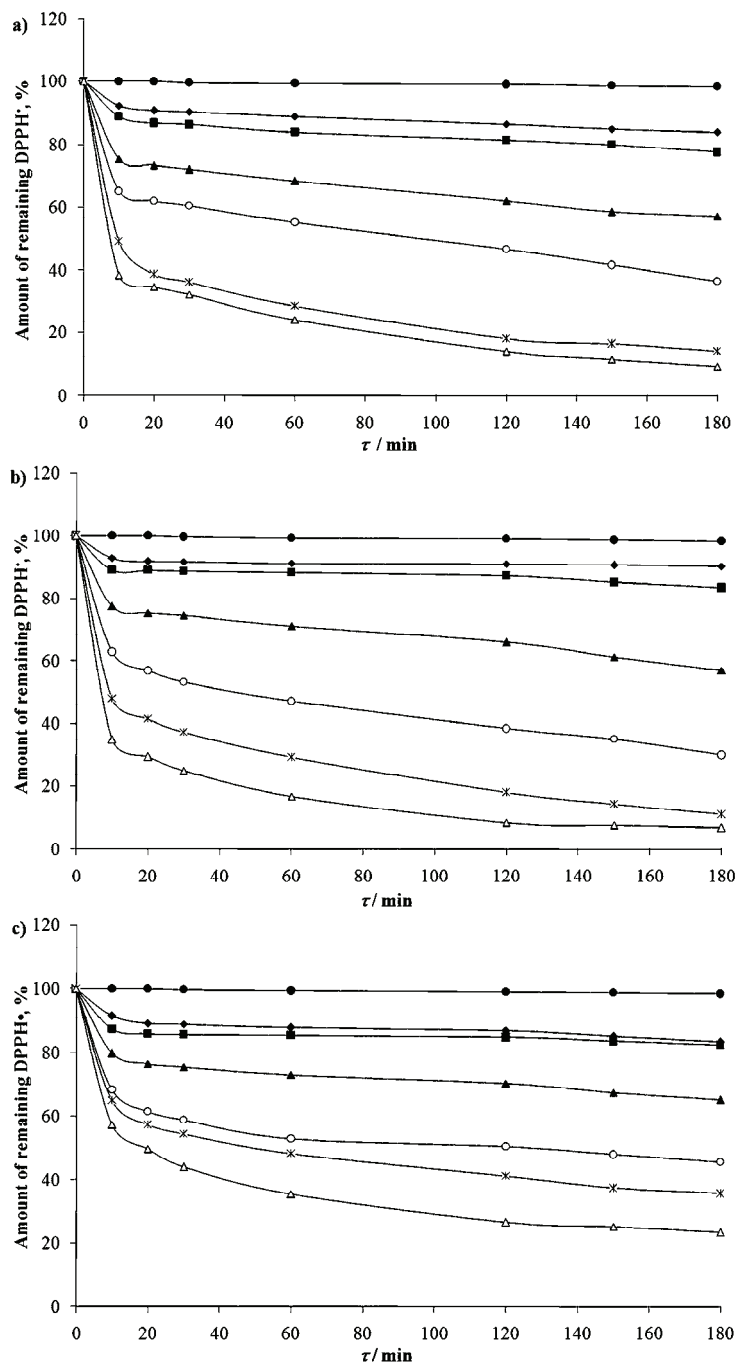
an absorption maximum at 515 nm. This purple colour generally fades/disappears when an antioxidant is present in the medium.¹⁶ Antioxidant molecules can quench DPPH free radicals (*i.e.*, by providing hydrogen atoms or by electron donation, conceivably *via* a free-radical attack on the DPPH molecule) and convert them to a colourless/bleached product (*i.e.*, 2,2-diphenyl-1-hydrazine, or a substituted analogous hydrazine), resulting in a decrease in absorbance at 515 nm.^{17,18}

Kinetic studies of the DPPH–extract reaction were performed to estimate the scavenging activity of the extracts as a function of time. The free DPPH radical is quite stable for more than 180 min at 20 °C in the reaction medium. Hence, it allows the evaluation of the radical scavenging activity of the extracts within that time. The kinetics of DPPH annihilation by different tomato waste extracts are shown in Figs. 1a–1f. Immediately after the addition of the tomato waste extracts to the reaction medium, the absorbance of DPPH at 515 nm dropped, due to the decrease of DPPH concentration in the medium. Clearly, the highest rate of DPPH decay occurs within the first 10 min of reaction. Although, the extract solutions maintained their antioxidant effect until the end of the experiment (180 min).

Based on the time required for the reaction to reach steady state, four reaction kinetic types (rapid, intermediate, slow and very slow) were found.^{8,10} For all tomato waste extracts, a steady state was not attained even after 180 min of reaction. Thus, the investigated extracts are classified as showing very slow behaviour. At each time, it was possible to compare the antioxidant activity of extracts.¹⁰ For example, in the presence of 37.04 mg of Novosadski niski extract per mg DPPH radicals, after 180 min, when the steady state was almost reached, about 23.39 % of the initial DPPH radicals remained in the medium. In the presence of the same concentration of O₂ extract, 4.40 % of initial DPPH radicals remained in the medium after the same time.

The concentrations required to decrease twofold the DPPH concentration at the chosen reaction time ($EC_{50,t}$) were calculated from the reaction kinetics obtained with different concentrations of the tomato waste extract. First, the remaining DPPH radicals percentage was plotted as function of extracts concentration at applied reaction time (10, 20, 30, 60, 120, 150 and 180 min). The $EC_{50,t}$ values were determined at all the kinetic times. The $EC_{50,t}$ values of tomato waste extracts and their kinetic classification are presented in Table I.

A lower $EC_{50,t}$ value indicates a higher DPPH radicals scavenging activity. Ascorbic and caffeic acid were used as reference radical scavengers. A comparison of the $EC_{50,t}$ values for the extracts showed that the DPPH radical scavenging activity of the extracts decreased in the order of O₂ > Knjaz > Bačka > Saint Pierre > Rutgers > Novosadski niski. The $EC_{50,t}$ value for ascorbic acid, was 0.14 mg mg⁻¹ DPPH• at 5 min (steady state < 5 min; rapid antioxidant), while the $EC_{50,t}$ value for caffeic acid was lower, 0.09 mg mg⁻¹ DPPH• at 20 min (5 min < steady state < 20 min; rapid–intermediate antioxidant). It was ob-



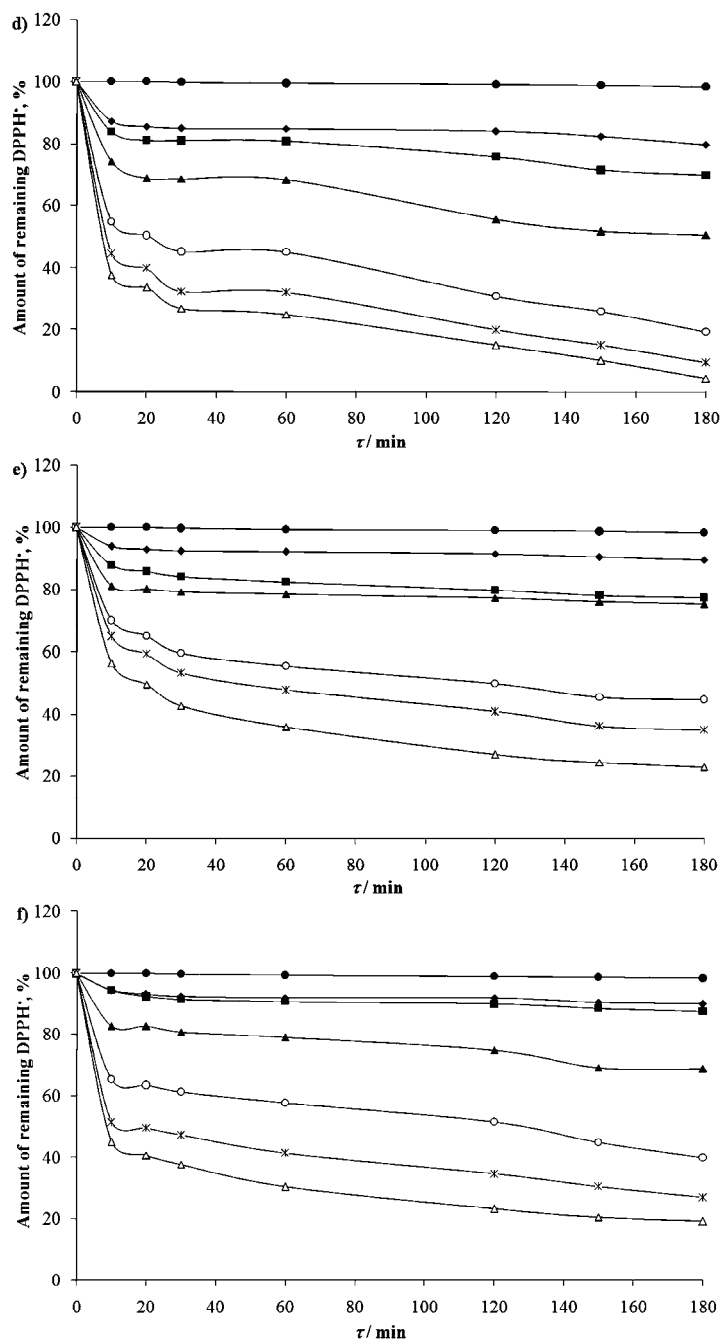


Fig. 1. Kinetic behaviour of: a) Bačka, b) Knjaz, c) Novosadski niski, d) O₂, e) Rutgers and f) Saint Pierre tomato waste extract. Concentrations of extracts in the medium are: ● 0; ◆ 0.93; ■ 1.85; ▲ 9.26; ○ 18.52; ✱ 27.50 and △ 37.04 mg extracts mg⁻¹ DPPH.

TABLE I. $EC_{50,t}$ (mg extract mg^{-1} DPPH) values of tomato waste extracts and their kinetic classification; the results are mean values of three determinations \pm standard deviation. Range of time to reach steady state: ≥ 180 min; kinetic classification: very slow

t / min	Genotype					
	Bačka	Knjaz	Novosadski niski	O ₂	Rutgers	Saint Pierre
10	27.3 \pm 1.21	26.6 \pm 1.24	47.1 \pm 2.15	22.9 \pm 1.06	46.8 \pm 2.15	30.0 \pm 1.35
20	23.3 \pm 1.08	22.7 \pm 1.04	36.9 \pm 1.64	18.9 \pm 0.87	36.6 \pm 1.71	27.6 \pm 1.26
30	22.5 \pm 1.05	20.4 \pm 0.98	31.8 \pm 1.35	16.6 \pm 0.71	30.7 \pm 1.36	26.0 \pm 1.02
60	20.3 \pm 0.96	17.4 \pm 0.76	25.4 \pm 1.20	16.6 \pm 0.65	25.0 \pm 1.05	23.0 \pm 1.00
120	16.5 \pm 0.72	14.6 \pm 0.65	19.1 \pm 0.90	11.3 \pm 0.50	18.4 \pm 0.86	17.3 \pm 0.60
150	13.9 \pm 0.54	13.2 \pm 0.52	17.6 \pm 0.85	9.9 \pm 0.42	17.1 \pm 0.64	16.6 \pm 0.63
180	12.5 \pm 0.52	11.7 \pm 0.51	16.4 \pm 0.74	9.4 \pm 0.38	16.9 \pm 0.70	15.3 \pm 0.59

served that the $EC_{50,t}$ value of the tomato waste extracts were higher than those of the individual antioxidant compounds.

According to literature data, phenolic compounds, vitamins, carotenoids, *etc.*, show different antiradical kinetic action. For example, ascorbic acid is a rapid antioxidant, caffeic acid was classified as a rapid–intermediate antioxidant, tocopherol and gallic acid show intermediate kinetic behaviour, while ferulic acid, quercetin and rutin are slow antioxidants.⁶ Furthermore, carotenoids act as intermediate or slow antioxidant.^{19,20} It can be proposed that the different kinetic behaviour of the phenolic compounds, present in tomato waste, as well as other constituents (vitamins, carotenoids *etc.*), determined the antiradical activity of this natural source of antioxidants.

CONCLUSIONS

In this study, DPPH radicals scavenging activity of tomato waste extracts (obtained from six genotypes) was applied to determine their kinetic behaviour. Expression of the results in terms of the kinetic approach not only takes into account the activity of an antioxidant, but also provides information on how quickly the antioxidant acts. All extracts showed a very slow kinetic action, which is probably result of the different kinetic behaviour of the antioxidants present in tomato waste. The chemical characteristics of the antioxidant compounds in tomato waste will be further investigated and more research is required to establish bioavailability and real benefits *in vivo*.

Acknowledgement. This research is part of the Project TR 31044 that is financially supported by the Ministry of Education, Science and Technological Development of the Republic of Serbia.

ИЗВОД

ДРРН АНТИРАДИКАЛСКО КИНЕТИЧКО ПОНАШАЊЕ
ЕКСТРАКАТА ОТПАДА ПАРАДАЈЗА

СЛАЂАНА М. САВАТОВИЋ, ГОРДАНА С. БЕТКОВИЋ, ЈАСНА М. ЧАНАДАНОВИЋ-БРУНЕТ И СОЊА М. БИЛАС

Технолошки факултет, Универзитет у Новом Саду, Булевар цара Лазара 1, 21000 Нови Сад

Кинетичко понашање екстраката отпада парадајза (добитених од шест генотипова) и антиоксидативних једињења (аскорбинска и кафена киселина) испитано је 2,2-дифенил-1-пикрилхидразил радикал тестом. На основу времена потребног за успостављање динамичке равнотеже реакције, испитивани екстракти су показали веома споро (≥ 180 min), аскорбинска киселина брзо (< 5 min), а кофеинска киселина умерено-брзо антирадикалско понашање (5 до 20 min). Ефективне концентрације у различитим кинетичким временима, $EC_{50,t}$, се користе као параметар за поређење антирадикалске активности антиоксиданата и екстраката прехранбених производа различитог кинетичког деловања и одређене су за све екстракте, аскорбинску и кофеинску киселину. Без обзира на разматрано време, поређењем $EC_{50,t}$ испитиваних екстраката утврђен је следећи редослед антирадикалске активности екстракта: $O_2 > \text{Књаз} > \text{Бачка} > \text{Сент Пјер} > \text{Rutgers} > \text{Новосадски ниски}$. Екстракти отпада парадајза су показали веома споро антирадикалско понашање, што је вероватно последица различитих кинетичких особина како фенолних једињења присутних у отпаду парадајза, тако и других присутних антиоксиданата (витамини, каротеноиди, итд.).

(Примљено 10. априла, ревидирано 16. јуна 2012)

REFERENCES

1. A. Schieber, F. C. Stintzing, R. Carle, *Trends Food Sci. Technol.* **12** (2001) 401
2. M. Del Valle, M. Cámara, M. E. Torija, *J. Sci. Food Agric.* **86** (2006) 1232
3. W. Peschel, F. Sánchez-Rabaneda, W. Diekmann, A. Plescher, I. Gartzia, D. Jiménez, R. Lamuela-Raventós, S. Buxaderas, C. Codina, *Food Chem.* **97** (2006) 137
4. D. Naviglio, F. Pizzolongo, L. Ferrara, B. Naviglio, A. Aragòn, A. Santini, *Afr. J. Food Sci.* **2** (2008) 37
5. R. Scherer, H. T. Godoy, *Food Chem.* **112** (2009) 654
6. C. Sanchez-Moreno, J. A. Larrauri, F. Saura-Calixto, *J. Sci. Food Agric.* **76** (1998) 270
7. A. K. Ratty, J. M. Sunatomo, N. P. Das, *Biochem. Pharmacol.* **37** (1988) 989
8. W. Brand-Williams, M. E. Cuvelier, C. Berset, *Food Sci. Technol.-Lebensm.-Wiss. Technol.* **28** (1995) 25
9. P. Stratil, B. Klejdus, V. Kubán, *J. Agric. Food Chem.* **54** (2006) 607
10. G. Kancsi, E. Dongo, C. Genot, *Nahrung* **47** (2003) 434
11. J. C. Espin, C. Soler-Rivas, H. J. Wichers, *J. Agric. Food Chem.* **48** (2000) 648
12. S. Savatović, G. Četković, J. Čanadanović-Brunet, S. Djilas, *Int. J. Food Sci. Nutr.* **63** (2012) 129
13. P. Terpinč, M. Bezjak, H. Abramović, *Food Chem.* **115** (2009) 740
14. B. Özcelik, J. H. Lee, D. B. Min, *J. Food Sci.* **68** (2003) 487
15. D. Villano, M. S. Fernández-Pachón, M. L. Moyá, A. M. Troncoso, M. C. García-Parrilla, *Talanta* **71** (2007) 230
16. B. Matthäus, *J. Agric. Food Chem.* **50** (2002) 3444
17. J. R. Soares, T. C. P. Dins, A. P. Cunha, L. M. Almeida, *Free Radical Res.* **26** (1997) 469

18. B. Ribeiro, J. Rangel, P. Valentão, P. Baptista, R. M. Seabra, P. B. Andrade, *J. Agric. Food Chem.* **54** (2006) 8530
19. C. Sgherri, C. Pinzino, F. Navari-Izzo, R. Izzo, *J. Sci. Food Agric.* **91** (2011) 1128
20. A. Jiménez-Escrig, I. Jiménez-Jiménez, C. Sánchez-Moreno, F. Saura-Calixto, *J. Sci. Food Agric.* **80** (2000) 1686.



J. Serb. Chem. Soc. 77 (10) 1391–1399 (2012)
JSCS–4360

Cobalt(II) and cadmium(II) compounds with adamantane-1-sulfonic acid

MILENA ĐORĐEVIĆ¹, DEJAN JEREMIĆ^{1#}, KATARINA ANĐELKOVIĆ^{1**},
MAJA GRUDEN-PAVLOVIĆ¹, VLADIMIR DIVJAKOVIĆ²,
MAJA ŠUMAR RISTOVIĆ^{1#} AND ILIJA BRČESKI^{1#}

¹Faculty of Chemistry, University of Belgrade, Studentski trg 12–16, 11000 Belgrade, Serbia
and ²Faculty of Sciences, University of Novi Sad, Trg D. Obradovića 4,
21000 Novi Sad, Serbia

(Received 12 April, revised 11 May 2012)

Abstract: In this work, the syntheses and characterization of two novel compounds of adamantane-1-sulfonic acid (1-AdSO₃H) with cobalt(II) and cadmium(II) are reported. The results of single crystal X-ray analysis of the compounds revealed that adamantane-1-sulfonate (1-AdSO₃[−]) in the monoanionic form plays different roles in the investigated compounds. Namely, while in compound [Co(H₂O)₆](1-AdSO₃)₂, six water molecules are coordinated to the cobalt(II) ion and 1-AdSO₃[−] serves as a counter ion, in compound [Cd(H₂O)₄(1-AdSO₃)₂], two molecules of 1-AdSO₃[−] are *trans*-coordinated to the cadmium(II) ion as a monodentate (O)-ligand and the other coordination sites are occupied by water molecules. The obtained compounds showed moderate activity against *Artemia salina*.

Keywords: X-ray structure determination; transition metal compounds; metal complexes; adamantane-1-sulfonate derivatives.

INTRODUCTION

Selective and efficient activation of C–H bonds in aliphatic hydrocarbons is one of the major challenges in chemistry and is the subject of extensive research.¹ Nevertheless, sulfoxidation of saturated hydrocarbons, as well as their possible application, has seen much slower progress, although the resulting products are stable compounds, suitable to serve as ligands and to form a coordination bond *via* oxygen.

As a part of on-going efforts to investigate the coordination behavior of alkane sulfonates,^{2,3} two novel compounds of 1-AdSO₃H with cobalt(II) (**1**) and cadmium(II) (**2**) are presented in this work.

* Corresponding author. E-mail: kka@chem.bg.ac.rs

Serbian Chemical Society member.

doi: 10.2298/JSC120419051D

Adamantane and its derivatives have gained much attention in the recent years, due to their significant biological activity.⁴ Coordination compounds of 1-adamantane derivatives are known only for the amino ($-\text{NH}_2$),^{5,6} and mercapto- ($-\text{SH}$) derivatives.^{7,8} It is noteworthy that information about compounds of 1-AdSO₃H with metal ions, both salts and coordination compounds, are very sparse.⁹ Therefore, to the best of our knowledge and according to the Cambridge Structural Database (CSD), herein the first crystal structures of any of the compounds of 1-AdSO₃H are presented. Evaluation of the biological activity of the synthesized compounds also formed part of this study.

EXPERIMENTAL

General procedures

For the synthesis of 1-AdSO₃H, the method of sulfoxidation of alkane using an SO₂/O₂ mixture in the presence of a catalytic amount of vanadium(IV) species [VO(acac)₂] was employed.¹⁰ This method was modified. Hence, unlike the original procedure, the gas was continuously blown through the mixture. Yield: 64 %.

1-AdSO₃H·H₂O (1.0 g, 4.2 mmol) was dissolved in methanol of technical purity. Into the clear solution of 1-AdSO₃H, cobalt(II) acetylacetonate (0.64 g, 2.5 mmol) was added. The obtained suspension was digested for 10 min on an ultrasonic bath at 20 °C. The reaction mixture was filtered and the filtrate was left for 7 days to crystallize at room temperature. The obtained brick-red crystals of the cobalt(II) complex had grown to a size of 5 mm and were suitable for crystallographic analyses. Yield of complex **1**: 58 %.

The cadmium(II) complex was prepared by the same procedure except cadmium(II) acetylacetonate (**3**) (0.78 g, 2.5 mmol) was added into the clear solution of 1-AdSO₃H. After 7 days of crystallization at room temperature, the obtained colorless crystals of the cadmium(II) complex had grown to a size of 1 mm and were suitable for crystallographic analyses. Yield of complex **2**: 57 %.

Elemental analyses (C and H) were performed by standard micro-methods using an ELEMENTARVario ELIII C.H.N.S O analyzer.

X-ray crystallography

The selected single crystals of the title compounds **1** and **2** were glued onto glass threads. The diffraction data were collected on an Oxford Diffraction KM4 four-circle goniometer equipped with Sapphire CCD detector. The crystal to detector distance in both cases was 45.0 mm and graphite monochromated MoK α ($\lambda = 0.71073$ Å) X-radiation was employed in the measurements. A frame width of 1° in ω , for 21.7 and 20.3 s, was used to acquire each frame for **1** and **2**, respectively. More than a hemisphere of three-dimensional data was collected in all measurements. The data were reduced using the Oxford Diffraction Program CrysAlisPro.¹¹ A semi-empirical absorption correction based upon the intensities of equivalent reflections was applied, and the data were corrected for Lorentz, polarization, and background effects. The scattering curves for neutral atoms, together with anomalous-dispersion corrections, were taken from International Tables for X-ray Crystallography.¹² The structures were solved by direct methods,¹³ and the figures were drawn using Mercury.¹⁴ The refinements were based on the F^2 values and performed by full-matrix least-squares¹⁵ with all non-H atoms anisotropic. The positions of all non H-atoms were located by direct methods. The positions of hydrogen

atoms were found from the inspection of the difference Fourier maps. The final refinement included atomic positional and displacement parameters for all non-H atoms.

The non-H atoms were refined anisotropically, while H sites of the water molecules were refined with isotropic displacement parameters. However, at the final stage of the refinement, H atoms belonging to the corresponding ligand were positioned geometrically (C–H, 0.97–0.98 Å) and refined using a riding model with fixed isotropic displacement parameters. The crystal data and refinement parameters are listed in Table I.

TABLE I. Crystal data and structure refinement for the obtained compounds

Compound	[Co(H ₂ O) ₆](1-AdSO ₃) ₂ (1)	[Cd(H ₂ O) ₄](1-AdSO ₃) ₂ (2)
Chemical formula	C ₂₀ H ₄₂ CoO ₁₂ S ₂	C ₂₀ H ₃₈ CdO ₁₀ S ₂
Formula weight	597.606	615.053
Wavelength, Å	0.71073	0.71073
Temperature, K	295(2)	295(2)
Crystal system	monoclinic	monoclinic
Space group	C2/m	C2/m
<i>a</i> / Å	11.058(5)	7.459(3)
<i>b</i> / Å	7.103(3)	10.488(4)
<i>c</i> / Å	18.099(8)	15.896(5)
β / °	106.057(5)	91.662(4)
<i>V</i> / Å ³	1366.13(11)	1243.0(8)
<i>Z</i>	2	2
<i>D</i> _{calc} / g cm ⁻³	1.453	1.643
μ / mm ⁻¹	0.84	1.10
<i>F</i> (000)	634	636
(θ_{\min} – θ_{\max}) / °	3.5–25.0	3.4–25.0
Diffraction measured fraction, θ_{\max}	0.998	0.998
Refined difference density, max/min	0.352/–0.220	0.64/–0.50
Reflection collected/unique/greater (<i>R</i> _{int})	2350/1309/1147 (0.023)	2286/1167/1136 (0.022)
Data/restraints/parameters	1309/0/104	1167/0/94
Goodness-of-fit on <i>F</i> ²	1.082	1.032
<i>R</i> indices (all data)	0.0442	0.0428
Final <i>R</i> indices [<i>I</i> > 2 σ (<i>I</i>)]	0.0367	0.0414

CCDC-844771 (**2**) and CCDC-844772 (**1**) contain the supplementary crystallographic data for this paper. These data can be obtained free of charge from The Cambridge Crystallographic Data Centre via www.ccdc.cam.ac.uk/data_request/cif.

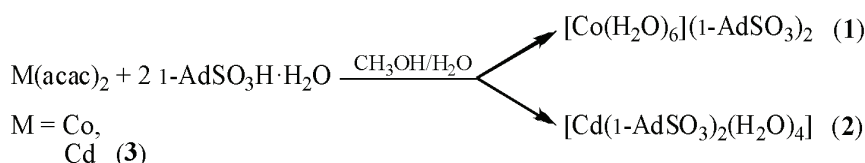
Biological activity evaluation – the brine shrimp test

A teaspoon of lyophilized eggs of the brine shrimp *Artemia salina* was added to 1 L of artificial sea water containing several drops of yeast suspension (3 mg of dry yeast in 5 mL distilled water), and air was passed through the suspension thermostated at 28 °C, under illumination for 24 h. Complex **2** and Cd(acac)₂ (**3**) were dissolved in DMSO. Since complex **1** is insoluble in DMSO and water, appropriate amounts of the compound dissolved in methanol were applied on paper disks (diameter 8 mm), and the solvent was evaporated. In a glass vial, 1–2 drops of yeast extract solution, 10–20 hatched nauplii in 5 mL of artificial seawater, and finally solutions of the tested compounds were added. For each concentration,

three determinations were performed. The vials were left at room temperature under illumination for 24 h, and afterwards the surviving nauplii were counted. The lethal concentration 50 (LC_{50}) was defined as the concentration of a substance that causes the death of 50 % of the nauplii. DMSO was inactive under the applied conditions.

RESULTS AND DISCUSSION

According to the procedure described in experimental section, 1-AdSO₃H as well as its derivatives with cobalt(II) **1** and cadmium(II) **2** were synthesized (Scheme 1) and characterized.



Scheme 1. Reaction of 1-AdSO₃H with the starting Co(II) and Cd(II) compounds.

1-AdSO₃H. Anal. Calcd. for C₁₀H₁₆O₃S: C, 55.56; H, 7.41 %. Found: C, 56.58; H, 7.39 %.

Cobalt complex 1. Anal. Calcd. for C₂₀H₄₂CoO₁₂S₂: C, 40.20; H, 7.04 %. Found: C, 40.24; H, 7.01 %.

Cadmium complex 2. Anal. Calcd. for C₂₀H₃₈CdO₁₀S₂: C, 39.06; H, 6.18 %. Found: C, 39.10; H, 6.12 %.

X-ray analysis

The results of the single crystal X-ray analysis revealed that the structural units of **1** are [Co(H₂O)₆]²⁺ and 1-AdSO₃⁻ additionally connected by strong hydrogen bonds, while the structural units of **2** are neutral [Cd(H₂O)₄(1-AdSO₃)₂] complex molecules mutually well separated, in which two 1-AdSO₃⁻ coordinate as monodentate (O)-ligands in the *trans* position. The structural units in **1** and **2** are involved in the formation of 2D networks of hydrogen bonds. In both compounds, the central ions are in a slightly distorted octahedral environment, consisting of six O-atoms of water molecules in **1**, or four O-atoms of water molecules and two O-atoms of sulfonate fragments in **2**. Structural units in both compounds exhibit a high degree of internal symmetry, as the majority of atoms that build up the 1-AdSO₃⁻ in **1** and **2** occupy a special position $4i$ (*m*), while the central ions are placed in positions $2b$ and $2d$ ($2/m$) of the $C2/m$ space group, respectively (Figs. 1 and 2). Pertinent crystallographic data for the two structures are given in Table I, the labeling schemes and corresponding symmetry elements are given in Figs. 1 and 2. Selected bond lengths and angles are listed in Table II. Both structures appear similar at the supramolecular level, caused by the relatively small number of hydrogen bonds (Table III). Hydrogen atoms from water molecules are involved in strong hydrogen bonding with free oxygen atoms of

the sulfonate fragment, building a 2D network of hydrogen bonds both along the *a* and *b* axes. As a result, along the *c* axis, “sandwiches” of thickness less than the size of axis *c* can be distinguished (Figs. 3 and 4). These “sandwiches” are on both outer sides covered with Ad-fragments, on which proper SO₃ groups are attached and oriented towards the core of the “sandwich”. The core consists of metal ions that are in **1** coordinated with six H₂O molecules, whereas in **2** the metal ions are coordinated with two O atoms from monodentate AdSO₃ ligands in the apical positions and four H₂O molecules in the equatorial plane. The distances between the “sandwiches” correspond to the C–C van der Waals contacts between the opposing Ad-fragments.

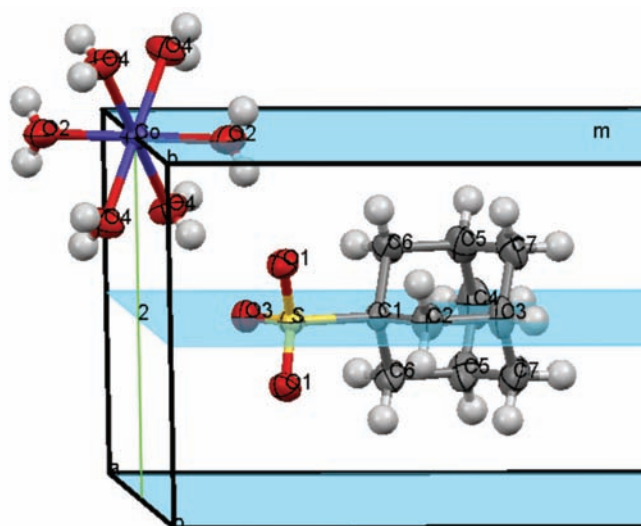


Fig. 1. Hexaaquacobalt(II)adamantane-1-sulfonate (**1**).

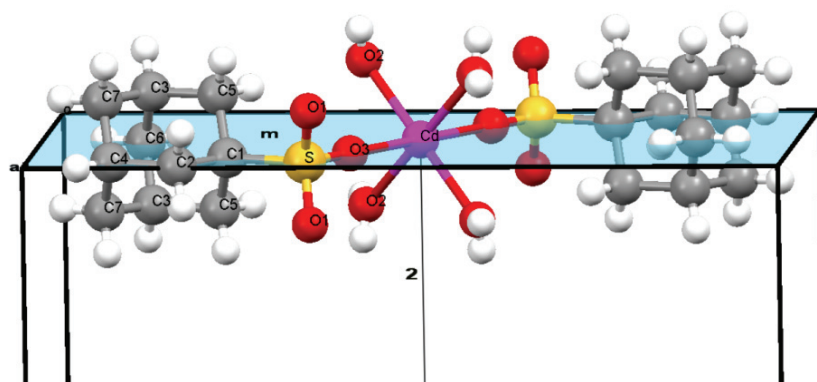


Fig. 2. Tetraaquabis(adamantane-1-sulfonato)cadmium(II) (**2**).

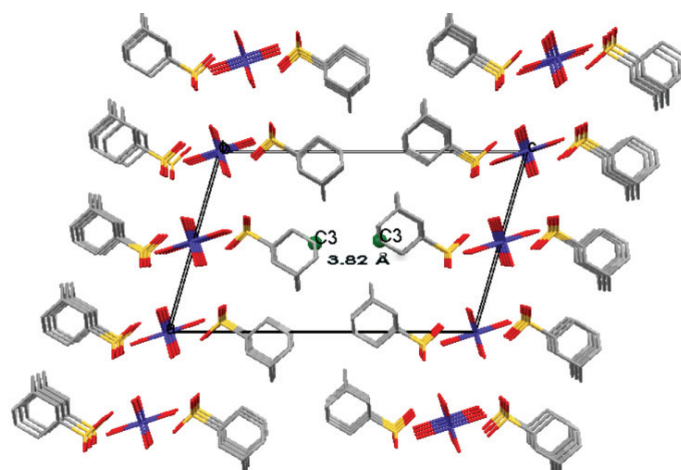
TABLE II. Selected bond lengths, Å, and angles, °, for complexes **1** and **2**

[Co(H ₂ O) ₆](1-AdSO ₃) ₂ (1)		[Cd(1-AdSO ₃) ₂ (H ₂ O) ₄] (2)	
Co–O2	2.043(3)	Cd–O2	2.233(4)
Co–O4	2.088(2)	Cd–O2 ^a	2.233(4)
O2–Co–O2 ^b	180.00	Cd–O3	2.250(5)
O4–Co–O4 ^c	180.00	S–O1	1.449(3)
O2–Co–O4	89.13(10)	S–O1 ^d	1.449(3)
O2–Co–O4 ^b	90.87(10)	S–O3	1.429(5)
O4–Co–O4 ^b	84.45(14)	S–C1	1.798(6)
O4–Co–O4 ^e	95.55(14)	O2–Cd–O3	92.4(2)
S–O3	1.457(2)	O2–Cd–O2 ^f	93.3(3)
S–O1	1.457(2)	O3–S–O1	112.1(2)
S–O1 ^g	1.457(2)	O3–S–O1 ^d	112.1(2)
S–C1	1.797(3)	O1–S–O1 ^d	112.1(3)
O3–S–O1	112.46(8)	O1–S–C1	107.0(2)
O1–S–O1 ^g	111.59(14)	O1 ^d –S–C1	107.0(2)
O3–S–C1	106.51(14)	O3–S–C1	106.2(3)
O1–S–C1	106.68(9)	Cd–O3–S	179.6(4)

^a $-x+1, y, -z+1$; ^b $-x+1, y, -z$; ^c $-x+1, -y+2, -z$; ^d $x, -y, z$; ^e $x, -y+2, z$; ^f $-x+1, y, -z+1$; ^g $x, -y+1, z$

TABLE III. Hydrogen bonding in complexes **1** and **2**

Bond	D–H, Å	H···A, Å	D···A, Å	D–H–A, °	Symmetry operation
1					
O4–H _A ···O3	0.74(3)	2.04(3)	2.770(3)	171(3)	$(-x+1, -y+1, -z)$
O4–H _B ···O1	0.78(3)	2.05(3)	2.815(3)	170(3)	$(-x+1/2, y+1/2, -z)$
O2–H _C ···O1	0.76(3)	1.99(3)	2.742(3)	167(3)	$(x, y+1, z)$
2					
O2–H1···O1	0.73(6)	2.08(6)	2.802(6)	167(6)	$(x-1/2, y-1/2, z)$
O2–H2···O1	0.82(6)	1.92(6)	2.739(6)	176(6)	$(x-1, -y, z)$

Fig. 3. Packing of the structural units in **1** with a view along the axis *b*.

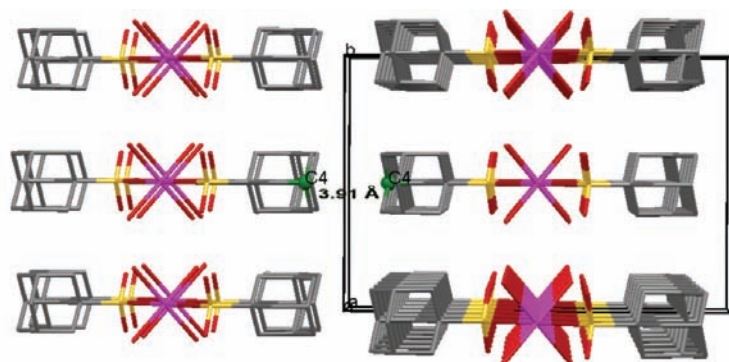


Fig. 4. Packing of the coordination units in **2** along the axis *a*.

Biological activity

In the *A. salina* test, which shows a good correlation with cytotoxic activity,¹⁶ all the substances had LC_{50} values in either the millimolar range or high micromolar range (Table IV). The tetraaquabis(adamantane-1-sulfonato)cadmium(II) complex (**2**) was more active than the starting Cd(II) compound **3**, probably due to its higher lipophilicity.

TABLE IV. Toxic effect (expressed as LC_{50} values) of the investigated compounds against *A. salina*

Compound	LC_{50} / mM
$[\text{Co}(\text{H}_2\text{O})_6](1\text{-AdSO}_3)_2$ (1)	3.05
$[\text{Cd}(\text{H}_2\text{O})_4(1\text{-AdSO}_3)_2]$ (2)	0.74
$\text{Cd}(\text{acac})_2$ (3)	3.03

CONCLUSIONS

In this work, the first crystal structures of inorganic compounds of 1-AdSO₃H were reported. While in compound $[\text{Co}(\text{H}_2\text{O})_6](1\text{-AdSO}_3)_2$, six water molecules are coordinated to the cobalt(II) ion and 1-AdSO₃⁻ serves as a counter ion, in the $[\text{Cd}(\text{H}_2\text{O})_4(1\text{-AdSO}_3)_2]$ compound, 1-AdSO₃⁻ acts as monodentate ligand and coordinates to the cadmium(II) ion through the oxygen atom in a monoanionic form. The phenomenon that 1-AdSO₃⁻ accomplished coordination with the Cd(II) ion but not with Co(II) can perhaps be explained by hard-soft-acid-base principle.¹⁷⁻¹⁹ In fact, it is more likely that the soft cadmium can make a coordination bond with a relatively soft alkane sulfonate group (much softer than the sulfate group), as opposed to the harder cobalt. Rigidity and hydrophobicity of the adamantane residue proved to be a difficulty in further attempts to synthesize adamantane-1-sulfonate compounds. The obtained compounds were tested against *A. salina* and showed moderate activity. Due to higher lipophilicity of compound **2**, it was more active than the starting Cd(II) compound **3**.

Acknowledgement. The authors are grateful to the Ministry of Education, Science and Technological Development of the Republic of Serbia for financial support (Project No. 172017).

ИЗВОД

НОВА ЈЕДИЊЕЊА КОБАЛТА(II) И КАДМИЈУМА(II) СА
АДАМАНТАН-1-СУЛФОНСКОМ КИСЕЛИНОМ

МИЛЕНА ЂОРЂЕВИЋ¹, ДЕЈАН ЈЕРЕМИЋ¹, КАТАРИНА АНЂЕЛКОВИЋ¹, МАЈА ГРУДЕН-ПАВЛОВИЋ¹,
ВЛАДИМИР ДИВЈАКОВИЋ², МАЈА ШУМАР РИСТОВИЋ¹ И ИЛИЈА БРЧЕСКИ¹

¹Хемијски факултет, Универзитет у Београду, Студентски штрк 12–16, 11000 Београд и ²Природно-математички факултет, Универзитет у Новом Саду, Трт Д. Обрадовића 4, 21000 Нови Сад

У овом раду приказана је синтеза и карактеризација два нова једињења адамантан-1-сулфонске киселине (1-AdSO₃H) са кобалтом(II) и кадмијумом(II). Резултати рендгенске структурне анализе датих једињења указују да моноанјон адамантан-1-сулфоната (1-AdSO₃ показује различит афинитет према Co(II) и Cd(II) јонима). У комплексу [Co(H₂O)₆](1-AdSO₃)₂, шест молекула воде се координује за Co(II) јон, док 1-AdSO₃ има улогу контрајона. У комплексу [Cd(H₂O)₄](1-AdSO₃)₂ два јона 1-AdSO₃ су координована за Cd(II) јон као монодентати у *trans* положају преко кисеоникових атома, док су остала координациона места заузета молекулима воде. Добијена једињења су показала умерену активност на *Artemia salina*.

(Примљено 12. априла, ревидирано 11. маја 2012)

REFERENCES

1. F. Parrino, A. Ramakrishnan, H. Kisch, *Angew. Chem. Int. Ed.* **47** (2008) 7107
2. D. A. Jeremić, G. N. Kaluderović, S. Gómez-Ruiz, I. D. Brčeski, B. Kasalica, V. M. Leovac, *Cryst. Growth Des.* **10** (2010) 559
3. D. A. Jeremić, G. N. Kaluderović, S. Gómez-Ruiz, I. D. Brčeski, K. Anđelković, *Acta Crystallogr. C* **65** (2009) m143
4. A. Kozubík, A. Vaculová, K. Souček, J. Vondráček, J. Turánek, J. Hofmanová, *Met.-Based Drugs* **2008** (2008) 417897
5. F. D. Rochon, M. Doyon, I. S. Butler, *Inorg. Chem.* **32** (1993) 2717
6. M. Westerhausen, T. Bollwein, A. Pfitzner, T. Nilges, H. J. Deiseroth, *Inorg. Chim. Acta* **312** (2001) 239
7. A. P. Purdy, A. D. Berry, C. F. George, *Inorg. Chem.* **36** (1997) 3370
8. Y. Matsunaga, K. Fujisawa, N. Ibi, M. Fujita, T. Ohashi, N. Amir, Y. Miyashita, K. Aika, Y. Izumi, K. Okamoto, *J. Inorg. Biochem.* **100** (2006) 239
9. I. Hitoshi, Y. Hiroshi, E. Hiroyuki, S. Masaharu, A. Kimisuke, (Nippon Electric Co, Jpn. Kokai Tokyo Koho), JKXXAF JP 07070312 A 19950314 (1995)
10. Y. Ishii, K. Matsunaka, S. Sakaguchi, *J. Am. Chem. Soc.* **122** (2000) 7390
11. CrysAlis CCD and CrysAlis RED software (Version 1.171), Oxford Diffraction, Yarnton, Oxfordshire, UK, 2000
12. J. A. Ibers, W. C. Hamilton, Eds., *International tables for X-ray crystallography*, vol. 4, Kynoch, Birmingham, UK, 1974
13. A. Altomare, M. C. Burla, M. Cavalli, G. Cascarano, C. Giacovazzo, A. Gagliardi, A. G. Moliterni, G. Polidori, R. Spagna, *Sir97: A New Program For Solving and Refining Cryst*

tal Structures, Istituto di Ricerca per lo Sviluppo di Metodologie Cristallografiche CNR, Bari, 1997

14. I. J. Bruno, J. C. Cole, P. R. Edgington, M. K. Kessler, C. F. Macrae, P. McCabe, J. Pearson, R. Taylor, *Acta Crystallogr., Sect. B* **58** (2002) 389
15. G. M. Sheldrick, *Acta Crystallogr., Sect. A* **64** (2008) 112
16. B.N. Meyer, N.R. Ferrigni, J.E. Putnam, L.B. Jacobsen, D.E. Nichols, J.L. McLaughlin, *Planta Med.* **45** (1982) 31
17. R. G. Pearson, *J. Am. Chem. Soc.* **85** (1963) 3533
18. R. G. Pearson, *J. Chem. Educ.* **45** (1968) 581
19. R. G. Pearson, *J. Chem. Educ.* **45** (1968) 643.



J. Serb. Chem. Soc. 77 (10) 1401–1408 (2012)
JSCS–4361

Verifying the modes of cyclic conjugation in tetrabenzo[bc,ef,op,rs]circumanthracene

IVAN GUTMAN^{*#}, JELENA ĐURĐEVIĆ^{**}, ZORAN MATOVIĆ and MARIJA MARKOVIĆ

Faculty of Science, University of Kragujevac, P. O. Box 60, 34000 Kragujevac, Serbia

(Received 19 May 2012)

Abstract: Cyclic conjugation in the “empty” central ring of tetrabenzo[bc,ef,op,rs]circumanthracene (TBCA) is stronger than in its neighboring “non-empty” rings, contradicting the predictions of Kekulé-structure-based theoretical models. Earlier examples of such anomalous cyclic conjugation were observed in highly strained, non-planar benzenoid systems. As the molecule of TBCA is perfectly planar and strain-free, it was possible to test and verify its cyclic conjugation pattern by means of high-level, B3LYP/6-311+G(d,p), *ab initio* DFT calculations.

Keywords: cyclic conjugation; energy effect (of cyclic conjugation); Kekulé-structure-based models; DFT calculation; benzo-annelated perylene; tetrabenzo-circumanthracene.

INTRODUCTION

Kekulé-structure-based models of cyclic conjugation

In polycyclic conjugated molecules, the location of the π -electrons usually cannot be represented by a single structural formula, but by several so-called Kekulé structures. In the 1970s and later, several approaches were put forward, aimed at quantitatively describing the π -electron properties of conjugated molecules, based on counting and analyzing their Kekulé structures. In particular, the Kekulé structure count K was used to predict the total π -electron energy^{1–3} and thermodynamic stability of benzenoid hydrocarbons.^{4–6} The aromaticity of an individual ring R in the conjugated system the molecular graph of which is G was assessed^{7,8} by means of the quantity $2K(G-R)/K(G)$. This idea was eventually elaborated in the so-called theory of conjugated circuits.^{9–12} A conjugated circuit in a Kekulé structure is a cycle in which single and double bonds alternate. Within the theory of conjugated circuits, cyclic conjugation in a ring R is assumed the consequence of the existence of conjugated circuits pertaining to R in

Corresponding authors. E-mail: (*)gutman@kg.ac.rs; (**)jddjurdjevic@gmail.com

Serbian Chemical Society member.

doi: 10.2298/JSC120518064G



the Kekulé structures. Clar¹³ proposed a diagrammatical method for drawing structural formulas, in which the most important cyclic conjugation modes (originating from the Kekulé structures) were indicated.¹⁴ Eventually, a quantitative version of the Clar theory was put forward.^{15,16} Kekulé structures were used to assess the distribution of π -electrons in polycyclic conjugated hydrocarbons and to estimate the π -electron content of individual rings.^{17–19} A similar approach based on the Clar formulas was also offered.^{20,21} Recently, ring currents in benzenoid hydrocarbons were also modeled by means of conjugated circuits.²²

Details on these Kekulé-structure-based models of cyclic conjugation can be found in a book²³ and in reviews.^{24–28}

Energy effect of cyclic conjugation

Also in the 1970s, a molecular-orbital- and graph-theory-based method for calculating the energy effect of individual cycles in polycyclic conjugated molecules was developed.²⁹ Its details can be found in the reviews^{30,31} and elsewhere.^{32–35} The energy effect ef of the ring R in the conjugated system whose molecular graph is G is computed by means of the formula

$$ef = ef(R) = \frac{2}{\pi} \int_0^{\infty} \ln \frac{\phi(G, ix)}{\phi(G, ix) + 2\phi(G - R, ix)} dx \quad (1)$$

where $\phi(G, x)$ is the characteristic polynomial of G and $i = \sqrt{-1}$.

The ef -values calculated by Eq. (1) are expressed in units of the HMO carbon–carbon resonance integral β . Therefore, positive ef -values indicate thermodynamic stabilization caused by cyclic conjugation. The greater is $ef(R)$, the stronger is the intensity of cyclic conjugation in the ring R .

For the considerations in the present paper, it is important to note that the ef -method is independent of any assumption based on Kekulé structures. Yet, in the majority of cases, its results are in full harmony with those obtained by means of Kekulé-structure-based approaches.^{30,31} In some cases, however, the ef -method leads to conclusions that differ from those implied by the Kekulé-structure-based models.^{32,33} These “anomalies” are outlined in the subsequent section, and then further elaborated and corroborated in the later parts of this article.

CYCLIC CONJUGATION IN PERYLENE AND ITS CONGENERS

The application of the ef -method to the six-membered rings of perylene is of particular interest because this benzenoid molecule possesses a so-called “empty” ring, namely a ring in which according to Kekulé-structure- and Clar-structure-based models, there is no cyclic conjugation. This is illustrated in Fig. 1 in which all the nine Kekulé structures of perylene are depicted. None of these has a conjugated circuit (*i.e.*, three double bonds) in the central ring. In fact, the two vertical carbon–carbon bonds in the central ring are single in all Kekulé structures.

Rings of this kind are referred to as “empty”.^{13,14,23} The central rings in perylene and all its congeners examined in this paper are “empty”. Recall that for such rings, the Randić local aromaticity index $2K(G-R)/K(G)$ is equal to zero, indicating a complete absence of cyclic conjugation.

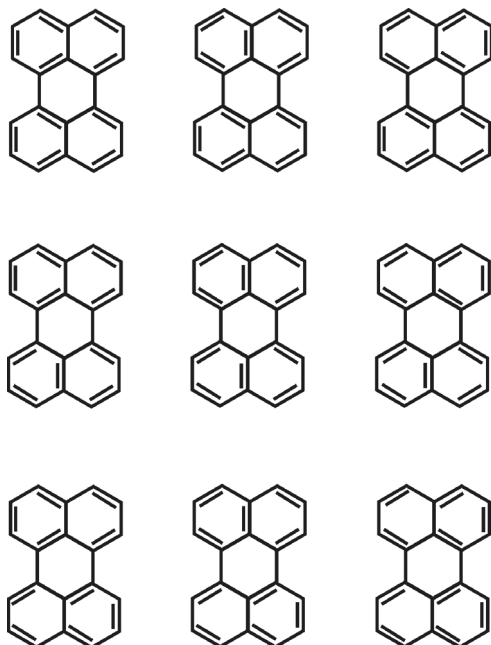


Fig. 1. The Kekulé structures of perylene. The two vertical carbon–carbon bonds in the central ring are always single. Therefore, within the Kekulé-structure-based models, this ring is claimed to be devoid of any cyclic conjugation.

In the case of perylene (**1** in Fig. 2), calculations based on the *ef*-model are in good agreement with the predictions of the Kekulé-structure- and Clar-structure-based models. Although the *ef*-value of the central “empty” ring (A) is not zero, it is nevertheless some five times smaller than the *ef*-value of the other four neighboring rings (B).

Due to a generally valid regularity,^{8,36} benzo-annulation (in the position indicated in **2** in Fig. 2) increases the intensity of cyclic conjugation in the central ring of perylene. When the same type of benzo-annulation is realized at all the four sites of perylene (**3**), then cyclic conjugation in the central “empty” ring is increased so much that it exceeds the magnitude of cyclic conjugation in the four neighboring rings. This phenomenon, discovered several years ago,³² was the first example when the pattern of cyclic conjugation in a benzenoid hydrocarbon violates the predictions of Kekulé-structure-based models. The “anomaly” of this kind can be strengthened by considering naphthalene-annulation (as shown in **4**). Although the *ef*-values of the central ring of benzoperylene (**3**) and naphthalenoperylene (**4**) differ only slightly, the cumulative effect in tetranaphthalenoperylene (**5**) is remarkable: in **5** the cyclic conjugation in the “empty” ring (A) is

found to be more than two times stronger than in the neighboring rings (B), and is also significantly greater than the analogous effect in the rings C, *cf.* Fig. 2.

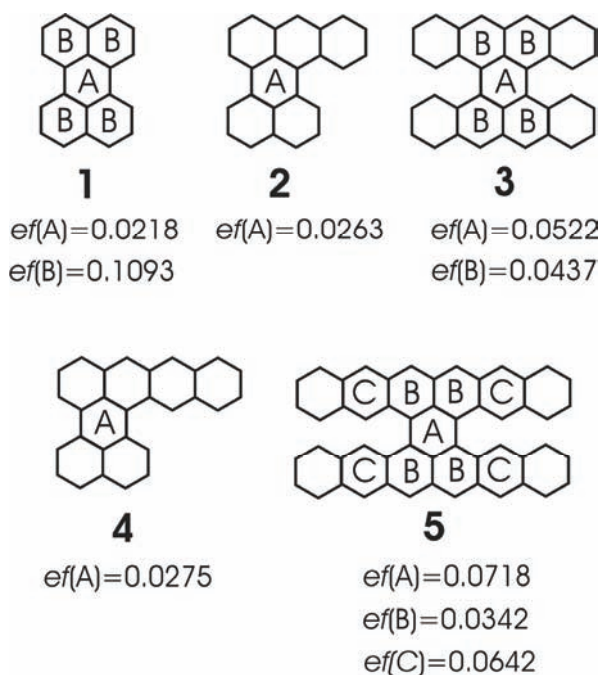


Fig. 2. Energy effects (in β units) of some six-membered rings of perylene (**1**) and its congeners. For details, see text.

HOW REALISTIC IS THE *ef*-METHOD?

The conclusions concerning cyclic conjugation in perylene and its congeners outlined in the preceding section are based on the energy effects *ef*, calculated according to formula (1). The natural dilemma is whether these results reflect real features of the π -electrons in the underlying molecules or whether they are artifacts originating from the crudeness of the HMO approximation. In order to resolve this problem, these conclusions have to be verified by means of more reliable theoretical approaches.

However, first a serious objection to the calculated cyclic conjugation patterns of tetrabenzo- and tetranaphtho-perylenes (**3** and **5**) needs to be addressed.

In HMO calculations, only the topology of the carbon-atom skeleton is taken into account. Consequently, steric effects are fully disregarded. In tetrabenzo- and tetranaphtho-perylenes, the near-lying hydrogen atoms impose a strong steric repulsion, which necessarily causes an extension of some carbon-carbon bonds, deformation of some six-membered rings and non-planarity of the entire molecule (Fig. 3). This, in turn, makes the results of any HMO-based calculation doubtful and inapplicable.

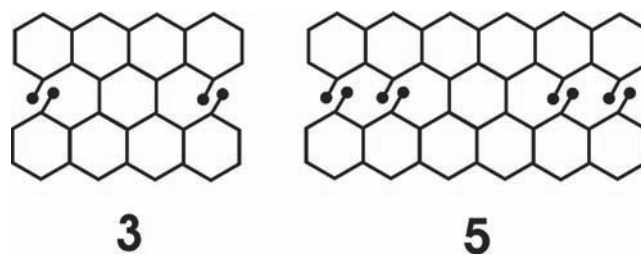


Fig. 3. Tetrabenzoperylene (**3**) and tetranaphthalenoperylene (**5**) in which the near-lying hydrogen atoms are indicated. Their repulsion causes strong sterical strain and deviation from planarity.

This difficulty would be overcome if instead of **3** and **5**, similar, but strain-free and strictly planar benzenoid systems would be considered. Such are obtained by replacing the overcrowded hydrogen atoms (indicated in Fig. 3) by carbon-carbon bonds. By this, one arrives at tetrabenzo[*bc,ef,kl,no*]coronene (**6**) and tetrabenzo[*bc,ef,op,rs*]circumanthracene (**7**), depicted in Fig. 4.

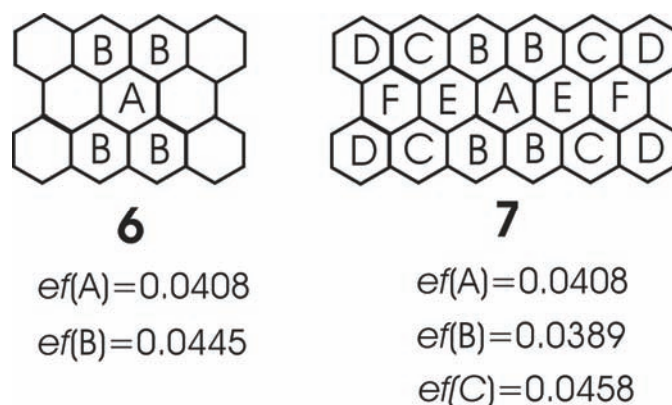


Fig. 4. Energy effects (in β units) of some six-membered rings of tetrabenzo[*bc,ef,kl,no*]coronene (**6**) and tetrabenzo[*bc,ef,op,rs*]circumanthracene (**7**).

These *ef*-values show that in **6**, the pattern of cyclic conjugation does not violate the predictions of the Kekulé-structure-based theoretical models, whereas in **7** it does, because $ef(A) > ef(B)$.

From the calculated *ef*-values of **6**, it can be seen that the transformation **3** \rightarrow **6** reduces the intensity of cyclic conjugation in the central ring A and increases it in the neighboring rings B. Consequently, $ef(A)$ becomes smaller than $ef(B)$, and the disagreement with the Kekulé-structure-based theories is lost. Fortunately, in **7**, the “anomaly” in the cyclic conjugation pattern remains, although much less pronounced than in the case of **5** (Fig. 4). Bearing these observations in mind, it was decided to test the modes of cyclic conjugation in tetrabenzo[*bc,ef,op,rs*]cir-

cumanthracene (TBCA) by independent, much more reliable quantum-theoretical methods.

A DENSITY-FUNCTION-THEORETICAL STUDY OF TBCA

The DFT calculations on tetrabenzo[*bc,ef,op,rs*]circumanthracene (TBCA) were realized using the Gaussian 09W package, version 0.1, at the B3LYP/6-311+G(d,p) level of theory.³⁷ Geometry optimization confirmed that the molecule is perfectly planar. Bond lengths were taken from the optimized geometry. The frequency calculations showed that the examined molecule has no imaginary vibration frequencies, *i.e.*, that the geometry determined corresponds to a true energy minimum. Nucleus independent chemical shift (NICS) values were calculated at the B3LYP/6-311+G(d,p) level through the gauge-including atomic orbital method (GIAO).³⁸

The results of the DFT study that are representative for the cyclic conjugation pattern of TBCA are presented in Table I. Full computational details can be obtained from the authors (J.Đ.) upon request.

From the data in Table I, it can be seen that the NICS method³⁹ indicates that the cyclic conjugation in ring A is stronger than that in ring B and even in ring C. Needless to say that the cyclic conjugation in ring A much exceeds also those in rings E and F. In fact, according to the NICS-values, only in the peripheral rings D is the cyclic conjugation more intense than in A. (Recall that the more negative a NICS-value is, the higher is the local aromaticity and cyclic conjugation in the underlying ring.^{39–41})

TABLE I. Properties of the rings of TBCA (**7**) according to the labeling indicated in Fig. 4. NICS(0) and NICS(1) are, respectively, the NICS values for the virtual charge located in the center of the ring and 1 Å above its center; Σ is the sum of the lengths (in pm) of the six carbon–carbon bonds forming the respective ring; Δ is the change of Σ relative to ring A ($\Delta < 0$ indicates bond compression and increased cyclic conjugation relative to ring A, $\Delta > 0$ indicates bond extension and decreased cyclic conjugation relative to ring A); *ef* is the energy effect computed by Eq. (1)

Ring	NICS(0)	NICS(1)	Σ	Δ	<i>ef</i>
A	−3.74	−7.09	852.8	0.0	0.0408
B	+2.11	−2.00	854.0	+1.2	0.0389
C	−2.47	−5.73	852.3	−0.5	0.0458
D	−5.74	−8.30	846.4	−6.4	0.0982
E	+0.26	−3.69	854.6	+1.8	0.0391
F	+8.03	2.81	861.8	+9.0	0.0277

Bond lengths may serve as another indicator of cyclic conjugation: With increasing magnitude of cyclic conjugation, the carbon–carbon bonds forming the respective ring will gain in double-bond character and thus become shorter. This effect is clearly seen from the bonds lengths of TBCA. The sums Σ of the lengths

of the six carbon–carbon bonds of the respective ring are given in Table I. Indeed, the Σ -value of ring A is smaller than those of the rings B, nearly equal to those of the rings C, and only exceeds those of the rings D. To see this effect better, the difference Δ between the Σ -value of a ring and the Σ -value of ring A are also presented.

For the sake of completeness, the *ef*-values of all six-membered rings of TBCA are also included in Table I.

CONCLUDING REMARKS

Based on the above-described DFT calculations and the data collected in Table I, it has been demonstrated that the results of the presented *ef*-method provide a reliable and realistic picture of the cyclic conjugation pattern of TBCA. Attention was focused on TBCA as a benzenoid molecule for which a breakdown of the Kekulé-structure-based theories is predicted by the *ef*-method. Therefore, by confirming the validity of the predictions of the *ef*-method, a case was also found for which, by considering Kekulé structures, one arrives at fallacious conclusions on the modes of cyclic conjugation and thus on local aromaticity. The example provided in this work, namely tetrabenzo[*bc,ef,op,rs*]circumanthracene (7), is a strain-free and planar benzenoid hydrocarbon, with a π -electron system for which Kekulé-structure-based theories were hitherto believed to be perfectly applicable. It can now be seen that the domain of applicability of these theories is somewhat more restricted than was previously thought.

Acknowledgement. The authors thank the Ministry of Education, Science and Technological Development of the Republic of Serbia for support (Grants No. 174033 and 41010).

ИЗВОД

ПОТВРЂИВАЊЕ НАЧИНА ЦИКЛИЧНЕ КОНЈУГАЦИЈЕ У ТЕТРАБЕНЗО[*bc,ef,op,rs*]ЦИРКУМАНТРАЦЕНУ

ИВАН ГУТМАН, ЈЕЛЕНА ЂУРЂЕВИЋ, ЗОРАН МАТОВИЋ и МАРИЈА МАРКОВИЋ

Природно–математички факултет Универзитета у Крагујевцу

Циклична конјугација у “празном” централом прстену тетрабензо[*bc,ef,op,rs*]циркумантрацена (ТВСА) је јача него у суседним “не-празним” прстеновима, што противречи предвиђањима добијеним помоћу модела заснованих на Кекулеовим структурама. Ранији примери овакве аномалне цикличне конјугације нађени су код непланарних бензеноидних система са великим стерним напонима. Будући да је молекул ТВСА потпуно планаран и лишен стерног напона, модови његове цикличне конјугација могли су се проверити и потврдити помоћу *ab initio* DFT прорачуна, на нивоу B3LYP/6-311+G(d,p).

(Примљено 19. маја 2012)

REFERENCES

1. G. G. Hall, *Int. J. Math. Educ. Sci. Technol.* **4** (1973) 233
2. J. Cioslowski, *MATCH Commun. Math. Chem.* **20** (1986) 95

3. I. Gutman, S. Marković, D. Vukičević, A. Stajković, *J. Serb. Chem. Soc.* **60** (1995) 93
4. W. C. Herndon, *J. Am. Chem. Soc.* **95** (1973) 2404
5. R. Swinborne-Sheldrake, W. C. Herndon, I. Gutman, *Tetrahedron Lett.* **16** (1975) 755
6. S. Radenković, I. Gutman, *J. Serb. Chem. Soc.* **74** (2009) 155
7. M. Randić, *Tetrahedron* **30** (1974) 2067
8. I. Gutman, A. T. Balaban, *J. Serb. Chem. Soc.* **76** (2011) 1505
9. M. Randić, *Chem. Phys. Lett.* **38** (1976) 68
10. M. Randić, *J. Am. Chem. Soc.* **99** (1977) 444
11. M. Randić, N. Trinajstić, *J. Am. Chem. Soc.* **109** (1987) 6923
12. T. Dolić, *MATCH Commun. Math. Comput. Chem.* **65** (2011) 775
13. E. Clar, *The Aromatic Sextet*, Wiley, London, 1972
14. A. T. Balaban, *Polycyclic Aromat. Compd.* **24** (2004) 83
15. H. Hosoya, T. Yamaguchi, *Tetrahedron Lett.* **16** (1975) 4659
16. W. C. Herndon, H. Hosoya, *Tetrahedron* **40** (1984) 3987
17. M. Randić, A. T. Balaban, *Polycyclic Aromat. Compd.* **24** (2004) 173
18. A. T. Balaban, M. Randić, *J. Chem. Inf. Comput. Sci.* **44** (2004) 50
19. A. T. Balaban, M. Randić, *New J. Chem.* **28** (2004) 800
20. I. Gutman, *Bull. Chem. Technol. Maced.* **22** (2003) 105
21. M. Randić, A. T. Balaban, *J. Chem. Inf. Model.* **46** (2006) 57
22. M. Randić, *Chem. Phys. Lett.* **500** (2010) 123
23. I. Gutman, S. J. Cyvin, *Introduction to the Theory of Benzenoid Hydrocarbons*, Springer, Berlin, 1989
24. W. C. Herndon, *J. Chem. Educ.* **51** (1974) 10
25. J. Cioslowski, *Topics Curr. Chem.* **153** (1990) 85
26. D. J. Klein, *J. Chem. Educ.* **69** (1992) 691
27. M. Randić, *Chem. Rev.* **103** (2003) 3449
28. A. T. Balaban, M. Randić, in: *Carbon Bonding and Structures*, M. V. Putz, Ed., Springer, Dordrecht, 2011, p. 159
29. I. Gutman, S. Bosanac, *Tetrahedron* **33** (1977) 1809
30. I. Gutman, *Monatsh. Chem.* **136** (2005) 1055
31. I. Gutman, in: *Mathematical Methods and Modelling for Students of Chemistry and Biology*, A. Graovac, I. Gutman, D. Vukičević, Eds., Hum, Zagreb, 2009, p. 13
32. I. Gutman, N. Turković, J. Jovičić, *Monatsh. Chem.* **135** (2004) 1389
33. I. Gutman, B. Furtula, J. Đurđević, R. Kovačević, S. Stanković, *J. Serb. Chem. Soc.* **70** (2005) 1023
34. S. Jeremić, S. Radenković, I. Gutman, *J. Serb. Chem. Soc.* **75** (2010) 943
35. M. Marković, J. Đurđević, I. Gutman, *J. Serb. Chem. Soc.* **77** (2012) 751
36. A. T. Balaban, I. Gutman, S. Jeremić, J. Đurđević, *Monatsh. Chem.* **142** (2011) 53
37. Gaussian 09, Revision A.01, Gaussian, Inc., Wallingford CT, USA, 2009
38. K. Wolinski, J. F. Hilton, P. Pulay, *J. Am. Chem. Soc.* **112** (1990) 8251
39. P. Ragué Schleier, C. Maerker, A. Drausfeld, H. Jiao, N. J. R. van Eikema Hommes, *J. Am. Chem. Soc.* **118** (1996) 6371
40. P. Ragué Schleier, H. Jiao, *Pure Appl. Chem.* **68** (1996) 209
41. J. A. N. F. Gomes, R. B. Mallion, *Chem. Rev.* **101** (2001) 1349.



J. Serb. Chem. Soc. 77 (10) 1409–1422 (2012)
JSCS–4362

An electrochemical study of the adsorptive behaviour of varenicline and its interaction with DNA

VALENTINA RADULOVIĆ¹, MARA M. ALEKSIĆ^{2**} and VERA KAPETANOVIĆ¹

¹University of Belgrade, Faculty of Pharmacy, Department of Analytical Chemistry, Vojvode Stepe 450, 11000 Belgrade, Serbia and ²University of Belgrade, Faculty of Pharmacy, Department of Physical Chemistry and Instrumental Methods, Vojvode Stepe 450, 11000 Belgrade, Serbia

(Received 20 April, revised 10 July 2012)

Abstract: The electrochemical behaviour of a novel nicotinic $\alpha_4\beta_2$ subtype receptor partial agonist varenicline (VAR), which is used for smoking cessation, was investigated in Britton–Robinson buffers (pH 2.0–12.0) by cyclic, differential pulse and square wave voltammetry at a hanging mercury drop electrode (HMDE). The influence of pH, scan rate, concentration, accumulation potential and time on the peak current and potential suggested that the redox process was adsorption controlled in alkaline media. In addition, the experimental value of the surface coverage, $\Gamma = 1.03 \times 10^{-10} \text{ mol cm}^{-2}$, was used to determine the conditions when VAR was fully adsorbed at the electrode surface. Bearing in mind the potential high toxicity of VAR due to the presence of a quinoxaline structure, its interaction with double stranded-DNA (ds-DNA) was postulated and studied when both compounds were in the adsorbed state at a modified HMDE. Using the adsorptive transfer technique, changes in potential and decreases in the normalized peak currents were observed. The estimated value of the ratio of surface-binding constants indicated that the reduced form of VAR interacted with ds-DNA more strongly than the oxidized form. Subtle DNA damage under conditions of direct DNA–VAR interaction at room temperature was observed. The proposed type of interaction was intercalation. This study employed a simple electroanalytical methodology and showed the potential of a DNA/HMDE biosensor for investigation of genotoxic effects.

Keywords: adsorption; DNA; interaction; varenicline; electrochemistry.

INTRODUCTION

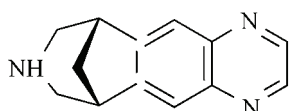
Varenicline (VAR, 7,8,9,10-tetrahydro-6,10-methano-6H-pyrazino(2,3-*h*)(3) benzazepine), (Scheme 1) is a novel nicotinic $\alpha_4\beta_2$ subtype receptor partial ago-

* Corresponding author. E-mail: mara@pharmacy.bg.ac.rs

Serbian Chemical Society member.

doi: 10.2298/JSC120420073R

nist approved by the Food and Drug Administration (FDA) for smoking cessation.¹ VAR is similar in structure to nicotine but, as a partial agonist, it does not produce the full effect of nicotine. VAR competitively blocks the ability of nicotine to bind and stimulate the dopamine system. Only a small portion of VAR is metabolized, so most of the active compound is excreted renally.



Scheme 1. Chemical structure of varenicline.

Since VAR possesses a quinoxaline core, which is known as a cytotoxic structure,² it can be supposed that varenicline also shows some cytotoxic effects.

There are only few reports on determination of VAR or its degradation products and impurities by different chromatographic methods in tablets^{3–7} and plasma samples.⁸ Recently, the electrochemical behaviour of VAR at several electrodes was reported.⁹ VAR undergoes reduction of the two C=N bonds of the substituted quinoxaline ring. In two consecutive, one electron steps the C=N bonds in VAR are reduced to give dihydrovarenicline, which undergoes further hydrogen ion-catalyzed chemical transformation and after the addition of two protons and two electrons, it is reduced to the final product, tetrahydrovarenicline. The critical factor governing the reduction processes of VAR is the pH of the solution. The overall process was possible only in acid solution and is represented by two reduction peaks, separated by more than 0.5 V. In alkaline medium, dihydrovarenicline is formed as the final product, which can be reversibly oxidized back to VAR.

Since the VAR molecule has a planar structure, it can be assumed that it will show considerable adsorption at an electrode surface. Bearing in mind its high toxicity, interactions with DNA molecule may be postulated.

The best way to study these interactions is to measure the electrode signal when both compounds are in the adsorbed state at the electrode surface.

Electrochemical DNA-based biosensors^{10–12} are often used for the determination of low-molecular weight compounds with affinity for nucleic acids and for the detection of the hybridisation reaction.¹³ There are many interesting applications of DNA biosensors for detection of different analytes in water, soil, plant, food samples and pharmaceuticals.¹⁴ It is well known that drugs bind to DNA both covalently and non-covalently. The covalent binding with DNA is irreversible and leads to complete inhibition of DNA processes and subsequent cell death. Non-covalent binding of small molecules to DNA can occur in three modes: intercalation into the base pairs, binding in the “major” or “minor” grooves, and by electrostatic interactions outside the helix.¹⁵ The intercalators are usually planar molecules which contain heterocyclic groups that stack between adjacent DNA base pairs and cause strong structural perturbations in the DNA molecule.

Since the structure of varenicline contains three planar heterocyclic rings, its potent interaction with DNA could be assumed.

Electrochemical analysis of DNA is based on the fact that the adenine and cytosine residues produce reducible signals, while guanine residues yield an anodic signal due to the oxidation of the guanine reduction product. For the detection of such signals, voltammetric techniques at a hanging mercury drop electrode (HMDE) are used most frequently.¹⁶ The interaction between drugs and DNA that cause DNA damage can be monitored by following the changes in the current intensity and the shift in the potential of the voltammetric peaks of DNA and investigated drug.

In this work, the preliminary results on the interaction of the nicotinic receptor agonist varenicline with calf thymus double-stranded DNA (ds-DNA) immobilized at a HMDE using adsorptive transfer stripping square wave voltammetry (AdTSSWV) are presented.

EXPERIMENTAL

Reagents and solutions

VAR was kindly donated by the Agency of Drugs and Medical Devices, Belgrade, Serbia. A stock solution (S_0) 1×10^{-3} mol dm⁻³ of VAR was prepared in redistilled water and stored in a freezer. More dilute solutions were prepared daily from the stock solution (S_0).

Double-stranded calf thymus DNA (MW = 10×10^6 – 15×10^6 g mol⁻¹) was purchased from Sigma-Aldrich (Deisenhofen, Germany). The stock solution of DNA was 1.3×10^{-4} mol dm⁻³ in 2×10^{-3} mol dm⁻³ phosphate buffer, pH 7.0, and its exact concentration was determined spectrophotometrically and related to the nucleotide content.

Britton-Robinson buffer solutions, used as the supporting electrolytes for VAR investigation, were prepared in the usual way.¹⁷ For the DNA studies, the adsorption was performed in phosphate buffer, and voltammetric measurements were realised in ammonium formate/sodium phosphate buffer. All the chemicals used for buffer preparation were of analytical grade.

Double distilled water was used throughout. All experiments were performed at room temperature.

Instrumentation

The measurements were performed with an μ AUTOLAB analyzer (EcoChemie, Utrecht, The Netherlands) connected to VA-Stand 663 (Metrohm, Herisau, Switzerland), and controlled by GPES 4.9 software. A standard three-electrode electrochemical cell was used. The working electrode was a hanging mercury drop electrode (HMDE) with drop area of 0.4 mm², the reference electrode was Ag/AgCl/3 mol dm⁻³ KCl, and a platinum wire was used as the auxiliary electrode.

Alternatively, in some voltammetric measurements, an Amel 433-A computerized polarographic analyzer was used, with a similar three-electrode system (working HMDE with a drop area of 1.9 mm², Ag/AgCl reference and Pt-auxiliary electrode).

A Radiometer PHM 220 pH meter with a Radiometer GK2401B combined pH electrode was used.

Cyclic (CV), differential pulse (DPV) and square wave (SWV) voltammetric techniques were used in this work. The CV mode was applied with the scan rates from 5 to 100 mV s⁻¹,

DPV was performed with pulse amplitude of 50 mV, pulse width 50 ms and scan rates of 20, 50 and 100 mV s⁻¹, while the parameters for the SWV mode were: amplitude 50 mV, scan increment 1–5 mV, frequency 125 Hz and sampling time 1 ms, and when required, the stirring speed of 300 rpm was applied. In the adsorptive stripping experiments, the adsorption accumulation potential and time were selected.

Procedure for the pH investigation

An appropriate volume of the supporting electrolyte of different pH values were placed in the electrochemical cell, de-aerated for 10 minutes with high purity nitrogen and then 0.15 ml of the VAR stock solution (S₀) was added to give a final VAR concentration of 1×10⁻⁵ mol dm⁻³ for cyclic voltammetry (CV) and differential pulse voltammetry (DPV). The solution was purged for a further 3 min and the current–voltage curves were recorded.

Procedure for adsorptive stripping voltammetric investigation

An aliquot of 15.00 ml of supporting electrolyte (BR buffer) solution was introduced into the electrochemical cell and de-aerated with pure nitrogen for 10 min. A selected accumulation potential was applied to the mercury drop for a selected accumulation period, while the solution was stirred at 300 rpm. The stirring was then stopped and after the rest period, adsorptive stripping square wave voltammetry was applied for reduction process over the range –0.2 to –1.2 V vs. Ag/AgCl. After the background voltammogram had been recorded, an adequate aliquot of the stock VAR solution was added to the cell and under the same conditions, the AdSSW voltammogram was recorded at a new drop.

Procedure for adsorptive transfer stripping technique (AdTS, ex situ)

DNA was adsorbed from a 5 µl sample drop onto the HMDE surface for 120 s. Then the electrode with an adsorbed DNA layer was washed with water and transferred into the background electrolyte, where the voltammetry was performed. The same procedure was employed with VAR under the same experimental conditions. The measurements were performed in the absence of oxygen, by passing nitrogen through the solution for 5 minutes before starting the measurements.

Alternatively, VAR and DNA were mixed, and after the selected incubation period (2–30 min) this mixture was adsorbed from a 5 µl drop onto the HMDE. The electrode modified with a VAR–DNA layer was washed and transferred into the background electrolyte and the SW voltammogram was recorded.

RESULTS AND DISCUSSION

Effect of pH

The study of the redox processes of VAR was performed in the pH range 2.0 to 12.0 in BR buffers. VAR exhibited electrochemical activity at all the investigated pH values. The voltammetric behaviour of VAR was examined using CV and DPV. Some representative voltammograms are presented in Fig. 1. Two reduction peaks (I and II) were present. Peak I was present over the whole pH range, and its reversibility increased with increasing pH. On the other hand, peak II was irreversible and not well developed. This peak appeared at negative potentials (–0.7 V < E_p < –1.0 V) and disappeared in neutral and alkaline media while the peak I attained full reversibility.

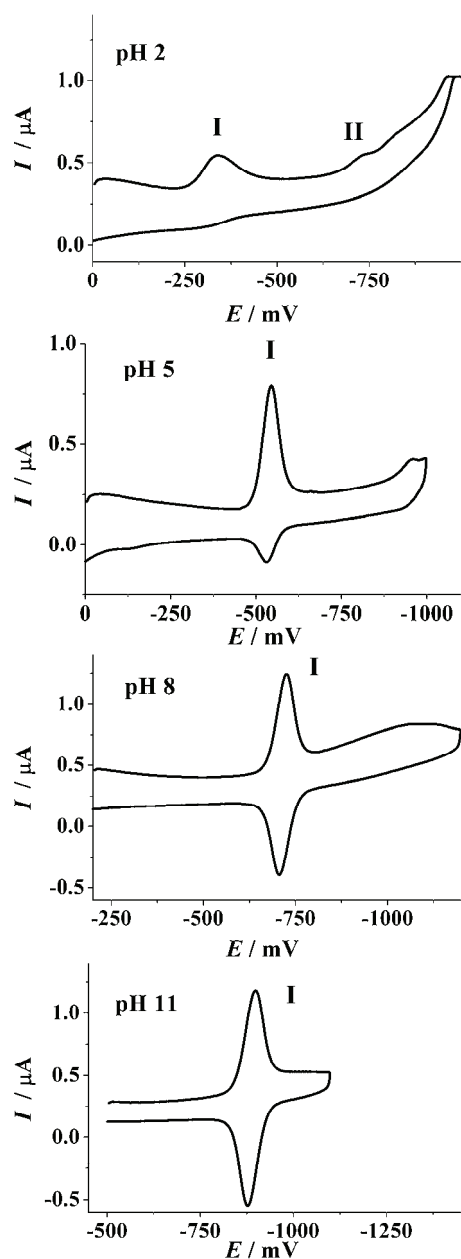


Fig. 1. Representative CV voltammograms of $1 \times 10^{-5} \text{ mol dm}^{-3}$ VAR in BR buffer: pH 2.0, 5.0, 8.0 and 11.0. Scan rate: 100 mV s^{-1} .

Attention was focussed on peak I, which is the consequence of the two-electron reduction of the C=N bond in VAR to give dihydrovarenicline.⁹ The peak current increased with the increasing pH, (Fig. 2A), indicating a higher rate of drug adsorption at the electrode surface in neutral and alkaline media. At the

same time, the peak potential was shifted towards more negative potentials, and linearly varied from -0.3 V at pH 2.0 up to -0.96 V at pH 12.0 (Fig. 2B), proving that protons participate directly in the reduction process.

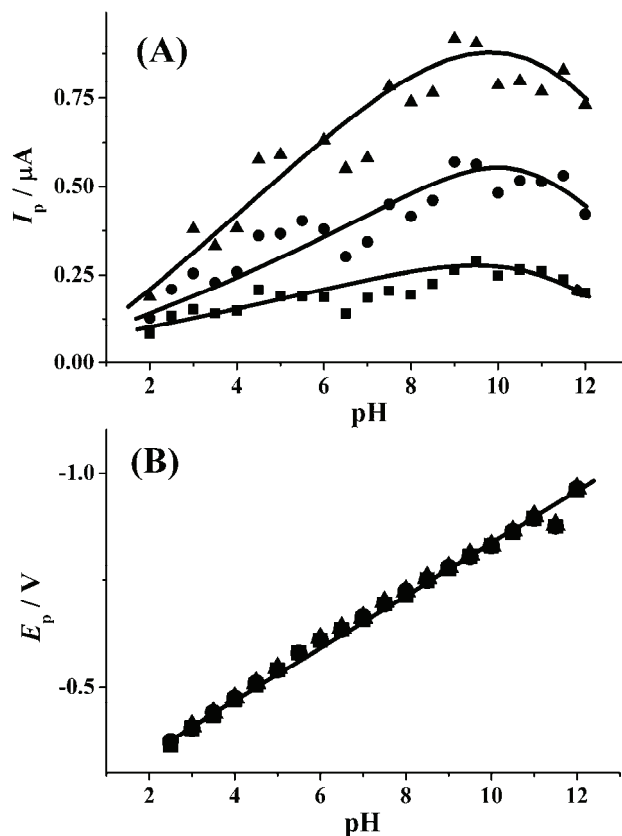


Fig. 2. The influence of pH on CV peak current (A) and peak potential (B) of 1×10^{-5} mol dm^{-3} VAR in BR buffer at different scan rates: 20 (■), 50 (●) and 100 mV s^{-1} (▲).

Using a VAR concentration of 1×10^{-5} mol dm^{-3} at different pH values and varying the scan rate over the range 5–100 mV s^{-1} , the voltammetric peak current was measured. At $\text{pH} < 4.0$, the I_p vs. ν dependence is nonlinear, but at $\text{pH} > 4.0$, a linear dependence was obtained, suggesting that the reduction process is controlled by adsorption. According to the values of the obtained slopes (Table I), it seems that the most pronounced adsorption of VAR at the mercury surface was observed at pH around 8. This means that the adsorbed form of VAR undergoes an electrode reduction process under these conditions.

The slope of the linear dependences of $\log I_p$ vs. $\log \nu$ at $\text{pH} > 4.0$ increases and becomes equal to the theoretical value of 1.0 at pH 8.0, which is characteristic for an entirely adsorption controlled processes. In addition, the small de-

crease of the slopes in the linear dependences $\log I_p$ vs. $\log v$ at $\text{pH} > 8.0$ expresses a weakened adsorption in highly alkaline solutions.

TABLE I. Regression equations of the $I_p = f(v)$ and $\log I_p = f(\log v)$ linear dependences, in acid and alkaline medium

pH	$I_p / \mu\text{A} = f(v / \text{V}^{-1} \text{ s})$	r	$\log I_p = f(\log v)$	r
2.0	Nonlinear	–	$\log I_p = 0.4831 \log v - 0.269$	0.997
4.0	Nonlinear	–	$\log I_p = 0.664 \log v + 0.267$	0.997
6.0	$I_p = 5.740v + 0.0466$	0.996	$\log I_p = 0.861 \log v + 0.668$	0.995
8.0	$I_p = 7.218v + 0.0143$	0.997	$\log I_p = 1.001 \log v + 0.882$	0.998
10.0	$I_p = 7.217v + 0.0851$	0.995	$\log I_p = 0.741 \log v + 0.642$	0.999
12.0	$I_p = 6.965v + 0.0553$	0.995	$\log I_p = 0.628 \log v + 1.292$	0.997

Adsorptive character of the drug

To improve the sensitivity for monitoring the accumulated drug, adsorptive stripping square-wave voltammetry was applied. The signal intensity of the AdSSW voltammetry was found to be 30 and 600 times higher than those of differential pulse (DP) and linear sweep (LS) adsorptive technique, respectively. The advantage of the application of an SW waveform was documented by trace analysis of several drugs that exhibited adsorption at the electrode surface.^{18–21} The SW response markedly depended on the parameters of the excitement signal. In order to obtain the maximum peak current, the optimum instrumental conditions (frequency of 125 Hz, scan increment of 5 mV and pulse amplitude of 50 mV) were applied in the further work.

Effect of accumulation time (t_{acc}) and potential (E_{acc})

The effect of accumulation time on the peak current for $1 \times 10^{-7} \text{ mol dm}^{-3}$ VAR was studied in the range from 1 to 30 s. The peak current increased with increasing accumulation time up to 10 s when adsorptive saturation on the mercury electrode surface was finally achieved. Under such conditions, interactions among the drug molecules in the adsorbed state became noticeable and the peak current commenced to decrease slightly. Hence, accumulation times longer than 10 s are required for work with an electrode surface covered with a VAR layer (Fig. 3A).

The potential range of -0.1 to -0.8 V was examined for $1 \times 10^{-7} \text{ mol dm}^{-3}$ VAR after a pre-concentration time of 10 s, to define the optimal accumulation potential. The highest current peak was obtained with a deposition potential of -0.4 V at pH 5.0 and -0.6 V at pH 8.0 (Fig. 3B). The observed gradual decrease in peak current intensity may be the consequence of desorption of the drug at much higher or lower potentials compared to the potential of zero charge, when the maximum adsorption of uncharged organic molecules is expected.

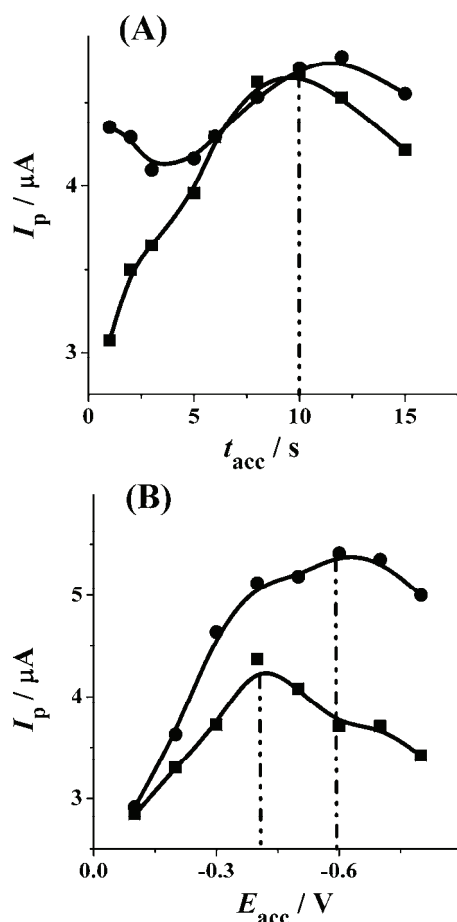


Fig. 3. The influence of (A) accumulation time (t_{acc}) and (B) accumulation potential (E_{acc}) on the AdSSWV current peak for $1 \times 10^{-7} \text{ mol dm}^{-3}$ VAR in BR pH 5.0 (■) and 8.0 (●) (B: $t_{\text{acc}} = 10$ s).

Effect of the drug concentration

Applying AdSSW voltammetry under the chosen optimal conditions for VAR concentrations above $10^{-7} \text{ mol dm}^{-3}$, the peak height increased linearly up to $4 \times 10^{-7} \text{ mol dm}^{-3}$, and then slightly decreased. Simultaneously, the peak potential was almost constant (Fig. 4).

This behaviour suggests that with increasing concentration, the electrode surface reaches its full coverage, and it can be assumed that at a VAR bulk concentration above $5 \times 10^{-7} \text{ mol dm}^{-3}$, a monolayer is completely formed and only the adsorbed VAR molecules undergo electron transfer processes. The CV response involving only the adsorbed species is characterized by symmetric cathodic and anodic peak shapes, which are noticeable in Fig. 1. The relative position of cathodic and anodic peaks depends on the relative adsorption energies of the oxidized and reduced species, and the corresponding peak current is given by:

$$I_p = \frac{n^2 F^2}{4RT} \nu A \Gamma \quad (1)$$

where n represents the number of electrons transferred in a reversible electrode reaction, A is the electrode surface area and Γ is the surface coverage in moles of adsorbed molecules per surface area. Applying this equation to the results obtained for the CV curves of $1 \times 10^{-5} \text{ mol dm}^{-3}$ VAR two electron reduction at pH 8.0, the amount of electroactive specie on the surface was evaluated, and the experimental surface coverage was found to be $\Gamma = 1.03 \times 10^{-10} \text{ mol cm}^{-2}$. To check whether this corresponds to a monolayer, the theoretical surface coverage was estimated by considering the varenicline molecule as a rectangle with an area of 1.5 nm^2 ($0.75 \text{ nm} \times 2 \text{ nm}$ corresponding to the bond lengths²²). A dense arrangement of these molecules should lead to a coverage of $\Gamma = 1.107 \times 10^{-10} \text{ mol cm}^{-2}$. This confirms that in the limit of the approximations made, the electrode was covered with a monolayer of varenicline.

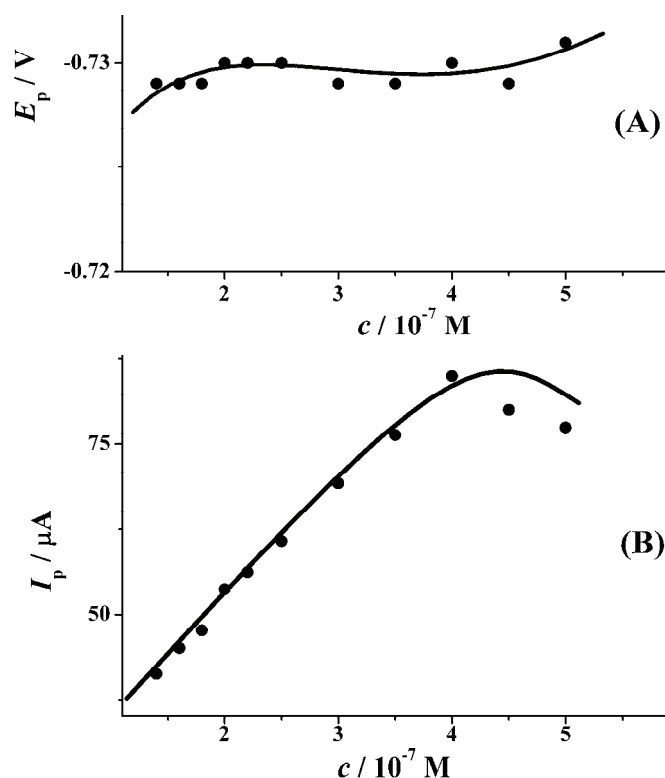


Fig. 4. Dependence of the AdSSWV peak potential (A) and current (B) on the VAR concentration in BR buffer at pH 8.0.

VAR–DNA Interaction

For the study of VAR–DNA interaction, DNA was pre-incubated with VAR in equal concentrations for different incubation periods. After this incubation period, the HMDE was modified with this mixture and the interaction was studied by comparing the obtained voltammogram with the signals obtained for HMDE/VAR and HMDE/DNA modified electrodes under the same conditions. The conditions pH (pH 7.0), ionic strength (5×10^{-2} mol dm⁻³ NaCl), concentrations (20 – 100×10^{-6} mol dm⁻³), and incubation time (2–30 min) were selected in order to ensure that both components are fully adsorbed at the electrode surface. After the incubation period, SWV measurements were performed using the adsorptive transfer stripping technique (AdTS).

The usual reduction and subsequent oxidation and electron transfer reactions characteristic for both components are shown in Fig. 5. The reversible reduction peak at -0.654 V corresponds to the two-electron reduction of VAR (curve 1, peak V), while DNA produces a cathodic peak at -1.426 V due to the reduction of adenine and cytosine (curve 2a, peak A/C) and an anodic peak of re-oxidized guanine at -0.253 V (curve 2b, peak G) after its reduction at extremely negative potentials.

After the incubation of VAR and DNA, the obtained voltammogram showed changes in the peak heights and potentials (curves 3a and 3b). All peak currents decreased, and the VAR peak potential was shifted to a more positive potential. This indicates that VAR and DNA interact and that the ds-DNA structure can be distorted as a result of subtle damage by this drug.

The changes in the current responses caused by VAR–DNA interaction were expressed as normalized peak currents: V (%), A/C (%), and G (%) using Eqs. (2)–(4):

$$V (\%) = 100I_{p,V}/I_{p0,V} \quad (2)$$

$$A/C (\%) = 100I_{p,A/C}/I_{p0,A/C} \quad (3)$$

$$G (\%) = 100I_{p,G}/I_{p0,G} \quad (4)$$

where $I_{p,V}$, $I_{p,A/C}$ and $I_{p,G}$ and $I_{p0,V}$, $I_{p0,A/C}$ and $I_{p0,G}$ are the peak currents of varenicline, adenine/cytosine and guanine after and before interaction, respectively. The obtained results are summarized in Table II. The normalized peak current of both compounds decreased after incubation.

The phenomenon of a change in the nature of the interaction from electrostatic to intercalative with increasing ionic strength was reported.²³ According to this study, the formal potential shift in the negative direction at low ionic strengths shows that the behaviour of the ds-DNA on the electrode surface was dominated by electrostatic interactions, while the formal potential shift in the positive direction at higher ionic strengths indicates intercalative interactions.

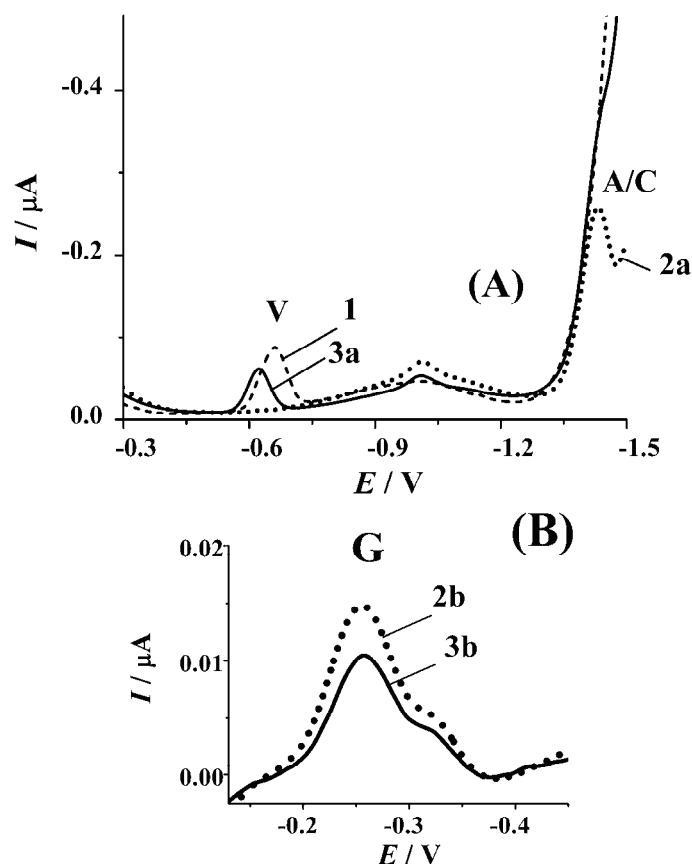


Fig. 5. AdTSSW voltammograms of: 1×10^{-5} mol dm $^{-3}$ VAR (1 - - -), ds-DNA (2a, 2b \cdots) and VAR-DNA mixture (3a, 3b \rightarrow). The compounds were adsorbed from 0.05 mol dm $^{-3}$ NaCl with 0.002 mol dm $^{-3}$ phosphate buffer, pH 7.0, for $t_{\text{acc}} = 120$ s, $E_{\text{acc}} = \text{OCP}$. The HMDE with adsorbed layers of (1), (2) or (3) were transferred to the blank background electrolyte 0.3 mol dm $^{-3}$ ammonium formate/sodium phosphate buffer, pH 6.86 and the SW voltammograms were recorded (frequency 25 Hz, amplitude 200 mV, potential range from 0 to -1.85 V). A) cathodic; B) anodic peaks.

The formal potential shift can be expressed as:

$$\Delta E^{0'} = E_{\text{surf}}^{0'} - E_{\text{sol}}^{0'} = \frac{RT}{nF} \ln \frac{K_{\text{Red}}}{K_{\text{Ox}}} \quad (5)$$

where $E_{\text{surf}}^{0'}$ and $E_{\text{sol}}^{0'}$ represent the formal potentials of the redox species immobilized on the electrode surface and in the solution, and K_{Red} and K_{Ox} are the surface-binding constants for the reduced and oxidized forms of the redox species, respectively. In the case of VAR, which undergoes a reversible, two-electron transfer at relatively high ionic strength (0.05 mol dm $^{-3}$), the ratio of $K_{\text{V,Red}}/$

$/K_{V,Ox}$ was estimated and is presented in Table II. These results indicate that the reduced form of VAR interacts with the ds-DNA on the modified electrode surface more strongly (3–14 times, depending on the incubation period) than the oxidized form. This behaviour is characteristic of intercalative interactions.²³ The shift in VAR peak potential, E_p , towards more positive potentials after VAR–DNA incubation supports this hypothesis.

TABLE II. The VAR–DNA interaction expressed by normalized values of the SW voltammetric responses, change in the peak potential, and surface binding constants ratio

Peak	E_p / V	$100I_p/I_{p0}$		$\Delta E_p / V$		$K_{V,Red}/K_{V,Ox}$	
		10	30	10	30	10	30
V	-0.654	74.9	31.1	34.0	15.0	14.0	3.0
A/C	-1.426	31.0	6.95	–	–	–	–
G	-0.253	72.5	68.7	–	–	–	–

CONCLUSIONS

The novelty of these investigations is based on the adsorption effects of VAR at a mercury surface, which enables the application of AdSSW voltammetry for studying the redox processes of VAR in the adsorbed state. The obtained values of surface coverage and accumulation potential and time were used to determine the conditions under which VAR is fully adsorbed at the electrode surface.

Association interaction of calf thymus ds-DNA with VAR at the modified HMDE was investigated. At room temperature and selected ionic strength, subtle DNA damage in the direct DNA–VAR interaction was observed, suggesting intercalation as the type of the interaction. The results lead to the conclusion that the toxicity of the investigated drug could be caused by this interaction. This study used simple electroanalytical methodology and showed the potential use of a DNA/HMDE biosensor for investigation of genotoxic effects.

Acknowledgement. This work was supported by the Ministry of Education, Science and Technological Development of the Republic of Serbia, Project No. 172033.

ИЗВОД

ЕЛЕКТРОХЕМИЈСКО ИСПИТИВАЊЕ АДСОРПЦИЈЕ И ИНТЕРАКЦИЈЕ ВАРЕНИКЛИНА И ДНК

ВАЛЕНТИНА РАДУЛОВИЋ¹, МАРА М. АЛЕКСИЋ² и ВЕРА КАПЕТАНОВИЋ¹

¹Универзитет у Београду, Фармацеушки факултет, Катедра за аналитичку хемију, Војводе Степе 450, 11000 Београд и ²Универзитет у Београду, Фармацеушки факултет, Катедра за физичку хемију и инструменталне методе, Војводе Степе 450, 11000 Београд

Електрохемијско понашање варениклина, новог парцијалног агонисте $\alpha_4\beta_2$ никотинског рецептора, који се користи за одвикавање од пушења, испитано је цикличном, диференцијално пулсном и волтаметријом правоугаоних таласа у Бритон–Робинсоновом пуферу (рН 2,0–12,0). На основу утицаја рН, брзине промене потенцијала, концен-

трације, потенцијала и времена акумулације на висину и положај пика, закључено је да је процес редукције у алкалној средини контролисан адсорпцијом варениклина. Коришћењем експериментално добијене вредности површинске запоседнутости, $\Gamma = 1,03 \times 10^{-10} \text{ mol cm}^{-2}$, одређени су услови под којима је варениклин потпуно адсорбован на површини електроде. Имајући у виду могућу високу токсичност варениклина, с обзиром на присуство хиноксалинског прстена у структури, претпостављено је да варениклин интерагује са ДНК када су оба молекула адсорбована на модификованој живиној електроди. Ова интеракција је испитана коришћењем „адсорптивне трансфер технике“ и примећене су промене потенцијала и смањење нормализованих струја волтаметријских пикова. На основу израчунате вредности односа константи везивања закључено је да се редуктовани облик варениклина јаче везује за ДНК од оксидованог. Претпостављено је да директна варениклин-ДНК интеракција на собној температури доводи до извесног оштећења ДНК и да је тип интеракције – интеркалација. Ова једноставна електроаналитичка методологија могла би наћи примену у виду потенцијалног биосензора за испитивање генотоксичних ефеката.

(Примљено 20. априла, ревидирано 10. јула 2012)

REFERENCES

1. J. W. Coe, P. R. Brooks, M. G. Vatelino, *J. Med. Chem.* **48** (2005) 3474
2. R. M. Rajurkar, V. A. Agrawal, S. S. Thonte, R. G. Ingate, *Pharmacophore* **1** (2010) 65
3. B. Satheesh, S. Kumarpulluru, V. Raghavan, D. Saravanan, *Acta Chromatogr.* **22** (2010) 207
4. A. A. Kadi, M. S. Mohamed, M. G. Kassen, I. A. Darwish, *Chem. Cent. J.* **5** (2011) 30
5. *Methods of Reducing Degradant Formation in Pharmaceutical Compositions of Varenicline*, <http://www.freepatentsonline.com/y2008/0026059.html> (accessed January 2012)
6. *Varenicline Standards and Impurity Controls*, <http://www.freepatentsonline.com/US2007/0224690.html> (accessed September 2011)
7. F. R. Busch, P. E. Concannon, R. E. Handfield, J. D. McKinley, M. E. McMahon, R. A. Singer, T. J. Watson, *Synth. Commun.* **38** (2008) 441
8. H. M. Faessel, B. J. Smith, M. A. Gibbs, J. S. Gobey, D. J. Clark, A. H. Burstein, *J. Clin. Pharmacol.* **46** (2006) 991
9. M. M. Aleksić, V. Radulović, N. Lijeskić, V. Kapetanović, *Curr. Anal. Chem.* **8** (2012) 133
10. J. Labuda, M. Fojta, F. Jelen, E. Paleček, in: *Encyclopaedia of Sensors*, Vol. 3, E.-F. C. A. Grimes, E. C. Dickey, M. V. Pishko, Eds., American Scientific Publishers, Valencia, USA, 2006, p. 201
11. J. Wang, in *Electrochemistry of Nucleic Acids and Proteins. Towards Electrochemical Sensors for Genomics and Proteomic*, E. Paleček, F. Sheeller, J. Wang, Eds., Elsevier, Amsterdam, The Netherlands, 2005, p. 175
12. M. Fojta, *Electroanalysis* **14** (2002) 1449
13. F. Lucarrelli, G. Marrazza, A. P. F. Turner, M. Mascini, *Biosens. Bioelectron.* **19** (2004) 515
14. K. J. Odenthal, J. J. Gooding, *Analyst* **132** (2007) 603
15. E. Palecek, M. Fojta, *Anal. Chem.* **73** (2001) 74A
16. E. Palecek, *Electroanalysis* **8/1** (1996) 7
17. D. D. Perrin, B. Dempsey, *Buffers for pH and Metal Ion Control*, Chapman and Hall, London, UK, 1974, p. 155

18. M. M. Ghoneim, A. M. Beltagi, *Talanta* **60** (2003) 911
19. A. H. Al-Ghamdi, O. M. Al-Ghamdi, M. A. Al-Omar, *Anal. Lett.* **41** (2008) 90
20. S. A. Ozkan, *Curr. Pharm. Anal.* **5** (2009) 127
21. M. Aleksić, V. Kapetanović, *J. Electroanal. Chem.* **593** (2006) 258
22. *Handbook of Chemistry and Physics*, 87th ed., D. R. Lide, Ed., CRC Taylor and Francis Group, Boca Raton, USA, 2006–2007, pp. 9–1
23. D. W. Pang, H. D. Abruna, *Anal. Chem.* **70** (1998) 3162.



J. Serb. Chem. Soc. 77 (10) 1423–1436 (2012)
JSCS–4363

Development and validation of a solid phase extraction-HPLC method for the determination of carbamazepine and its metabolites, carbamazepine epoxide and carbamazepine *trans*-diol, in plasma

PREDRAG DŽODIĆ^{1*}, LJILJANA ŽIVANOVIĆ², ANA PROTIĆ², IVANA IVANOVIĆ³,
RADMILA VELIČKOVIĆ-RADOVANOVIĆ¹, MIRJANA SPASIĆ¹, STEVO LUKIĆ¹
and SLAVOLJUB ŽIVANOVIĆ¹

¹University of Niš, Faculty of Medicine, Bulevar dr Zorana Đinđića 81, 18000 Niš, Serbia,

²University of Belgrade, Faculty of Pharmacy, Department of Drug Analysis, Vojvode Stepe
450, 11221 Belgrade, Serbia and ³Avantor Performance Materials, Teugseweg 20,
7400 AA Deventer, The Netherlands

(Received 6 January, revised 11 June 2012)

Abstract: A solid phase extraction-HPLC method has been developed and validated for the rapid analysis of carbamazepine and its two metabolites, carbamazepine epoxide and carbamazepine *trans*-diol, in human plasma. The analysis was performed using a C18 Bakerbond-BDC analytical column (250 mm×4.6 mm i.d., particle size 5 μm). The optimal conditions for the separation were established with the mobile phase acetonitrile – 10 mM phosphate buffer, pH 7.0 (30:70, v/v) at a flow rate of 1.5 mL min⁻¹ and temperature of 35 °C, with UV detection at 210 nm. The total run time was about 8 minutes. The SPE procedure for the extraction of the analytes from a plasma sample was developed using Oasis HLB cartridges and subsequently, the eluate was injected into the HPLC system for analysis. Afterwards, the SPE-HPLC method was subjected to validation. Linearity was obtained over the concentration range of 0.2–25 μg mL⁻¹ for carbamazepine, carbamazepine epoxide and carbamazepine *trans*-diol, with correlation coefficients higher than 0.995. The method showed good intra-day and inter-day precision with a relative standard deviation below 7.96 %, while the accuracy ranged from 92.09 to 108.5 % for all analytes. Finally, the method was successfully applied to the analysis of the plasma samples of epileptic patients in mono- and polytherapy.

Keywords: human plasma; carbamazepine; carbamazepine epoxide; carbamazepine *trans*-diol; solid phase extraction.

* Corresponding author. E-mail: pdzodic@gmail.com
doi: 10.2298/JSC120106084D



INTRODUCTION

Carbamazepine (CBZ, Fig. 1a) is a tricyclic lipophilic compound used in the treatment of epilepsy, trigeminal neuralgia and bipolar disorders.^{1–3} A CBZ plasma concentration ranging from 4 to 12 $\mu\text{g mL}^{-1}$ is associated with seizure control.^{4,5} CBZ is a strong inducer of microsomal enzymes (cytochrome P450 in liver) which can quicken its own metabolism and those of co-administered drugs.⁵ Hence, polytherapy may be associated with drug interactions and undesired toxicity.

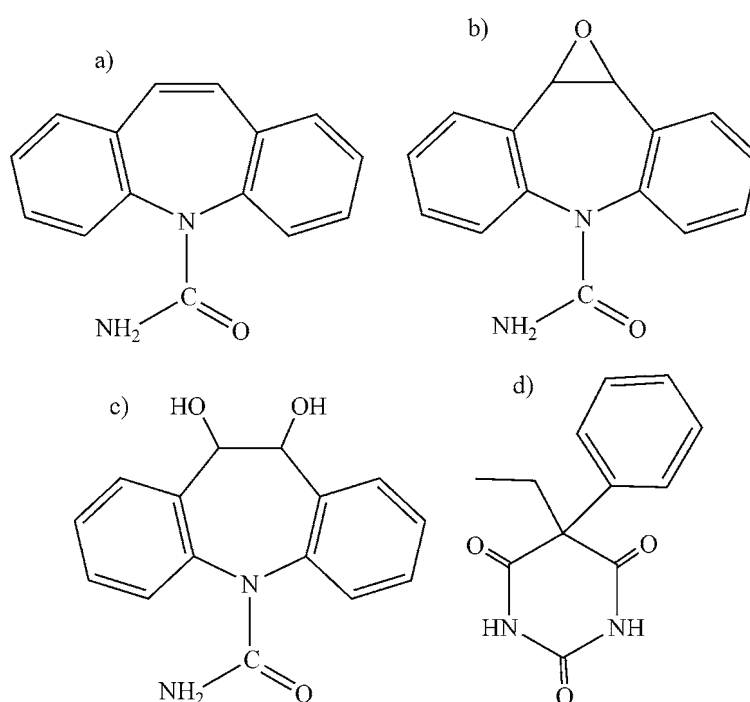


Fig. 1. Structures of carbamazepine, CBZ (a), carbamazepine epoxide, CBZ-E (b), carbamazepine *trans*-diol, CBZ-DIOH (c) and the internal standard phenobarbital (d).

Carbamazepine epoxide (CBZ-E, Fig. 1b) is the most important among its 33 metabolites, because CBZ-E exerts pharmacological activity as does its parent compound.⁶ Afterwards, CBZ-E is mainly metabolized by epoxide hydrolases to carbamazepine *trans*-diol (CBZ-DIOH, Fig. 1c). CBZ-DIOH is fairly conjugated with glucuronic acid and excreted in urine.⁷ Therefore, regular measurement of the plasma levels of CBZ and its metabolites and dosage adjustment are necessary for patients undergoing chronic treatment with CBZ.

Commercially immunoassays are available for the determination of the concentration of CBZ. However, CBZ-E cannot be routinely monitored using immu-

noassays and therefore measurement of both CBZ and CBZ-E requires chromatographic analysis.⁸

According to a literature survey, HPLC and HPLC-MS methods have been published for the quantitative analysis of CBZ, its metabolites and other medications in human plasma. The HPLC-MS techniques are not widely used because the required expensive equipment is not available in most clinical laboratories. Prior to HPLC analysis, human plasma samples were subjected to protein precipitation, liquid-liquid extraction⁹⁻¹⁵, stir bar-sorptive extraction¹⁶ or solid phase extraction (SPE).^{7,17-21} Unfortunately, these methods^{7,17-21} are time-consuming on account of eluate evaporation and subsequent reconstitution in comparison with the SPE-HPLC method proposed herein. After the employed SPE procedure, the eluate is injected into the HPLC system without performing evaporation and reconstitution steps. Since the total time for sample preparation is shorter than 10 min, the proposed SPE-HPLC method is advantageous over the previously published SPE-HPLC methods^{7,17-21} in routine application.

An automated and sensitive SPE-HPLC method for analysis of CBZ, CBZ-E and CBZ-DIOH was found. This method was applied to the analysis of plasma samples obtained from rats treated with CBZ,²² but the applicability of the method to samples obtained from epileptic patients was not examined. According to the chromatogram of spiked drug-free plasma, interfering substances from human plasma were not completely separated from peaks of the analytes and internal standard.²² Considering the proposed SPE-HPLC method, the total chromatographic run time was about 8 min with excellent peak shapes and good resolution between the investigated compounds and interfering plasma substances. Furthermore, expenses and the overall time of therapeutic drug monitoring are reduced, which is important in the individualization of therapy of patients undergoing chronic treatment with CBZ.

SPE-HPLC method was subjected to validation according to US Food and Drug Administration (FDA)²³ and International Conference on Harmonisation (ICH)²⁴ guidelines. It fulfills the validation criteria in every segment of validation. Finally, the developed method was successfully applied to routine analysis of plasma samples of epileptic patients under both mono- and polytherapy. It could be used for cost-effective therapeutic drug monitoring of CBZ due to its appropriate sensitivity and selectivity.

EXPERIMENTAL

Chemicals and reagents

CBZ and internal standard phenobarbital (IS, Fig. 1d) as solid standard compounds were kindly provided by pharmaceutical company Galenika (Belgrade, Serbia). CBZ-E and CBZ-DIOH as solid standard compounds were kindly provided by pharmaceutical company Novartis Pharma (Basel, Switzerland). Acetonitrile and methanol HPLC gradient grade were purchased from Avantor Performance Materials (Deventer, The Netherlands). Sodium hydro-

xide and sodium dihydrogen phosphate suitable for HPLC were obtained from Merck (Darmstadt, Germany).

Instrumentation and materials

HPLC analysis was performed with an Agilent Technologies 1200 (Wilmington, DE, USA) chromatographic system equipped with on-line degasser, binary pump, column oven and photo diode array detector. Sample injection of 10 μL was performed using an Agilent 1200 Series high performance autosampler G1367B. Water for chromatography was obtained from a Smart 2 Pure (TKA, Niederelbert, Germany) purification system. Before use, the mobile phase was degassed and purified by vacuum filtration through 0.45 μm regenerated cellulose membrane filters (Agilent, Böblingen, Germany). The compounds were separated on a C18 Bakerbond-BDC analytical column (250 mm \times 4.6 mm; 5 μm) (Avantor performance materials, Deventer, The Netherlands). Data were acquired with Agilent ChemStation software. Statistical analysis was performed using Microsoft Excel software.

The SPE procedure was performed using a Visiprep-DL Vacuum Manifold, 12-port model from Supelco (Bellefonte, USA) coupled to a vacuum pump from KNF Neuberger (Freiburg, Germany). Oasis HLB cartridges (30 mg, 1 mL, particle size 30 μm) were purchased from Waters (Milford, MA, USA).

Chromatographic conditions

The mobile phase was 30:70 (v/v) acetonitrile–10 mM sodium dihydrogen phosphate (pH 7.0 adjusted with 1 M sodium hydroxide). The flow rate was 1.5 mL min^{-1} and the column temperature was set at 35 $^{\circ}\text{C}$. Detection was performed at 210 nm.

Human plasma samples

Patients and healthy volunteers who donated plasma samples gave written informed consent, and all investigations were approved by the Ethical committee (Faculty of Medicine, University of Niš, Serbia). Blank plasma was obtained from ten different healthy volunteers. Plasma samples from patients were obtained from Clinic of Neurology (University Clinical Centre Niš, Serbia). Blood samples were collected into vacutainers containing EDTA-Na, and separated by centrifugation at 3000 g for 10 min. All samples were stored at -80°C before analysis.

Standard solutions, calibration standards and quality control samples

Four standard stock solutions of CBZ, CBZ-E, CBZ-DIOH and IS were prepared in acetonitrile at a concentration of 10 mg mL^{-1} . The standard working solutions of CBZ, CBZ-E, CBZ-DIOH and IS contained 1 mg mL^{-1} in the mobile phase. Standard stock solutions were stored at -20°C and standard working solutions were stored at 4–8 $^{\circ}\text{C}$ for 1 month. No stability related problems were encountered during this period.

Each analyte was added separately for the preparation of standard curve samples. Volumes of 0.1, 0.3, 2.5, 5, 7.5, 10 and 12.5 μL of 1 mg mL^{-1} CBZ, CBZ-E and CBZ-DIOH standard working solutions were transferred to seven Eppendorf tubes containing 0.5 mL of blank human plasma. Five μL of 1 mg mL^{-1} IS standard working solution was added to each of the Eppendorf tubes. After dilution and the SPE procedure 0.2, 0.6, 5, 10, 15, 20 and 25 $\mu\text{g mL}^{-1}$ of CBZ, CBZ-E and CBZ-DIOH were obtained in the eluates. Concentration of IS was 10 $\mu\text{g mL}^{-1}$. The zero plasma samples were prepared by adding IS to drug-free human plasma to yield a final concentration of 10 $\mu\text{g mL}^{-1}$.

The quality control (QC) plasma samples were prepared to final concentrations of 0.6 (low), 10 (medium) and 20 $\mu\text{g mL}^{-1}$ (high) of all the investigated compounds. The concentra-

tion of IS was $10 \mu\text{g mL}^{-1}$. QC (medium) samples were used for the optimization of the SPE procedure.

QC samples were prepared daily, and parts of the low and high QC samples were stored at -80°C to study their stability after three freeze–thaw cycles and long-term stability.

Solid phase extraction procedure

Phosphate buffer (10 mM of sodium dihydrogen phosphate, pH 7.0) was added to the prepared samples (calibration standards, QC samples) to a volume of 1 mL, which was followed by brief vortex mixing.

The flow rate during the SPE procedure was maintained at about 1.0 mL min^{-1} . The SPE cartridges were conditioned with 1 mL of methanol, and 1 mL of the phosphate buffer (10 mM; pH 7.0). The diluted plasma samples (1 mL) were loaded onto the cartridges. A wash step was performed with 1 mL of phosphate buffer (10 mM; pH 7.0) and subsequently 1 mL of methanol – 10 mM phosphate buffer, pH 7.0 (20:80, v/v). The cartridges were then dried under vacuum (-40 kPa) for 30 s. Finally, the analytes and IS were eluted with 0.5 mL of acetonitrile – 10 mM phosphate buffer, pH 7.0 (60:40, v/v). A $10 \mu\text{L}$ volume of the eluate was injected into the HPLC system for analysis.

RESULTS AND DISCUSSION

Development of the HPLC method

At the beginning of the investigation, $\log D$ values of the compounds were calculated using MarvinSketch software.²⁵ The $\log D$ values of CBZ-DIOH, CBZ-E and CBZ were 0.81, 1.97 and 2.77, respectively (Table I). The $\log D$ values were pH independent except for CBZ-DIOH, the ionic form of which appeared at pH values higher than 9.80. Therefore, the $\log D$ values of CBZ-DIOH, CBZ-E and CBZ are equivalent to their $\log P$ values at pH values lower than 9.80. Due to the lipophilic nature of CBZ-E and CBZ, a C18 column package was chosen. The following columns were investigated: Bakerbond-BDC C18 (150 mm \times 4.6 mm; 5 μm), Bakerbond-BDC C18 (250 mm \times 4.6 mm; 5 μm) and Symmetry C18 (150 mm \times 4.6 mm; 5 μm). The Bakerbond-BDC C18 analytical columns are better than the classical C18 columns owing to improved peak symmetry, lower back pressure and a longer column lifetime. By using Bakerbond-BDC C18 (150 mm \times 4.6 mm; 5 μm) it was not possible to adequately separate the interfering plasma compounds from the analytes (CBZ, CBZ-E and CBZ-DIOH). Therefore, a longer column Bakerbond-BDC C18 (250 mm \times 4.6 mm; 5 μm) was used. As a result, the analytes were successfully separated from the plasma compounds.

TABLE I. $\text{p}K_{\text{a}}$ and $\log D$ values of the investigated compounds

Parameter	CBZ-DIOH	CBZ-E	CBZ
$\log D$	0.81	1.97	2.77
$\text{p}K_{\text{a}}$	12.80	–	–

When methanol was a constituent of a mobile phase, peak symmetry and resolution between the contiguous analytes were poor. Considering the absorption of methanol at 210 nm, acetonitrile was examined as a constituent of the mobile phase.

CBZ and CBZ-E are neutral analytes, and CBZ-DIOH is a weak acid ($pK_a = 12.80$). The examined pH range during the development of a chromatographic method is usually lower than 11. Therefore, it could be concluded that the pH of the mobile phase would not influence the retention of the investigated compounds, which was confirmed by a few experiments (mixtures 30:70 (v/v) acetonitrile–the phosphate buffer (10 mM) were used with a flow rate of 1.5 mL min^{-1} and column temperature at $35 \text{ }^\circ\text{C}$ with the pH adjusted to 6.2, 7 and 8.2). Furthermore, it was decided to use a mobile phase with the pH adjusted to 7. This decision was based on the chromatographic behavior of IS in order to shorten its retention time and hence the total run time.

Three variables were left to be optimized: percentage of acetonitrile, flow rate and temperature of the column. Firstly, a mixture 40:60 (v/v) acetonitrile–water was used as the mobile phase at a flow rate of 1 mL min^{-1} and with the column temperature at $30 \text{ }^\circ\text{C}$. Under these chromatographic conditions, very poor retention of CBZ-DIOH was achieved. Afterwards, the percentage of water was increased and a mixture 35:65 (v/v) acetonitrile–water was used as the mobile phase, while the other chromatographic conditions remained the same. The retention factor of CBZ-DIOH was 0.37, although it was noticed that the decrease in the percentage of acetonitrile led to an increase in the retention factors of all the investigated compounds. Subsequently, a mixture 35:65 (v/v) acetonitrile–phosphate buffer (10 mM; pH 7.0) was used as the mobile phase at a flow rate of 1 mL min^{-1} and a column temperature of $30 \text{ }^\circ\text{C}$. Addition of the phosphate buffer resulted in a better symmetry of the analyte peaks. Although the critical resolution of IS and CBZ-E peaks was improved, the retention factor of CBZ-DIOH was still less than 1. Therefore, the percentage of acetonitrile in mobile phase was decreased again and a mixture 30:70 (v/v) acetonitrile–phosphate buffer (10 mM; pH 7.0) was used at a flow rate of 1 mL min^{-1} and column temperature at $30 \text{ }^\circ\text{C}$. Now the separation was successful and retention factor of CBZ-DIOH was 0.98, but chromatographic run lasted about 12 minutes. Hence, the flow rate was increased to 1.5 mL min^{-1} and the column temperature was increased to $35 \text{ }^\circ\text{C}$. As a result, the total chromatographic run was shortened to about 8 min. Excellent peak shapes, good resolution between the contiguous peaks, and a number of theoretical plates of more than 17000 for all peaks were achieved. Retention factor of CBZ-DIOH was 1.02. Thus, these chromatographic conditions were chosen.

Development of the SPE procedure for sample pretreatment

Due to the different polarity of the neutral analytes (CBZ, CBZ-E and CBZ-DIOH), Oasis HLB cartridges were chosen since the polymeric sorbent retains both polar and non-polar compounds.²⁶

As the analytes are neutral compounds and it was proven during development of the HPLC method that pH had no influence on the retention of the analytes, it was decided to use the buffer which was a constituent of the mobile phase (10 mM sodium dihydrogen phosphate, pH 7.0) for the conditioning of the cartridges, as well as for the wash and the elution steps. The selectivity was enhanced by tuning the ratio of the organic solvent to the phosphate buffer (10 mM; pH 7.0). Absolute recovery values of the investigated compounds were calculated for the optimization of the SPE procedure.

After load step of QC medium samples, the sorbent completely retained the analytes and IS. The first wash step was performed by passing 1 mL of the phosphate buffer (10 mM; pH 7.0), which did not remove any analyte or IS from the cartridge. For the second wash step, 1 mL of the mixtures 5:95, 10:90, 15:85, 20:80 and 30:70 (v/v) methanol–phosphate buffer (10 mM; pH 7.0) were investigated. The mixture 20:80 (v/v) methanol–phosphate buffer (10 mM; pH 7.0) was the highest percentage of methanol that did not remove any analyte or IS from the cartridge.

For the elution step, 0.5 mL of 30:70, 40:60, 50:50, 60:40 and 70:30 (v/v) acetonitrile–phosphate buffer (10 mM; pH 7.0) were investigated. The mixture 60:40 (v/v) acetonitrile–phosphate buffer (10 mM; pH 7.0) was the lowest percentage of acetonitrile which completely eluted the analytes and IS from the cartridge. The total time for sample preparation was shorter than 10 min.

Method validation

The new SPE-HPLC method was validated following FDA²³ and ICH²⁴ guidelines. The following validation characteristics were evaluated: selectivity, sensitivity, linearity, precision, accuracy, absolute recovery and stability.

The proposed method is selective since co-elution was not spotted at the retention times of CBZ, CBZ-E, CBZ-DIOH and IS from freshly prepared spiked samples at LLOQ levels compared to the blank plasma obtained from 10 healthy volunteers. The corresponding chromatogram of blank plasma sample is shown in Supplementary material to this paper.

The calibration curves showed good linearity over the investigated concentration range (0.2–25 $\mu\text{g mL}^{-1}$ for all analytes). The obtained calibration curves were:

$$y = 0.1347x - 0.0118; r^2 = 0.9964 \text{ for CBZ-DIOH} \quad (1)$$

$$y = 0.1749x - 0.0725; r^2 = 0.9951 \text{ for CBZ-E} \quad (2)$$

and

$$y = 0.1426x - 0.0436; r^2 = 0.9976 \text{ for CBZ} \quad (3)$$

where y is peak area ratio, x is concentration of the compound and r is the correlation coefficient. The intercepts of the calibration curves were tested using the student's t -test. The following results were found for the standard deviation of

the slope (Sa), standard deviation of the intercept (Sb) and the confidence factor (t_{α}): $Sa = 0.0051$, $Sb = 0.0716$ and $t_{\alpha} = 0.1642$ for CBZ-DIOH; $Sa = 0.0078$, $Sb = 0.1093$ and $t_{\alpha} = 0.663$ for CBZ-E; and $Sa = 0.0044$, $Sb = 0.0615$ and $t_{\alpha} = 0.7093$ for CBZ. The deviation of the intercepts from zero were found to be insignificant ($p = 0.05$ and $t_{tab} = 2.37$). The corresponding chromatograms obtained from plasma sample spiked with IS, and plasma sample spiked with the analytes and IS in Supplementary material to this paper.

Limit of detection (LOD) and lower limit of quantification ($LLOQ$) values for all compounds were found to be $0.02 \mu\text{g mL}^{-1}$ and $0.2 \mu\text{g mL}^{-1}$, respectively. The accuracy and precision were evaluated in five replicates at the $LLOQ$ level. Accuracy is reported as recovery (R in %), precision as relative standard deviation (RSD in %) and the assessed values are given in Table II.

TABLE II. Intra-day precision and accuracy at $LLOQ$, low QC, medium QC, and high QC concentrations in plasma samples for CBZ-DIOH, CBZ-E and CBZ ($n = 5$)

Parameter	Nominal concentration in plasma, $\mu\text{g mL}^{-1}$			
	0.2	0.6	10	20
CBZ-DIOH				
Precision (RSD / %)	5.42	7.3	7.15	2.89
Accuracy (R / %)	102.63	92.72	108.50	103.27
Found concentration, $\mu\text{g mL}^{-1}$	0.205	0.556	10.85	20.65
CBZ-E				
Precision (RSD / %)	7.24	6.41	0.97	1.58
Accuracy (R / %)	114.41	98.60	98.95	98.30
Found concentration, $\mu\text{g mL}^{-1}$	0.229	0.592	9.895	19.659
CBZ				
Precision (RSD / %)	11.24	5.20	1.20	3.41
Accuracy (R / %)	89.05	102.77	98.71	103.87
Found concentration, $\mu\text{g mL}^{-1}$	0.178	0.617	9.87	20.77

After investigation of the intra-day and inter-day accuracy and precision at QC concentration levels, it was found that the obtained results for RSD (%) and recovery (R , %) were pursuant to FDA guidance²³ (precision of 20 % and accuracy of 80–120 % at the $LLOQ$; and precision of 15 % and accuracy of 85–115 % at the low QC, medium QC and high QC levels). The results are listed in Tables II and III.

To evaluate efficiency of the SPE procedure, the absolute recovery values were calculated. Spiked drug-free plasma samples at low QC, medium QC and high QC levels were diluted to 1 ml with the phosphate buffer and subjected to the SPE procedure. These samples were compared to blank plasma that had been extracted following the same SPE procedure and then spiked at the same concentration levels. The absolute recovery values as well as the estimated concentrations from human plasma for the investigated compounds are displayed in Table

IV. The absolute recovery values of all analytes did not appear to be dependent on concentration.

TABLE III. Inter-day precision and accuracy at *LLOQ*, low QC, medium QC, and high QC concentrations in plasma samples for CBZ-DIOH, CBZ-E and CBZ ($n = 5$)

Parameter	Nominal concentration in plasma, $\mu\text{g mL}^{-1}$		
	0.6	10	20
CBZ-DIOH			
Precision (<i>RSD</i> / %)	7.96	4.11	0.81
Accuracy (<i>R</i> / %)	92.09	104.58	100.90
Found concentration, $\mu\text{g mL}^{-1}$	0.55	10.46	20.18
CBZ-E			
Precision (<i>RSD</i> / %)	3.99	1.65	3.54
Accuracy (<i>R</i> / %)	93.34	98.23	104.04
Found concentration, $\mu\text{g mL}^{-1}$	0.56	9.82	20.81
CBZ			
Precision (<i>RSD</i> / %)	1.14	2.16	5.42
Accuracy (<i>R</i> / %)	98.06	100.00	106.31
Found concentration, $\mu\text{g mL}^{-1}$	0.59	10.00	21.26

TABLE IV. Absolute recoveries of CBZ-DIOH, CBZ-E and CBZ from plasma samples ($n = 5$)

Parameter	Nominal concentration in plasma, $\mu\text{g mL}^{-1}$		
	0.6	10	20
CBZ-DIOH			
Recovery, %	96.51	90.75	100.12
<i>RSD</i> / %	9.30	5.58	0.81
Found concentration, $\mu\text{g mL}^{-1}$	0.579	9.07	20.02
CBZ-E			
Recovery, %	104.04	95.89	93.80
<i>RSD</i> / %	3.99	0.97	3.54
Found concentration, $\mu\text{g mL}^{-1}$	0.624	9.589	18.76
CBZ			
Recovery, %	102.18	87.39	94.46
<i>RSD</i> / %	1.14	1.20	5.42
Found concentration, $\mu\text{g mL}^{-1}$	0.613	8.74	18.89

After performing the stability tests at low QC and high QC levels (short term, post-preparative, long-term stability and freeze–thaw cycles), the *RSD* values for the investigated compounds were below 8.39 %, while recovery values ranged from 90.84 to 112.35 %. Hence, the stability of the analytes was appropriate during all investigations. The results of the stability tests are given in Tables V–VIII.

Clinical application

Results of the assay of plasma samples obtained from nine epileptic patients under chronic treatment with CBZ are listed in Table IX. Along with CBZ, the

patients were co-administrated with amlodipine, bromazepam, dihydroergotoxine mesylate, aminophylline, fenoterol bromide, ipratropium bromide, beclomethasone dipropionate, prednisone, ramipril, losartan, acetylsalicylic acid, α -tocopherolacetate, nicergoline, lamotrigine, sodium valproate, topiramate, clonazepam, diazepam, lorazepam, phenytoin and ethosuximide. In all cases, no co-elution was observed at the retention times of the analytes and IS. To investigate additionally the selectivity of the method, plasma samples from healthy volunteers who had been administrated with the above-mentioned drugs were assayed and no interferences were registered.

On balance, the applicability of the method to routine analysis of plasma samples of epileptic patients under mono- and polytherapy was demonstrated. It allows for therapeutic drug monitoring of CBZ. However, the proposed method cannot be applied to analysis of plasma samples of patients co-administrated with CBZ and Phenobarbital, since it is used as an internal standard.

TABLE V. Results of short-term stability tests at low QC and high QC concentrations in plasma samples ($n = 5$)

Parameter	Nominal concentration in plasma, $\mu\text{g mL}^{-1}$	
	0.6	20
CBZ-DIOH		
Recovery, %	99.71	105.49
RSD / %	2.93	4.44
Found concentration, $\mu\text{g mL}^{-1}$	0.598	21.10
CBZ-E		
Recovery, %	90.84	104.26
RSD / %	8.39	1.01
Found concentration, $\mu\text{g mL}^{-1}$	0.545	20.85
CBZ		
Recovery, %	91.82	110.22
RSD / %	3.81	1.43
Found concentration, $\mu\text{g mL}^{-1}$	0.551	22.04

TABLE VI. Results of the post-preparative stability test at low QC and high QC concentrations in plasma samples ($n = 5$)

Parameter	Nominal concentration in plasma, $\mu\text{g mL}^{-1}$	
	0.6	20
CBZ-DIOH		
Recovery, %	101.56	99.77
RSD / %	6.81	0.64
Found concentration, $\mu\text{g mL}^{-1}$	0.609	19.95
CBZ-E		
Recovery, %	96.18	99.82
RSD / %	5.57	1.28
Found concentration, $\mu\text{g mL}^{-1}$	0.577	19.96

TABLE VI. Continued

Parameter	Nominal concentration in plasma, $\mu\text{g mL}^{-1}$	
	0.6	20
	CBZ	
Recovery, %	96.42	100.66
<i>RSD</i> / %	5.47	2.52
Found concentration, $\mu\text{g mL}^{-1}$	0.579	20.132

TABLE VII. Results of the freeze–thaw stability test at low QC and high QC concentrations in plasma samples ($n = 5$)

Parameter	Nominal concentration in plasma, $\mu\text{g mL}^{-1}$	
	0.6	20
	CBZ-DIOH	
Recovery, %	112.35	102.66
<i>RSD</i> / %	2.20	1.36
Found concentration, $\mu\text{g mL}^{-1}$	0.674	20.53
	CBZ-E	
Recovery, %	102.40	102.66
<i>RSD</i> / %	7.29	1.69
Found concentration, $\mu\text{g mL}^{-1}$	0.614	20.53
	CBZ	
Recovery, %	105.42	103.63
<i>RSD</i> / %	2.64	1.22
Found concentration, $\mu\text{g mL}^{-1}$	0.63	20.73

TABLE VIII. Results of the long-term stability test at low QC and high QC concentrations in plasma samples ($n = 5$)

Parameter	Nominal concentration in plasma, $\mu\text{g mL}^{-1}$	
	0.6	20
	CBZ-DIOH	
Recovery, %	110.18	99.71
<i>RSD</i> / %	2.39	5.96
Found concentration, $\mu\text{g mL}^{-1}$	0.661	19.94
	CBZ-E	
Recovery, %	102.31	101.06
<i>RSD</i> / %	3.60	5.23
Found concentration, $\mu\text{g mL}^{-1}$	0.614	20.21
	CBZ	
Recovery, %	109.32	97.09
<i>RSD</i> / %	2.02	4.39
Found concentration, $\mu\text{g mL}^{-1}$	0.656	19.42

TABLE IX. Results of the assay of plasma samples obtained from nine epileptic patients under treatment with CBZ ($n = 5$)

Patient	Hours from last dosage	CBZ dosage, mg day ⁻¹	(Mean concentration ^a ± SD ^b) / µg mL ⁻¹		
			CBZ	CBZ-E	CBZ-DIOH
S.A	10.5	400	6.47±0.03	1.36±0.06	1.06±0.01
R.J.	10	600	8.74±0.05	2.06±0.02	3.06±0.04
M.L.	1	200	4.72±0.03	1.34±0.02	0.88±0.03
I.I.	9	400	7.12±0.07	1.44±0.03	1.40±0.06
A.D.	12	600	11.95±0.12	2.24±0.08	4.53±0.07
B.V.	13	1200	16.91±0.11	3.99±0.05	6.84±0.06
I.S	4	600	5.43±0.05	1.48±0.03	1.75±0.03
P.B.	3	400	8.7±0.07	1.69±0.04	1.48±0.09
T.R.	10.5	600	ND ^c	ND	ND

^aMean concentration in plasma, µg mL⁻¹; ^bstandard deviation, µg mL⁻¹; ^cnot determined, concentration was below the *LLOQ*

CONCLUSIONS

The chromatographic behavior of the investigated compounds was examined. As a result, an SPE-HPLC method was developed and validated. It showed satisfactory precision and accuracy with *RSD* values in the range from 0.81 to 11.24 % and recovery (*R*, %) values from 89.05 to 114.41 %. The linearity of the method was adequate in the range 0.20–25 µg mL⁻¹ with a correlation coefficient higher than 0.9951 for the investigated compounds. The efficiency of the extraction procedure was established with the assistance of absolute recovery values, which were calculated to be from 87.39 to 104.04 %. During analysis of plasma samples obtained from patients, no interferences from endogenous compounds and co-administered drugs were found. Therefore, the developed chromatographic method was shown to be suitable for the simultaneous determination of CBZ and its metabolites CBZ-E and CBZ-DIOH in the plasma of epileptic patients. The short chromatographic run time and the rapid SPE procedure are important advantages of the proposed SPE-HPLC method for its routine application. In conclusion, the applicability of the method to therapeutic drug monitoring of patients under chronic treatment with CBZ was proved.

SUPPLEMENTARY MATERIAL

Representative chromatograms of blank plasma, blank plasma spiked with internal standard, blank plasma spiked with CBZ, CBZ-E, CBZ-DIOH and internal standard and plasma sample of an epileptic patient after receiving an oral dose of CBZ are available electronically from <http://www.shd.org.rs/JSCS/>, or from the corresponding author on request.

Acknowledgments. This research was supported by the Ministry of Education, Science and Technological Development of the Republic of Serbia as part of Project No. OI 172033. Carbamazepine and phenobarbital as solid standard compounds were kindly provided by the pharmaceutical company Galenika (Belgrade, Serbia). Carbamazepine epoxide and carbamazepine *trans*-diol as solid standard compounds were kindly provided by the pharmaceutical company Novartis Pharma (Basel, Switzerland).

ИЗВОД

РАЗВОЈ И ВАЛИДАЦИЈА SPE-HPLC МЕТОДЕ ЗА ОДРЕЂИВАЊЕ КАРБАМАЗЕПИНА И МЕТАБОЛИТА КАРБАМАЗЕПИН ЕПОКСИДА И КАРБАМАЗЕПИН *trans*-ДИОЛА У ПЛАЗМИ

ПРЕДРАГ ЦОДИЋ¹, ЉИЉАНА ЖИВАНОВИЋ², АНА ПРОТИЋ², ИВАНА ИВАНОВИЋ³, РАДМИЛА ВЕЛИЧКОВИЋ-РАДОВАНОВИЋ¹, МИРЈАНА СПАСИЋ¹, СТЕВО ЛУКИЋ¹ и СЛАВОЉУБ ЖИВАНОВИЋ¹

¹Универзитет у Нишу, Медицински факултет, Булевар др Зорана Ђинђића 81, 18000 Ниш,

²Универзитет у Београду, Фармацеутички факултет, Капелгра за анализику лекова, Војводе Сіеице 450, 11221 Београд и ³Avantor Performance Materials, Teugseweg 20, 7400 AA Deventer, The Netherlands

SPE-HPLC метода је развијена и валидирана у циљу брзог анализирања карбамазепина и метаболита карбамазепин епоксида и карбамазепин *trans*-диола у хуманој плазми. C18 Bakerbond-BDC аналитичка колона (250 mm×4,6 mm; 5 μm) је коришћена ради извођења анализе. Оптимални услови за хроматографско раздвајање су мобилна фаза ацетонитрил – 10 mM фосфатни пуфер, рН 7,0 (30:70, v/v), проток од 1,5 ml min⁻¹, температура 35 °C и детекција на 210 nm. Укупно трајање хроматографског рана износи око 8 min. SPE процедура за екстракцију анализата из узорака плазме је развијена уз коришћење Oasis HLB кетрица након чега се елуат ињектује у HPLC систем ради анализирања. Затим је извршена валидација SPE-HPLC методе. Линеарност је потврђена у концентрационом опсегу 0,2–25 μg/ml за карбамазепин, карбамазепин епоксид и карбамазепин транс-диол са вредношћу корелационих коефицијената вишом од 0,995. Прецизност методе у току једног и у току више дана је добра са релативном стандардном девијацијом нижом од 7,96 %, док тачност методе обухвата вредности у опсегу од 92,09 до 108,5 % за све анализате. На крају је метода успешно примењена у циљу анализирања узорака плазме пацијената оболелих од епилепсије на монотерапији и политерапији.

(Примљено 6. јануара, ревидирано 11. јуна 2012)

REFERENCES

1. L. L. Brunton, J. S. Lazo, K. L. Parker, *Goodman & Gilman's the Pharmacological Basis of Therapeutics*, McGraw-Hill, New York, USA, 2006, p.533
2. H. Levert, P. Odou, H. Robert, *Biomed. Chromatogr.* **16** (2002) 19
3. A. Martinavarró-Domínguez, M. E. Capella-Peiró, M. Gil-Agustí, J. V. Marcos-Tomás, J. Esteve-Romero, *Clin. Chem.* **48** (2002) 1696
4. B. Koristkova, U. Bergman, M. Grundmann, H. Brozmanova, F. Sjöqvist, *Ther. Drug Monit.* **28** (2006) 594
5. L. A. Bauer, *Applied Clinical Pharmacokinetics*, 2nd ed., McGraw-Hill, New York, USA, 2008, pp. 548, 554
6. E. K. Oh, E. Ban, J. S. Woo, C. K. Kim, *Anal. Bioanal. Chem.* **386** (2006) 1931
7. R. Mandrioli, F. Albani, G. Casamenti, C. Sabbioni, M. A. Raggi, *J. Chromatogr., B* **762** (2001) 109
8. G. A. McMillin, J. M. Juenke, G. Tso, A. Dasgupta, *Am. J. Clin. Pathol.* **133** (2010) 728
9. T. Yoshida, K. Imai, S. Motohashi, S. Hamano, M. Sato, *J. Pharm. Biomed. Anal.* **41** (2006) 1386
10. L. Budakova, H. Brozmanova, M. Grundmann, J. Fischer, *J. Sep. Sci.* **31** (2008) 1
11. G. F. Van Rooyen, D. Badenhorst, K. J. Swart, H. K. L. Hundt, T. Scanes, A. F. Hundt, *J. Chromatogr., B* **769** (2002) 1

12. H. Breton, M. Cociglio, F. Bressolle, H. Peyriere, J. P. Blayac, D. Hillaire-Buys, *J. Chromatogr., B* **828** (2005) 80
13. Z. Ates, T. Özden, S. Özilhan, S. Toptan, *Chromatographia* **66** (2007) S123
14. C. L. Ma, Z. Jiao, Y. Jie, X. J. Shi, *Chromatographia* **65** (2007) 267
15. C. Heideloff, D. R. Bunch, S. Wang, *Ther. Drug Monit.* **32** (2010) 102
16. R. H. C. Queiroz, C. Bertucci, W. R. Malfará, S. A. C. Dreossi, A. R. Chaves, D. A. R. Valério, M. E. C. Queiroz, *J. Pharm. Biomed. Anal.* **48** (2008) 428
17. L. Franceschi, M. Furlanut, *Pharmacol. Res.* **51** (2005) 297
18. F. Bugamelli, C. Sabbioni, R. Mandrioli, E. Kenndler, F. Albani, M. A. Raggi, *Anal. Chim. Acta* **472** (2002) 1
19. M. Subramanian, A. K. Birnbaum, R. P. Remmel, *Ther. Drug Monit.* **30** (2008) 347
20. A. Fortuna, J. Sousa, G. Alves, A. Falcão, P. Soares-da-Silva, *Anal. Bioanal. Chem.* **397** (2010) 1605
21. R. Mandrioli, N. Ghedini, F. Albani, E. Kenndler, M. A. Raggi, *J. Chromatogr., B* **783** (2003) 253
22. M. C. Rouan, J. Campestrini, V. Le Clanche, J. B. Lecaillon, J. Godbillon, *J. Chromatogr.* **573** (1992) 65
23. US Food and Drug Administration, *Guidance for Industry: Bioanalytical Method Validation*, Center for Drug Evaluation and Research, Center for Veterinary Medicine, US Department of Health and Human Services, Rockville, MD, USA, 2001. Available from: www.fda.gov/downloads/Drugs/GuidanceComplianceRegulatoryInformation/Guidances/UCM070107.pdf
24. ICH Harmonised Tripartite Guideline Q2(R1), *Validation of analytical procedures: text and methodology*, *Fed. Regist.* **62** (1997) 27463
25. <https://www.chemaxon.com/marvin/sketch/index.php>
26. N. J. K. Simpson, *Solid-phase Extraction: Principles, Techniques and Applications*, Marcel Dekker, New York, USA, 2000, p. 42.



J. Serb. Chem. Soc. 77 (10) S187–S188 (2012)

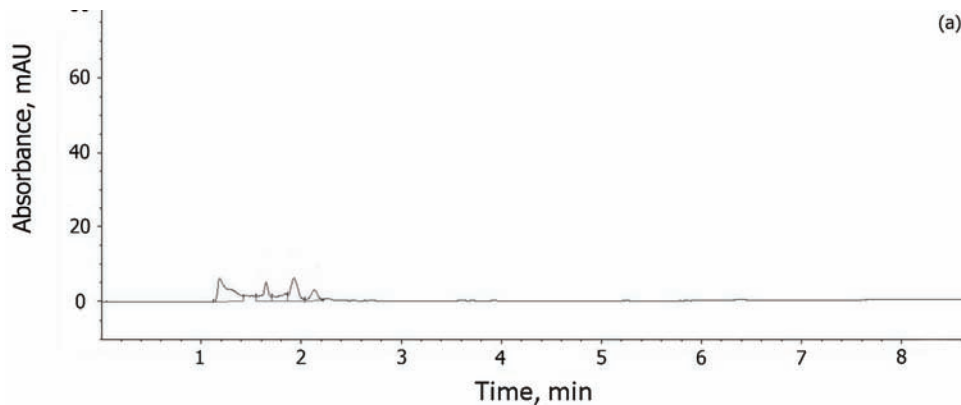
SUPPLEMENTARY MATERIAL TO
**Development and validation of a solid phase extraction-HPLC
method for the determination of carbamazepine and its
metabolites, carbamazepine epoxide and carbamazepine
trans-diol, in plasma**

PREDRAG DŽODIĆ^{1*}, LJILJANA ŽIVANOVIĆ², ANA PROTIĆ², IVANA IVANOVIĆ³,
RADMILA VELIČKOVIĆ-RADOVANOVIĆ¹, MIRJANA SPASIĆ¹, STEVO LUKIĆ¹
and SLAVOLJUB ŽIVANOVIĆ¹

¹University of Niš, Faculty of Medicine, Bulevar dr Zorana Đinđića 81, 18000 Niš, Serbia,

²University of Belgrade, Faculty of Pharmacy, Department of Drug Analysis, Vojvode Stepe
450, 11221 Belgrade, Serbia and ³Avantor Performance Materials, Teugseweg 20,
7400 AA Deventer, The Netherlands

J. Serb. Chem. Soc. 77 (10) (2012) 1423–1436



* Corresponding author. E-mail: pdzodic@gmail.com

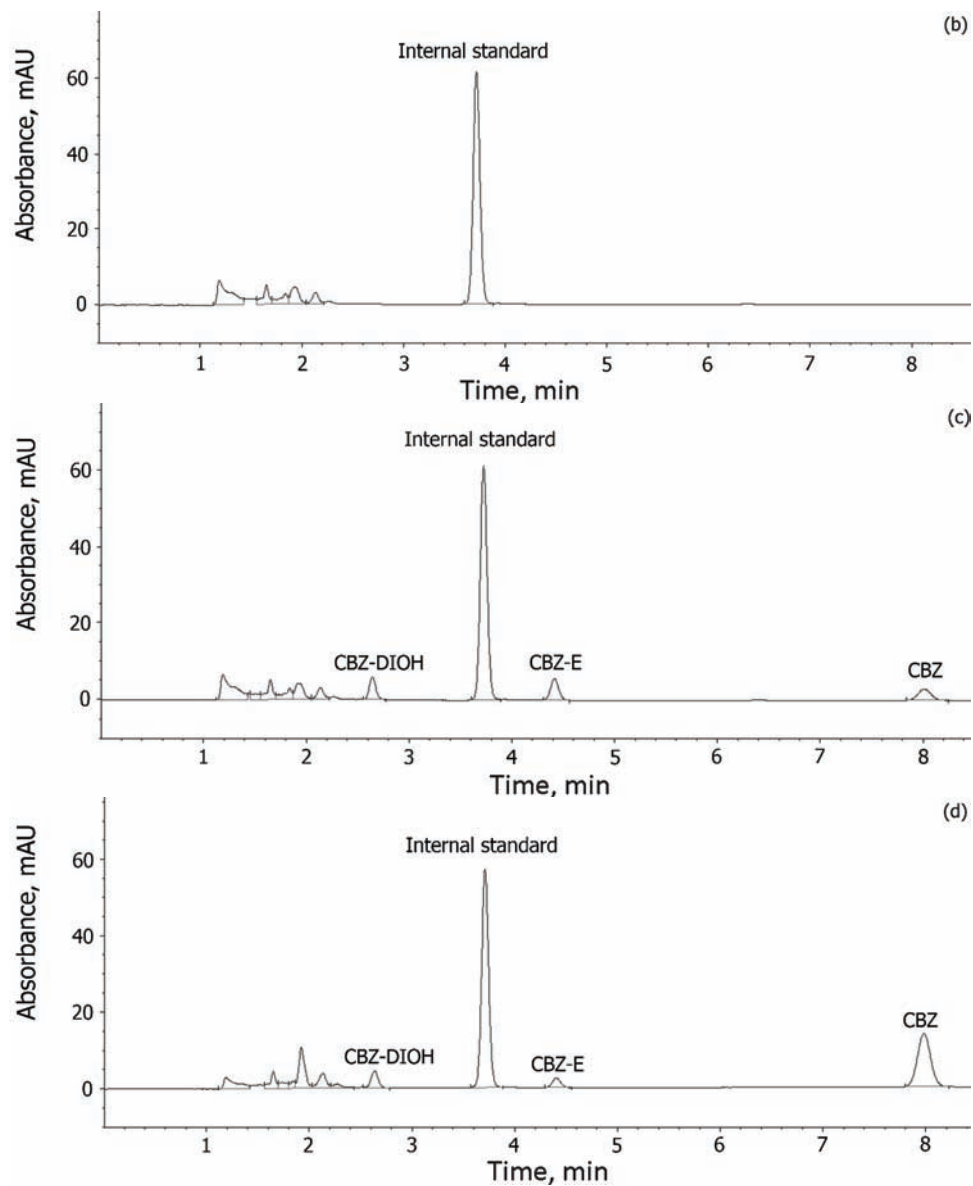


Fig. S-1. Representative chromatograms of blank plasma (a), blank plasma spiked with $10 \mu\text{g mL}^{-1}$ of internal standard (b), blank plasma spiked with $0.6 \mu\text{g mL}^{-1}$ of CBZ, CBZ-E, CBZ-DIOH and $10 \mu\text{g mL}^{-1}$ of internal standard (c) and plasma sample of an epileptic patient (concentrations of CBZ, CBZ-E and CBZ-DIOH were 7.12 , 1.44 and $1.40 \mu\text{g mL}^{-1}$, respectively) at 9.0 h after receiving an oral dose of 200 mg CBZ (d).



J. Serb. Chem. Soc. 77 (10) 1437–1442 (2012)
JSCS–4364

NOTE

Determination of lisinopril in pharmaceuticals by a kinetic spectrophotometric method

MIRA ČAKAR* and GORDANA POPOVIĆ

*Faculty of Pharmacy, University of Belgrade, P. O. Box 146, Vojvode Stepe 450,
11000 Belgrade, Serbia*

(Received 31 January, revised 23 July 2012)

Abstract: A kinetic spectrophotometric method for determination of lisinopril in pharmaceuticals has been developed. The method is based on the activator action of lisinopril on Cu(II) ions catalysing the oxidation of Nile Blue A with hydrogen peroxide in borate buffer (pH 9.3). A decrease of the absorbance was recorded at 635 nm after 5 min at 25 °C. Linearity was established by application of the tangent method within the concentration range of lisinopril from 0.8–6.4 µg mL⁻¹, the detection and quantification limits being 0.158 and 0.480 µg mL⁻¹, respectively. The method was successfully applied to three brands of tablets containing lisinopril alone or in combination with hydrochlorothiazide.

Keywords: lisinopril; Nile Blue A; spectrophotometry; kinetic determination; pharmaceuticals.

INTRODUCTION

Lisinopril, (S)-1-[N²-(1-carboxy-3-phenylpropyl)-L-lysyl]-L-proline, belongs to the group of angiotensin converting enzyme (ACE) inhibitors, widely applied in the treatment of high blood pressure.¹ Due to its wide application in medicine, there is an increasing interest for the development of sensitive and highly selective methods for lisinopril determination in pharmaceuticals and biological materials. Several spectrophotometric^{2–16} and spectrofluorimetric^{3,17} procedures have been described for lisinopril determination. Thus, zero order⁵ and derivative spectrophotometry^{2,7–9} have been proposed for the direct determination of lisinopril. Considering the very low absorbance of lisinopril in the UV region, some authors have applied derivatisation in order to increase the sensitivity of the determination.^{3,4,6,10–16} The methods based on derivatisation are time consuming, usually require heating and cooling of the reaction mixture and the use of organic

* Corresponding author. E-mail: mcakar@pharmacy.bg.ac.rs
doi: 10.2298/JSC120131079C

solvents. Furthermore, finding out an appropriate reagent that would quantitatively react with the analysed substance represents an additional problem of derivatisation. Of all the spectrophotometric methods hitherto proposed for lisinopril determination, only Rahman *et al.*¹² recently reported a kinetic procedure.

The present study was aimed at the development of a rapid and sensitive kinetic spectrophotometric method for lisinopril determination in pharmaceuticals. The procedure is based on the activator effect of lisinopril on the oxidation reaction of Nile Blue A with hydrogen peroxide, catalysed by Cu(II) ions. The method is more sensitive than the already reported spectrophotometric approaches, which are listed in the literature,¹⁵ and lisinopril is determined avoiding derivatisation and the use of organic solvents.

EXPERIMENTAL

Apparatus

A GBC Cintra 20 spectrophotometer (GBC Scientific Equipment Pty Ltd., Dandenog, Australia) with 1.0 cm quartz cuvettes and software for kinetic measurements was used. The temperature of the samples was maintained at 25 ± 0.1 °C using a Huber Polistat CC2 thermostat.

Materials and reagents

Lisinopril dihydrate and hydrochlorothiazide were kindly provided by the Medicines and Medical Devices Agency of Serbia (Belgrade, Serbia) and Zdravlje Actavis Company (Leskovac, Serbia), respectively. Water content in lisinopril dihydrate standard was determined by titrimetry at time of use for analysis. Pharmaceutical lisinopril preparations, such as Loril® (Srbolek, Serbia), Skopryl® (Alkaloid, Macedonia) and Lizopril® H (Bosnalijek, Bosnia and Herzegovina) were purchased from a local market. Claimed lisinopril content per tablet in the examined samples was 5 mg lisinopril dihydrate (Loril®), *i.e.*, 10 mg lisinopril (Skopryl®) and 10 mg lisinopril dihydrate plus 12.5 mg hydrochlorothiazide (Lizopril® H). Nile Blue A (Sigma–Aldrich), hydrogen peroxide 30 % (Merck), disodium tetraborate decahydrate (Baker) and anhydrous copper(II) sulphate (Merck) were of analytical reagent grade. Other reagents used throughout the present study were of analytical grade purity. All solutions were prepared in double distilled water. The concentrations of the stock solutions were: Nile Blue A, 1.00×10^{-4} mol L⁻¹, and Cu(II) sulphate, 1.00×10^{-4} mol L⁻¹. Borate buffer (0.1 mol L⁻¹), pH 9.3, was prepared by dissolving sodium tetraborate in water. Hydrogen peroxide solution (3.92×10^{-1} mol L⁻¹) was obtained by diluting 30 % H₂O₂ with water.

Procedure

The reaction was performed in a reaction-mixture vessel with three compartments for rapid mixing of the stock solutions, designed by L.I. Budarin.¹⁸ The measured amounts of Nile Blue A and Cu(II) solutions were placed in the first compartment of the vessel, and borate buffer, lisinopril solution and water (up to a total volume of 25 mL) in the second compartment. After thermostating at 25 °C, hydrogen peroxide solution was added into the third compartment and the reaction initiated by mixing the reactants (zero time). After 30 s, the absorbance was recorded at 635 nm for 5 min at 30 s intervals. To study the effects of hydrochlorothiazide on the determination of lisinopril, a solution of hydrochlorothiazide was stored in lisinopril-containing compartment.

Calibration curve. A calibration curve was obtained by the described procedure for the following amounts of the reagents: 0.8 mL hydrogen peroxide ($3.92 \times 10^{-1} \text{ mol L}^{-1}$), 5 mL $1.00 \times 10^{-4} \text{ mol L}^{-1}$ Nile Blue A solution, 4 mL $1.00 \times 10^{-4} \text{ mol L}^{-1}$ Cu(II) solution, 5 mL borate buffer, pH 9.3 (0.1 mol L^{-1}), aliquots of 0.5–4.0 mL of the solution containing $40 \mu\text{g mL}^{-1}$ lisinopril and water up to a total volume of 25 mL.

Analysis of pharmaceuticals. Twenty lisinopril-containing tablets were precisely weighed and pulverised. The amount of the obtained powder corresponding to the mass of a single tablet was transferred to a 100 mL volumetric flask and water added up to the volume. The mixture was treated for 10 min in an ultrasonic bath and filtered. For further analyses, 0.8 mL (Skopryl® and Lizopril® H tablets) and 1.6 mL (Loril® tablets) aliquots of the resulting filtrates were used.

RESULTS AND DISCUSSION

The presence of Cu(II) ions decreased the absorbance in the system Nile Blue A – hydrogen peroxide, thus demonstrating that copper ions acted as a catalyst of this reaction. Addition of lisinopril to this system led to a further decrease of the absorbance, indicating an increased reaction rate and demonstrating the activator action of lisinopril. In order to optimise experimental conditions for lisinopril determination, the kinetics of the catalytic reaction of the system Nile blue A – hydrogen peroxide – Cu(II), in the presence and in the absence of lisinopril, was examined. The reaction rate was recorded spectrophotometrically at 635 nm, applying the tangent method.¹⁸ The concentration ranges of the reagents and selected optimal conditions for lisinopril determination are listed in Table I.

TABLE I. Concentration range and optimal concentrations of the reagents for the determination of lisinopril by the proposed kinetic spectrophotometric method

Reagent	Range	Optimal values
Cu(II), mol L ⁻¹	0.40×10^{-5} – 2.00×10^{-5}	1.60×10^{-5}
H ₂ O ₂ , mol L ⁻¹	0.625×10^{-2} – 1.57×10^{-2}	1.25×10^{-2}
Borate buffer, pH	8.6–9.3	9.3
Borate buffer (pH 9.3), mol L ⁻¹	1.00×10^{-2} – 3.00×10^{-2}	2.00×10^{-2}

A linear relationship was established within lisinopril concentration range 0.80 – $6.40 \mu\text{g mL}^{-1}$ (0.197×10^{-5} – $1.58 \times 10^{-5} \text{ mol L}^{-1}$), and the parameters obtained by regression analysis are given in Table II. The precision of the method was estimated by performing six determinations of 1.60 , 3.20 and $5.60 \mu\text{g mL}^{-1}$ lisinopril. The results obtained are listed in Table III. The accuracy of the method was established by performing recovery experiments at three levels (by adding 80, 100 and 120 % lisinopril of the claimed tablet content) using the standard addition method. The analysed samples, Skopryl® and Loril® tablets, were spiked with additional 8, 10 and 12 mg, *i.e.*, 4, 5 and 6 mg lisinopril, respectively, and the content of lisinopril determined by the proposed method. The recoveries ranged from 99.16 to 101.4 % (Table IV).

The proposed method was applied to the determination of the lisinopril content in three different commercial tablets (loril, skopryl and lizopril H).

TABLE II. Statistical data of lisinopril determination by the proposed kinetic spectrophotometric method ($n = 6$)

Parameter	Value
Concentration range, $\mu\text{g mL}^{-1}$	0.80–6.40
Calibration equation	$2.097 \times 10^{-4} + 1.578 \times 10^{-5}c$
Correlation coefficient (r)	0.9997
Standard deviation of slope	1.81×10^{-7}
Standard deviation of intercept	7.57×10^{-7}
Limit of detection ($LOD / \mu\text{g mL}^{-1}$)	0.158
Limit of quantification ($LOQ / \mu\text{g mL}^{-1}$)	0.480

TABLE III. Precision test of the proposed kinetic spectrophotometric method for lisinopril determination (six independent determinations)

Analysed lisinopril amount, $\mu\text{g mL}^{-1}$	SD	$RSD / \%$	Standard analytical error
1.60	0.049	3.15	0.020
3.20	0.040	1.22	0.016
5.60	0.028	0.48	0.011

TABLE IV. Accuracy of the proposed kinetic spectrophotometric method for the determination of lisinopril ($n = 6$)

Pharmaceutical formulation analyzed	Amount of lisinopril, mg					
	In analysed tablets	Standard added	Total	SD	$RSD / \%$	Recovery, %
Skopryl	9.850	8.00	17.94	0.095	1.17	101.1
	9.850	10.00	19.78	0.127	1.28	99.30
	9.850	12.00	21.75	0.027	0.23	99.16
Loril	4.544	4.00	8.601	0.088	2.17	101.4
	4.544	5.00	9.522	0.092	1.85	99.56
	4.544	6.00	10.55	0.115	1.91	100.1

The selectivity of the proposed method was investigated by the determination of $4 \mu\text{g mL}^{-1}$ lisinopril solution in the presence of various water soluble compounds commonly found in lisinopril tablets within a relative error of $\pm 5 \%$. The co-existing soluble ingredients did not interfere with the determination (mass ratio to lisinopril): Ca^{2+} (1000); HPO_4^{2-} (100) and mannitol (10 000). Since lizopril H tablets in addition to lisinopril (10 mg in the form of dihydrate) also contain hydrochlorothiazide (12.5 mg), the effects of the latter component on the determination of lisinopril by the proposed kinetic method were examined. The results clearly showed that hydrochlorothiazide did not interfere up to the mass ratio lisinopril:hydrochlorothiazide of 1:1.4. Since commercially available pharmaceutical preparations contain at the most a 1.25 higher content of hydrochlorothiazide than lisinopril, the proposed kinetic procedure described in the present

work could be successfully applied for the determination of lisinopril in these preparations. The obtained results of lisinopril determination in tablets are summarized in Table V.

TABLE V. Determination of lisinopril in commercial tablets by the proposed kinetic spectrophotometric method ($n = 6$)

Commercial tablets	Claimed content per tablet, mg	Found mg	Found content calculated as lisinopril dihydrate, mg	In relation to claimed content, %
Loril	5 ^a	4.544 ^b	4.947	98.94
Skopryl	10 ^b	9.850 ^b	–	98.50
Lizopril H	10 ^a	9.286 ^b	10.11	101.1

^aLisinopril dehydrate; ^blisinopril

Acknowledgement. This work was supported by the Ministry of Education, Science and Technological Development of the Republic of Serbia, Grant No. 172033.

ИЗВОД

ОДРЕЂИВАЊЕ ЛИЗИНОПРИЛА У ФАРМАЦЕУТСКИМ ПРЕПАРАТИМА ПРИМЕНОМ КИНЕТИЧКЕ СПЕКТРОФОТОМЕТРИЈСКЕ МЕТОДЕ

МИРА ЧАКАР и ГОРДАНА ПОПОВИЋ

Фармацеутички факултет и Универзитет у Београду, и. пр. 146, Војводе Свеште 450, 11000 Београд

Развијена је кинетичка спектрофотометријска метода за одређивање лизиноприла у фармацеутиским препаратима. Метода се заснива на активаторском дејству лизиноприла на реакцију оксидације боје нил плавог-А водоник-пероксидом у боратном пуферу (pH 9,3), а која је катализована Cu(II) јонима. Смањење апсорбације мерено је на 635 nm у временском периоду од 5 мин на температури 25 °C. Линеарност је утврђена применом методе тангенса у опсегу концентрација лизиноприла 0,8–6,4 µg mL⁻¹, са лимитом детекције 0,158 µg mL⁻¹ и лимитом одређивања 0,480 µg mL⁻¹. Метода је примењена за анализу три комерцијална препарата која су садржала лизиноприл и лизиноприл у комбинацији са хидрохлортиазидом.

(Примљено 31. јануара, ревидирано 23. јула 2012)

REFERENCES

1. *Martindale*, The Complete Drug Reference, 33rd ed., Pharmaceutical Press, London, UK, 2002, p. 921
2. D. Bonazzi, R. Gotti, V. Andrisano, V. Cavrini, *J. Pharm. Biomed. Anal.* **16** (1997) 431
3. A. El-Gindy, A. Ashour, L. Abdel-Fattah, M. M. Shabana, *J. Pharm. Biomed. Anal.* **25** (2001) 913
4. A. A. El-Emam, S. H. Hansen, M. A. Moustafa, S. M. El-Ashry, D. T. El-Sherbiny, *J. Pharm. Biomed. Anal.* **34** (2004) 35
5. N. Erk, M. Kartal, *Anal. Lett.* **32** (1999) 1131
6. O. Abdel Razak, S. F. Belal, M. M. Bedair, N. S. Barakat, R. S. Haggag, *J. Pharm. Biomed. Anal.* **31** (2003) 701
7. A. El Gindy, A. Ashour, L. Abdel-Fattah, M. M. Shabana, *J. Pharm. Biomed. Anal.* **25** (2001) 923
8. D. Ozer, H. Senel, *J. Pharm. Biomed. Anal.* **21** (1999) 691

9. N. Erk, *Spectrosc. Lett.* **31** (1998) 633
10. N. Rahman, M. R. Siddiqui, S. N. H. Azmi, *Chem. Anal. (Warsaw)* **52** (2007) 465
11. A. Raza, T. M. Ansari, Atta-ur-Rehman, *J. Chin. Chem. Soc.* **52** (2005) 1055
12. N. Rahman, M. Singh, Md-N. Hoda, *J. Braz. Chem. Soc.* **16** (2005) 1001
13. A. Rajasekaran, S. Udayavani, *J. Indian Chem. Soc.* **78** (2001) 485
14. G. Paraskevas, J. Atta-Politou, M. Koupparis, *J. Pharm. Biomed. Anal.* **29** (2002) 865
15. K. Basavaiah, K. Tharpa, S. G. Hiriyanna, K. B. Vinay, *J. Food Drug Anal.* **17** (2009) 93
16. G. Cetin, S. Sungur, *Rev. Anal. Chem.* **25** (2006) 1
17. C. K. Zacharis, P. D. Tzanavaras, D. G. Themelis, G. A. Theodoridis, A. Economou, P. G. Rigas, *Anal. Bioanal. Chem.* **379** (2004) 759
18. K. B. Yatsimirski, *Kinetic Methods of Analysis*, Pergamon Press, Oxford, 1966, pp. 29 and 39.



Quantitative structure–toxicity relationship study of some natural and synthetic coumarins using retention parameters

EL HADI M. A. RABTTI¹, MAJA M. NATIĆ^{1#}, DUŠANKA M. MILOJKOVIĆ-OPSENICA^{1#}, JELENA Đ. TRIFKOVIĆ^{1#}, TOMISLAV TOSTI^{1#}, IVAN M. VUČKOVIĆ¹, VLATKA VAJS² and ŽIVOSLAV Lj. TEŠIĆ^{1#*}

¹Faculty of Chemistry, University of Belgrade, P. O. Box 51, 11158 Belgrade, Serbia and

²Institute of Chemistry, Technology and Metallurgy, University of Belgrade, Njegoševa 12, 11000 Belgrade, Serbia

(Received 16 July, revised 6 September 2012)

Abstract: Four lipophilicity descriptors (R_M^0 , b , C_0 and PCI) for twelve coumarin derivatives were determined by reversed-phase thin-layer chromatography in order to analyze the descriptor which best describes the lipophilicity of the investigated coumarins. Moreover, possible chemical toxicity of coumarins, expressed as the probability of a compound to cause organ-specific health effects, was calculated using ACD/Tox Suite program. The quantitative relationships between toxicity and molecular descriptors, including experimentally determined lipophilicity descriptors obtained in current study were investigated using partial least square regression. The best models were obtained for kidney and liver health effects. Quantitative structure–toxicity relationship models revealed the importance of electric polarization descriptors, size descriptors and lipophilicity descriptors. The obtained models were used for the selection of the structural features of the compounds that are significantly affecting their absorption, distribution, metabolism, excretion and toxicity.

Keywords: lipophilicity parameters; thin-layer chromatography; toxicity; partial least squares regression.

INTRODUCTION

Lipophilicity of a compound is an important physico-chemical parameter. It determines biological processes as it is related to absorption, bioavailability, hydrophobic drug-receptor interactions, metabolism and toxicity. The lipophilic nature of a drug might be represented by the logarithm of the octanol–water partition coefficient, $\log P$, introduced into medicinal chemistry by Hansch and Fujita.¹ Instead of the traditional shake-flask method, partition chromatographic data can be used for quantitative comparisons of relative lipophilicities. For this

* Corresponding author. E-mail: ztesic@chem.bg.ac.rs

Serbian Chemical Society member.

doi: 10.2298/JSC120716091R

purpose, the most suitable are the intercepts of the linear relationships between the logarithm of retention constants R_M and the volume fraction of the organic modifier in a binary mobile phase obtained in reversed-phase thin-layer chromatographic (RP TLC) experiments. The relation is given by Eq. (1):

$$R_M = R_M^0 + b\varphi \quad (1)$$

where φ stands for the concentration of the organic component in the mobile phase and b is the slope, which indicates the rate at which the solubility of the solute in the mobile phase increases with changes in its composition. Parameter b is related to the specific hydrophobic surface area of the solutes in contact with the non-polar stationary phase.² Two theories relate the slope with the specific hydrophobic surface area. The first one correlates the slope to the number of mobile phase molecules in the solvation sphere of the solute, which are released after formation of the stationary phase–solute complex.³ This depends on the non-polar (hydrophobic) area of a molecule in the case of reversed-phase chromatography. Another approach is based on the explanation that the surface tension of the mobile phase changes with its composition, thereby altering the energy of vacancy formation required for the accommodation of solute molecules.²

Besides the lipophilicity parameter R_M^0 , the parameter C_0 , defined as the ratio of the intercept and slope values, is frequently used in this type of investigations:⁴

$$C_0 = -R_M^0/b \quad (2)$$

C_0 could be understood as the concentration of an organic modifier in the mobile phase for which the distribution of the solute between the two phases is equal, *i.e.*, $R_M = 0$, $R_F = 0.5$. It could also be interpreted as the hydrophobicity per unit of specific hydrophobic surface area.

Several studies show that the retention is much better correlated with lipophilicity parameters if principal component analysis (PCA) is employed.^{5,6} Principal components (PCs) combine all chromatographic data in one single feature, possessing in this way properties of interpolated quantities, while R_M^0 , b and C_0 are extrapolated. PCA is a multivariate statistical method that is usually used to reduce the dimensionality (number of variables) of a large number of interrelated variables, while retaining as much of the information (variation) as possible. The first principal component (PC1, *i.e.*, a linear combination of the R_M values obtained under different chromatographic conditions) is chosen in the direction of the largest variance in the dataset, followed by the second one that encloses the rest of the variability and so on.^{7,8}

All the above-mentioned chromatographic descriptors are equally present in the literature and are commonly used for assessing the lipophilicity of unknown solutes.

Different computational and mathematical models can be a very useful approach in prediction of biological activity of novel compounds. Quantitative structure–activity relationships (QSARs) are mathematical models that are used to correlate molecular descriptors with biological activity of a given group of compounds. Similar to QSARs, quantitative structure–retention relationships (QSRRs) relate molecular descriptors to chromatographic retention. Among the many examples of the measures that may be predicted from QSARs, modeling health effects could be considered as one of the most diverse.⁹ A wide range of software tools are available for predicting physico-chemical properties and biological effects. Many of these packages are commonly used in the assessment of chemical toxicity. ToxBboxes (now called ACD/Tox Suite), marketed by ACD/Labs and Pharma Algorithms, provides predictions of various toxicity endpoints, including human Ether-à-go-go Related Gene (hERG) channel inhibition, genotoxicity, cytochrome P450 (CYP3A4) inhibition, Estrogen Receptor (ER) binding affinity, irritation, rodent acute lethal toxicity (LD_{50}), aquatic toxicity, and organ-specific health effects (<http://www.acdlabs.com/products/admet/tox/>). The predictions are associated with confidence intervals and probabilities, thereby providing a numerical expression of prediction reliability. The software incorporates the ability to identify and visualize specific structural toxicophores, giving insight into which parts of the molecule are responsible for the toxic effect.¹⁰ Continuing research on the screening of plant extracts,^{11–14} in this paper, attention is focused on naturally occurring coumarins, compounds of diverse pharmacological properties.¹⁵ The majority of coumarins have been isolated from green plants. The genus *Seseli*, part of Apiaceae family, is a well-known source of linear or angular pyranocoumarins, an interesting subclass of coumarins possessing antiproliferative,¹⁶ antiviral¹⁷ and antibacterial activities.¹⁸ Numerous species of the genus have been used in folk medicine since ancient times.

In addition to previous research on chromatographic behavior of the mentioned coumarins,¹⁴ the first goal of this study was to determine the descriptors that best describe their lipophilicity based on thin-layer chromatographic data. The research was focused on the calculation of the probability of a compound causing organ-specific health effects; on the identification of structural features that contribute to diverse health effects; and on establishing a relationship between toxicity data and molecular descriptors, using partial least square regression, in order to determine crucial factors governing activity, *i.e.*, to reveal mechanisms of action and to propose structural features that would contribute to improved ADME-Tox profiles of the compounds.

EXPERIMENTAL

Reagents

The structures of the twelve studied coumarins are presented in Fig. 1. Coumarins **1–5** were isolated from *Seseli montanum* subsp. *tommasinii*.¹⁹ Coumarin **6** was isolated from the

roots of *Seseli annuum*²⁰ and coumarin **7** was obtained from *Achillea tanacetifolia*.²¹ Compounds **8–12** were purchased from Sigma–Aldrich (Steinheim, Germany). Their purity was proven by HPLC or NMR spectroscopy.

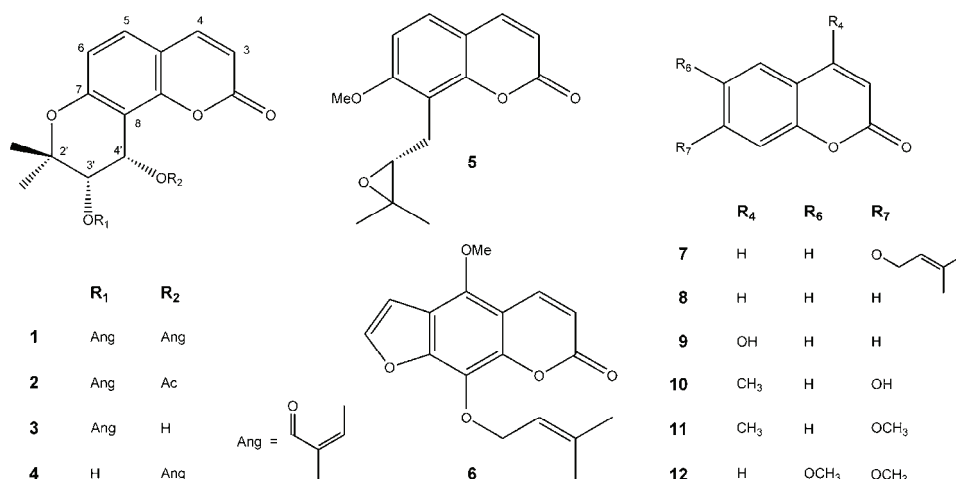


Fig. 1. Chemical structures of the investigated coumarins: anomalin (**1**), isopteryxin (**2**), isolaserpitin (**3**), laserpitin (**4**), meranzin (**5**), phellopterin (**6**), 7-*O*-prenylumbelliferone (**7**), coumarin (**8**), 4-hydroxycoumarin (**9**), 7-hydroxy-4-methylcoumarin (**10**), 7-methoxy-4-methylcoumarin (**11**) and 6,7-dimethoxycoumarin (**12**).

Thin-layer chromatography

The analytical procedure for the TLC was described in detail previously.¹⁹

Software

Software-predicted lipophilicity of the compounds was calculated with the available programs (<http://www.vcclab.org/lab/alogps/>). The ALOGPS 2.0 program package for prediction of lipophilicity and aqueous solubility of compounds was developed using the efficient partition algorithm and an associative neural network (ASNN) approach. The database used in the current program included 13,360 compounds with experimental values for lipophilicity ($\log P$) covering a diverse range.²²

The prediction of toxicity was realized using ADME/Tox WEB Software (<http://pharma-algorithms.com/webboxes/>). The predictions of genotoxicity by ToxBboxes are based on the probability of a query compounds to be genotoxic in the Ames test. The training data used in the software contained the results of Ames genotoxicity assays for several strains of *S. typhimurium*, with or without metabolic activation. A neural network model was built using structural fragments as descriptors. The molecules were decomposed into atomic- and chain-based fragments. Fragments containing 2 to 5 atoms present in at least 10 training set molecules were used to develop the model. The model makes a prediction if the chemical structure is more than 75 % covered by fragments in the training set.¹⁰

Optimized geometrical representations of the coumarins were obtained by Hyperchem Professional software (version 7.0, Hypercube). Molecular Modeling Program Plus (MMP Plus) software was employed for the calculation of the physicochemical properties (<http://www.norgwyn.com/com/mmpplus.html>). PCA and Partial least square regression (PLS)

were performed using PLS_Toolbox statistical package (Eigenvectors Inc. v. 5.7) from MATLAB, v. 7.4.0.287 (R2007a) (MathWorks INC, Natick, MA, USA). PCA was performed as an exploratory data analysis using a singular value decomposition algorithm (SVD) and a 0.95 confidence level for Q and T^2 Hotelling limits for outliers. The PLS method was employed using the SIMPLS algorithm without forcing orthogonal conditions to the model in order to condense Y-block variance into first latent variables. Model calibration was performed using the random samples cross-validation method. The calibration model was characterized by the root mean square errors of calibration ($RMSEC$) and root mean square errors of cross-validation ($RMSECV$). The explained variances are defined as the sum of squares due to regression divided by the sums of the squares about the mean: R^2Y (cum), the square of the multiple correlation coefficients for the calibration objects, and Q^2Y (cum), the square of the multiple correlation coefficients for the cross-validation segments.^{7,8} The data were mean-centered and scaled to unit variance before statistical analyses. Autoscaling of the data was chosen as a pretreatment method in order to prevent highly abundant components from dominating components present in much smaller quantities. The values of the probabilities of health effects were the dependent variables in the quantitative structure–toxicity relationship (QSTR) equations, and they were regressed against the molecular structural descriptors (*i.e.*, independent variables).

RESULTS AND DISCUSSION

Lipophilicity of the compounds

Retention behavior of the investigated coumarins was described in detail in a previous work.¹⁹ Reversed-phase thin-layer chromatography was performed on an octadecyl-modified silica stationary phase with three different binary solvent systems composed of water and organic modifier (methanol, tetrahydrofuran or acetonitrile). Data for linear correlation between R_M and the volume fraction of organic modifier in the mobile phase along with slopes, the correlation coefficients and standard errors of estimation were previously reported.¹⁹ The calculated R_M^0 values were different for the individual compounds due to different substituents. The aforementioned paper also described the determination of octanol–water partition coefficients, $\log P_{OW}$, as a measure of the lipophilicity of tested compounds. The $\log P_{OW}$ values were experimentally obtained using eight standard solutes with known $\log P_{OW}$ values, which were analyzed under the chosen chromatographic condition (methanol–water, 75/25 %, v/v), the same as for the target substances.¹⁹ The determined lipophilicity of the investigated compounds was in accordance with their chromatographic behavior. The experimentally established R_M^0 and $\log P_{OW}$ values, obtained with methanol as the organic modifier, were correlated against $\log P$ values calculated using different software packages. It was concluded that the RPTLC retention constants, R_M^0 , and the $\log P_{OW}$ values of the investigated compounds reflect their lipophilicity.

In addition to mentioned observations, correlations between R_M^0 (intercept) and b (slope) of the linear relationship between R_M and the volume percent of organic modifier in the aqueous mobile phase was performed in order to evaluate the possibility of the use of the slopes as lipophilicity parameters. These linear

relations are presented as equations given together with correlation coefficients (r), standard deviation (s), and Fisher test (F) calculated for the 95 % level of significance. Highly significant linear relationships between the retention constants R_M^0 and b were obtained (the calculated Student's t -values were greater than the critical one):

$$b_{(\text{ACN})} = -1.067(\pm 0.215) - 0.758(\pm 0.012) R_M^0$$

$$r = 0.7890, \quad s = 1.06, \quad F = 42.106, \quad t = 4.06 \quad t_{\text{cr}} = 2.26$$

$$b_{(\text{MeOH})} = -0.807(\pm 0.063) - 0.905(\pm 0.021) R_M^0$$

$$r = 0.9940, \quad s = 0.08, \quad F = 1772.254, \quad t = 28.74 \quad t_{\text{cr}} = 2.26$$

$$b_{(\text{THF})} = -0.900(\pm 0.273) - 1.123(\pm 0.015) R_M^0$$

$$r = 0.8950, \quad s = 0.55, \quad F = 94.652, \quad t = 6.34 \quad t_{\text{cr}} = 2.26$$

The obtained statistically significant relationships indicate that the slopes could be considered as an alternative to the intercepts lipophilicity parameters. The slopes were further compared with the previously calculated $\log P$ values¹⁹ and the statistical parameters of these dependences are given in Table I.

TABLE I. Relationships between the slopes and the $\log P$ values determined using different computational programs

b vs. $\log P$	Organic modifier	Equation	r	s
$b - \text{Alog } P_s$	Acetonitrile	$b = -0.618(0.265) - 0.613(0.090)\text{Alog } P_s$	0.806	0.972
	Methanol	$b = -0.341(0.275) - 1.033(0.093)\text{Alog } P_s$	0.918	1.046
	Tetrahydrofuran	$b = 1.696(0.234) - 0.641(0.079)\text{Alog } P_s$	0.854	0.759
$b - \text{AClog } P$	Acetonitrile	$b = -0.5745(0.252) - 0.647(0.088)\text{AClog } P$	0.829	0.859
	Methanol	$b = -0.276(0.245) - 1.087(0.085)\text{AClog } P$	0.936	0.810
	Tetrahydrofuran	$b = -1.597(0.158) - 0.696(0.055)\text{AClog } P$	0.935	0.338
$b - \text{Alog } P$	Acetonitrile	$b = -0.539(0.267) - 0.634(0.090)\text{Alog } P$	0.816	0.923
	Methanol	$b = -0.217(0.279) - 1.064(0.094)\text{Alog } P$	0.921	1.004
	Tetrahydrofuran	$b = -1.566(0.187) - 0.679(0.063)\text{Alog } P$	0.914	0.450
$b - \text{Mlog } P$	Acetonitrile	$b = 0.390(0.775) - 1.168(0.328)\text{Mlog } P$	0.515	2.435
	Methanol	$b = 1.690(0.979) - 2.111(0.414)\text{Mlog } P$	0.694	3.886
	Tetrahydrofuran	$b = -0.306(0.611) - 1.365(0.259)\text{Mlog } P$	0.710	1.512
$b - \log P_{\text{KOWWIN}}$	Acetonitrile	$b = -1.045(0.231) - 0.496(0.081)\log P_{\text{KOWWIN}}$	0.767	1.167
	Methanol	$b = -1.039(0.249) - 0.844(0.088)\log P_{\text{KOWWIN}}$	0.893	1.354
	Tetrahydrofuran	$b = -2.086(0.160) - 0.541(0.056)\log P_{\text{KOWWIN}}$	0.892	0.562
$b - \text{Xlog } P_2$	Acetonitrile	$b = -0.492(0.382) - 0.739(0.115)\text{Xlog } P_2$	0.783	1.088
	Methanol	$b = -0.139(0.351) - 1.240(0.134)\text{Xlog } P_2$	0.884	1.470
	Tetrahydrofuran	$b = -1.546(0.258) - 0.779(0.098)\text{Xlog } P_2$	0.847	0.796
$b - \text{Xlog } P_3$	Acetonitrile	$b = -0.669(0.338) - 0.642(0.124)\text{Xlog } P_3$	0.701	1.502
	Methanol	$b = -0.358(0.389) - 1.108(0.143)\text{Xlog } P_3$	0.843	1.980
	Tetrahydrofuran	$b = -1.664(0.261) - 0.705(0.096)\text{Xlog } P_3$	0.828	0.896

The lower r values obtained for the analyzed correlations indicate that it is necessary to use a proper statistical test to see whether the correlation coefficients are indeed significant, bearing in mind the number of points used in the calibration. The t -test for the correlation confirmed that no linear relationship between S and $M\log P$ was obtained with the chromatographic system using acetonitrile as the organic modifier ($t = 1.90$, $t_{cr(0.05;10)} = 2.23$). In all other cases, the correlations were statistically significant ($t = 3.05 - 8.41$). Although the results indicate that the slopes of RPTLC equations may be applied for lipophilicity expression of the investigated compounds, it could be noticed that intercepts, as a parameter of lipophilicity, are more reliable according to the Pearson's coefficients and standard errors of estimation. Within the observed correlations, the best results were obtained for methanol, *i.e.*, the correlation coefficients are the highest and deviations from the ideal correlation (slope ≈ 1 and intercept ≈ 0) are less pronounced than in the case of the other two organic modifier. In addition, the best correlations were achieved between the slopes and the $AC\log P$ values.

Lower quality correlations were obtained between R_M^0 and parameter C_0 :

$$C_{0(\text{ACN})} = 0.324(\pm 0.084) + 0.215(\pm 0.046)R_M^0$$

$$r = 0.6570, \quad s = 0.16, \quad F = 22.068, \quad t = 2.75 \quad t_{cr} = 2.26$$

$$C_{0(\text{MeOH})} = 0.497(\pm 0.055) + 0.109(\pm 0.019)R_M^0$$

$$r = 0.7480, \quad s = 0.06, \quad F = 33.615, \quad t = 3.56 \quad t_{cr} = 2.26$$

$$C_{0(\text{THF})} = 0.458(\pm 0.066) + 0.085(\pm 0.028)R_M^0$$

$$r = 0.4270, \quad s = 0.03, \quad F = 9.204, \quad t = 1.49 \quad t_{cr} = 2.26$$

and C_0 was not further considered as a potential parameter of lipophilicity.

PCA was performed on the set of retention data (R_M values obtained for the three chromatographic systems) in order to reveal possible similarities among the studied compounds governed by both their intrinsic structural properties and specific interactions that occurred in the different chromatographic systems, and to obtain the values of PCI , as a measure of lipophilicity. PCA applied on the entire set of molecular descriptors resulted in a three-component model explaining 97.64 % of the data variation (first principal component comprised 91.76 % of the variances).

The scores plot of the first two principal components (Fig. 2) indicates that there were no outliers among the analytes (all the data lie inside the Hotelling T^2 ellipse). Samples are clustered into two main separate groups, similar to PCA analysis of molecular descriptors of investigated substances, reported previously.¹⁹ Clustering was performed according to the lipophilicity of the coumarins. PC1 distinguished samples consistent to the number of the rings present in the molecule (bicyclic and tricyclic compounds). The exception was compound 7

with the hydrophobic side-chain substituent, 3-methylbut-2-enyloxy, which exhibits positive *PCI* score values together with the tricyclic compounds.

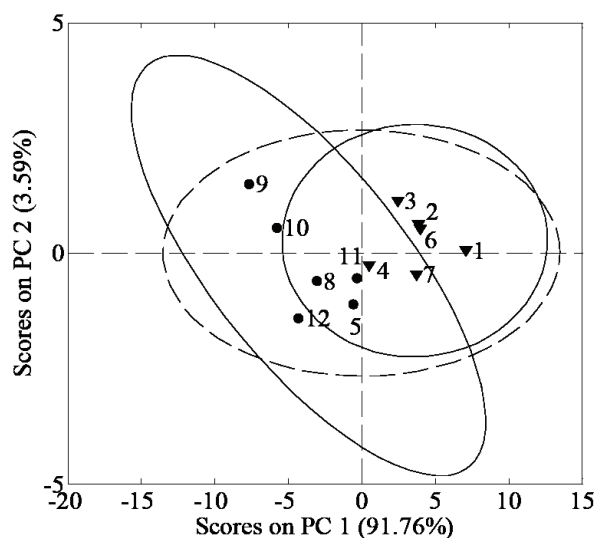


Fig. 2. Score values of the first and second PCs.

Highly significant linear relationships between the retention constants R_M^0 and *PCI* were obtained:

$$\begin{aligned}
 PCI &= -8.434(\pm 0.939) + 5.099(\pm 0.511) R_{M(\text{ACN})}^0 \\
 r &= 0.9000, \quad s = 20.24, \quad F = 99.715, \quad t = 6.53 \quad t_{\text{cr}} = 2.62 \\
 PCI &= -9.445(\pm 0.615) + 3.556(\pm 0.211) R_{M(\text{MeOH})}^0 \\
 r &= 0.9620, \quad s = 7.58, \quad F = 282.967, \quad t = 11.14 \quad t_{\text{cr}} = 2.62 \\
 PCI &= -16.461(\pm 1.188) + 7.181(\pm 0.502) R_{M(\text{THF})}^0 \\
 r &= 0.9490, \quad s = 10.35, \quad F = 204.468, \quad t = 9.52 \quad t_{\text{cr}} = 2.62
 \end{aligned}$$

Taking into account the satisfactory quality of the obtained relationships, the values of *PCI* were correlated with the calculated $\log P$ values. The statistical parameters of these dependences are listed in Table II. Statistically significant correlations were obtained in all the investigated linear dependences, indicating that *PCI* could be used as a parameter of lipophilicity for the investigated coumarins.

A general remark related to the previous discussion could be that the variables describing directly the partitioning of the solute between the stationary and mobile phase, such as R_M^0 , are more suitable for lipophilicity estimation of the investigated coumarins than the parameter proportional to the molecular hyd-

rophobic surface area (b) or the interpolated quantity that combines all chromatographic data (PCI).

TABLE II. Relationships between the PCI and the $\log P$ values determined using different computational programs

PCI vs. $\log P$	Equation	r	s
$PCI - A\log P_s$	$PCI = -11.136(1.049) + 4.008(0.477)A\log P_s$	0.864	27.527
$PCI - AC\log P$	$PCI = -11.434(1.285) + 4.235(0.448)AC\log P$	0.889	22.367
$PCI - A\log P$	$PCI = -11.682(1.380) + 4.155(0.464)A\log P$	0.878	24.599
$PCI - M\log P$	$PCI = -19.948(3.686) + 8.592(1.561)M\log P$	0.727	55.093
$PCI - \log P_{KOWWIN}$	$PCI = -8.758(0.879) + 3.407(0.309)\log P_{KOWWIN}$	0.916	16.902
$PCI - X\log P_2$	$PCI = -11.755(1.808) + 4.746(0.693)X\log P_2$	0.807	38.995
$PCI - X\log P_3$	$PCI = -11.455(1.485) + 4.451(0.545)X\log P_3$	0.857	28.926

Quantitative structure–toxicity relationship

In a previous study, PLS modeling was performed in order to qualify relationships between the factors governing the lipophilicity of the studied coumarins.¹⁹ The two proposed PLS models (the dependent variables were R_M^0 and $\log P_{OW}$) were statistically significant and their statistical quality was comparable. From these models, it could be seen that the descriptors that describe the size and the shape of the molecule as well as their polar properties determined the lipophilic behavior of the investigated compounds.

Continuing this previous investigation, the toxicity of the analyzed substances, expressed as organ-specific health effects, was predicted and correlated with the molecular descriptors and retention parameters for all three chromatographic systems, as parameters of lipophilicity.

The numerical expressions of the prediction reliability for different health effects (blood, cardiovascular system, gastrointestinal system, kidney, liver and lungs) for the twelve investigated coumarins are given in Table III. Compounds **1–4** have pronounced toxic effects on blood, the cardiovascular system, the gastrointestinal system, and kidney. Compound **6** has a considerable impact on all the investigated health effects and among the observed analogs, it is the most active one. Compounds **11** and **12** have the largest influence on the gastrointestinal system.

The structural features contributing to the diverse health effects are presented in Figs. S1–S12 (Supplementary material) for all the analyzed substances. The mentioned structural features are identified on the molecules with highlighting and color mapping (red – associated with toxic action, green – unrelated to the health effects under investigation).

In order to qualify the relationships between the factors governing the toxicity of the studied compounds, PLS modeling was performed on the data of the probabilities of health effects. The number of latent variables (Num. LVs) was

selected based on minimum *RMSECV* and the minimum difference between *RMSEC* and *RMSECV*. The obtained models are summarized in Table IV.

TABLE III. The values of the probabilities of health effects for the investigated coumarins

Compd.	Probability of health effects					
	Blood	Cardiovascular system	Gastrointestinal system	Kidney	Liver	Lungs
1	0.94	0.98	0.90	0.73	0.46	0.44
2	0.82	0.97	0.87	0.54	0.60	0.41
3	0.89	0.95	0.91	0.65	0.75	0.40
4	0.86	0.94	0.90	0.67	0.44	0.40
5	0.93	0.54	0.49	0.17	0.33	0.33
6	0.90	0.94	0.72	0.86	0.73	0.70
7	0.34	0.44	0.41	0.13	0.07	0.35
8	0.27	0.29	0.23	0.09	0.09	0.16
9	0.45	0.11	0.18	0.04	0.02	0.32
10	0.23	0.04	0.28	0.07	0.03	0.19
11	0.33	0.68	0.87	0.10	0.17	0.12
12	0.60	0.77	0.78	0.12	0.19	0.13

TABLE IV. The statistical parameters of the derived PLS models

Parameter	Probability of health effects					
	Blood	Cardiovascular system	Gastrointestinal system	Kidney	Liver	Lungs
R^2Y	0.738	0.867	0.798	0.823	0.959	0.899
Q^2Y	0.508	0.446	0.276	0.638	0.634	0.124
<i>RMSEC</i>	0.141	0.122	0.125	0.125	0.052	0.050
<i>RMSECV</i>	0.191	0.260	0.254	0.182	0.158	0.169
<i>Num. LVs</i>	2	3	3	2	4	4

The contribution of the molecular descriptors and lipophilicity parameters that exhibit the strongest influence on toxic activity was analyzed using variable importance in projection scores (*VIP*). The variables with *VIP* scores higher than 1 were considered as the most relevant for the explanation of the dependant variable *Y*, while those significantly lower than 1 (arbitrarily a value lower than 0.5 is taken) have extremely low or almost no contribution. The descriptors included in the final models are presented in Table V in descending order of their coefficient values in regression graphs together with the notification of the sign of their contribution to the dependent variable.

The statistical parameters calculated for the models obtained after elimination of the variables that only contribute to noise (variables with low values of coefficients and low *VIP* values) confirmed that only in the case of the gastrointestinal system and kidney toxic activity was a simpler and better model obtained (gastrointestinal system – $R^2Y = 0.792$; $Q^2Y = 0.508$; *RMSEC* = 0.126; *RMSECV* = 0.199; *Num. LVs* – 3; kidney – $R^2Y = 0.914$; $Q^2Y = 0.738$; *RMSEC* = 0.088; *RMSECV* = 0.154; *Num. LVs* – 2). Taking into account the parameters

that represent the quality of the model, it could be concluded that the PLS models for kidney and liver health effects are statistically significant.

TABLE V. Molecular descriptors included in the PLS models

Probability of health effects	Molecular descriptors
Blood	LUMO (–), Molecular width (+), Polar surface area (+), Molecular depth (+), Total energy (–), Molecular weight (+), Mass (+), Volume (+), Binding energy (–), Refractivity (+), Polarizability (+), Parachor (+), MR (+), Surface area (+)
Cardiovascular system	Hansen dispersion (–), LUMO (–), HOMO (+), $R_M^0(\text{ACN})$ (–), Total energy (–), Molecular weight (+), Mass (+), $R_M^0(\text{MeOH})$ (–), Molecular depth (–), Surface area (–), Refractivity (+), Polarizability (+), Parachor (+), MR (+), Binding energy (–), $R_M^0(\text{THF})$ (–), Volume (+)
Gastrointestinal system	HOMO (+), Hansen dispersion (–), $R_M^0(\text{ACN})$ (–), Polar surface area (+), H bond acceptor (+), Total energy (–), Molecular depth (–), Surface area (–)
Kidney	LUMO (–), Molecular width (+), Hydrophilic surface area (+), Polar surface area (+), $R_M^0(\text{THF})$ (+), Refractivity (+), Mass (+), Molecular weight (+), Volume (+), Surface area (+), MR(+), Parachor (+), $R_M^0(\text{MeOH})$ (+), Total energy (–), Binding energy (+), $R_M^0(\text{ACN})$ (+)
Liver	LUMO (–), Molecular width (+),
Lungs	LUMO (–), Molecular width (+), $R_M^0(\text{THF})$ (+)

The most relevant descriptors influencing the probabilities of health effects are electric polarization descriptors, size descriptors and lipophilicity descriptors. All the obtained models indicate the importance of the LUMO parameter with a negative contribution to toxicity. The mentioned descriptor is related to the electron affinity and is a measure of the electrophilicity of a molecule. Other electric polarization descriptors that encode information about the charge distribution in the molecule, such as polarizability and refractivity index, have a positive influence on the values of the biological activities, while the Hansen dispersion exhibits a negative influence. Descriptors related to the size of the molecule, such as molecular weight, depth, width, mass and volume, have a positive impact on all the observed health effects. The polar surface area, present in the model for blood and the gastrointestinal system, is defined as the part of the surface area of the molecule associated with oxygens, nitrogens, sulfurs and the hydrogens bonded to any of these atoms. This surface descriptor, which is related to the hydrogen-bonding ability of the compounds, has a positive impact on two mentioned health effects. On the contrary, the surface area of a substance, as the sum of all areas that cover the surface of the molecule, have different influences subject to the determined toxicity. Experimentally obtained lipophilicity parameters $R_M^0(\text{ACN})$, $R_M^0(\text{MeOH})$ and $R_M^0(\text{THF})$ are present with negative influences in the models for

the cardiovascular and gastrointestinal systems, and in models for kidney and lungs with a positive impact. Lipophilicity parameters are not included in the final models for blood and liver. This leads to the assumption that the toxicity of the investigated coumarins in these cases is probably not determined by their lipophilicity, but by specific interactions with the receptor active center. Similar results could be found elsewhere in the literature.^{23,24}

CONCLUSIONS

The present work focused on identifying the most important descriptors affecting the lipophilicity of twelve coumarin derivatives. Four commonly used descriptors for assessing the lipophilicity of unknown solutes, obtained from the thin-layer chromatographic data, were compared. As a general remark, it could be stated that a variable describing directly the solute partitioning between the stationary and mobile phase, such as R_M^0 , are more suitable for lipophilicity estimation of the investigated coumarins than the parameter proportional to the molecular hydrophobic surface area (b), or the interpolated quantity that combined all chromatographic data (PCI).

The toxicity of the coumarins was used for establishing QSTRs including calculated and experimentally determined molecular descriptors, and also partial least square regression. Taking into account the parameters that represent the quality of the QSTR model, it could be concluded that the best models were obtained for kidney and liver health effects. Descriptors included in the final equations were electric polarization descriptors, size descriptors and lipophilicity descriptors. The obtained models were used for the selection of the structural features of the compounds that significantly affect their absorption, distribution, metabolism, excretion and toxicity.

SUPPLEMENTARY MATERIAL

Structural features of compounds **1–12** contributing to diverse health effects are available electronically from <http://www.shd.org.rs/JSCS/>, or from the corresponding author on request.

Acknowledgements. This work was supported by the Ministry of Education, Science and Technological Development of the Republic of Serbia, Grant No. 172017.

ИЗВОД

АНАЛИЗА ЗАВИСНОСТИ СТРУКТУРЕ И ТОКСИЧНОСТИ НЕКИХ ПРИРОДНИХ И СИНТЕТИЧКИХ КУМАРИНА КОРИШЋЕЊЕМ РЕТЕНЦИОНИХ ПАРАМЕТАРА

EL NADI M. A. RABTTI¹, MAJA M. NATIĆ¹, DUŠANKA M. MILOJKOVIĆ-OPSENIĆA¹, JELENA B. TRIFKOVIĆ¹, TOMISLAV TOŠIĆ¹, IVAN M. VUČKOVIĆ¹, VLATKA VAJČIĆ² и ЖИВОСЛАВ Љ. ТЕШИЋ¹

¹Хемијски факултет Универзитета у Београду, П. фах 51, 11158 Београд и ²Институт за хемију, технологију и металургију Универзитета у Београду, Њешићева 12, 11000 Београд

Применом реверзно-фазне танкослојне хроматографије на дванаест деривата кумарина одређена су четири параметара липофилности (R_M^0 , b , C_0 и PCI). Корелацијом добијених резултата са израчунатим $\log P$ вредностима утврђен је дескриптор који на

најбољи начин описује липофилност испитиваних кумарина. Поред тога израчуната је могућа хемијска токсичност кумарина, изражена као вероватноћа утицаја поменутих једињења на специфичне органе (крв, кардиоваскуларни систем, гастроинтестинални систем, бубреге, јетру и плућа) а која је израчуната применом ACD/Tox Suite програма. Добијене вредности токсичности корелисане су са молекулским дескрипторима и експериментално одређеним параметрима липофилности, применом методе парцијалне регресије најмањих квадрата (*partial least square regression*). Узимајући у обзир параметре који описују квалитет модела зависности структуре и токсичности, утврђено је да су најбољи модели добијени за утицај кумарина на бубреге и јетру. Сви добијени модели указују на значај електрично поларизационих дескриптора, као и дескриптора који описују величину и липофилност једињења, а употребљени су за утврђивање структурних карактеристика које значајно утичу на њихову апсорпцију, дистрибуцију, метаболизам, излучивање и токсичност.

(Примљено 16. јула, ревидирано 6. септембра 2012)

REFERENCES

1. C. Hansch, T. Fujita, *J. Am. Chem. Soc.* **86** (1964) 1616
2. C. Horváth, W. Melander, I. Molnar, *J. Chromatogr.* **125** (1976) 129
3. F. Murakami, *J. Chromatogr.* **178** (1979) 393
4. M. L. Bieganowska, A. Doraczynska-Szopa, A. Petruczynik, *J. Planar Chromatogr. - Mod. TLC* **8** (1995) 122
5. C. Sarbu, T. Sorina, *J. Chromatogr., A* **822** (1998) 263
6. C. Sarbu, K. Kuhajda, S. Kevresan, *J. Chromatogr., A* **917** (2001) 361
7. R. G. Brereton, *Chemometrics: Data Analysis for the Laboratory and Chemical Plant*, Wiley, Chichester, UK, 2003, p. 297–323
8. K. Varmuza, P. Filzmaser, *Introduction to Multivariate Statistical Analysis in Chemometrics*, CRC Press, Taylor & Francis Group, Boca Raton, FL, 2008
9. T. W. Schultz, M. T. D. Cronin, T. I. Netzeva, *J. Mol. Struct. THEOCHEM* **622** (2003) 23
10. A. Worth, S. Lapenna, E. Lo Piparo, A. Mostrag-Szlichtyng, R. Serafimova, *JRC Scientific and Technical Reports*, EUR 24705 EN, Publications Office of the European Union, European Union, Luxembourg, 2011
11. M. Sajewicz, D. Staszek, M. Natic, M. Waksmundzka-Hajnos, T. Kowalska *J. Chromatogr. Sci.* **49** (2011) 560
12. M. Sajewicz, L. Wojtal, M. Natic, D. Staszek, M. Waksmundzka-Hajnos, T. Kowalska, *J. Liq. Chromatogr. Related Technol.* **34** (2011) 848
13. M. Sajewicz, D. Staszek, M. Natic, L. Wojtal, M. Waksmundzka-Hajnos, T. Kowalska, *J. Liq. Chromatogr. Related Technol.* **34** (2011) 864
14. A. B. Abubaker, M. Natic, T. B. Tosti, D. M. Milojkovic-Opsenica, I. Z. Djordjevic, V. V. Tesevic, M. B. Jadranin, S. M. Milosavljevic, M. J. Lazic, S. S. Radulovic, Z. Lj. Testic, *Biomed. Chromatogr.* **23** (2009) 250
15. I. Rostova, *Curr. Med. Chem. - Anti-Cancer Agents* **5** (2005) 29
16. P. Magiatis, E. Melliou, A. L. Skaltsounis, S. Mitaku, S. Léonce, P. Renard, A. Pierré, G. Atassi, *J. Nat. Prod.* **61** (1998) 982
17. L. Xie, Y. Takeuchi, L. M. Cosentino, K. H. Lee, *J. Med. Chem.* **42** (1999) 2662
18. E. Melliou, P. Magiatis, S. Mitaku, A. L. Skaltsounis, E. Chinou, I. Chinou, *J. Nat. Prod.* **68** (2005) 78

19. E. H. M. A. Rabtti, M. M. Natić, D. M. Milojković-Opsenica, J. Đ. Trifković, I. M. Vučković, V. E. Vajs, Ž. Lj. Tešić, *J. Braz. Chem. Soc.* **23** (2012) 522
20. I. Vučković, V. Vajs, M. Stanković, V. Tešević, S. Milosavljević, *Chem. Biodiv.* **7** (2010) 698
21. S. Trifunović, *PhD. Thesis*, Comparative investigation of the chemical composition of selected *Achilea* species, Faculty of Chemistry, University of Belgrade, Belgrade, Serbia 2006.
22. I. Tetko, V. Yu. Tanchuk, *J. Chem. Inf. Comput. Sci.* **42** (2002) 1136
23. S. Šegan, F. Andrić, A. Radoičić, D. Opsenica, B. Šolaja, M. Zlatović, D. Milojković-Opsenica, *J. Sep. Sci.* **34** (2011) 2659
24. S. Šegan, J. Trifković, T. Verbić, D. Opsenica, M. Zlatović, J. Burnett, B. Šolaja, D. Milojković-Opsenica, *J. Pharm. Biomed. Anal.*, 2012, In press, DOI: 10.1016/j.jpba.2012.08.025.



J. Serb. Chem. Soc. 77 (10) S189–S201 (2012)

SUPPLEMENTARY MATERIAL TO

Quantitative structure–toxicity relationship study of some natural and synthetic coumarins using retention parameters

EL HADI M. A. RABTTI¹, MAJA M. NATIĆ^{1#}, DUŠANKA M. MILOJKOVIĆ-OPSENICA^{1#}, JELENA Đ. TRIFKOVIĆ^{1#}, TOMISLAV TOSTI^{1#}, IVAN M. VUČKOVIĆ¹, VLATKA VAJS² and ŽIVOSLAV Lj. TEŠIĆ^{1#*}

¹*Faculty of Chemistry, University of Belgrade, P. O. Box 51, 11158 Belgrade, Serbia and*

²*Institute of Chemistry, Technology and Metallurgy, University of Belgrade, Njegoševa 12, 11000 Belgrade, Serbia*

J. Serb. Chem. Soc. 77 (10) (2012) 1443–1456

* Corresponding author. E-mail: ztesic@chem.bg.ac.rs

Serbian Chemical Society member.

STRUCTURAL FEATURES OF COMPOUNDS 1–12 CONTRIBUTING TO DIVERSE HEALTH EFFECTS

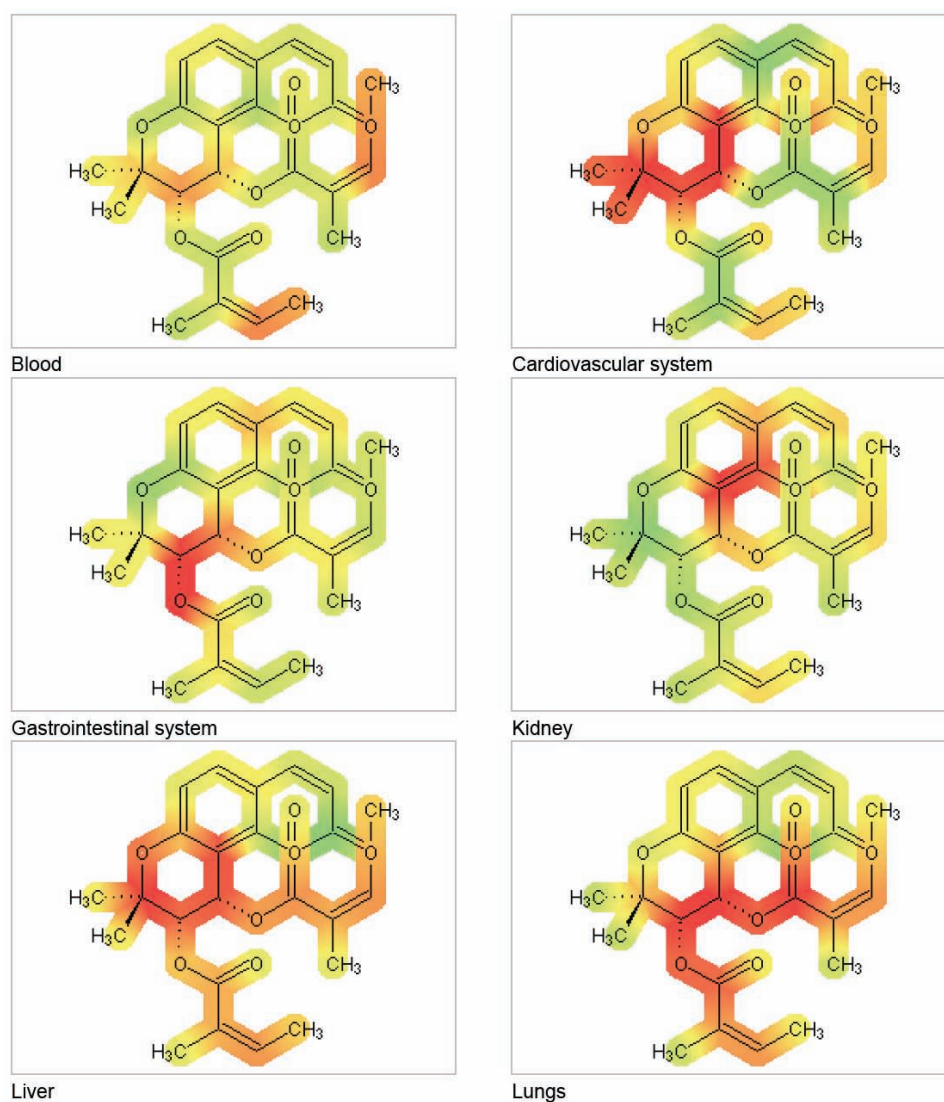


Figure S-1. Structural features of compound 1 contributing to diverse health effects.

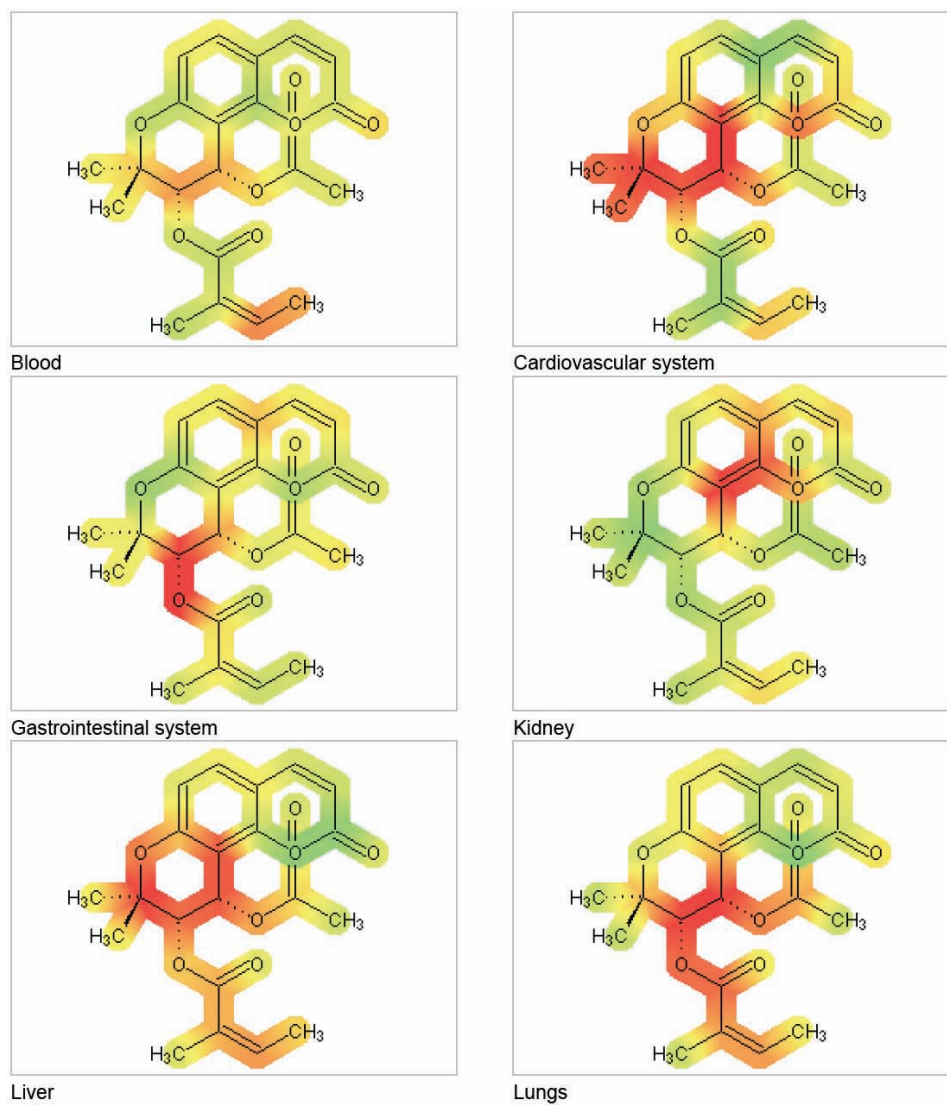


Figure S-2. Structural features of compound 2 contributing to diverse health effects.

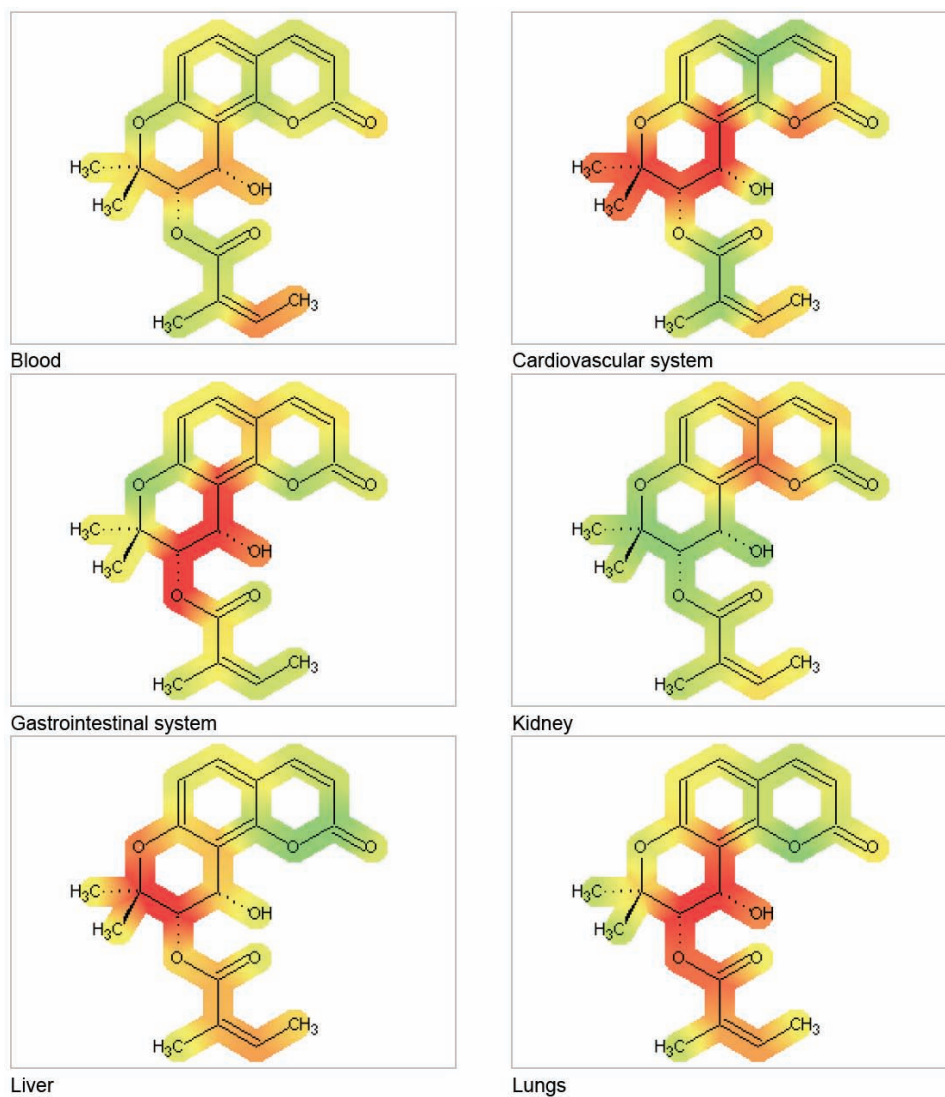


Figure S-3. Structural features of compound **3** contributing to diverse health effects.

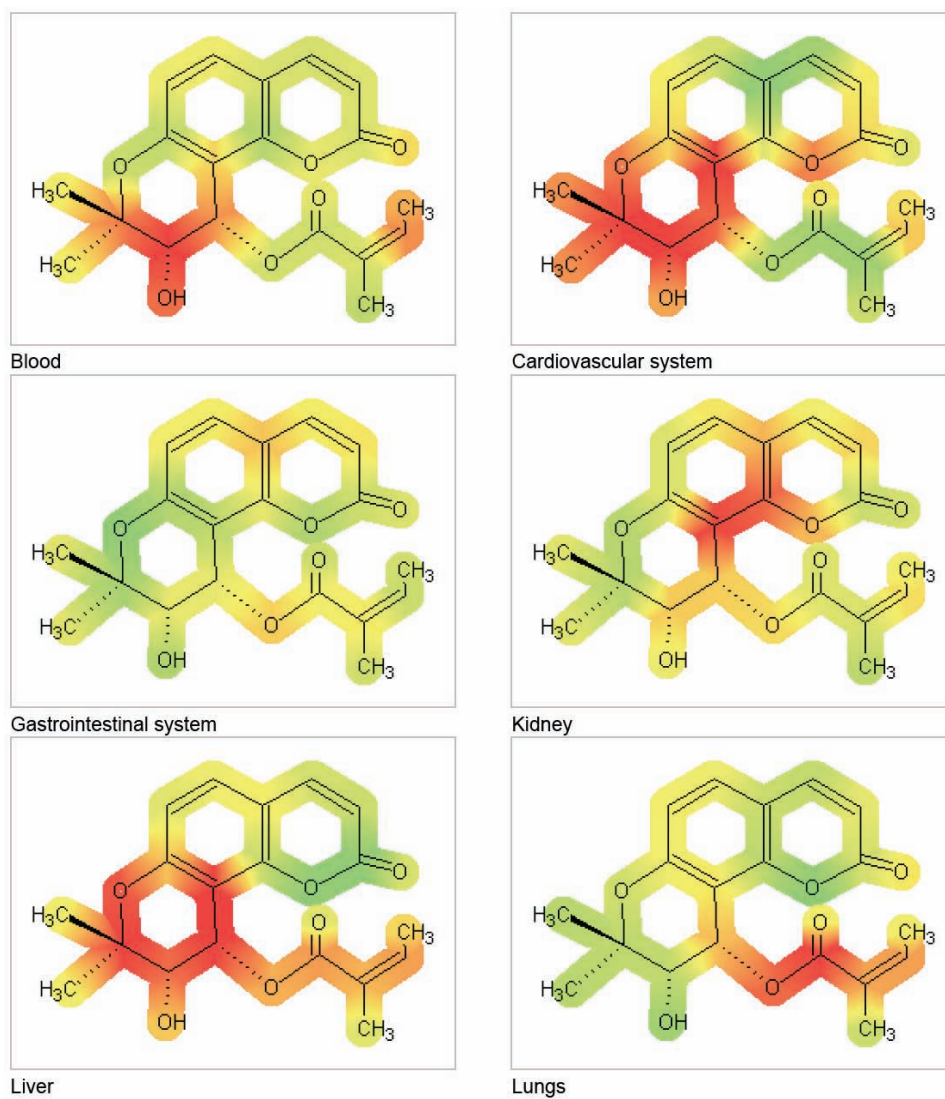


Figure S-4. Structural features of compound 4 contributing to diverse health effects.

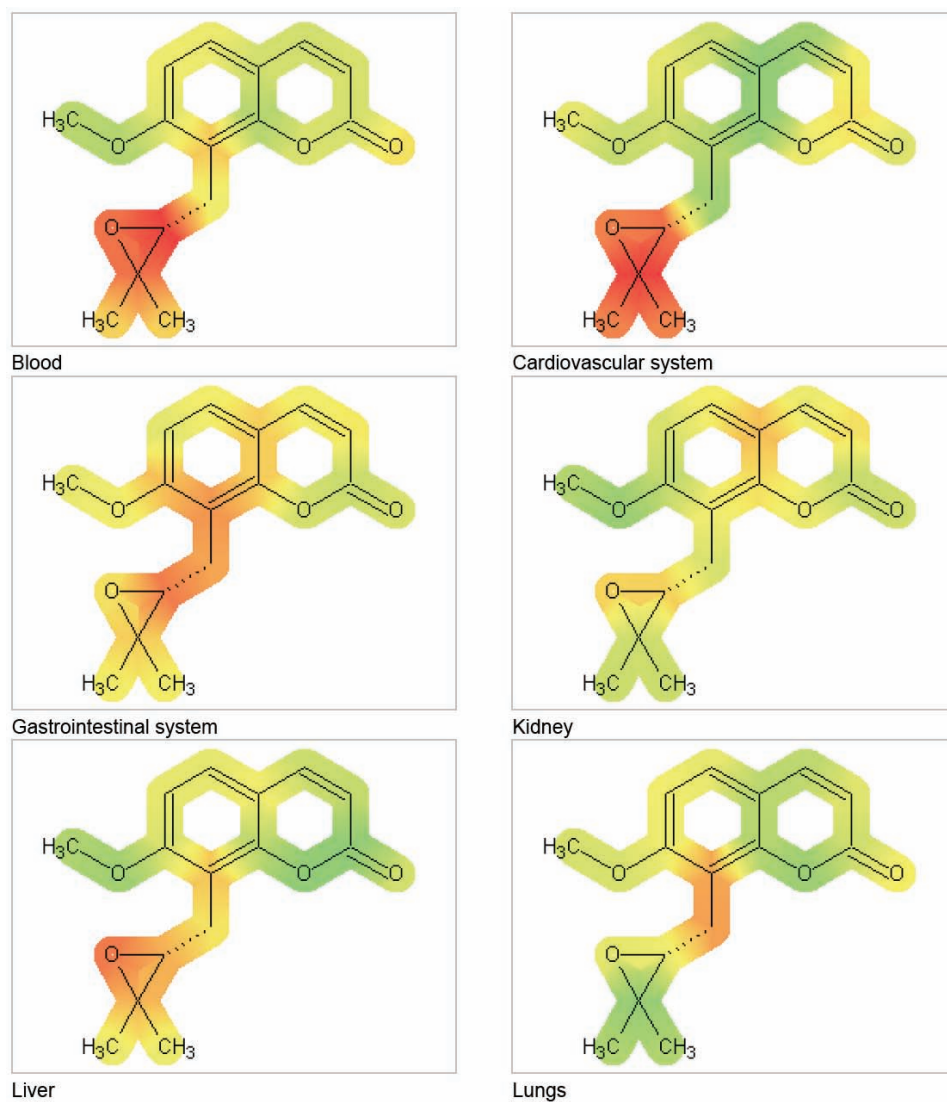


Figure S-5. Structural features of compound 5 contributing to diverse health effects.

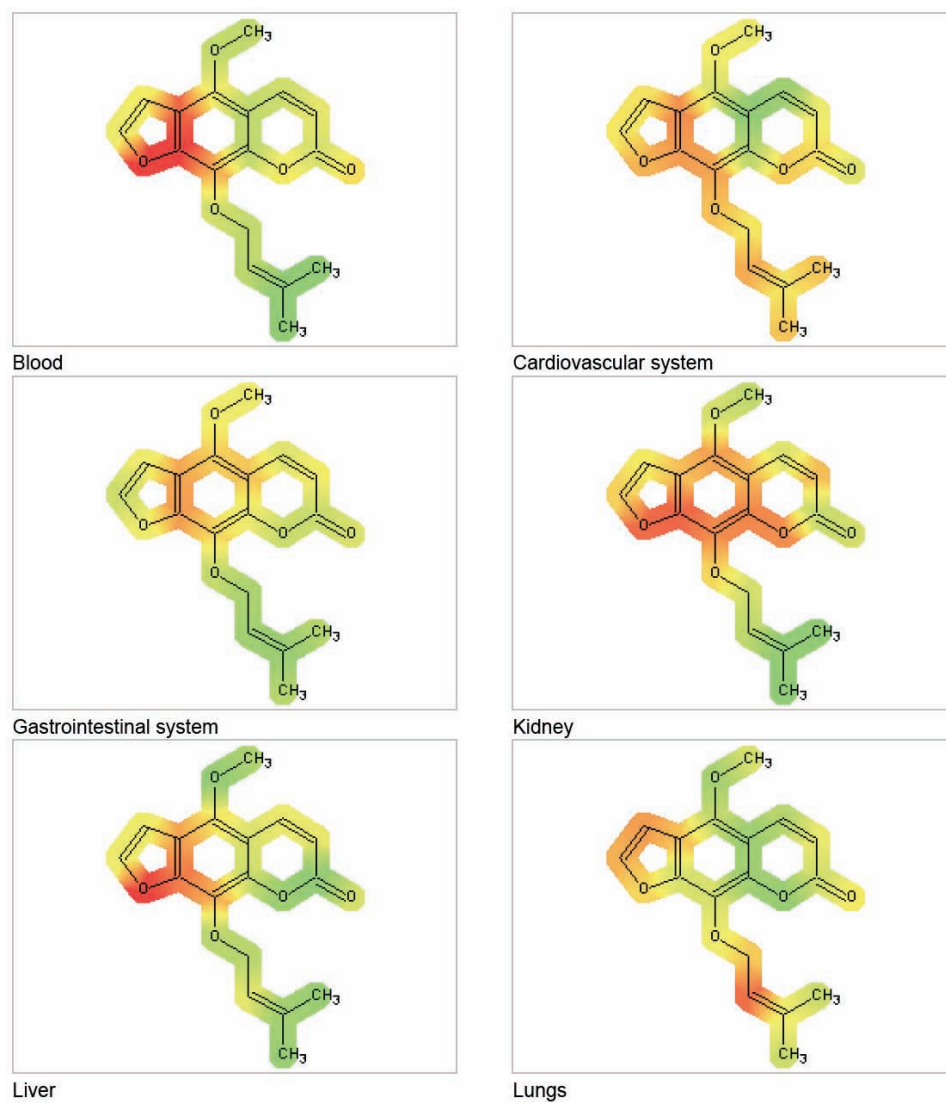


Figure S-6. Structural features of compound 6 contributing to diverse health effects.

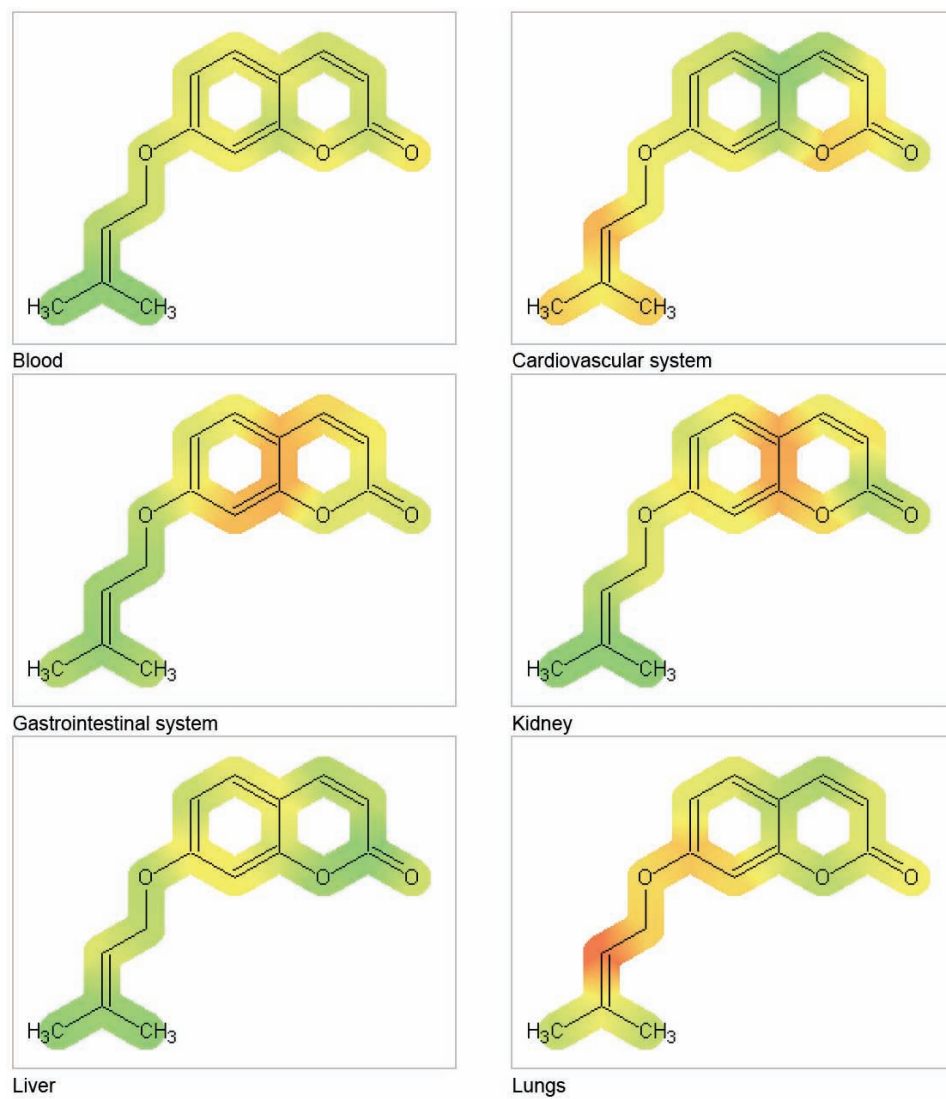


Figure S-7. Structural features of compound 7 contributing to diverse health effects.

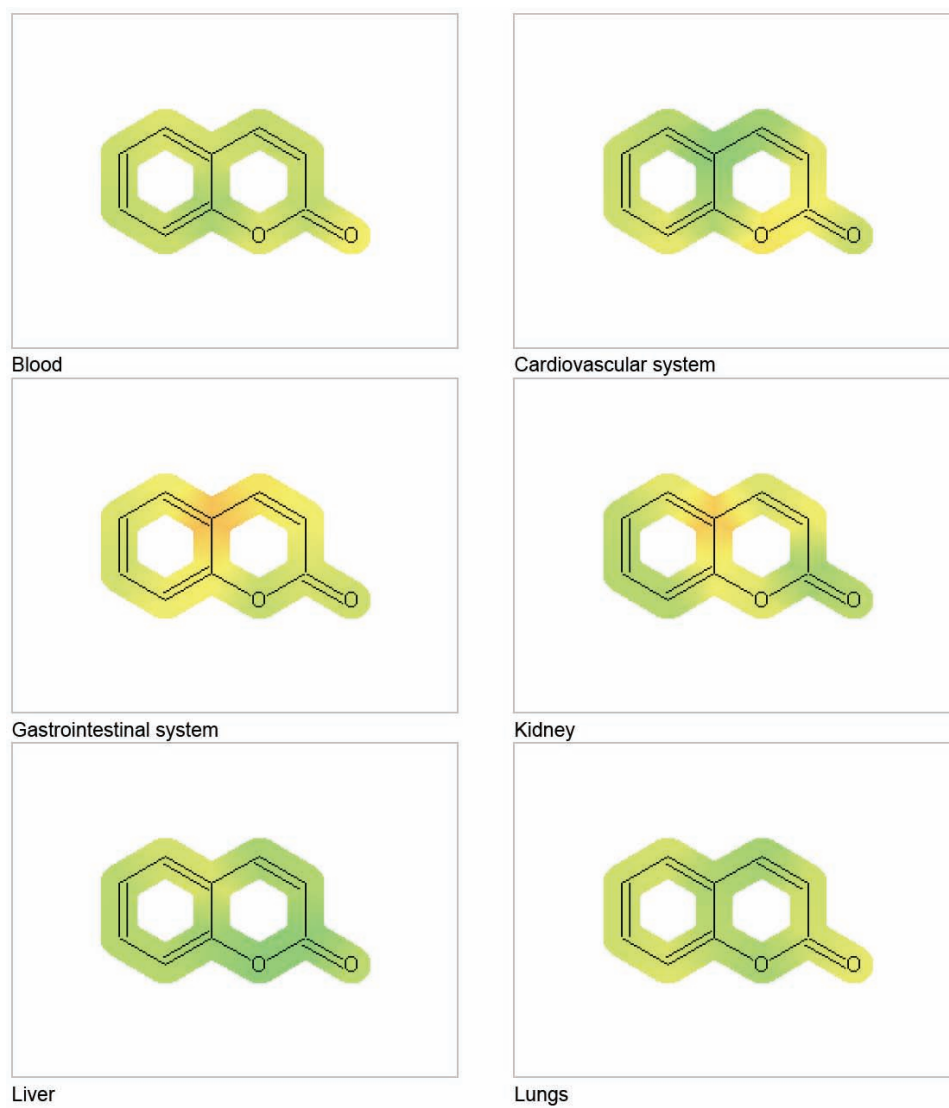


Figure S-8. Structural features of compound **8** contributing to diverse health effects.

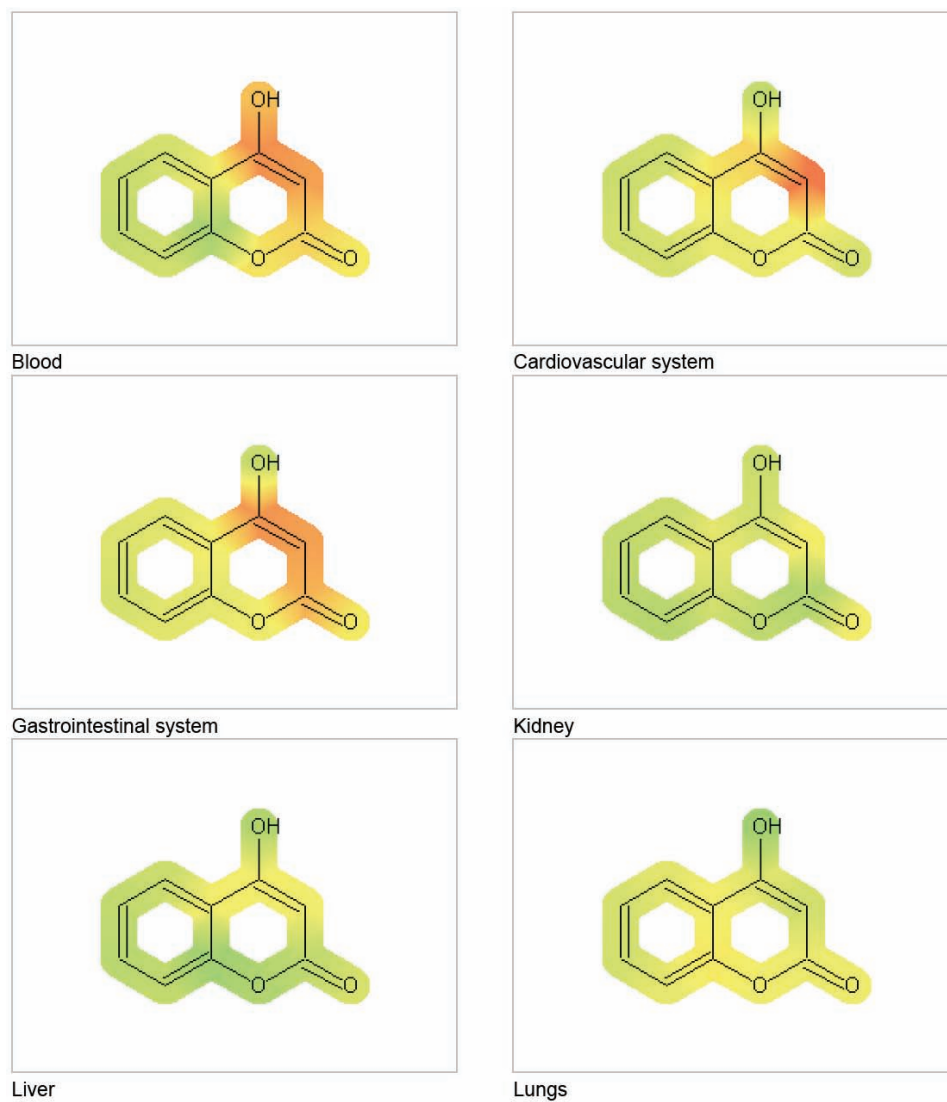


Figure S-9. Structural features of compound 9 contributing to diverse health effects.

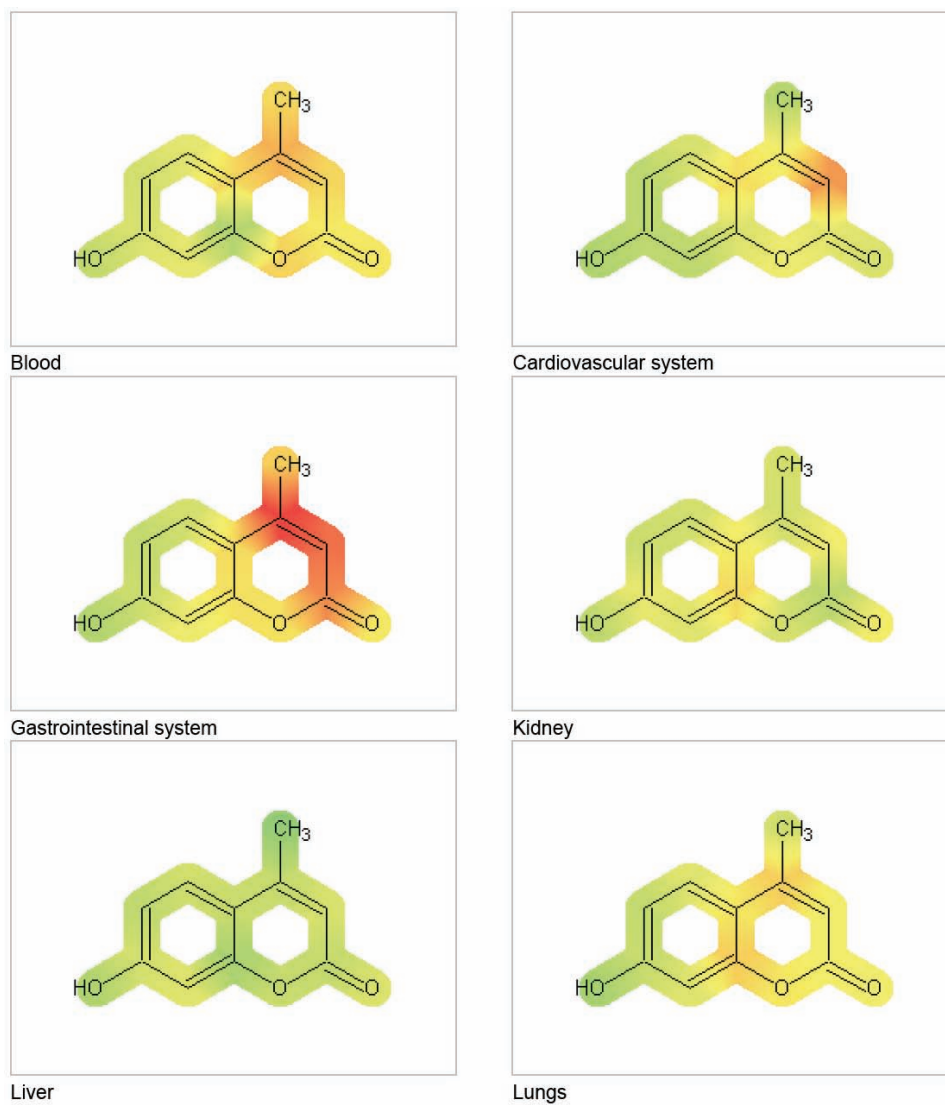


Figure S-10. Structural features of compound 10 contributing to diverse health effects.

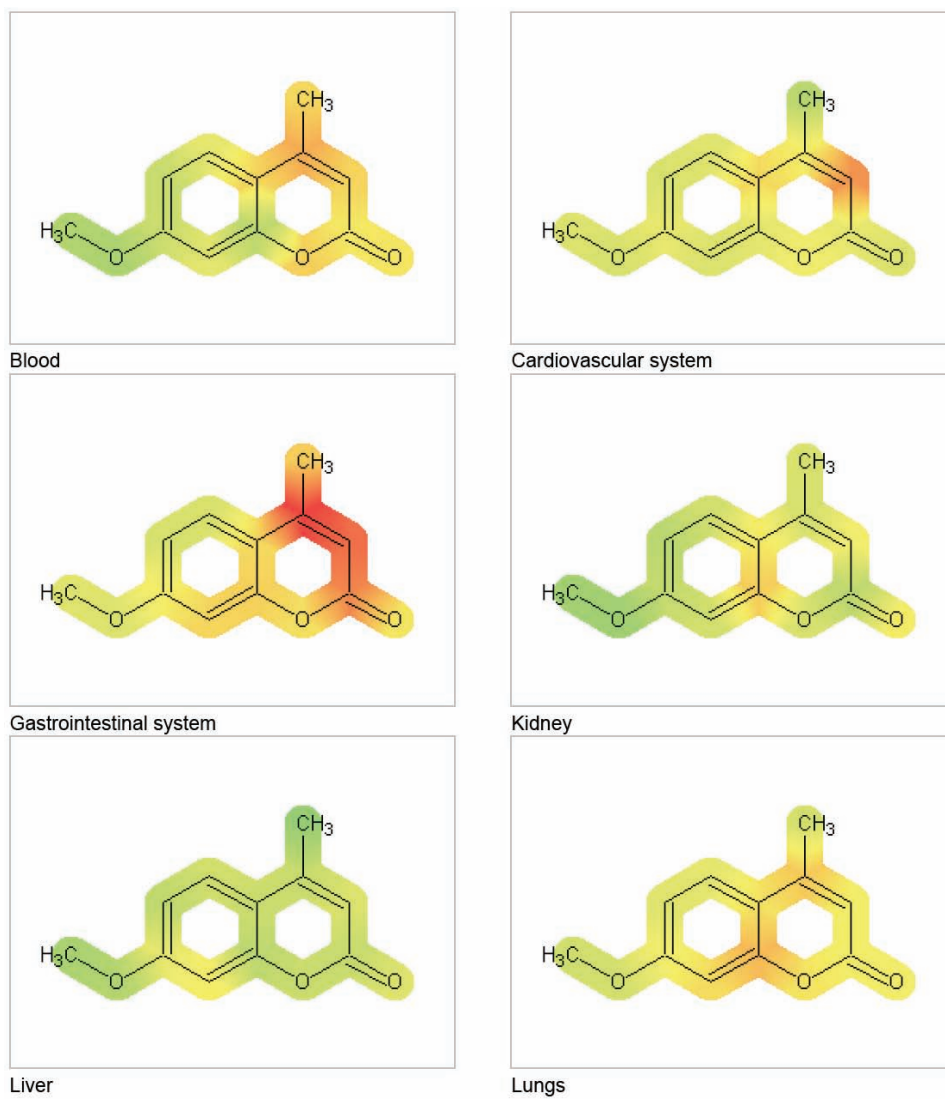


Figure S-11. Structural features of compound **11** contributing to diverse health effects.

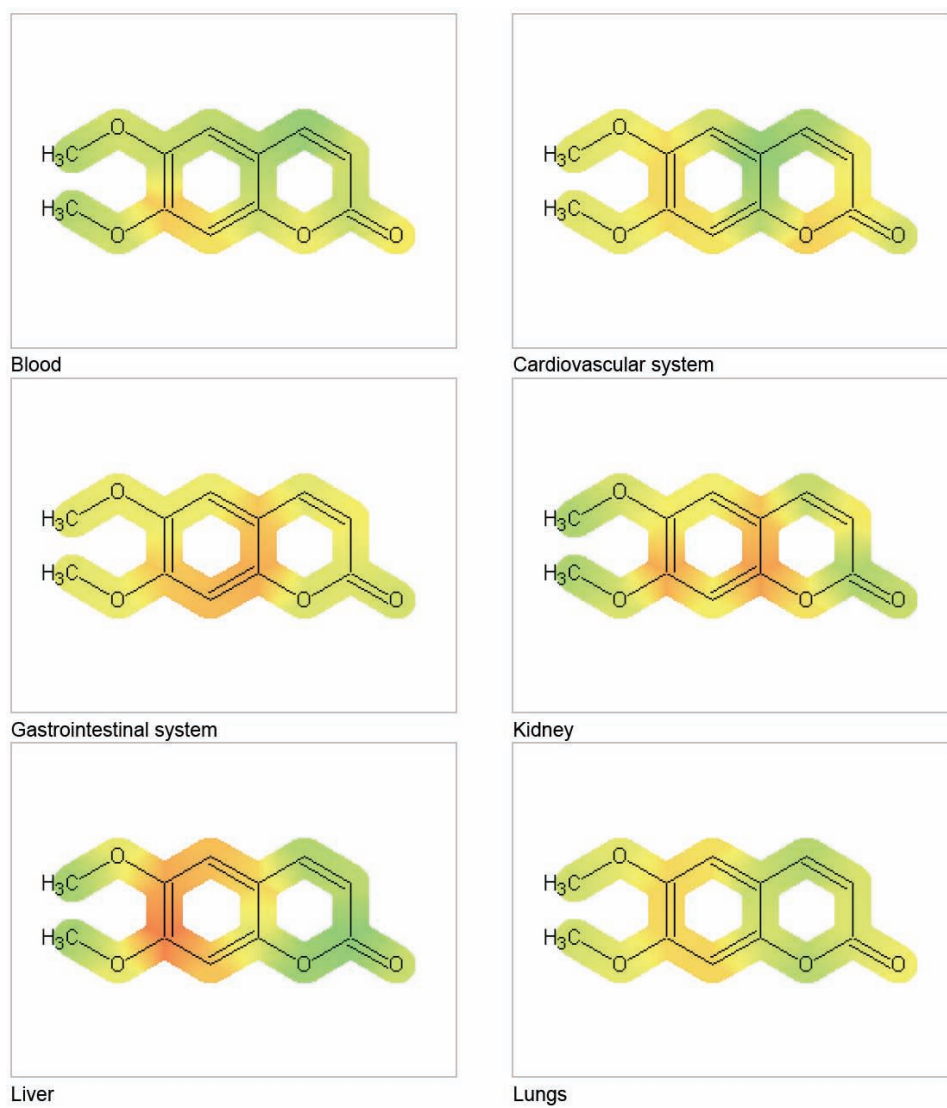


Figure S-12. Structural features of compound **12** contributing to diverse health effects



J. Serb. Chem. Soc. 77 (10) 1457–1481 (2012)
JSCS–4366

The effect of polar solvents on the synthesis of poly(urethane–urea–siloxane)s

MILICA BALABAN¹, VESNA ANTIĆ^{2*#}, MARIJA PERGAL^{3#},
IOLANDA FRANCOLINI⁴, ANDREA MARTINELLI⁴ and JASNA DJONLAGIĆ^{5#}

¹University of Banja Luka, Faculty of Science, Banja Luka, Bosnia and Herzegovina,
²University of Belgrade, Faculty of Agriculture, Belgrade, Serbia, ³University of Belgrade,
Institute of Chemistry, Technology and Metallurgy, Belgrade, Serbia, ⁴University of Rome
“Sapienza”, Dept. of Chemistry, Rome, Italy and ⁵University of Belgrade, Faculty of
Technology and Metallurgy, Belgrade, Serbia

(Received 25 October 2011, revised 9 April 2012)

Abstract: Segmented poly(urethane–urea–siloxanes) (PUUS) based on 4,4'-methylene diphenyl diisocyanate–ethylene diamine (MDI–ED) hard segments and hydroxypropyl-terminated poly(dimethylsiloxane) (PDMS, $\bar{M}_n = 1000 \text{ g mol}^{-1}$) soft segments were prepared under various experimental conditions. The copolymers with constant molar ratio of hard and soft segments (PDMS:MDI:ED = 1:2:1; 20 wt. % of the hard segments) were synthesized in two different solvent mixtures, by a two-step polyaddition procedure. The first one was tetrahydrofuran/*N,N*-dimethylacetamide (THF/DMAc) with different co-solvent ratios (1/1, 1/2 and 1/9, v/v), whereas the second one was tetrahydrofuran/*N*-methylpyrrolidone (THF/NMP, 1/9, v/v). The reaction conditions were optimized by varying the co-solvents ratio, the concentration of the catalyst, the initial monomer concentration, as well as the time of the first and the second step of the reaction. The effects of the experimental conditions on the size of the PUUS were investigated by gel permeation chromatography (GPC) and dilute solution viscometry. The copolymers with the highest molecular weights were obtained in the THF/NMP mixture (1/9, v/v). The structure and composition of the copolymers were determined by ¹H-NMR and FTIR spectroscopy. The morphology of the synthesized copolymers was investigated by atomic force microscopy (AFM), while the thermal properties were studied by differential scanning calorimetry (DSC) and thermogravimetric analysis (TGA). The surface properties were evaluated by measuring the water contact angle (WCA). The copolymers exhibited phase-separated microstructure and were stable up to 200 °C in nitrogen.

Keywords: urethane–urea–siloxane copolymers; two-step polyaddition; reaction conditions; optimization; thermal properties; microphase separation.

* Corresponding author. E-mail: vantic@agrif.bg.ac.rs

Serbian Chemical Society member.

doi: 10.2298/JSC111025056B

INTRODUCTION

Poly(urethane–urea) (PUU) copolymers represent an important subclass of segmented polyurethanes (PU) in which diamines are used as the chain extenders rather than diols. The soft segments in both PU and PUU copolymers are usually aliphatic polyesters or polyethers with number average molecular weights in range from 1000 to 5000 g mol⁻¹, while the hard segment content is between 15 and 40 wt.%. Due to the stronger hydrogen bonding in the hard domains, the PUU possess improved mechanical properties compared to conventional thermoplastic PU.^{1–4}

Segmented PU and PUU with polydimethylsiloxane (PDMS) as the soft segment (PUS and PUUS, respectively) have found substantial interest because of the many unique properties of the PDMS segments, including low glass transition temperature, low surface energy, high permeability to many gases, biocompatibility and thermal stability, which made them suitable for applications such as elastomers, coatings and biological implants.^{5,6} The extremely large differences in the solubility parameters of PDMS and urethane and urea groups (15.6, 37.2 and 45.6 J^{1/2} cm^{-3/2}, respectively),⁷ which results in almost complete phase separation between the hard and soft segments in copolymer, together with strong hydrogen bonding which occurs in the hard segments, should lead to improved mechanical properties of PUUS copolymers. However, the initial attempts to synthesize PDMS-based poly(urethane–urea)s resulted in copolymers with rather low molecular weight and poor mechanical properties, mainly due to solubility problems during synthesis.^{6,7}

The solvent mixture usually used for the synthesis of PUUSs is THF/DMAc, tetrahydrofuran/*N,N*-dimethylacetamide, of different co-solvent ratios. DMAc is responsible for the dissolution of polar monomers and segments, while the presence of THF is necessary because of the dissolution of the non-polar PDMS segments.^{8–10} The use of 2-propanol (2-PA) as a solvent for the preparation of the PDMS–urea copolymers with high urea contents and high molecular weights has also been demonstrated.^{11,12} Considering the large difference in polarity between the urethane/urea hard segments and the siloxane soft segments, there are now two general approaches to the synthesis of PUUS copolymers. The first involves the presence of polyether- or polyester-segments as co-soft segments, in order to improve miscibility of PDMS with the urethane and urea units.^{13–15} The presence of the second soft segment, which has the ability to form hydrogen bonds with the hard segments, leads to extensive phase mixing of the hard and the soft segments and to a deterioration in mechanical properties, due to the decrease of the phase separation in the copolymers.^{16,17} In addition, it was established that typical aliphatic polyether and polyester soft segments are susceptible to oxidative and hydrolytic degradation *in vivo*, which restricts their long-term use as biomedical implants.¹⁸

The second approach to the synthesis of segmented PUUSs is based on using end-functionalized PDMS as a single soft segment, whereby the terminal units attached to the ends of the siloxane oligomers act as a “compatibilizer” between the highly polar urethane/urea hard segments and the non-polar siloxane soft segments.^{6,14} Over the years, the use of hydroxybutyl-, hydroxyhexyl-, as well as aminopropyl- and secondary aminoalkyl-terminated PDMS oligomers for the preparation of polyurethane, polyurea and poly(urethane–urea) copolymers has been reported.^{12,19,20} Recently, segmented PUUS based on fluorinated hydroxypropyl-terminated PDMS were prepared.²¹ Generally, the synthesis of segmented PUUS is very difficult to realize due to the extremely high immiscibility of the highly polar combination of urethane/urea hard segments with non-polar siloxane soft segments, regardless of the kind of used end-functionalized PDMS. The selection of the appropriate solvent is critical to promote solubilization and to prevent premature precipitation of the growing chains, thus ensuring copolymers of high molecular weight.

This work focused on the synthesis of PUUS copolymers derived from hydroxypropyl-terminated PDMS as the soft segment and 4,4'-methylene diphenyl diisocyanate–ethylene diamine (MDI–ED) as the hard segment. The molar ratio of the reacting monomers was constant (PDMS:MDI:ED = 1:2:1), which resulted in the copolymers with the predetermined content of the hard segments of 20 wt. %. The copolymers were prepared in two different solvent mixtures, DMAc/THF and NMP/THF. The aim of this work was to optimize the experimental conditions for the synthesis of PUUS in order to obtain high-molecular weight copolymers. The effects of the co-solvents ratio, the catalyst concentration, the reaction time and the initial monomer concentration in the reaction mixture on the molecular weight were studied. The goal was to compare molecular weights of the PUUS obtained in the DMAc/THF mixtures, which are usually used for the synthesis of this kind of copolymers, with those of the products obtained in more polar NMP/THF solvent combination. The structure of the obtained copolymers was characterized by NMR and FTIR spectroscopy, while their thermal properties were studied by DSC and TG analysis. The morphology of the PUUSs was investigated by AFM. It was also investigated whether the small variation in the structure and composition of the copolymers synthesized under different experimental conditions had an influence on their properties.

EXPERIMENTAL

Materials

α,ω -Dihydroxypropyl-poly(dimethylsiloxane) (α,ω -dihydroxypropyl-PDMS, $\bar{M}_n = 1000$ g mol⁻¹, from ABCR) was dried over molecular sieves. The structure and the number-average molecular weight of PDMS were confirmed by ¹H-NMR spectroscopy. 4,4'-Methylene diphenyl diisocyanate (MDI, from Aldrich) with an isocyanate content of 33.6 wt. %, and ethylene diamine (ED, from Zorka, Serbia), were used as received. *N,N*-Dimethylacetamide

(DMAc, from Acros) was dried over calcium hydride and distilled under vacuum. *N*-Methylpyrrolidone (NMP, from Acros) was purified by low-pressure distillation prior to use. Tetrahydrofuran (THF, from J. T. Baker) was dried over lithium aluminum hydride and distilled before use. The stannous octanoate ($\text{Sn}(\text{Oct})_2$) catalyst was obtained from Aldrich and used without further purification. The catalyst was used as a dilute solution (0.01 g cm^{-3}) in an anhydrous mixture THF/DMAc (1/1, v/v) or THF/NMP (1/9, v/v).

Synthesis

Two series of the PUUS copolymers were prepared by a two-step polyaddition procedure in solution, using α,ω -dihydroxypropyl-PDMS, MDI and ED as chain extenders. The first series was synthesized in a mixture of THF and DMAc (1/1, 1/2 or 1/9, v/v), while the second series was obtained in a mixture of THF and NMP (1/9, v/v). All copolymers were prepared at a constant molar ratio of the reacting monomers (PDMS:MDI:ED = 1:2:1), which resulted in a content of hard segments of 20 wt. %. The reaction temperature was varied from 40 to 80 °C, while the catalyst concentration was varied between 0 and 0.10 mol % $\text{Sn}(\text{Oct})_2$, based on PDMS.

For all the used combinations of the reaction conditions, the time of the first reaction step was determined in preliminary experiments, by the standard dibutylamine back-titration method.²² The reaction time of the first step was measured from the moment of completion of the addition of the solution of PDMS and $\text{Sn}(\text{Oct})_2$ into the solution of MDI. The second step (chain-extension) was performed for 1 or 3 h. The exceptions were the experiments in which optimization of the reaction time of the second step was performed, when reaction was extended up to 8 h. The initial concentration of the monomers in the reaction mixture was varied between 7.5 and 25 wt. % (Table I).

TABLE I. Reaction conditions for the synthesis of PUUSs at 40 °C, intrinsic viscosities, the results of the GPC and ¹H-NMR analysis and yields of the copolymers

Sample ^a	Time of 1 st step min	$[\eta]$ dL g ⁻¹	\bar{M}_n g mol ⁻¹	\bar{M}_w g mol ⁻¹	\bar{M}_w/\bar{M}_n	Content HS, mol % (NMR) ^b	Content HS, wt. % (NMR) ^b	<i>l</i> HS ^c	Yield ^d %
Series I									
PUUS7.5-0.1	27	0.15	9400	20420	2.17	52.5	21.5	1.1	62
PUUS10-0.1	20	0.17	8250	16300	1.97	41.9	15.2	0.7	84
PUUS10-0.05	25	0.18	7800	14500	1.86	33.6	11.1	0.5	79
PUUS15-0.1	15	0.15	8050	14400	1.79	43.4	16.0	0.8	83
PUUS15-0.05	20	0.18	9020	16750	1.86	48.2	18.7	0.9	90
		(0.22)	(12200)	(25230)	(2.07)	(55.8)	(23.9)	(1.3)	(88)
PUUS15-0	29	(0.24)	(12440)	(25650)	(2.06)	(60.3)	(27.3)	(1.5)	(85)
PUUS15A-0.05 ^e	17	(0.25)	(14300)	(28730)	(2.01)	(54.8)	(23.1)	(1.2)	(90)
PUUS15B-0 ^f	29	(0.28)	(18500)	(73500)	(3.97)	(60.1)	(27.2)	(1.5)	(89)
Series II									
PUUS10-0.05	19	0.19	8230	13850	1.68	42.0	15.2	0.7	86
PUUS15-0.05	17	0.23	11050	19500	1.76	54.0	22.6	1.2	89
PUUS25-0.05	15	0.28	13040	25120	1.92	45.7	17.3	0.8	91
		(0.29)	(19540)	(58100)	(2.97)	(51.2)	(20.7)	(1.0)	(93)

^aThe values without brackets are for an extension step of 1 h, while the values in brackets are for an extension step of 3 h; ^bcalculated according to 1 soft segment; ^cthe HS content predetermined by the composition of the reaction mixtures was 50 mol % and 20 wt. %; ^dcalculated after precipitation of the copolymer; ^esolvent mixture: THF/DMAc (1/2, v/v); ^fsolvent mixture: THF/DMAc (1/9, v/v)

A typical synthesis for the sample PUUS15-0.05 from Series I, in THF/DMAc (1/1, v/v), at a concentration of the catalyst of 0.05 mol % and the concentration of the monomers of 15 wt. %, is described herein. The reaction was performed in a four-necked round-bottomed flask equipped with an overhead stirrer, a dry argon inlet, a reflux condenser and a dropping funnel. In the first step the solution of 5.00 g (5.0 mmol) PDMS in 33.2 cm³ of THF/DMAc (1/1, v/v) and the catalyst (1.0 mg, 2.5·10⁻³ mmol) was slowly added from the dropping funnel into the flask containing required amount of MDI (2.50 g, 10.0 mmol) and 16.6 cm³ of THF/DMAc (1/1, v/v). The solution of MDI had previously been heated to 40 °C in a silicone oil bath. The reaction mixture was stirred for 20 min at 40 °C to prepare the isocyanate-terminated prepolymer. After the theoretical NCO content of 5.60 wt. % in the reaction mixture was reached, the prepolymer was chain-extended by the dropwise addition of the stoichiometric amount of ED (0.30 g, 5.0 mmol) in 2.0 cm³ of solvent mixture, and the reaction was continued at the same temperature for 3 h. The synthesized copolymer was precipitated into methanol/water (1/1) solution, filtered and dried to the constant weight in a vacuum oven at 40 °C. The yields of synthesized PUUS copolymers after precipitation in methanol/water mixture were in the range of 79–93 %, except for sample PUUS7.5-0.1 (62 %) (Table I).

Film preparation

The copolymer films (0.2–0.3 mm thickness) utilized for characterization were cast from NMP solution (10 wt. %) into Teflon molds. First, the solvent was slowly evaporated for 48 h at 40 °C in a force-draft oven. The obtained films were dried under vacuum at 40 °C for 48 h.

Characterization methods

The ¹H-NMR spectra were recorded on a Bruker Avance 500 spectrometer (500.13 MHz) equipped with 5 mm inverse detection z-gradient probe at 25 °C using DMSO-*d*₆ as solvent.

The FTIR spectra were recorded on an ATR-IR Nicolet 380 instrument with a diamond crystal of refractive index 2.4 and an incidence angle of 45°. All spectra were collected using 64 scans in the spectral region between 4000 and 400 cm⁻¹, at a resolution of 4 cm⁻¹.

The intrinsic viscosities, [η], were measured in an Ubbelohde viscometer at 25 °C using NMP as the solvent.

The GPC measurements were conducted using a Waters 600E instrument equipped with a refractive index detector, on three Supelco Pl-Gel columns connected in line (crosslinked polystyrene with pore sizes of 10⁻⁵, 10⁻⁶ and 10⁻⁷ m). NMP was used as the mobile phase at 60 °C, with a flow rate of 1.5 cm³ min⁻¹. The volume of the sample solutions (1 wt. % in NMP) injected was 60 μL in all cases. The system was calibrated with a number of polystyrene standards (from Sigma-Aldrich) ranging from 1700 to 55100 g mol⁻¹.

Differential scanning calorimetry (DSC) was performed on a Mettler-Toledo DSC822 thermal analyser, under a nitrogen atmosphere, at a heating rate of 10 °C min⁻¹ and the cooling rate of 40 °C min⁻¹ over a temperature range from -150 to 200 °C. The weight of the samples was approximately 5 mg.

The thermal stabilities of the polymers were determined using a Mettler-Toledo DSC822 thermal analyser in the temperature range from 25 to 600 °C, at heating rate of 10 °C min⁻¹. The TG scans were recorded under dynamic nitrogen atmosphere at flow rate of 50 cm³ min⁻¹. The average weights of the samples were around 3 mg.

Water contact angle (WCA) measurements of the polymer films were realized employing a Krüss DSA100, using the sessile drop method. Single drops of distilled water with a volume of 20 μL were deposited on the polymer film surface and the contact angles were measured at

26 °C after 30 s by means of a camera connected to software for image analysis. The contact angle values were obtained from the average of five measurements.

The surface topography of the PUUS samples was observed by atomic force microscopy (AFM). The AFM characterizations were performed with an AutoProbe CP-Research SPM (TM Microscopes-Veeco) instrument using 90 μm large area scanner. Measurements were performed in air using the contact AFM mode. Veeco phosphorus (n) doped silicon contact metrology probes-model MPP-31123-10 with an Al reflective coating and a symmetric tip were used.

Sample designation

The samples are denoted by 'PUUS' with two numbers denoting the initial monomer concentration and the catalyst concentration in the reaction mixture. For example, PUUS7.5-0.1 means that the initial monomer concentration in the reaction mixture was 7.5 wt. %, while the catalyst concentration was 0.1 mol % Sn(Oct)₂, based on PDMS. The samples that were prepared in the THF/DMAc mixtures at co-solvent ratios different to 1/1, v/v, are additionally denoted as "A" (THF/DMAc = 1/2, v/v) and "B" (THF/DMAc = 1/9, v/v).

RESULTS AND DISCUSSION

Determination of the optimal conditions for the synthesis of PUUSs

The PUUS copolymers were synthesized by the two-step polyaddition method ("prepolymer method"), as shown in Scheme 1.

The hard segment content of 20 wt.%, predetermined by the composition of the reaction mixtures, was calculated based on the copolymer structure given in Scheme 1. In this way, only the portion of MDI that reacted with diamine contributes to the hard segments, while the other MDI portion that reacted with the PDMS prepolymer gives the soft segments.

Two series of the copolymers with constant hard segment content (20 wt. %) were prepared in different solvent mixtures: THF/DMAc (1/1, 1/2 or 1/9, v/v) and THF/NMP (1/9, v/v). In the first step of the reaction, isocyanate-terminated prepolymer was prepared by reaction of MDI in an excess with PDMS, *i.e.*, the mole ratio of NCO and OH groups was 2:1. The required reaction time for the first step had previously been determined in separate experiments for all the employed combinations of the reaction conditions, using the standard dibutylamine back-titration method. The time of the first reaction step was the time required to reduce the concentration of the NCO groups to half of the initial value, and it is given in Table I. In the second step, the prepolymer was chain-extended with the stoichiometric amount of ED under various experimental conditions. The influence of the concentration of the catalyst and monomer in the reaction mixture, as well as the time of the second reaction step, on the molecular weight of the resulting copolymers was studied in order to determine the optimal experimental conditions for the synthesis of PUUS. The molecular weights of PUUS were monitored by measuring the intrinsic viscosity of the copolymer solutions and by GPC. The most important results of the optimization in THF/DMAc and THF/NMP

are summarized in Table I. The copolymers prepared in the THF/DMAc and THF/NMP solvents mixture are assigned as Series I and Series II, respectively. All syntheses given in Table I were realized at 40 °C.

Series I

The experiments in the first series commenced in the solvent mixture THF/DMAc (1/1, v/v). This solvent mixture is, with various volumetric ratios of co-solvents, usually used for the synthesis of the PDMS-based segmented poly(urethane-urea)s.^{8–10} In the beginning, the influence of the reaction temperature on the time required to complete the first step of reaction, *i.e.*, the reaction between PDMS and MDI, was investigated. The dependence of the concentration of NCO groups on the time at different temperatures (40, 60 and 80 °C) is shown in Fig. 1. The initial NCO content in the reaction mixture was 11.2 wt. % and ideally it should have decreased to 5.6 wt. %, *i.e.*, to half of the initial value. However, due to the presence of excess of isocyanate and traces of moisture, side reactions occurred (allophanate and biuret). Consequently, the NCO groups reacted further and their concentration decreased to below the theoretical value, as can be seen in Fig. 1. The first step was generally very fast, especially at temperatures at 80 and 60 °C, when it was completed in 7 or 12 min, respectively. If the first step proceeds very rapidly, the possibility of the side reactions is also pronounced, which acts adversely on the molecular weight and the structure of the copolymers.

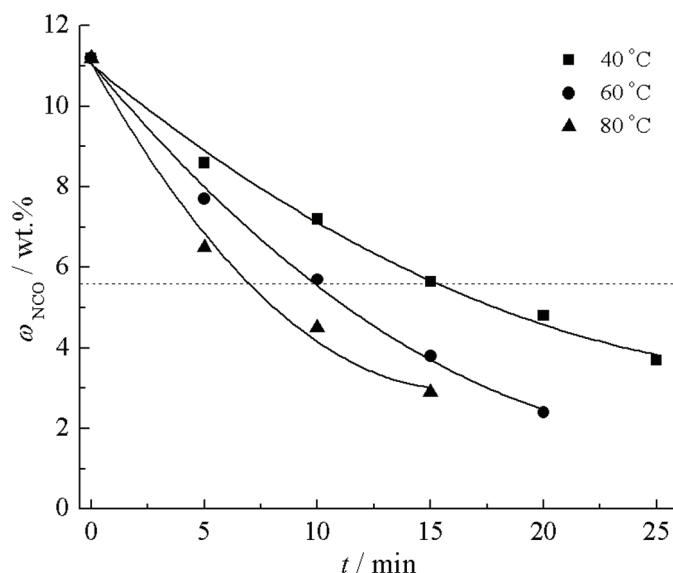


Fig. 1. The concentration of NCO groups as a function of the time of the first reaction step, for the syntheses in THF/DMAc (1/1, v/v) solvent mixture, at different temperatures (40, 60 and 80 °C) and at constant concentration of the monomers (15 wt. %) and catalyst (0.1 mol %).

When the reaction was performed at 40 °C, the reaction was completed in 15 min, which is a reasonable time for the first step. For these reasons, it was decided to perform all further reactions at 40 °C. It was also demonstrated that the time of the first reaction step was shorter with higher concentrations of catalyst and monomers in the reaction mixture (Table I).

The effect of the reaction time of the second phase on the size of the obtained PUUSs, at different concentrations of the catalyst and monomers in the reaction mixture, was also investigated. When the second phase (*i.e.*, the chain-extension step) lasted 1 h, the values of the intrinsic viscosity of all samples synthesized in THF/DMAc (1/1, v/v) were similar (0.15–0.18 dL g⁻¹, Table I), regardless the concentration of the catalyst or the monomers in the reaction mixture. By increase the reaction time of the second phase to 3 h, both the intrinsic viscosity and the molecular weight of the copolymers increased (the values given in brackets in Table I). In addition, it was noticed that a copolymer with a slightly higher molecular weight was obtained in the absence of the catalyst. This can be explained by side-reactions, which occur to a higher degree in the presence of the catalyst, leading to a reduction of the molecular weight. The effect of the time of the second step of reaction on the intrinsic viscosity of PUUSs, with a monomer concentration of 15 wt. % and without the catalyst is shown in Fig. 2. Increasing the reaction time to above 3 h (to 6 and 8 h) provoked a decrease in the viscosity, as it can be seen in Fig. 2. This is probably due to the longer exposure of the copolymer to traces of moisture, *i.e.*, its hydrolysis, and again due to the side-reac-

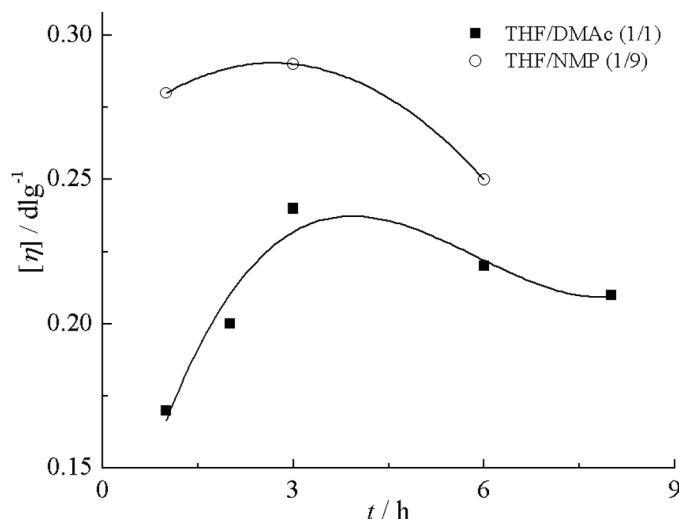


Fig. 2. The effect of the time of the second step on the intrinsic viscosity of PUUSs prepared in THF/DMAc (1/1, v/v at a monomer concentration of 15 wt.% without catalyst) and THF/NMP (1/9, v/v, at a monomer concentration of 25 wt.% and a catalyst concentration of 0.05 mol%) reaction mixtures.

tions of the isocyanate groups, which are related to a disruption of the stoichiometry, and are more pronounced during prolonged polymerization time. The highest values of intrinsic viscosity and molecular weight in the 1/1 (v/v) THF/DMAc mixture were obtained for the sample PUUS15-0, synthesized without the catalyst, with the initial concentration of monomers of 15 wt. % and the time of the second step of 3 h. Intrinsic viscosity of the sample PUUS15-0 amounted 0.24 dL g^{-1} , while the number average molecular weight determined by GPC was 12440 g mol^{-1} (Table I).

In the presence of the highest catalyst concentration (0.1 mol %), a slow decrease in the molecular weights of the copolymers (from 9400 to 8050 g mol^{-1}) with increasing monomer concentration (samples PUUS7.5-0.1, PUUS10-0.1 and PUUS15-0.1) was observed. The highest molecular weight of the sample PUUS7.5-0.1, obtained with the lowest monomer concentration, could be a consequence of polymer fractionation during precipitation and the loss of low molecular weight fractions, as was supported by the low polymer yield (62 %). Further decreases in molecular weight (samples PUUS10-0.1 and PUUS15-0.1) could be explained by the higher probability of side reactions at the highest catalyst concentration of 0.1 mol %, with increasing the monomer concentration. The side reactions were less pronounced at the lower catalyst concentration of 0.05 mol %, and an increase of the molecular weight of the copolymer could be observed with increasing monomer concentration (samples PUUS10-0.05 and PUUS15-0.05).

As was already stated, a key factor for the successful synthesis of PDMS-based poly(urethane-urea)s is the proper selection of the solvent. During the chain extension step in the 1/1 (v/v) THF/DMAc solvent mixture, an undesirable macroscopic separation of the reaction mixture was observed, as well as a premature precipitation of the copolymer, which resulted in low molecular weight of the copolymers. It is obvious that the employed solvent mixture was not polar enough to dissolve efficiently the growing copolymer chains. To overcome this problem, it was decided to increase the proportion of polar DMAc in the mixture.

The increase in the proportion of DMAc to 1/2 (v/v) THF/DMAc led to optically clearer, but not perfectly homogeneous reaction mixture, and to a certain increase in both the intrinsic viscosity and molecular weight of the obtained copolymers, in comparison with the syntheses in 1/1 (v/v) THF/DMAc (Table I). A further increase in the proportion of the polar co-solvent to the ratio 1/9 (v/v) THF/DMAc led to copolymer precipitation in the presence of the catalyst, very soon after the chain extender had been added. It was not possible to analyze this sample because it was not completely soluble in NMP, used for both the viscosity and GPC measurements. All previous samples were completely soluble in NMP, but only partially soluble in DMAc.

Then a new copolymer was prepared under the same conditions, in 1/9 (v/v) THF/DMAc mixture, but without the catalyst. The reaction mixture was clear

and homogeneous in this case, and consequently, the molecular weight of obtained copolymer was significantly higher. It was noticed that a molecular weight of the copolymer increased from 12440 to 18500 g mol⁻¹ when the THF/DMAc ratio was changed from 1/1 to 1/9, at an initial monomer concentration of 15 wt. % in the absence of the catalyst in both cases. A further increase in the proportion of DMAc would be unfavorable because it would lead to a reduction in the solubility of the siloxane prepolymer in the reaction mixture. A certain minimum concentration of THF in the solvent mixture was necessary to maintain the PDMS molecules in solution until they had completely reacted with MDI.

Furthermore, the synthesis with monomer concentrations higher than 15 wt. % (for instance with 25 wt. %) was not successful, since precipitation of the copolymer again occurred.

According to the presented results, the copolymer with the highest molecular weight in Series I was obtained when the following reaction conditions were employed in the second phase of the synthesis: a reaction time of 3 h; a ratio of THF/DMAc co-solvents 1/9 (v/v); a monomer concentration of 15 wt. % and in the absence of the catalyst.

However, further attempts to synthesize PUUSs with a content of the hard segment higher than 20 wt.% under these conditions, again resulted in the premature precipitation of copolymers from the reaction mixture. It could be concluded that DMAc as a co-solvent is not sufficiently polar to provoke dissociation of the very strong hydrogen bonding between the urea groups, the concentration of which in the polymer chain increases with increasing hard segment content.

Series II

As was shown above, increasing the proportion of the more polar DMAc in the mixture with THF did not lead to the desired increase in molecular weight of PUUSs. In most cases, the reaction mixtures were turbid during the synthesis, due to precipitation of the copolymer, and consequently the viscosities and molecular weights of obtained samples were rather low. To overcome these problems, it was decided to replace DMAc as the polar component in the solvent mixture with NMP. NMP is also an aprotic solvent which is often used for the synthesis of thermoplastic poly(urethane-urea)s,¹⁵ polyureas,^{23,24} poly(amide-urea)s,²⁵ and poly(ester-urea)s,²⁶ but is slightly more polar than DMAc.²⁷

To study the effect of the change of polar component of the reaction solvent, on the molecular weight of PUUSs, Series II was prepared in a THF/NMP (1/9, v/v) solvent mixture. Analogously to Series I, the time that was required to complete the first step of reaction was independently determined for all the syntheses and these values are given in Table I. The reaction time was found to decrease (from 19 to 15 min) with increasing concentration of both catalyst and reactants,

similar to when the THF/DMAc solvent mixtures were used. It was also registered that the rate of the reaction between PDMS and MDI was significantly higher in the THF/NMP mixture and showed less dependence on the initial concentration of monomers.

In Series II, the effect of the monomer concentration in the reaction mixture and reaction time of the second phase on the intrinsic viscosity and molecular weight of the obtained copolymers was investigated. The results are presented in Table I and Fig. 2. Unlike the syntheses in THF/DMAc, the reactions in THF/NMP proceeded in a perfectly clear solution after the addition of chain extender and precipitation was not observed regardless of any change in the reaction conditions. The molecular weight of the copolymers synthesized at reaction time of 1 h with a catalyst concentration of 0.05 mol % increased significantly with the concentration of the monomers in the reaction mixture, as was found for Series I. Moreover, in this solvent mixture, it was possible to synthesize PUUSs at a higher initial concentration of the monomers, *i.e.*, 25 wt. %. The values of \bar{M}_n were 8230, 11050 and 13040 g mol⁻¹ for monomer concentrations of 10, 15 and 25 wt. %, respectively (Table I). The reaction mixtures were perfectly homogeneous throughout the reactions and no precipitation was observed with any of the monomer concentrations polymerized in THF/NMP. Similar to Series I, a further increase of the reaction time to 3 hours resulted in increased viscosity and molecular weight of the copolymer to 19540 g mol⁻¹ when the synthesis was performed at a monomer concentration of 25 wt. % in the presence of 0.05 wt. % of the catalyst. When the reaction time was increased to 6 hours, the viscosity of the copolymer decreased, *i.e.*, the trend was very similar to that in Series I (Fig. 2).

Despite the higher molecular weights obtained without a catalyst in the mixture of THF/DMAc (Table I), the syntheses in the THF/NMP mixture were performed in the presence of the catalyst because it was believed that the control of the reaction would be better. As will be shown later, the copolymer composition, *i.e.*, the hard segment content was determined by analysis of the ¹H-NMR spectra of the obtained copolymers. A better agreement with theoretical hard segment content was obtained for the samples that were synthesized in the presence of the catalyst than without (Table I).

Generally, the molecular weights of the PUUSs of Series II were higher than those prepared in the THF/DMAc mixture under the same conditions. The differences were more obvious with increasing concentration of the monomers in the reaction mixture, which was a consequence of better solubility of the PUUSs in THF/NMP than in THF/DMAc. This also shows that besides the choice of solvent, a very important factor for the successful synthesis of PUUS copolymers is a higher concentration of the monomers in the reaction mixture.

The yields of synthesized PUUS copolymers after precipitation in methanol/water mixture were between 62 and 90 % in Series I, while in Series II they

ranged between 86 and 93 %. The highest yield of 93 %, as well as the highest number average molecular weight of 19540 g mol^{-1} was obtained for the sample PUUS25-0.05 synthesized in the THF/NMP mixture. The polydispersity index was about 2 in most cases (Table I), indicating typical products of step polymerization.

Based on all the results presented herein, it could be concluded that the optimal experimental conditions for the synthesis of PUUSs are THF/NMP (1/9, v/v) solvent mixture, a temperature of $40 \text{ }^\circ\text{C}$, a catalyst concentration of 0.05 mol % and a reaction time of the second step of 3 h.

The structure and composition of PUUSs

The structure of the copolymers was verified by $^1\text{H-NMR}$ and $^{13}\text{C-NMR}$ spectroscopy. The $^1\text{H-NMR}$ spectrum of the PUUS25-0.05 sample from Series I is shown in Fig. 3.

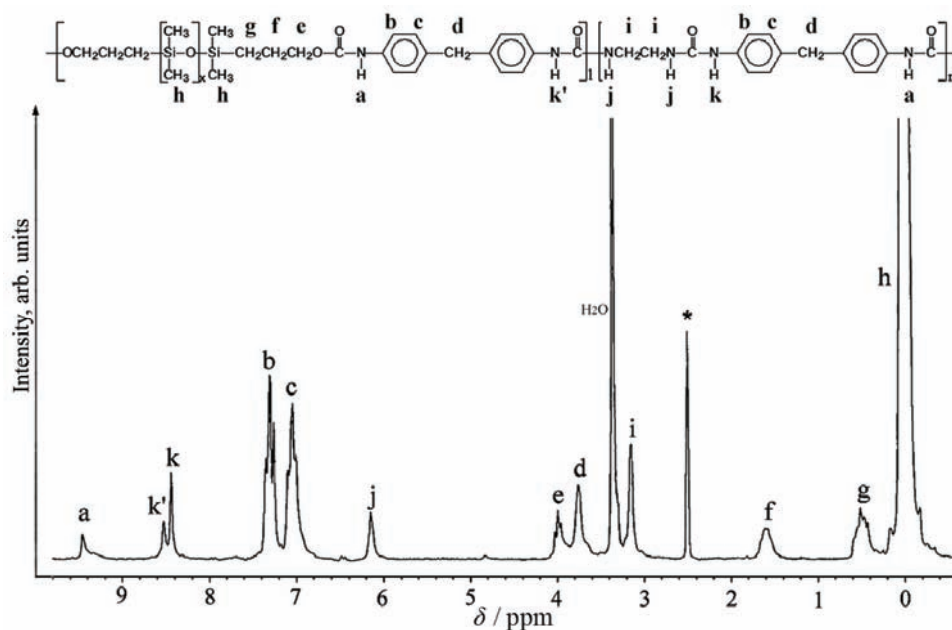


Fig. 3. $^1\text{H-NMR}$ Spectrum of the sample PUUS25-0.05 (the reaction time of the second step was 3 h).

In the $^1\text{H-NMR}$ spectrum the following characteristic signals were observed: 0.04 ppm of the Si-CH₃ protons; 0.53, 1.60 and 3.99 ppm of the CH₂ protons from the PDMS propylene residue; 3.15 ppm of the CH₂-CH₂ protons from the ethylene diamine residue; 3.75 ppm of the MDI methylene protons and 7.04 and 7.30 ppm of the aromatic protons from the MDI residue; 6.14 ppm of the NH urea protons next to ethylene diamine residue; 8.44 and 8.52 ppm of the NH

protons next to the aromatic rings, from the hard and soft segments, respectively; and 9.46 ppm of the NH urethane protons.

The content of hard segments was calculated from the $^1\text{H-NMR}$ spectra from the ratio of intensities of the aliphatic proton signals from the ED residues and the methyl proton signals from the $-\text{SiCH}_3$ groups, according to the following formulas:

$$x_{\text{HS}} = \frac{I(\text{CH}_2 - \text{CH}_2)}{\frac{I(\text{SiCH}_3)}{6 \cdot \bar{X}_x + 6} + \frac{I(\text{CH}_2 - \text{CH}_2)}{4}}; \quad x_{\text{SS}} = 1 - x_{\text{HS}}$$

$$w_{\text{HS}} = \frac{x_{\text{HS}} \cdot M_{\text{HS}}}{x_{\text{SS}} \cdot \bar{M}_{\text{SS}} + x_{\text{HS}} \cdot M_{\text{HS}}}; \quad w_{\text{SS}} = 1 - w_{\text{HS}} \quad w_{\text{SS}} = 1 - w_{\text{HS}}$$

where x_{HS} and x_{SS} are the mole fractions of hard and soft segments, respectively; w_{HS} and w_{SS} are the weight fractions of the hard and soft segments, respectively; $M_{\text{HS}} = 310 \text{ g mol}^{-1}$, molecular weight of the MDI-ED unit; $\bar{M}_{\text{SS}} = 1250 \text{ g mol}^{-1}$, molecular weight of the PDMS-MDI unit; $\bar{X}_x = 11.3$, the degree of polymerization of the PDMS prepolymer.

The experimental contents of the hard segments of the synthesized copolymers are presented in Table I. Better agreement of the experimental contents of the hard segments with the content predetermined by the composition of the initial reaction mixtures (20 wt. %) was obtained for the samples synthesized when the second step lasted 3 h. The highest deviation was observed for the samples synthesized without catalyst – the wt. % of HS was 27.3 and 27.2 for the samples PUUS15-0 and PUUS15B-0 from Series I. This was probably the result of the thermal instability of the hydroxypropyl end groups of the siloxane prepolymer under the polymerization conditions. Earlier studies showed that hydroxypropyl end groups undergo a cyclization reaction when heated, thereby losing their functionality and reactivity.^{28–30} In the absence of the catalyst, the hydroxypropyl end groups preferentially degraded rather than reacted with the present NCO groups. This further suggests that the presence of the catalyst is very important for fast building of urethane bonds between MDI and PDMS residues, and for obtaining the predicted copolymer composition. The lengths of the hard segment, $l(\text{HS})$, calculated as the number of MDI-ED units per one soft segment, are also given in Table I. The values of $l(\text{HS})$ were in range from 0.5 to 1.5, while the theoretical value, predetermined by the composition of the reaction mixture, was 1MDI-ED unit per 1 soft segment.

The molecular structure of the copolymers was also confirmed by FTIR spectroscopy. Characteristic absorption bands appeared at 2960 and 2905 cm^{-1} (ν_s and ν_{as} of C-H), 1595 and 1410 cm^{-1} ($\nu_{(\text{C}=\text{C})_{\text{arom}}}$), 1538 and 1510 cm^{-1}

(Amide II bands), 1303 cm^{-1} (Amide III band). The presence of the bands at 1072 and 1015 cm^{-1} ($\nu_{\text{Si-O-Si}}$), 1258 cm^{-1} $\gamma_{\text{Si-CH}_3}$ and 792 cm^{-1} $\delta_{\text{Si-CH}_3}$ confirmed the incorporation of the PDMS soft segments into the copolymer chains.

It is well established that the morphologies and the physical properties of segmented poly(urethane-urea)s mainly depend on the extent of hydrogen bonding between the copolymer chains.³¹⁻³⁴ There are two regions in the FTIR spectrum related to the hydrogen bonding of the hard segments. The first is the absorption region at $1620\text{--}1760\text{ cm}^{-1}$, corresponding to stretching vibrations of the C=O groups, where multiple bands were found. An intensive peak located at 1634 cm^{-1} is assigned to $\nu(\text{C=O})$ absorbance of the ordered hydrogen-bonded urea bonds, while the absorption peaks at 1733 cm^{-1} ($\nu(\text{C=O})_{\text{non-bonded urethane}}$), 1708 cm^{-1} ($\nu(\text{C=O})_{\text{hydrogen-bonded urethane}}$), 1694 cm^{-1} ($\nu(\text{C=O})_{\text{non-bonded urea}}$) and $1670\text{--}1680\text{ cm}^{-1}$ ($\nu(\text{C=O})_{\text{hydrogen-bonded urea, disordered}}$) appear as small shoulders. The C=O region of the spectra of the samples was fitted by the Gaussian deconvolution technique, using the PeakFit v4.12 (SeaSolve Software Inc.) program, whereby the locations and areas of each of these bands was given (Table II). The Gaussian deconvolution procedure showed very good agreement between observed and generated values (Fig. 4). The C=O and N-H stretching regions of the FTIR spectra of selected PUUS samples are shown in Figs. 5a and 5b, respectively. In the carbonyl region of FTIR spectra of the PUUS copolymers, the C=O absorption peak of hydrogen bonded urea dominated (Fig. 5a) and its area ranged from 49 to 59 %.

TABLE II. Curve fitting results (area, %) for the C=O stretching region of the FTIR spectra of some of the synthesized PUUSs

Sample	ν/cm^{-1}				$X_{\text{b,UT}}$	$X_{\text{b,UA}}$	$X_{\text{o,UA}}$	$X_{\text{d,UA}}$	
	1733	1708	1694	1670–1680					1634
Series I (the reaction time of the second step was 3 h)									
PUUS15-0.05	11.5	19.8	4.6	5.2	58.9	63.3	93.3	85.7	7.6
PUUS15-0	12.0	22.6	6.0	6.9	52.5	65.3	88.4	80.3	9.2
PUUS15A-0.05	10.4	25.8	9.5	4.1	50.3	71.3	85.1	78.7	6.4
PUUS15B-0	12.8	22.4	4.5	7.3	53.0	63.6	93.1	81.8	11.3
Series II									
PUUS15-0.05 (1 h)	12.2	27.1	6.7	4.6	49.4	69.0	89.0	81.4	7.6
PUUS25-0.05 (1 h)	12.6	25.1	8.5	3.9	49.9	66.7	86.4	80.1	6.2
PUUS25-0.05 (3 h)	11.4	24.7	7.6	3.1	53.2	68.4	88.1	83.3	4.8

FTIR Spectroscopy has also been used for the analysis of phase separation in PU and PUU copolymers. The degree of phase separation is reflected in the size and perfection of the domains. The success in the utilization of FTIR spectroscopy for investigating phase separation depends on the existence of bands sensitive to mixed and phase separated states. It was proposed that the degree of microphase separation in poly(urethane-urea) copolymers could be assessed

based the degree of hydrogen bonding of the urea C=O, whereby the extent of microphase separation is directly related to the intensity of the ordered urea absorbance at 1634 cm^{-1} . Simultaneously, the relative intensity of the absorbance of disordered hydrogen bonded urea carbonyls is a measure of the phase mixing between the hard and soft segments.^{35–37} The degree of hydrogen bonding of urethane groups ($X_{b,UT}$) and urea groups ($X_{b,UA}$), as well as the percentage of ordered ($X_{o,UA}$) and disordered ($X_{d,UA}$) urea–urea hydrogen bonds were calculated in following way:²¹

$$X_{b,UT} = \frac{\text{Area}(1708\text{ cm}^{-1})}{\text{Area}(1708\text{ cm}^{-1}) + \text{Area}(1733\text{ cm}^{-1})}$$

$$X_{b,UA} = \frac{\Sigma \text{Area}(\text{bonded})}{\Sigma \text{Area}(\text{bonded}) + \text{Area}(1694\text{ cm}^{-1})}$$

$$X_{o,UA} = \frac{\text{Area}(1634\text{ cm}^{-1})}{\Sigma \text{Area}(\text{bonded}) + \text{Area}(1694\text{ cm}^{-1})}$$

$$X_{d,UA} = \frac{\text{Area}(1670-1680\text{ cm}^{-1})}{\Sigma \text{Area}(\text{bonded}) + \text{Area}(1694\text{ cm}^{-1})}$$

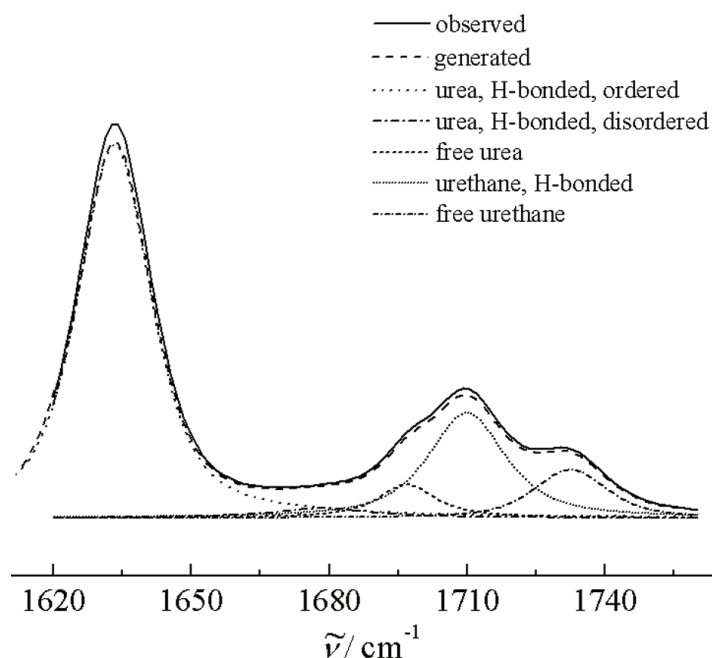


Fig. 4. Deconvolution of the carbonyl absorbance region of the FTIR spectrum for sample PUUS25-0.05 (reaction time of the second step was 3 h).

The $\Sigma Area(\text{bonded})$ is given as the sum of the areas at 1634 cm^{-1} (ordered hydrogen bonded urea bonds) and at $1670\text{--}1680 \text{ cm}^{-1}$ (disordered hydrogen-bonded urea bonds):

$$\Sigma Area(\text{bonded}) = Area(1634 \text{ cm}^{-1}) + Area(1670\text{--}1680 \text{ cm}^{-1})$$

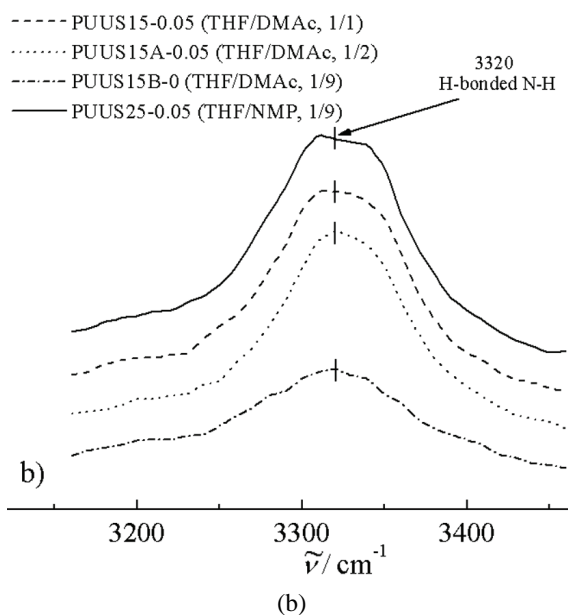
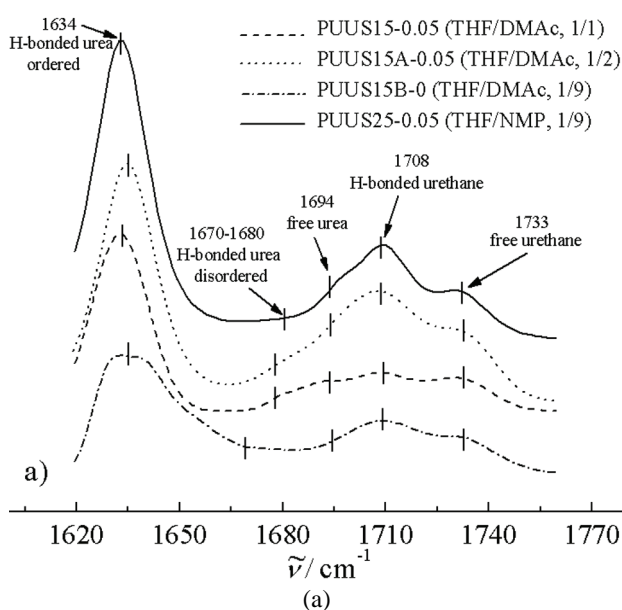


Fig. 5. FTIR Spectra of selected PUUS copolymers in the C=O (a) and N–H (b) stretching region (the reaction time of the second step was 3 h).

The results of these calculations for the prepared copolymers are given in Table II. It can be seen that the $X_{o,UA}$ values referring to urea ordered hydrogen bonding were similar in all samples and ranged from 79 to 86 %, indicating a high degree of microphase separation in the PUUS copolymers. The percentages of disordered hydrogen bonding urea, $X_{d,UA}$, ranged from 4.8 to 11.3 %, whereby somewhat higher values of $X_{d,UA}$ were calculated for the PUUS15-0 and PUUS15B-0, copolymers obtained without a catalyst in the mixture of THF/DMAc. This confirms the earlier conclusion that better control of reaction was enabled by the presence of the catalyst.

The second region related to hydrogen bonding was the N–H stretching region between 3100 and 3500 cm^{-1} , where a single peak centered at 3320 cm^{-1} was observed. This absorbance was assigned to the stretching vibrations of hydrogen-bonded N–H in both the urea and urethane units, indicating that all N–H groups in the PUUSs participated in hydrogen bonding. Using the Peakfit program, it was not possible to separate the peaks of disordered, hydrogen bonded N–H groups and free N–H groups, which for the PUU copolymers are characterized by absorbances at 3390 and 3450 cm^{-1} , respectively.³³ However, by comparison of the absorbance shape and intensity in this region, some qualitative assessment can be given.³⁷ Namely, the shapes and relative intensities of N–H absorbances were similar for most samples with a relatively sharp band at 3320 cm^{-1} , indicating a similar degree of phase separation (Fig. 5b). The broadening of the N–H band observed for the PUUS15B-0 sample implies a certain increase of phase mixing between the hard and soft segments, which is consistent with the previous analysis of the C=O region.

Thermal properties of the PUUSs

The results of DSC (first scan) and TG analyses of the PUUS synthesized in different solvent mixtures are summarized in Table III. In the DSC thermograms of PUUSs (Fig. 6), the glass transition temperatures of the soft segments were observed in the range from -112 to -99 °C, indicating that the PDMS was microphase separated from the hard segment phase. A relatively broad endothermic peak was observed between 50 and 68 °C. According to Seymour and Cooper, this peak relates to disruption of short-range ordering between the hard segments, *i.e.*, to dissociation of the hydrogen bonds.³⁸ The changes of the enthalpies of the endothermic peaks were in range from 0.83 to 1.22 J g^{-1} . In the second scan, this endothermic peak was not present, indicating that it was not possible to reform hydrogen bonds during the relatively fast cooling of the sample in the calorimeter.³⁹ For this reason, the first scan is presented in Fig. 6. The values of the glass transition temperatures of the soft segment did not changed significantly in the second scan.

TABLE III. DSC and TGA data of selected PUUSs under a nitrogen atmosphere (the reaction time of the second step was 3 h)

Sample ^a	Reaction solvent	T_g (PDMS) °C	T , endo-peak °C	$T_{5\%}$ °C	$T_{10\%}$ °C	$T_{50\%}$ °C	$T_{90\%}$ °C	DTG_{max} °C	Residual weight at 600 °C, %
PUUS10-0.05	THF/DMAc 1/1	-109	50	219	256	348	579	278/349/473	7.7
PUUS15-0.05	THF/DMAc 1/1	-99	58	252	269	374	610	287/361/489	11.5
PUUS15-0	THF/DMAc 1/1	-112	52	216	271	374	537	291/348/472	1.3
PUUS15A-0.05	THF/DMAc 1/2	-107	56	256	276	373	592	288/352/488	8.9
PUUS25-0.05	THF/NMP 1/9	-99	68	163	239	380	556	285/338/472	1.4

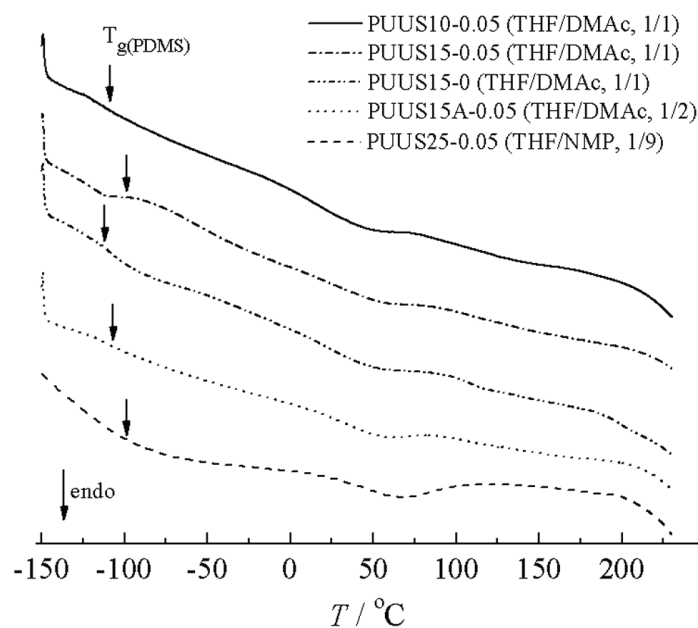


Fig. 6. DSC Analysis of selected PUUS copolymers (the reaction time of the second step was 3 h).

High temperature transitions were not detected in DSC thermograms, since the thermal degradation of the urea and urethane bonds begins around 200 °C, before melting the hard segments of the PUUS. This corresponds to the results of the TG analysis and to the proposed mechanism of degradation of poly(urethane-urea)s.⁴⁰

The thermal stability and degradation behavior of the synthesized PUUSs were investigated by thermogravimetric analysis under a nitrogen atmosphere.

The TG and DTG curves (Fig. 7) indicate that thermal degradation occurs in three steps. The characteristic temperatures for weight losses of 5, 10, 50 and 90 %, respectively, as well as the residual weight at 600 °C are considered. The $T_{5\%}$ value is considered to represent the beginning of mass loss. The results show that

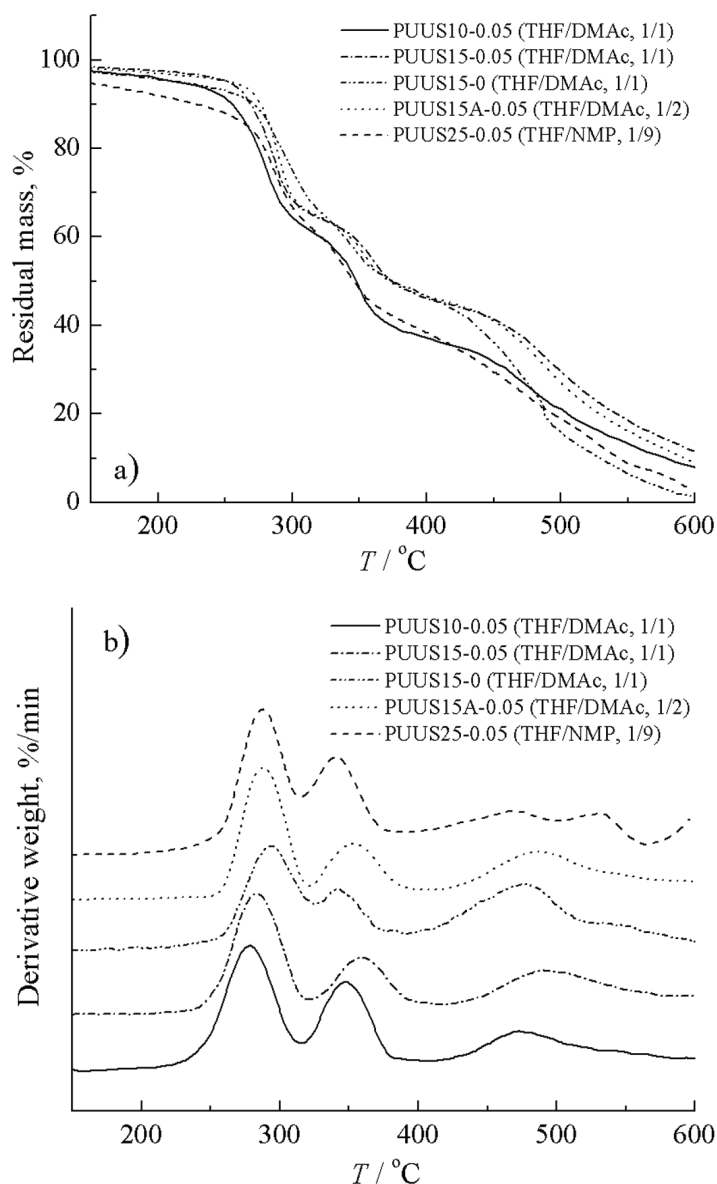


Fig. 7. TG and DTG analysis of selected PUUS copolymers (the reaction time of the second step was 3 h).

degradation of copolymers commenced above 200 °C, with the exception of the sample PUUS25-0.05, synthesized in THF/NMP, which lost 5 % of its weight by 163 °C (Table III). In this case, the weight loss begins at a lower temperature probably due to the presence of traces of NMP solvent in the sample, which is low volatile solvent and because of that cannot be easily removed from the sample. The temperatures of the maximal rate of degradation occurred around the same value for all samples, regardless of the reaction solvent (Table III).

It is well known that the thermally weakest link in polyurethane copolymers is the urethane bond, which commences to dissociate at around 200 °C. Three mechanisms of decompositions of urethane bonds have been suggested and the reactions may proceed simultaneously: dissociation to the original polyol and isocyanate, formation of a primary amine, an alkene, and carbon dioxide, and formation of a secondary amine and carbon dioxide.⁴¹

The thermal degradation of the synthesized PUUSs was a process, which occurred in three main steps under a nitrogen atmosphere. The thermal degradation of the copolymers commenced with decomposition of the urethane and urea bonds (the first and the second main DTG peaks), followed by degradation of the soft PDMS segments (the third DTG peak, between 400 and 500 °C). Further decomposition in the region between 500 and 600 °C corresponds to carbonization of the aromatic structures of MDI.^{41,42}

The residual weights of the PUUS samples at 600 °C ranged from 1.4 to 11.5 % (Table III). The residual weight originated mainly from the “organic”-fraction (MDI–ED), while the PDMS chains under a nitrogen atmosphere degraded by depolymerization, giving cyclosiloxanes as the degradation products.⁵

Water contact angle of the PUUSs

Special attention was focused on the wettability and hydrophobicity of the PUUSs surface, through the measurement of the static water contact angle (WCA). The determined values of the WCA for the PUUS copolymers are reported in Table IV. A water contact angle of 90° or higher indicates a non-wetting (hydrophobic) surface. The values of the WCA for the PUUSs were in a very narrow range from 87.4 to 91.3°, which could be explained by the similar contents of hard and soft segments. Thus, the surfaces of the obtained copolymers were on the border between weak hydrophilic and weak hydrophobic. In an environment other than water, they could rearrange very rapidly from hydrophilic to hydrophobic and *vice versa*, in dependence on the polarity of the surrounding environment. In an environment more polar than water, the hard segments are on the top of the surface, while a non-polar environment causes migration of the PDMS, which covered most of the surface of the PUUSs. This behavior is due to the very low surface energy of PDMS. As a comparison, the values of the water contact angle for thermoplastic poly(urethane–siloxane) elastomers, based on

MDI, BD and α,ω -dihydroxy-[poly(caprolactone)-poly(dimethylsiloxane)-poly(caprolactone)] (1:2:1 molar ratio of the reactants) were in the range from 93.7 to 99.9°, and these copolymers were considered to be hydrophobic.⁴³ Similarly, the contact angles of poly(ester-siloxane)s based on poly(butylene terephthalate) as the hard segments and poly(caprolactone)-poly(dimethylsiloxane)-poly(caprolactone) as the soft segments were in the range from 97 to 125°, depending on the hard to soft segment ratio, which classified these copolymers again as hydrophobic.⁴⁴

TABLE IV. WCA values for selected PUUS

Sample	Contact angle, °
Series I (the reaction time of the second step was 3 h)	
PUUS15-0.05	87.4±1.5
PUUS15-0	89.0±1.4
PUUS15A-0.05	91.3±1.7
PUUS15B-0	89.8±1.0
Series II	
PUUS15-0.05 (1h)	89.5±1.1
PUUS25-0.05 (1h)	88.6±0.8
PUUS25-0.05 (3h)	90.8±0.9

Topographical investigation of the PUUSs by AFM

The morphology of the PUUS copolymers was investigated by AFM. A contact mode AFM image of the surface topology of the sample PUUS25-0.05 is presented in Fig. 8. The distribution of hard and soft phases of the copolymer surface was analyzed by 3D- and 2D-topographic images. Based on prior studies, it is known that the bright regions represent the hard phase (hard ordered domains or crystalline regions in a copolymer), while the darker regions represent the soft PDMS phase. The AFM images clearly showed that the PUUS copolymers formed a two-phase microstructure and crystallized in the form of sphere-

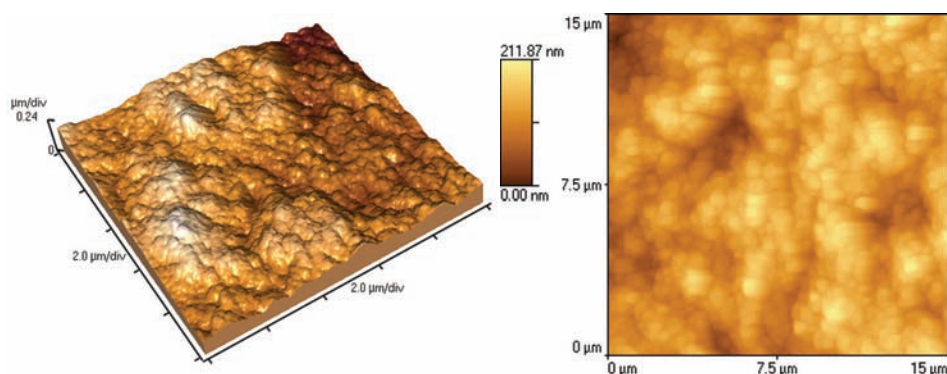


Fig. 8. 3D- and 2D-AFM images of the sample PUUS25-0.05 (size 15 μm).

litic superstructures. The average diameter of the hard segment domains, dispersed in the soft PDMS matrix was about 600 nm. AFM also confirmed that the hard-segment had a crystalline structure, which was not observed by DSC since the degradation of copolymers began before melting.

CONCLUSIONS

Segmented PUUSs were prepared by a two-step polymerization procedure in two different reaction mediums. It was demonstrated that the more polar THF/NMP mixture was a better solvent system for the synthesis of PUUSs than THF/DMAc. Copolymers with higher molecular weight were obtained in the THF/NMP mixture. It was also shown that not only was the solvent selection an important factor for the successful synthesis of the PUUS copolymers, but also a higher concentration of the monomers in the reaction mixture. Based on the obtained results, it was concluded that the following conditions were optimal for the synthesis of PUUSs in THF/NMP mixture: a temperature of 40 °C, a catalyst concentration of 0.05 mol % (calculated to PDMS), a monomer concentration of 25 wt. % in the reaction mixture and a reaction time for the second step of 3 h. The structure and composition of the PUUSs were confirmed by ¹H-NMR and FTIR spectroscopy. Small variations in the structure were obtained in dependence on the reaction conditions applied for the synthesis. A better agreement of the experimental hard segment content, determined by analysis of ¹H-NMR spectra of copolymers, with the theoretical hard segment content was obtained for the samples that were synthesized in the presence of catalyst than in its absence. FTIR Spectroscopy was employed for an analysis of the phase separation in the PUUS copolymers. It was calculated that the fraction of ordered hydrogen-bonded urea groups ranged from 79 to 86 %, indicating a high degree of microphase separation in the PUUS copolymers. DSC and AFM analysis also revealed that the copolymers show a phase-separated structure. The glass transition temperatures of the soft segments were observed in the range from -112 to -99 °C and a relatively broad endothermic peak was observed between 50 and 68 °C, which was related to the disruption of short-range ordering between hard segments. Thermal gravimetric analysis under nitrogen showed that the PUUSs were stable up to 200 °C. Since the values of the water contact angle were about 90°, the copolymers could possess slightly hydrophilic or hydrophobic surface properties, depending on the surrounding environment. The synthesis of a series of PUUS copolymers of different composition, *i.e.*, different hard/soft segment ratio, under the optimal conditions presented in this manuscript will be the subject of future work. Moreover, the influence of the structure and composition on the properties of the obtained copolymers will be investigated.

Acknowledgement. This work was financially supported by the Ministry of Education, Science and Technological Development of the Republic of Serbia (Project No. 172062).

ИЗВОД

УТИЦАЈ ПОЛАРНИХ РАСТВОРАЧА НА СИНТЕЗУ ПОЛИ(УРЕТАН–УРЕА–СИЛОКСАНА)

МИЛИЦА БАЛАБАН¹, ВЕСНА АНТИЋ², МАРИЈА ПЕРГАЛ³, IOLANDA FRANCOLINI⁴,
ANDREA MARTINELLI⁴ и ЈАСНА ЂОНЛАГИЋ⁵

¹Универзитет у Бањој Луци, Природно–математички факултет, Бања Лука, Босна и Херцеговина,
²Универзитет у Београду, Пољопривредни факултет, Београд, ³Универзитет у Београду, Институт
за хемију, технологију и металургију, Београд, ⁴University of Rome “Sapienza”, Department of
Chemistry, Rome, Italy и ⁵Универзитет у Београду, Технолошко–металуршки факултет, Београд

Сегментирани поли(уретан–уреа–силоксани) (PUUS), са тврдим сегментима на бази 4,4'-метиленидифенилдиизоцијаната и етилендиаминa (MDI–ED) и меким сегментима на бази хидроксипропил–терминираног поли(диметилсилоксана) (PDMS, $M_n = 1000 \text{ g mol}^{-1}$), синтетисани су под различитим експерименталним условима. Кополимери са константним молским односом тврдиx и меких сегмената (PDMS:MDI:ED = 1:2:1; 20 мас. % тврдиx сегмената), синтетисани су у две различите смеше растварача као реакционог медијума, методом двостепене полиадисије. Прва комбинација растварача је била смеша тетрахидрофурана (THF) и *N,N*-диметилацетамида (DMAc), док је у другом случају коришћена смеша THF-а и *N*-метилпиролидона (NMP). Реакциони услови су оптимизовани у погледу односа ко-растварача, концентрације катализатора, почетне концентрације мономера и времена одигравања прве и друге фазе реакције. Испитан је утицај примењених експерименталних услова на величину PUUS применом гел-пропусне хроматографије (GPC) и вискозиметрије разблажених раствора $[\eta]$. Кополимери највећих моларних маса су добијени у смеси THF/NMP (1/9, v/v). Структура и састав кополимера су окарактерисани ¹H-NMR и FTIR спектроскопијом. Морфологија синтетисаних кополимера је испитана микроскопијом атомских сила (AFM), док су термичка својства испитана диференцијалном скенирајућом калориметријом (DSC) и термогравиметријском анализом (TGA). Површинска својства кополимера су испитана одређивањем контактних углова са водом (WCA). Кополимери су показали двофазну микроструктуру и били су стабилни до 200 °C у атмосфери азота.

(Примљено 25. октобра 2011, ревидирано 9. априла 2012)

REFERENCES

1. Z. S. Petrovic, J. Ferguson, *Prog. Polym. Sci.* **16** (1991) 695
2. C. I. Chiriac, in *Encyclopedia of Polymer Science and Engineering*, H. F. Mark, N. M. Bikales, C. G. Overberger, G. Menges, J. I. Kroschwitz, Eds., Vol. 13, Wiley, New York, 1988, p. 212
3. J. T. Garrett, J. Runt, J. S. Lin, *Macromolecules* **33** (2000) 6353
4. H. Li, B. D. Freeman, O. M. Ekiner, *J. Membr. Sci.* **369** (2011) 49
5. P. R. Dvornic, R. W. Lenz, *High Temperature Siloxane Elastomers*, Hüthing & Wepf, Heidelberg and New York, 1990, p. 1
6. I. Yilgör, J. McGrath, *Adv. Polym. Sci.* **86** (1988) 1
7. J. P. Sheth, A. Aneja, G. L. Wilkes, E. Yilgor, G. E. Atilla, I. Yilgor, F. L. Beyer, *Polymer* **45** (2004) 6919
8. F. Lim, C. Z. Yang, S. L. Cooper, *Biomaterials* **15** (1994) 408
9. R. W. Hergenrother, X. H. Yu, S. L. Cooper, *Biomaterials* **15** (1994) 635
10. H. B. Park, C. K. Kim, Y. M. Lee, *J. Membr. Sci.* **204** (2002) 257
11. E. Yilgor, G. E. Atilla, A. Ekin, P. Kurt, I. Yilgor, *Polymer* **44** (2003) 7787

12. I. Yilgor, T. Eynur, E. Yilgor, G. L. Wilkes, *Polymer* **50** (2009) 4432
13. P. A. Gunatillake, G. F. Meijs, S. J. McCarthy, R. Adhikari, *J. Appl. Polym. Sci.* **76** (2000) 2026
14. R. Hernandez, J. Weksler, A. Padsalgikar, J. Runt, *Macromolecules* **40** (2007) 5441
15. Y. H. Lee, E. J. Kim, H. D. Kim, *J. Appl. Polym. Sci.* **120** (2011) 212
16. J. P. Sheth, E. Yilgor, B. Erenturk, H. Ozhalici, I. Yilgor, G. L. Wilkes, *Polymer* **46** (2005) 8185
17. E. Yilgor, E. Burgaz, E. Yurtsever, I. Yilgor, *Polymer* **41** (2000) 849
18. K. Stokes, R. McVenes, J. M. Anderson, *J. Biomater. Appl.* **9** (1995) 321
19. X. H. Yu, M. R. Nagarajan, T. G. Grasel, P. E. Gibson, S. L. Cooper, *J. Polym. Sci.* **23** (1985) 2319
20. E. Yilgor, I. Yilgor, *Polymer* **42** (2001) 7953
21. C. Liu, C. P. Hu, *Polym. Degrad. Stab.* **94** (2009) 259
22. A. Marand, J. Dahlin, D. Karlsson, G. Skarping, M. Dalene, *J. Environ. Monit.* **6** (2004) 606
23. S. Mallakpour, H. Raheno, *J. Appl. Polym. Sci.* **89** (2003) 2692
24. U. P. Ojha, C. Ramesh, A. Kumar, *J. Polym. Sci.* **43** (2005) 5823
25. S. M. Ataei, N. B. Laleh, *Polym. Adv. Technol.* **19** (2008) 291
26. S. M. Ataei, N. B. Laleh, A. Rabei, S. Saidi, *High Perform. Polym.* **19** (2007) 283
27. J. L. M. Abboud, R. Notario, *Pure Appl. Chem.* **71** (1999) 645
28. J. L. Speier, M. P. David, B. A. Eynon, *J. Org. Chem.* **25** (1960) 1637
29. I. Yilgor, E. Yilgor, M. Spinu, J. S. Riffle, R. S. Ward, in *Proceedings of 5th Int. Symp. Ring-Opening Polymerization*, Blois, France, 1986, p. 91
30. I. Yilgor, E. Yilgor, *Polym. Bull.* **40** (1998) 525
31. L. Ning, W. D. Ning, Y. S. Kang, *Polymer* **37** (1996) 3577
32. S. S. Sarva, A. J. Hsieh, *Polymer* **50** (2009) 3007
33. J. T. Garrett, J. S. Lin, J. Runt, *Macromolecules* **35** (2002) 161
34. X. Lu, Y. Wang, X. Wu, *Polymer* **35** (1994) 2315
35. E. Yilgor, I. Yilgor, E. Yurtsever, *Polymer* **43** (2002) 6551
36. E. Yilgor, E. Yurtsever, I. Yilgor, *Polymer* **43** (2002) 6561
37. J. T. Garrett, R. Xu, J. Cho, J. Runt, *Polymer* **44** (2003) 2711
38. R. W. Seymour, S. L. Cooper, *Macromolecules* **6** (1973) 48
39. T. Choi, J. Weksler, A. Padsalgikar, J. Runt, *Polymer* **51** (2010) 4375
40. L. F. Wang, Q. Ji, T. E. Glass, T. C. Ward, J. E. McGrath, M. Muggli, G. Burns, U. Sorathia, *Polymer* **41** (2000) 5083
41. F. S. Chuang, W. C. Tsen, Y. C. Shu, *Polym. Degrad. Stab.* **84** (2004) 69
42. T. Hentschel, H. Münstedt, *Polymer* **42** (2001) 3195
43. M. V. Pergal, V. V. Antic, M. N. Govedarica, D. Godjevac, S. Ostojic, J. Djonlagic, *J. Appl. Polym. Sci.* **122** (2011) 2715
44. V. V. Antic, M. V. Pergal, M. N. Govedarica, M. P. Antic, J. Djonlagic, *Polym. Int.* **59** (2010) 796.